

Advanced Magnetic Thin-Film Heads Under Read-While-Write Operation

by

Frank Zhigang Wang

A thesis submitted to the University of Plymouth
in fulfilment for the degree of

DOCTOR OF PHILOSOPHY

Centre for Research in Information Storage Technology
School of Electronic, Communication and Electrical Engineering
Faculty of Technology
University of Plymouth
United Kingdom

In collaboration with Hewlett Packard

March 1999

LIBRARY STORE

90 0398916 0



UNIVERSITY OF PLYMOUTH	
Item No.	9003989160
Date	- 3 JUL 1999 T
Class No.	T621.38234 WAN
Contl. No.	X703909206
LIBRARY SERVICES	

REFERENCE ONLY

This copy of the thesis has been supplied on condition that anyone who consults it is understood to recognise that its copyright rests with its author and that no quotation from the thesis and no information derived from it may be published without the author's prior written consent.

© Frank Zhigang Wang, 1999.

To my wife.

Abstract

Advanced Magnetic Thin-Film Heads Under Read-While-Write Operation

Frank Zhigang Wang

A Read-While-Write (RWW) operation for tape and/or potentially disk applications is needed in the following three cases: 1. High reliability; 2. Data servo systems; 3. Buried servo systems. All these applications mean that the read (servo) head and write head are operative simultaneously. Consequently, RWW operation will require work to suppress the so-called crossfeed field radiation from the write head.

Traditionally, write-read crossfeed has been reduced in conventional magnetic recording heads by a variety of screening methods, but the effectness of these methods is very limited. On the other hand, the early theoretical investigations of the crossfeed problem concentrating on the flux line pattern in front of a head structure based on a simplified model, may not be comprehensive. Today a growing number of magnetic recording equipment manufacturers employ thin-film technology to fabricate heads and thereby the size of the modern head is much smaller than in the past. The increasing use of thin-film metallic magnetic materials for heads, along with the appearance of other new technologies, such as the MR reproductive mode and keepered media, has stimulated the need for an increased understanding of the crossfeed problem by advanced analysis methods and a satisfactory practical solution to achieve the RWW operation.

The work described in this thesis to suppress the crossfeed field involves both a novel reproductive mode of a Dual Magnetoresistive (DMR) head, which was originally designed to gain a large reproduce sensitivity at high linear recording densities exceeding 100 kFCI, playing the key role in suppressing the crossfeed (the corresponding signal-noise ratio is over 38 dB), and several other compensation schemes, giving further suppression. Advanced analytical and numerical methods of estimating crossfeed in single and multitrack thin-film/MR heads under both DC and AC excitations can often help a head designer understand how the crossfeed field spreads and therefore how to suppress the crossfeed field from the standpoint of an overall head configuration. This work also assesses the scale of the crossfeed problem by making measurements on current and improved heads, thereby adapting the main contributors to crossfeed. The relevance of this work to the computer industry is clear for achieving simultaneous operation of the read head and write head, especially in a thin-film head assembly. This is because computer data rates must increase to meet the demands of storing more and more information in less time as computer graphics packages become more sophisticated.

Acknowledgements

I would like very much to thank the following people for their help and support throughout the project:

My first supervisor, Professor Desmond J. Mapps, Head of Centre for Research in Information Storage Technology, to whom I am deeply indebted for instigating the project during the registration for the degree, and then supplying me with a constant stream of support and encouragement; and without whom this project would not have been possible.

My second supervisor, Dr. David T. Wilton, Deputy Head of School of Mathematics and Statistics, for his valuable guidance, enthusiasm and fruitful criticism, whose experience and expertise have been of enormous benefit to me during the course of my research.

Professor Barry K. Middleton, Victoria University of Manchester, Dr. Terry Donnelly, University of Plymouth, Professor Warwick W. Clegg, Head of School of Electronic, Communication and Electrical Engineering, University of Plymouth, and Professor Kevin O'Grady, University of Wales, for their constructive comment and the encouragement.

Dr. Rick Barndt, Hewlett-Packard, Palo Alto, California, USA, and Dr. Ron Kennedy, Hewlett-Packard, Loveland, Colorado, USA, for their help during their visits to Plymouth. Dr. Catherine Slater, the European Research Laboratories of Hewlett-Packard, Bristol, England, for her encouragement. Professor John Mallinson, California, USA, for his discussion.

All of the staff within Centre for Research in Information Storage Technology, especially Mr. Nick Fry, Dr. Daniel F. Smith (now IBM), Dr. Paul Davey, Mr. Stuart C. Warner, Mr. Phil J. Brown, Mr. David C. Groom and Mr. Adrian F.A. Jerram, for their interest and help with both the simulations and the experiments.

The thesis is dedicated to my wife, Dr. Lianna He, Research Assistant of University of Plymouth. No-one could have asked for, or received more, assistance and encouragement than I have been given by her, for which I am extremely grateful.

Frank Zhigang Wang

Author's Declaration

This work was performed under the British Government EPSRC project GR/L39803 and a Hewlett-Packard Research Grants Programme. At no time during the registration for the degree of Doctor of Philosophy has the author been registered for any other University award.

Publications during the registration:

[1]D.J.Mapps, Z.G.Wang, D.T.Wilton, L.N.He and W.W.Clegg, "Suppression of Cross-Feed Field for Magnetic Recording", 7th European Magnetic Materials and Applications Conference, EMMA98-08012, Zaragoza, Spain, September 9-12, 1998; accepted by J. Magn. Mater.;

[2]Z.G.Wang, D.J.Mapps, D.T.Wilton, L.N.He, "Read-While-Write Operation in Magnetic Recording", in press, J. Magn. Mater., 1999;

[3]L.N. He, Z.G. Wang, D.J. Mapps, P. Robinson, D. Jenkins and W.W. Clegg, "Nano-Scale Positioning for Magnetic Recording", in press, Sensors and Actuators A: Physical, 1999;

[4]Z.G. Wang, L.N.He, D.J. Mapps, D.T.Wilton and W.W. Clegg, "Crossfeed Response of DMR vs. SAL Multitrack Heads", IEEE Trans. Magn., Vol.34, No.4, pp.1456-1458, July 1998;

[5]L.N. He, Z.G. Wang, D.J. Mapps, W.W. Clegg and D.T. Wilton, , "Perpendicular Kepered Media Reproduction with Dual MR Heads", Journal of the Magnetics Society of Japan, Vol.21, No.S2, pp.273-276, 1997;

[6]Z.G. Wang, L.N. He, D.J. Mapps, D.T. Wilton and W.W. Clegg, "Kepered Media Reproduction with Dual MR Heads", IEEE Trans. Magn., Vol.34, No.4, pp.1982-1984, July 1998;

[7]Z.G. Wang, D.J. Mapps, D.T.Wilton, L.N.He, "Crossfeed problems in read-while-write inductive/MR tape head", IEEE Trans. Magn., Vol.33, No.4, p.2531-2537, July 1997;

[8]L.N.He, Z.G. Wang, Bin Liu, D.J. Mapps, D.T. Wilton and W.W. Clegg, D.T.Wilton and Y.Nakamura, "Estimation of Track Misregistration by Using Dual-Stripe MR Heads", IEEE Trans. Magn., Vol.34, No.4, pp.2348-2355, July 1998.

Conferences attended during the registration:

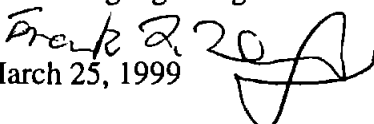
[1] 7th International Conference on Magnetic Recording Media, August, 1998, in Maastricht, the Netherlands, to present the poster WP1-22 "Read-While-Write Operation in Magnetic Recording";

[2] 2nd European Conference on Magnetic Sensors and Actuators, July, 1998, in Sheffield, UK, to present the poster "Nano-Scale Positioning for Magnetic Recording";

[3] 3rd International Symposium on Metallic Multilayers (MML'98) jointly with the EMRS Symposium on Magnetic Ultrathin Films and Ultrathin Film Nanostructures, Vancouver, British Columbia, Canada, June, 1998.

Frank Zhigang Wang

Frank Z. Wang
March 25, 1999



Contents

1	Introduction	1
1.1	Generalization	1
1.2	Concept of Read-While-Write (RWW) Operation	4
1.3	Application I: High Reliability	7
1.4	Application II: Data Servo Systems	11
1.5	Application III: Buried Servo Systems	16
1.6	Early Work	18
1.7	Motivation	27
1.8	Outline of This Work	28
2	Magnetostatics	29
2.1	Introduction	29
2.2	Concepts of MR and DMR	30
2.3	2D Analytical Model	33
2.4	3D Analytical Model: Multi-track Case	38
2.5	3D Finite Element Methodology (FEM)	46
2.5.1	Model Space	47
2.5.2	Mesh Generation and Discretisation Strategy	48
2.5.3	Topology of the Potential Space	49
2.5.4	Magnetostatic Analysis	50
2.5.5	Source Currents in Three Dimensions	51
2.5.6	Boundary Conditions	52
2.5.7	Material Properties	52

2.5.8	Laminations	53
2.5.9	Anisotropy	54
2.6	RWW Head Designs	54
2.7	Different Coil Shapes	60
2.8	A By-product of Different Core Width Design	64
2.9	Head Field Intensity	64
2.10	Crossfeed Response in Three Designs	68
2.11	Laminating Effect	76
2.12	Underpole and Underlayer Designs	77
2.13	Replay Processes	80
2.14	Summary	86
3	Magnetodynamics	90
3.1	Introduction	90
3.2	3D FEM Magnetodynamic Methodology	92
3.2.1	Vector Potential in Three Dimensions	93
3.2.2	Fields in Non-Conducting and Conducting Volumes	94
3.2.3	Time Variation in ELEKTRA	94
3.2.4	Computational Effort	95
3.2.5	An Eddy Current Example	95
3.3	Magnetodynamic RWW Head Model	99
3.4	Three Dimensional Dynamic Magnetic Field	100
3.5	Using Low Conductivity Materials	104
3.6	Cutting a Slot	109
3.7	Interconnecting Shields	114
3.8	RWW Operation in the Presence of Kepered Media	117
3.8.1	Background to Kepered Media	117
3.8.2	Reproductive Principle	118
3.8.3	Crossfeed Analysis	123
3.8.4	Summary of RWW in the Presence of a Kepered Medium	127
3.9	Summary	127

4	Experimental Assessment of Heads	130
4.1	Introduction	130
4.2	Experimental Apparatus	131
4.3	Experimental Assessments	133
4.3.1	Read-Rite TR5 Heads	135
4.3.2	Read-Rite DSMR Heads	143
4.3.3	Philips DCC Heads	145
4.4	Summary	148
5	Conclusions	150
5.1	Summary of This Work	150
5.2	Magnetostatics	151
5.2.1	Writing Coils	153
5.2.2	Read and Write Gap Separation	153
5.2.3	Screening Schemes	154
5.2.4	Other Compensation Schemes	155
5.2.5	MR Sensor	155
5.2.6	Dual-Magneto-Resistive (DMR) Sensor	156
5.2.7	Track Arrangement	157
5.3	Magnetodynamics	160
5.4	Experimental Assessment of Heads	161
5.5	Scientific/Technological Relevance	163
5.6	Future Work	164
	References	165
	Appendices	
	Published papers	
	Software	i
A.1	Crossfeed Calculation: Borland C++	i
A.2	Crossfeed Calculation and Plotting: MATLAB	viii
A.3	Stage Control: Turbo C	xv
A.4	Piezoelectric Ceramic Actuator Control: Turbo C	xvii
	List of Figures	xx
	List of Tables	xxxiii
	Index	xxxiv

Chapter 1

Introduction

1.1 Generalization

Magnetic recording systems are now becoming very important for the storage of digital information used in modern computer and communication systems. The increasing demands of the information super highways mean that large quantities of information must be stored after being transmitted in the super highways, prior to processing inside computers. The needs of personal computers themselves are increasingly significant as new, more user-friendly, suites of software are developed, often containing information-intensive graphics packages[1].

The basic structure of a magnetic recording head for writing is a magnetic circuit with a small gap in it and a coil wound around the magnetic core. Electric current in the core magnetises the material of the core causing a fringing field near the gap which magnetises the magnetic coating on the disk or tape drive being scanned across the head, as shown in Figure 1.1. In the read process, also shown in Figure 1.1, the magnetic field emanating from transitions is picked up by the magnetoresistive (MR) read element[2]. MR read heads produce very high signal per unit trackwidth and can provide media noise-limited system performance at very high areal storage density.

A practical thin-film head is shown in Figure 1.2. This is a typical thin-film head

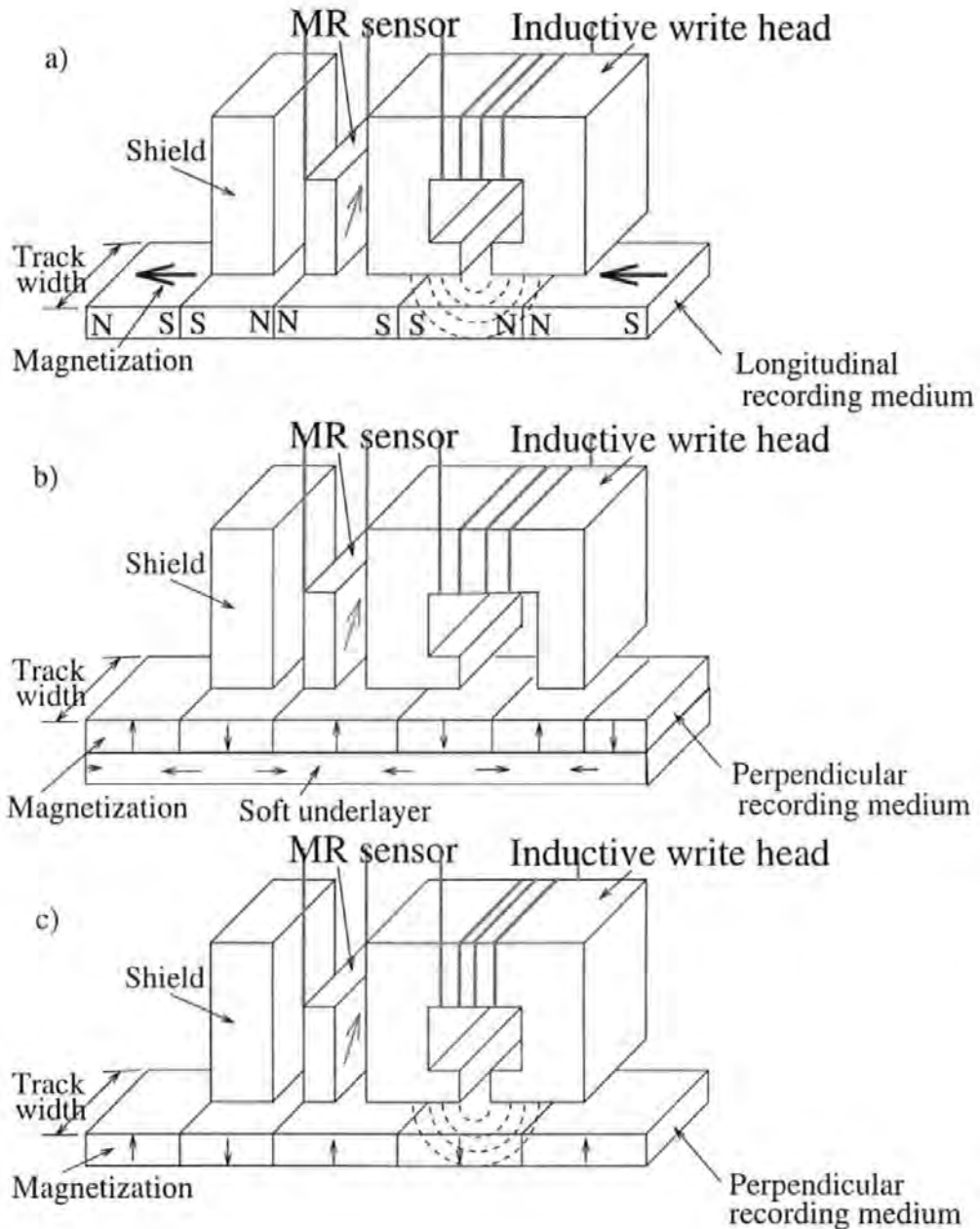


Figure 1.1: The write and read heads for longitudinal recording (a) and Type 1 and 2 perpendicular recording, (b) and (c), respectively. Type 1 perpendicular recording requires a special write head and a soft magnetic layer under the perpendicular recording medium. Type 2 requires only a perpendicular medium and a special equalizer to process asymmetric bi-polarity readback waveform across a transition in an otherwise conventional system.

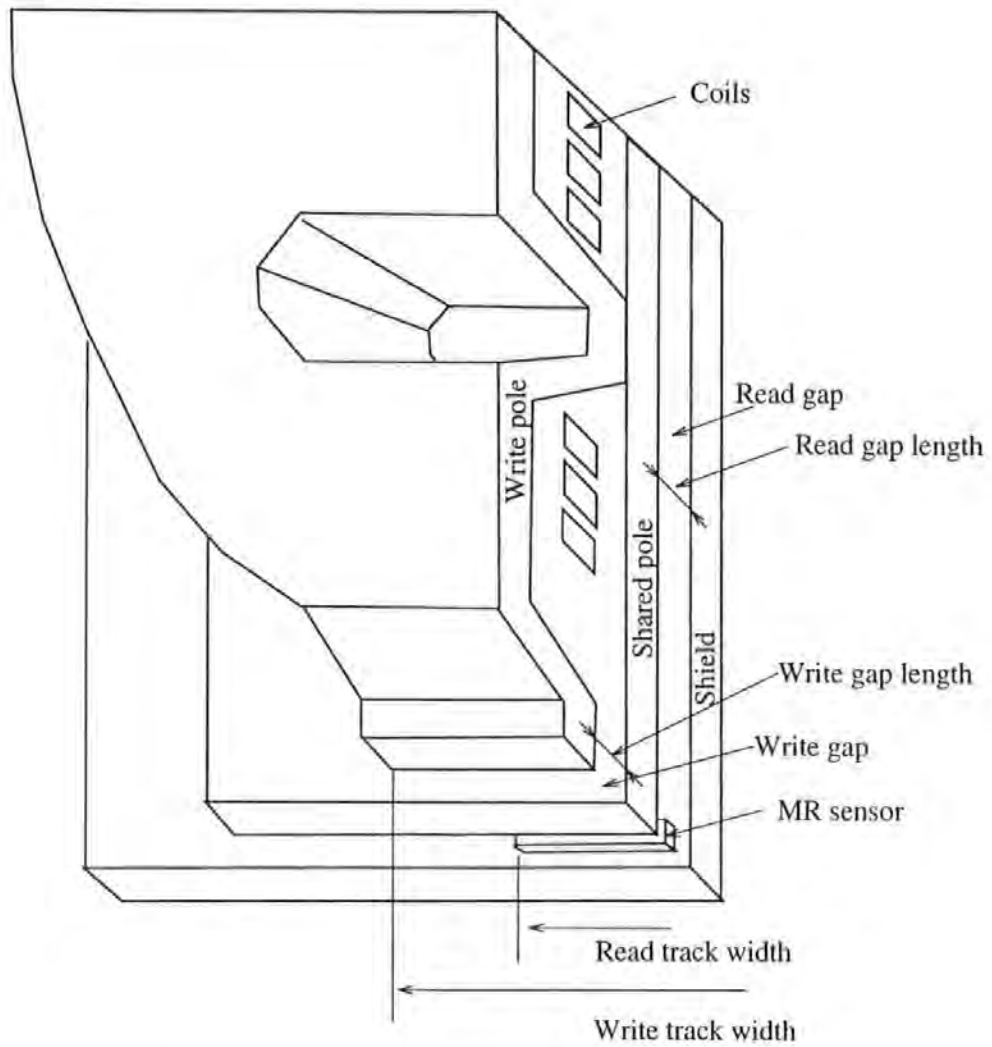


Figure 1.2: A typical design for a practical thin-film Inductive/Magneto-Resistive (MR) head, based on a shared-pole sensor-in-gap structure. In the read process, the magnetic field emanating from transitions is picked up by the magnetoresistive (MR) read element, inserted between shields.

and the fabrication technique has been borrowed from the semiconductor industry for fabrication of integrated circuits. There are many advantages to this approach, with perhaps the most important being the ability to produce extremely narrow pole tips and recording gap widths in the thin-film process. These narrow pole tips, in turn, permit the density of magnetic recording to be increased. As the linear recording density of magnetic disk storage systems increases, recording heads which can produce strong fields with steep field gradients are necessary in order to record the data patterns with sufficient overwrite characteristics on high coercivity media. As shown in Figure 1.2, different layers are deposited onto an insulating substrate (silicon). The copper has been shaped into a multi-turn conductor and magnetic top and bottom cores are jointed at the center of this conductor and there is no back gap. The front gap for an inductive head is controlled by a thin insulating layer. A Magneto-Resistive (MR) reproducing element is inserted between two shields.

In the hierarchy of computer peripherals, the magnetic tape drive is a commercially important contribution to the world industry. It is also undergoing rapid development to keep pace with hard disk drives. The progress of this technology in the future needs very sophisticated recording heads, tape media and electronic data channels. The work described in this thesis is mainly to help overcome a potentially serious problem (write-read crossfeed) in Read-While-Write operation.

1.2 Concept of Read-While-Write (RWW) Operation

In some applications, the read head and write head need to be in operation simultaneously. This is named "Read-While-Write (RWW)" operation. This means, as shown in Figure 1.3, that the read head may receive not only a signal flux from the medium but also an unwanted flux component from the write head. The flux component picked up by the read head from the write head is normally of signif-

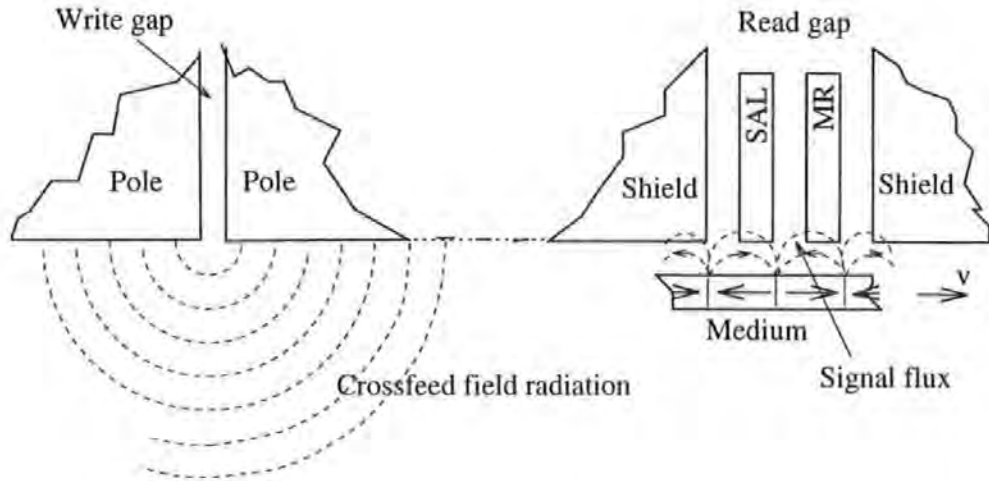


Figure 1.3: Concept of Read-While-Write (RWW) operation. In the RWW operation, the read head (here is a SAL [Soft Adjacent Layer] biased MR head) may receive not only a signal flux from the medium but also a flux component from the write head.

icant magnitude compared with the signal flux, especially when a high coercivity medium is used, and is given the name of "crossfeed field". In principle, four different sources of crossfeed field can easily be distinguished, as shown in Figure 1.4, namely:

- (a) Capacitive coupling from the writing to the reading bump;
- (b) Inductive coupling from the writing to the reading winding;
- (c) Magnetic flux leaking around the screen, which separates writing and reading bumps;
- (d) Magnetic flux penetrating through the screen.

Also, in multitrack thin-film/MR heads, there may be several write heads operating at the same time, all contributing a different amplitude and phase of different signals at any one time to any particular reading head in the array.

It is proposed in this research project to study the main contributing factors to crossfeed in single and multitrack heads and then explore and adapt some methods

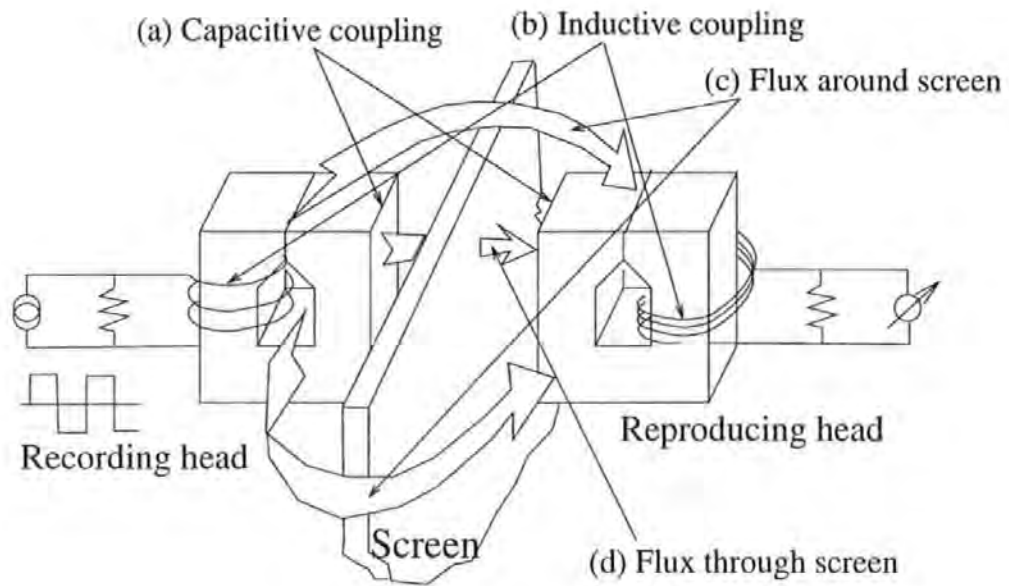


Figure 1.4: Schematic illustration of four different sources of crossfeed field. They are: (a) Capacitive coupling from the writing to the reading bump; (b) Inductive coupling from the writing to the reading winding; (c) Magnetic flux leaking around the screens; (d) Magnetic flux penetrating through the screens. Here the reproducing head is an example of an inductive head. If an MR reproducing head is used, it is equivalent to a one-turn coil with respect to the crossfeed field source (b).

to reduce crossfeed field for use in thin-film/MR heads. Analytical and numerical methods of estimating crossfeed in single and multitrack thin-film/M-R heads under both DC and AC excitations can often help a head designer understand how the crossfeed field spreads and therefore how to suppress the crossfeed field from a standpoint of an overall head configuration.

In the following three sections, we will demonstrate three possible applications of RWW operation. They are high reliability, data servo systems and buried servo systems, respectively.

1.3 Application I: High Reliability

Magnetic tape units are vital components in data measurement and computer systems[1]. Their demise has been predicted numerous times, and each time they have survived – lately in the form of numerous back-up drives. Using advanced tapes allows higher track densities to be achieved with the current recording channel and detection system in the DigaMaxTM recorder[3]. Track widths smaller than 10 μm become possible. The first generation already allows 13 GBytes per 1000 feet of tape using 37.5 μm tracks. At 10 μm track widths it would be possible to store around 50 GBytes. When this is combined with the high data rate of 2 MBytes/s we see that, even 100 years on from Valadimir Poulsen's first demonstration of magnetic recording, interesting developments can still be made.

Tape drives employ cassettes, cartridges or reels with tapes of different widths and lengths. The tape transport must satisfy several requirements. Very fast starts and stops are necessary and movement of the tape must be in a perfectly straight path. This requirement is particularly critical in parallel track applications with high bit densities; here the bits from the tracks need to be read simultaneously. Such high accelerations were not possible in early digital tape drives. It was common to bring the tape into motion by pressing it against a rotating shaft called a

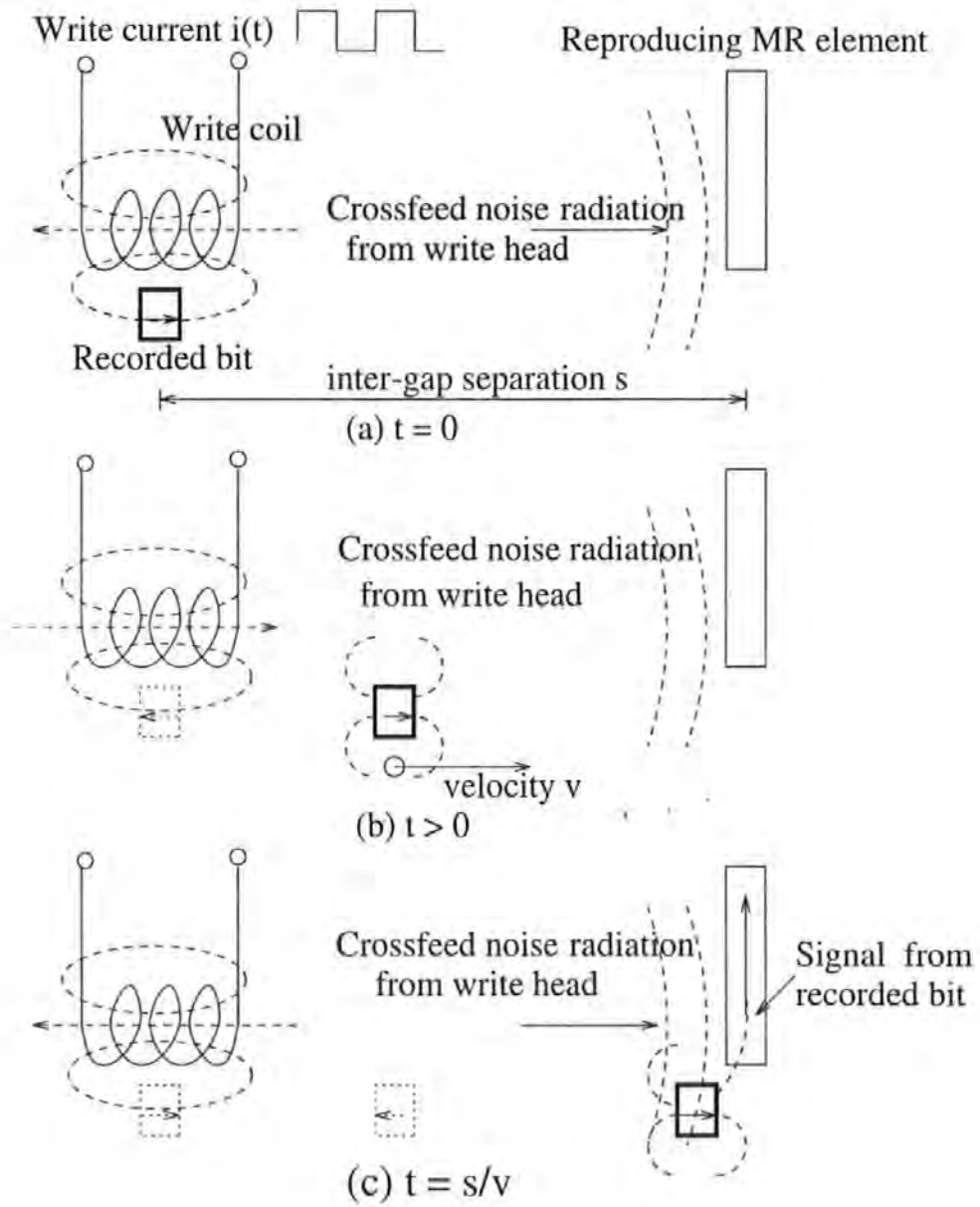


Figure 1.5: Schematic illustration of the crossfeed problem in RWW heads for the purpose of high reliability.

capstan by means of a puck. This system was improved by introducing a perforated capstan wherein a vacuum would attract the tape and move it with the capstan. To stop the tape, air pressure would force the tape against a fixed surface near the capstan.

It is necessary in some tape drives to write information on tape and verify it by reading with a read head a short time later, as illustrated in Figure 1.5. For example, defects in the tape material and in the contact between the head and tape may give rise to errors in the recorded information. In order to detect such "drop-outs" a reproducing head placed closely behind the recording head in each track is employed to check-read the information stored on the tape. For information being recorded and verified continuously, this means that the read head and write head are in operation simultaneously. The magnitude of the flux sensed by the read head on the tape is of the order of pico-webers (i.e. very small). In contrast, the writing flux can be very large, especially if a high-coercivity medium is being used. This means that the read head may receive a flux component from the write head which is of significant magnitude compared with the signal flux it is detecting from the tape and this is especially true if the write head and read head are close together—an essential design-aim if the "dead" tape at the end of a recorded block of information (the inter-block gap) is to be minimized.

In intermittent operation of the tape-unit, the tape stops when the end of the record passes the reproducing gaps. Unless the tape is spooled backwards before the next recording takes place, an inter-record gap arises in this way, the length of which is determined by the distance between the recording and reproducing-transducer gap and by the starting and stopping time of the tape transport mechanism.

For efficient use of the available storage space a short distance between the head gaps is thus required. An additional benefit from tight write-to-read gap spacing is fewer off-track errors due to the skew of the tape (Figure 1.6) and azimuth alignment of the head as it passes over the head. Bytes are written in parallel in several

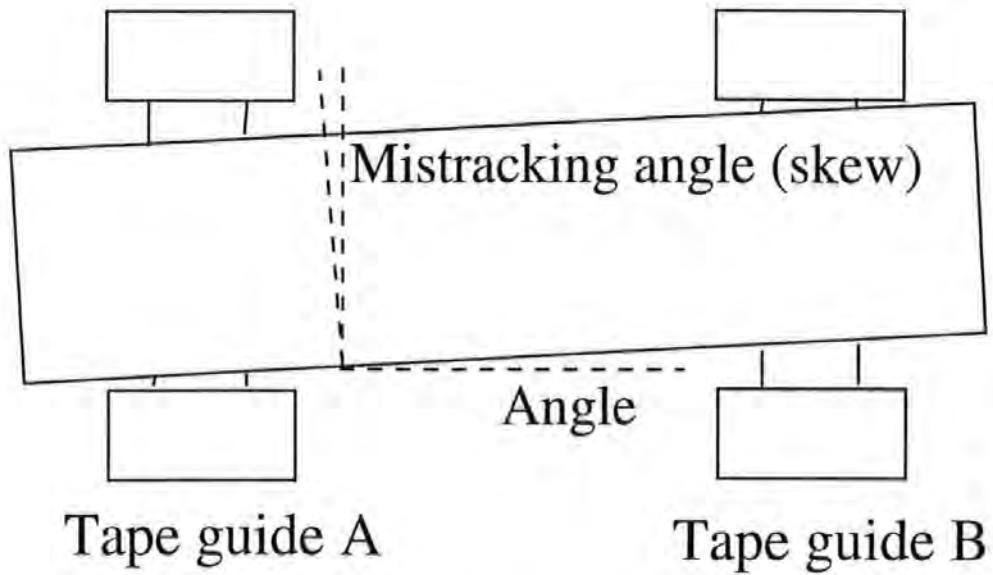


Figure 1.6: Tape skew.

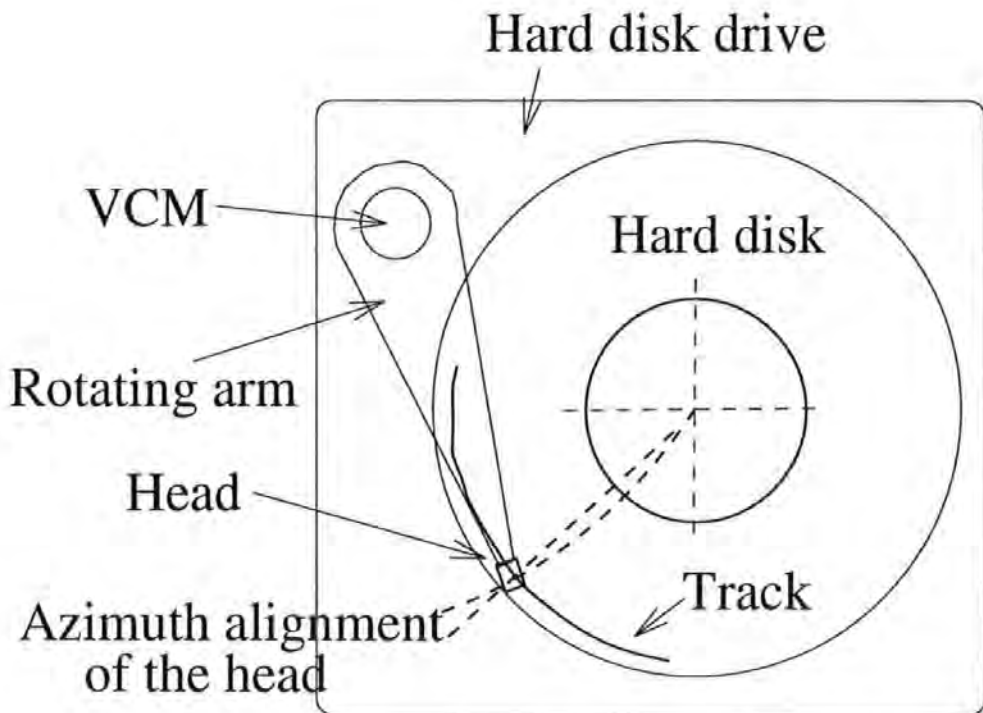


Figure 1.7: The azimuth alignment of the head in hard disk drive.

tracks and they should be read back simultaneously. This situation difficulty exists in practice because of tolerances in the manufacture of multitrack heads and in the slitting of tapes. The curvature may, among other factors, cause the tape to "weave" through the drive and it could depart from the ideal, straight path. In modern thin-film/MR heads the write and read gaps can be very close together (eg. 10 μm) and in some cases head parts can be shared, as shown in Figure 1.2, so write-read crossfeed can be unacceptable when both head functions are used at the same time.

As stated earlier, the RWW operation can potentially be applied to disk drives as well. A similar requirement of a short distance between the head gaps is also needed due to the azimuth alignment of the head (Figure 1.7) in hard disk drives with rotary VCMs (Voice Coil Motor).

1.4 Application II: Data Servo Systems

The computer industry is developing rapidly towards more and more powerful systems requiring the storage of large amounts of data onto hard disk. The dramatic increase in areal density in magnetic recording has been made possible through numerous developments, including the reduction in flying heights and decreased head dimensions. Taken to an extreme, one can imagine a "head", which has nanometer-scale dimensions, moving in contact or near-contact over the surface of a disk. Correspondingly, better servoing will be required to ensure acceptable error performance. In traditional sector servo systems, as shown in Figure 1.8, the servo signal is intermittent because data sectors and servo sectors are distributed alternately over the hard disk surface, thereby yielding a possible misregistration from the track when the head is passing through data sectors (inertia-dependent track following). A new track following method has been proposed, by which the head's position error signal (PES) can be directly and continuously extracted from data sequences[4].

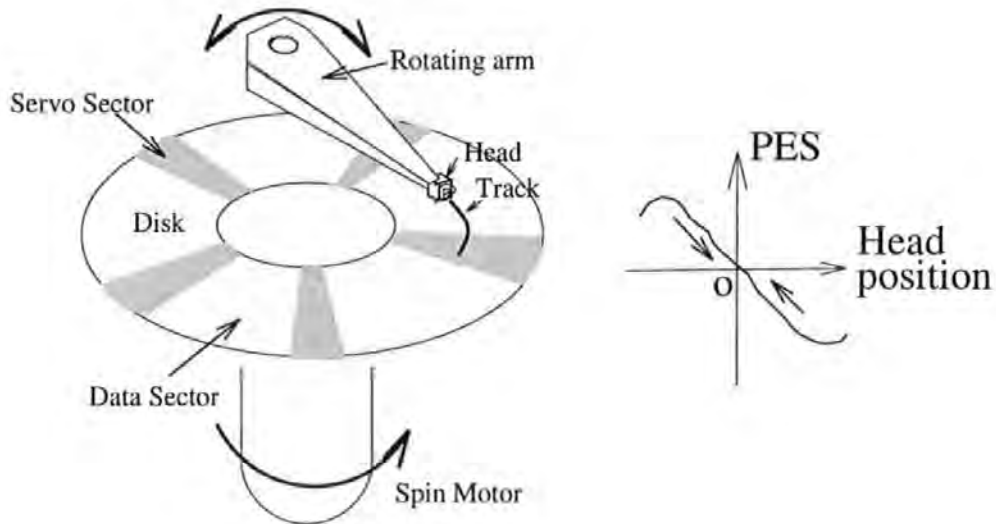


Figure 1.8: A traditional sector servo system. Here the servo signal is intermittent because data sectors and servo sectors are distributed alternately over the hard disk surface, thereby yielding a possible misregistration from the track when the head is passing through data sectors.

To satisfy the needs of nanoscale positioning, in this section, we will describe the design and development of a new concept of servoing with dual-strip MR (DSMR) heads which uses the asymmetric microtrack profile of the MR element to estimate the data and provide servo information[5]. In 4-terminal DSMR[6], the magnetizations of the individual stripes are biased by the sense current passing through the opposite stripe, as shown in Figure 1.9. This means that the magnetizations scissor from their nominal parallel positions, one is at 45° , the other is at -45° . The nominal parallel magnetization configuration without sense current flowing is caused by permanent magnet films placed in the off-track wing regions (not shown in the figure) to control the magnetization orientation, thus avoiding multidomain formation within the soft films[7][8]. In Figure 1.9, the two MR stripes are exposed to the same stray field from a medium transition and thus the DSMR head produces a maximum output(one MR stripe has a resistance increase, and the other has a resistance decrease, but in the DSMR one looks at the differential signal).

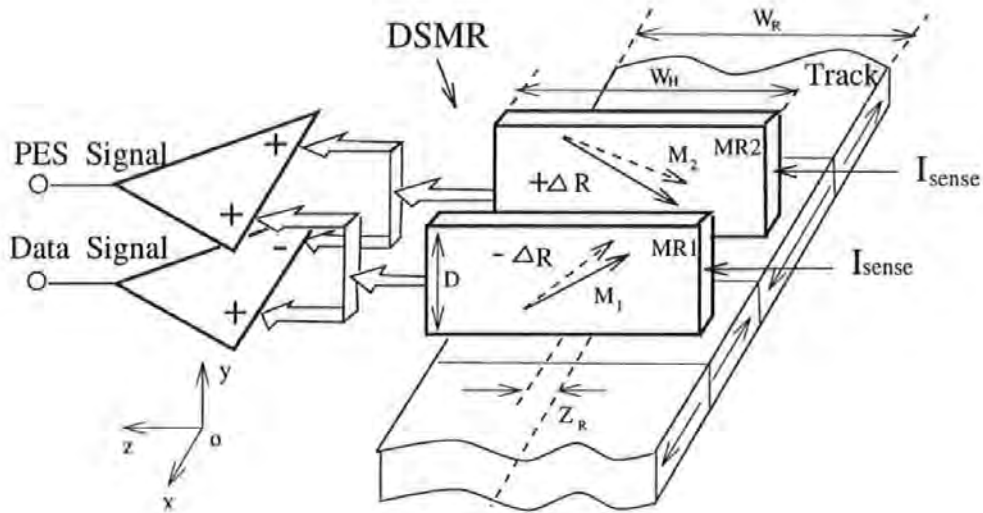


Figure 1.9: Track and head configuration for misregistration Z_R . When exposed to the same stray field from a medium transition, one MR stripe has a resistance increase, and the other has a resistance decrease. The difference of these two stripes' signals is taken as DSMR's effective output whereas the sum of these two stripes' signals is taken as a PES (Position Error Signal) for servo purposes.

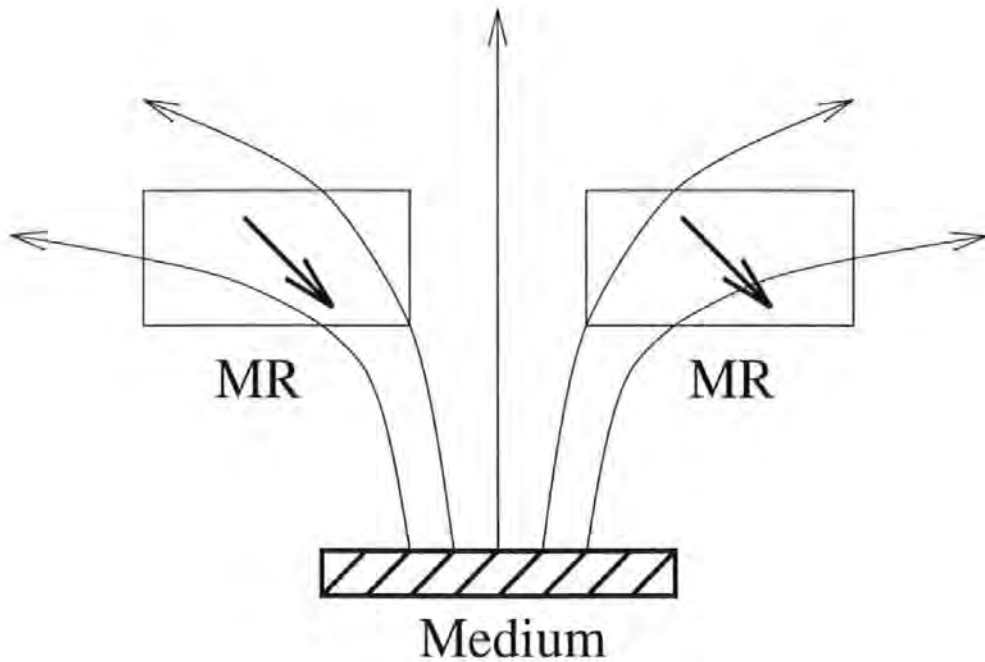


Figure 1.10: Illustration of fields in the (y,z) MR element plane from a recorded longitudinal medium. The biased MR element is shown in two positions to illustrate off-track asymmetry.

Due to the intrinsic asymmetry of the 45° bias in the single domain MR film, MR heads generally have asymmetric off-track responses[9]. In other words, the output voltage in a single MR film cannot reach its maximum value even when the transverse displacement of the head from the recorded track is zero. The reason for this asymmetric behavior is illustrated in Figure 1.10. A sketch of the magnetic field from the magnetized medium in the (y,z) plane of the element is shown. Also shown is the MR element, biased nominally at 45° to the $-z$ direction, in off-track positions on either side of the finite track width recording. For the element on the right (corresponding to transverse misregistration $Z_R < 0$) the signal field is generally orthogonal to the MR bias magnetization. In this case the torque on the magnetization is large, and large rotations occur giving large resistance changes. For the element shown on the left ($Z_R > 0$), the signal field is generally parallel to the MR magnetization, yielding small rotations and correspondingly small resistance changes. In a word, the response is asymmetric with respect to off-track displacement. Not only does the maximum response not occur for zero displacement ($Z_R = 0$), but the response decreases at different rates depending on the direction of displacement.

We plotted the normalized response voltages versus Z_R , in Figure 1.11. In the figure, $\lambda = 0.5 \mu m$ is the characteristic length of flux decay, $W = 7.5 \mu m$ is the total width of the MR stripe including the off-track wing regions, $W_H = 1.5 \mu m$, $W_R = 2 \mu m$. The stripe depth D is optimized to $0.8 \mu m$ because the slope of the PES around the zero-crossing point becomes sharp with the stripe's depth decreasing. It is obvious that the individual stripe's response is asymmetric and the peak shifts right or left, respectively. Within a range of 30% of the track width (about $\pm 0.3 \mu m$) around the track centric line, PES is proportional to the misregistration Z_R and when $Z_R = 0$ the head is aligned with the recorded track. A reasonable servoing ability through DSMR has been confirmed.

So far, studies have mainly focused on how to reduce this asymmetry of the microtrack profile, which is present for each individual MR sensor[8][10][11]. An ex-

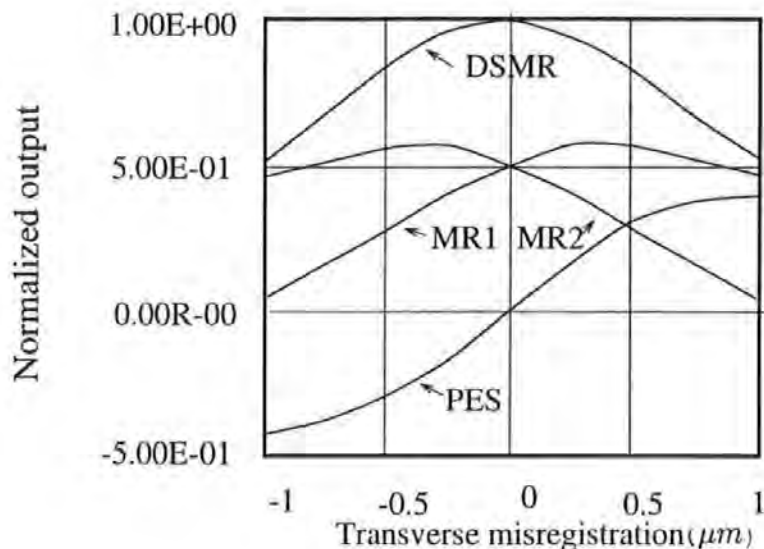


Figure 1.11: Normalized voltages amplitude versus the transverse misregistration Z_R of the head from the recorded track. Due to the intrinsic asymmetry of the 45° bias, the individual stripe's response is asymmetric and the peak shifts right (for MR1) or left (for MR2), respectively. But the DS MR signal retrieved from MR1 and MR2 is symmetry. When $-0.3 \mu m \leq Z_R \leq +0.3 \mu m$, a good linearity with PES can be seen.

ample is the DS MR configuration that eliminates off-track asymmetry by differential detection and yields symmetric off-track responses[12]. Other methods to reduce the off-track asymmetry include biasing the magnetizations into anti-symmetric states for the two MR films and using a soft underlayer beneath the medium to alter flux propagation paths[13]. Conversely, we actively make use of the asymmetry phenomenon to estimate the off-track perturbation. This estimation will be executed continuously even when the head is passing through data sectors, while in conventional sector servo systems the servo signal is intermittent because data sectors and servo sectors are distributed alternately over the hard disk surface. We claim this new concept meets the challenge of high density magnetic recording, in which better servoing[5] is required to ensure acceptable error performance. For such a continuous data servo system, this means that the servo (read) head and write head are operative simultaneously, i.e. the concept of RWW operation applies here.

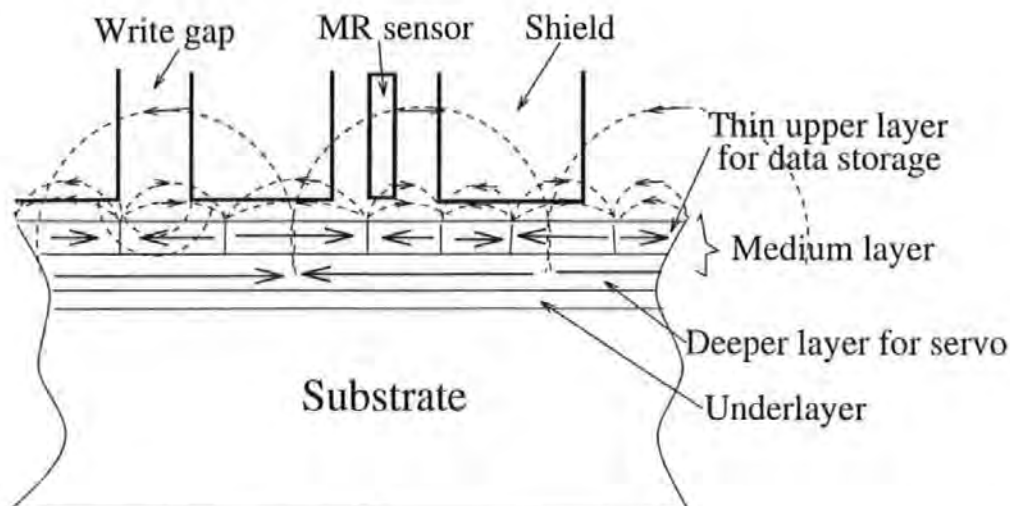


Figure 1.12: Schematic diagram of the buried servo. A buried servo method can obtain a positioning signal continuously, in which servo and data share a medium layer by using the thin upper layer for data only and deeper layer for servo only. Both the data and the servo signals are reproduced by an identical MR sensor.

1.5 Application III: Buried Servo Systems

As mentioned in the previous section, continuous servo meets the challenge of high density magnetic recording, in which better servoing is required to ensure acceptable error performance. A buried servo method[3] offers another possibility of continuous servo. Its schematic is shown in Figure 1.12, in which servo and data share a medium layer by using the thin upper layer for data only and deeper layer for servo only. The thin upper layer contains exclusively data bits and is magnetized densely. The deeper layer is exclusively for servo bits magnetized at relatively low linear density. Both the data and the servo signals are reproduced by the same MR sensor. During the reading and writing of data, an actuator keeps the head on the track center using prerecorded buried servo information. These buried servo tracks are written deep into the magnetic coating in one pass with a dedicated thin-film servo writer. Writing the servo information below the data tracks leaves the full tape area available for the recording of data. The major advantages of this servo method are that the servo signal is continuous, its quality has low sensitivity to medium defects and is no longer limited by the data trackwidth.

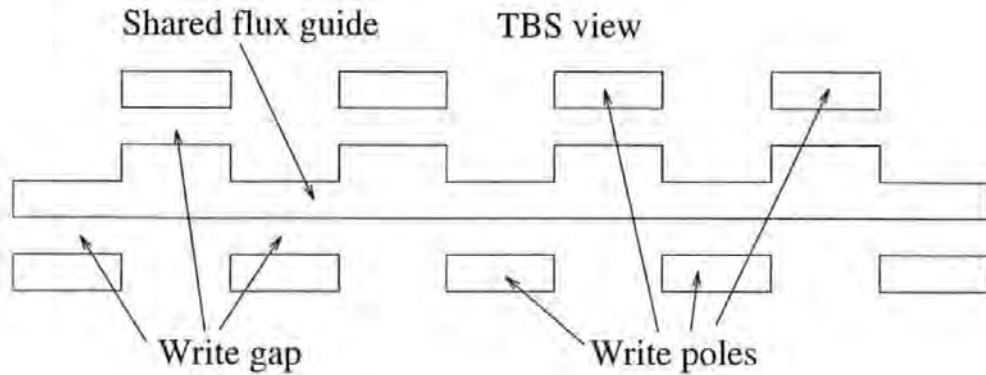


Figure 1.13: Schematic Tape Bearing Surface (TBS) view of a servo write head.

The buried servo information consists of AC bias recorded servo tracks. The servo wavelength is much longer than maximum data bit length, which enables sensing of the servo tracks by the data read head during writing and reading of data. Servo and data signals are separated in the read-channels by low-pass and high-pass filtering.

A schematic description of the servo writer is shown in Figure 1.13. It consists of structured upper and lower soft magnetic flux guides on both sides of a continuous shared flux guide. By this design, the write poles cover 100 % of the tape width. The optimal gap length for deep-recording is a few microns. The upper and lower writers each have their own single turn common write coil by which servo tracks with a signal phase difference of 180 degrees between adjacent tracks are written. The data head is 'on track' if the signals of two neighbouring servo tracks cancel each other, resulting in zero output of the sensing read channel at the servo signal frequency. In the buried servo system three channels detect a 0-180 degree servo track intersection, three channels detect a 180-0 degree intersection, and two channels detect a wide reference servo track to obtain the phase and frequency of the servo signal. The track position indicated by the error signal generated from these eight signals is insensitive to small variations in the width or signal amplitude of

the servo tracks[3]. The servo track signals should be large enough, even after many overwrites by the write head. This is ensured by the fact that the servo tracks are recorded deep into the tape, whereas the data tracks are written in a thin upper layer of the tape.

For such a continuous buried servo system, this also means that the servo (read) head and write head are operative simultaneously.

1.6 Early Work

Traditionally, write-read crossfeed has been reduced in conventional heads by a variety of screening methods to achieve Read-While-Write(RWW) operation.

Pioneering work on compensating techniques of crossfeed field was done by G.I. Walther, Philips Research Laboratories, Eindhoven, the Netherland, in 1964[14]. He studied the influence of various screening configurations and screening materials on the crossfeed from writing to reading transducers. As a result, a crossfeed track attenuation of 17.3 dB, which was satisfactory in the early digital recording systems, where the dimension of the heads was of centimetre order, was obtained by relatively simple means.

Walther's experimental apparatus is indicated in Figure 1.14. A recording and reproducing head were positioned on the same track, leaving sufficient space for screen to be placed between the cores. The electric circuits associated with the windings on both heads were damped. The writing transducer was energized by a square wave current of sufficient strength to saturate the tape. The high frequency components present in the writing current were dependent on the rise time, which in this case was of the order of $0.1 \mu\text{sec}$. The repetition frequency was adjusted to a value where, at a step-change of the current, the contribution of the preceding step to the voltage induced in the reading coil was negligibly small. Alternatively,

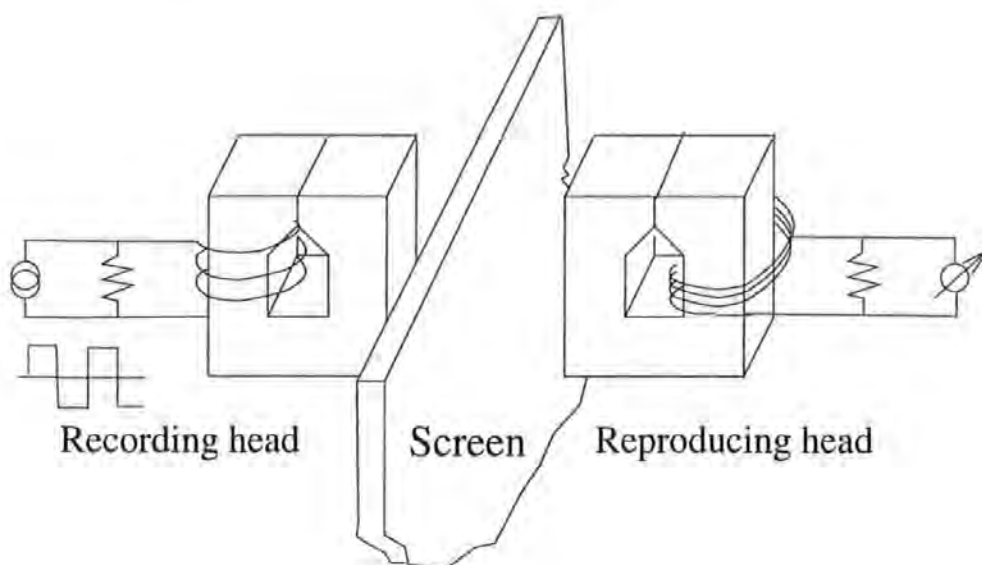


Figure 1.14: Walther's experimental situation in 1964.

crossfeed measurements was carried out with sinusoidal currents. In the experiments copper was used as a conductive screen material, whereas mu-metal and ferrite were employed in the magnetic layers of the screens.

Walther's various experimental screening configurations are shown in Figure 1.15. Without any screening measures, the crossfeed was +35 dB above the normal reading level at a tape speed of 150 inch/sec. The effect of the magnetic flux diffusing through the screens was determined by placing a full screen between the transducer heads (Figure 1.15(a)). The assumption that the leakage flux was the most serious part of the crossfeed was justified by this impractical arrangement. This conclusion was emphasized by the increase of the crossfeed voltage when the full screen was reduced to a half-plane ending at the surface of contact between the head and the tape, as shown in Figure 1.15(b). A conducting screen of 1 mm total thickness was shown to have this source of crossfeed of +23dB above the normal reading level and when a combination of electric and magnetic screens was employed, the crossfeed was reduced to +7.4 dB. In many applications the internal screens could be completed by screens at the back of the tape, as shown in Figure 1.15(c), giving further

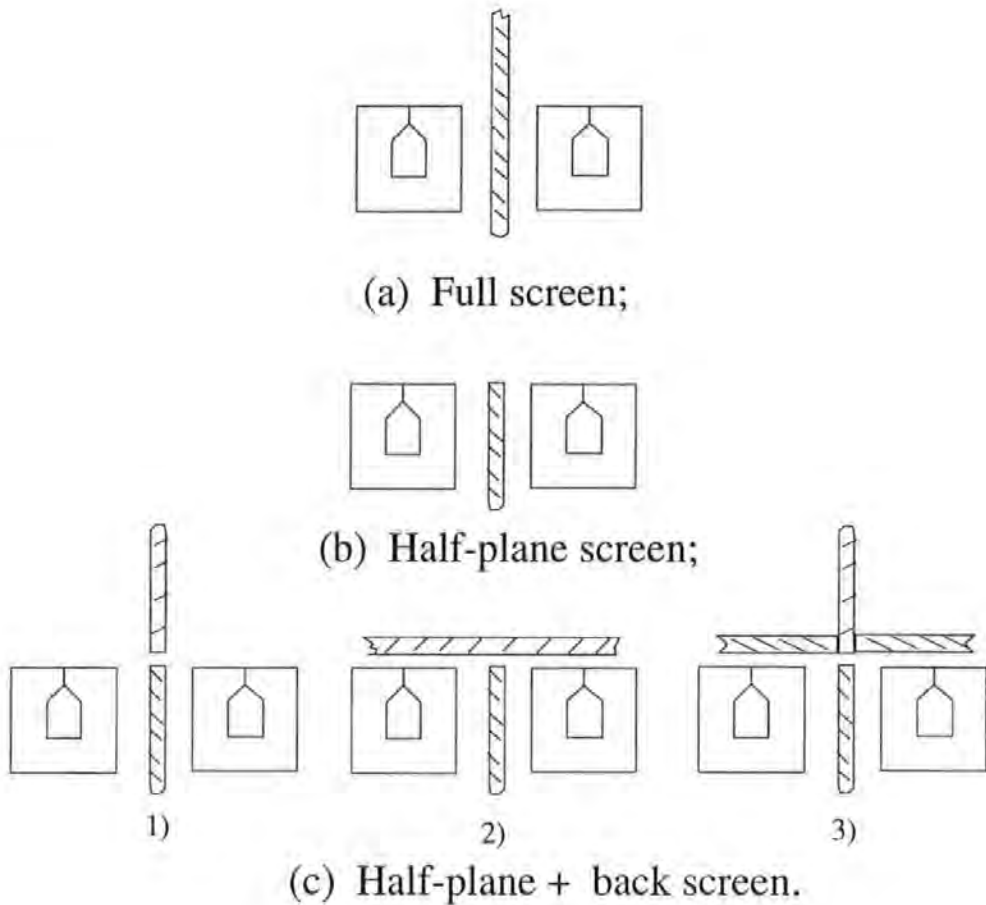


Figure 1.15: Different screening configurations by Walther.

reduction of the crossfeed. A useful improvement was also obtained by interconnecting the conducting screens on both sides of the tape, thereby reducing the leakage flux through the gap between the screens, as a result of the flow of induction currents around this gap. Although with the above-mentioned measures the crossfeed could be reduced to an acceptable level, complicated internal and external screens were required, as well as careful adjustment of the screens at the back of the tape. In practical heads screens were sometimes employed with as many as twenty or thirty layers forming an alternating sequence of conducting and magnetic material.

Also in 1964 J.A.Geurst of Philips, carried out a theoretical investigation of crossfeed based on the Cauchy-Riemann relations[15]. Some of Walther's work was

justified by this analytical model. Nevertheless, it may not be safe to assume that three-dimensional effects such as the influence of finite track-width, would not alter the flux line pattern in front of a head structure substantially.

In 1976 H.N. Bertram and J.C. Mallinson, Ampex Corporation, USA, presented a novel theory wherein it was assumed that flux flows only in a skin layer which covers all the surface of the head[16]. The gap regions were treated as magnetic transmission lines. This model was simple enough to be readily applied to the design of heads made from conductive materials. In particular, this theory yielded insights into the the main contributing factors to crossfeed under AC excitation.

In 1976, D.J. Sansom, Data Recording Heads Ltd., England, investigated factors affecting the design and performance of digital recording heads with reference to multi-track write/read heads for use with thin high-coercivity disc media[17]. He took account of the flux leakage paths round each ferrite core to calculate the core efficiency and crosstalk from an adjacent core. Values obtained with cores approximating to this model and for which sufficient data were available, indicated that absolute levels of inductance, write current, peak output and crosstalk were calculable to $\pm 15\%$ accuracy using the techniques described. The above calculation discrepancy was attributed to calculation error because only the leakage of the flux had been taken into account. In the real case the AC bias effect increased the crosstalk by 5 dB over the calculated value described above.

In 1977, A. van Herk, Philips, studied the side fringing field and write and read crosstalk of narrow magnetic recording heads[18]. An analytical expression, based on Lindholm's work, was derived that describes the response of a magnetic read head of finite width to a magnetized track of finite width shifted in the lateral direction. With this expression the side fringing field and the crosstalk from adjacent tracks were calculated.

In 1984, K.Tanaka, Mitsubishi Corporation, Japan, measured the crosstalk in

the recording process and the playback process in multihead digital tape recorder applications[19]. It was concluded that the limitation of track density in multitrack digital recording is determined by intertrack crosstalk. That is to say, signal-to-noise ratio (SNR) was proportional to the square root of the track width and inversely proportional to the second power of linear density. This relationship meant that increasing the track density would degrade the SNR of the playback signal less than increasing linear density.

Figure 1.16 shows the schematic shape and arrangement of the cores in a head in Tanaka's work. Only four are shown, but more could be possible in practice, together with dummy cores on either side. Coils were wound on the back bars connecting them to the pole pieces. A symmetric design is presented here. The crosstalk level was calculated when each core dimension of the head was changed individually. It was clear from the calculation results that crosstalk could be improved greatly with a change in the guard space, the inclination of the top core, the gap depth, or the core width. The guard space cannot be changed because it changes the recorded track format. In manufacturing the head, the core width may easily be changed. The gap depth should be as small as possible under the consideration of adequate durability. In summary, a reduction of the area of the cores facing one another reduced the crosstalk without reducing the efficiency of the head.

In Tanaka's work, the SNR could be further improved by electrical cancellation of the crosstalk signal. An improvement by about 15-20 dB was possible with a very simple circuit, as shown in Figure 1.17.

In 1992, J.M. Coutellier, et al, Laboratoire Central de Recherches, Cedex, France[20], realized a $32(\text{data}) \times 12(\text{selection}) = 384$ track fixed recording head, as shown in Figure 1.18, constructed with the ability to record a very large number of parallel tracks on a magnetic tape. A conventional addressing technique was used to multiplex the recording process. Each head was located at the crossing of two coils, the row wire being used to feed the data to be recorded, and the column wire to select the desired

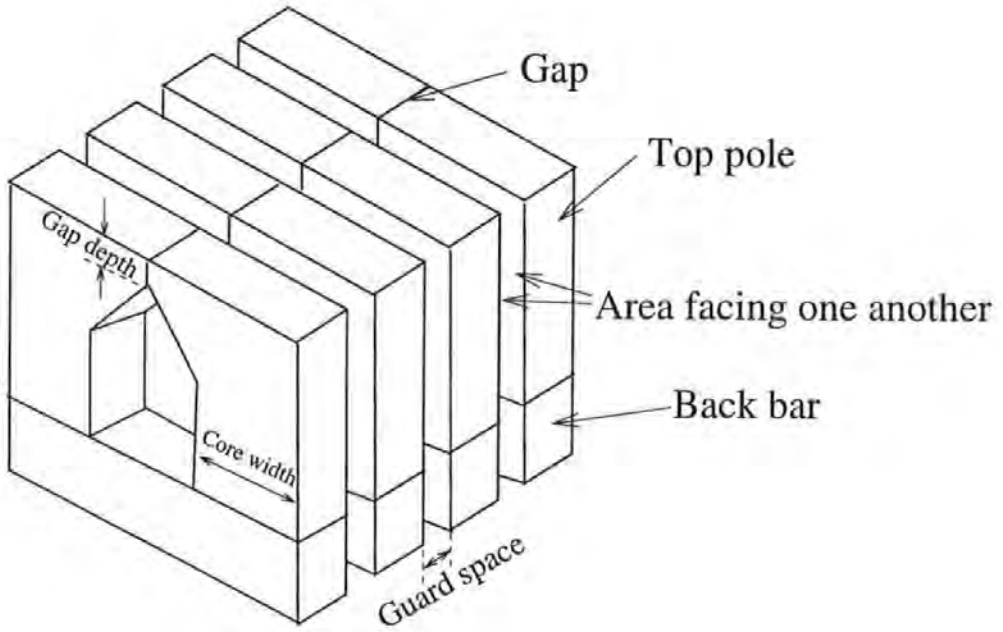


Figure 1.16: Schematic arrangement of the cores in a head in Tanaka's work.

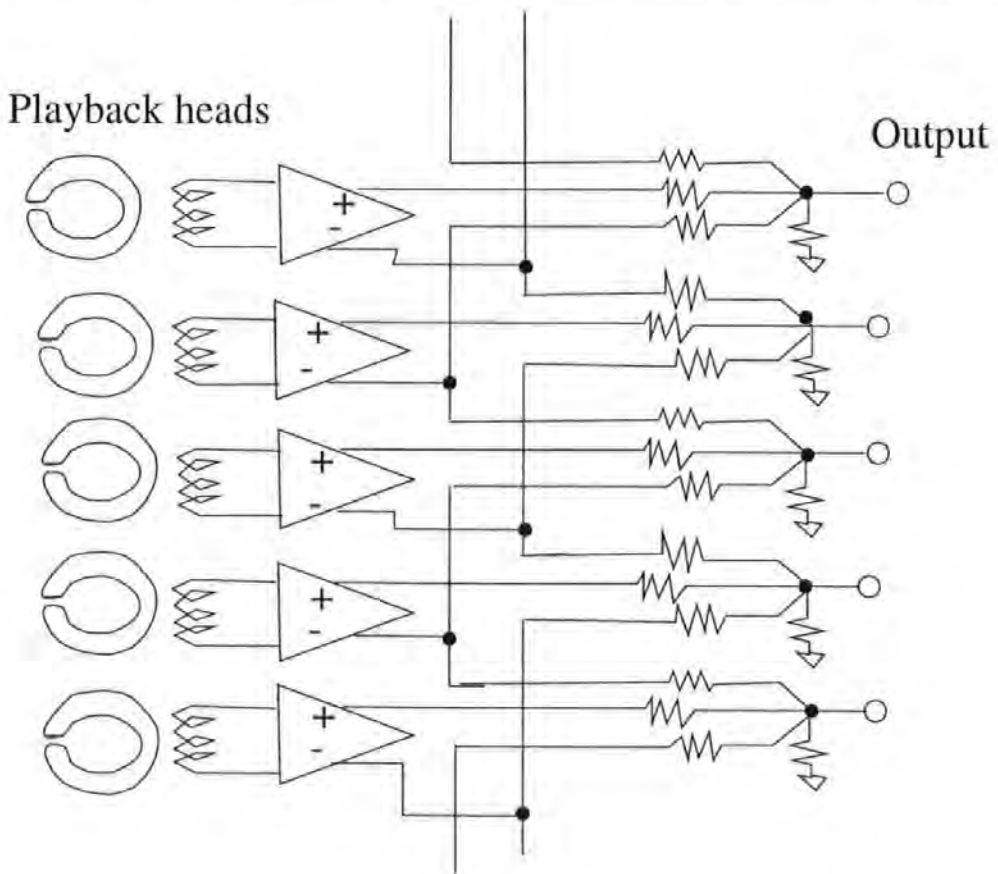


Figure 1.17: Circuit diagram of the crosstalk canceller in Tanaka's work.

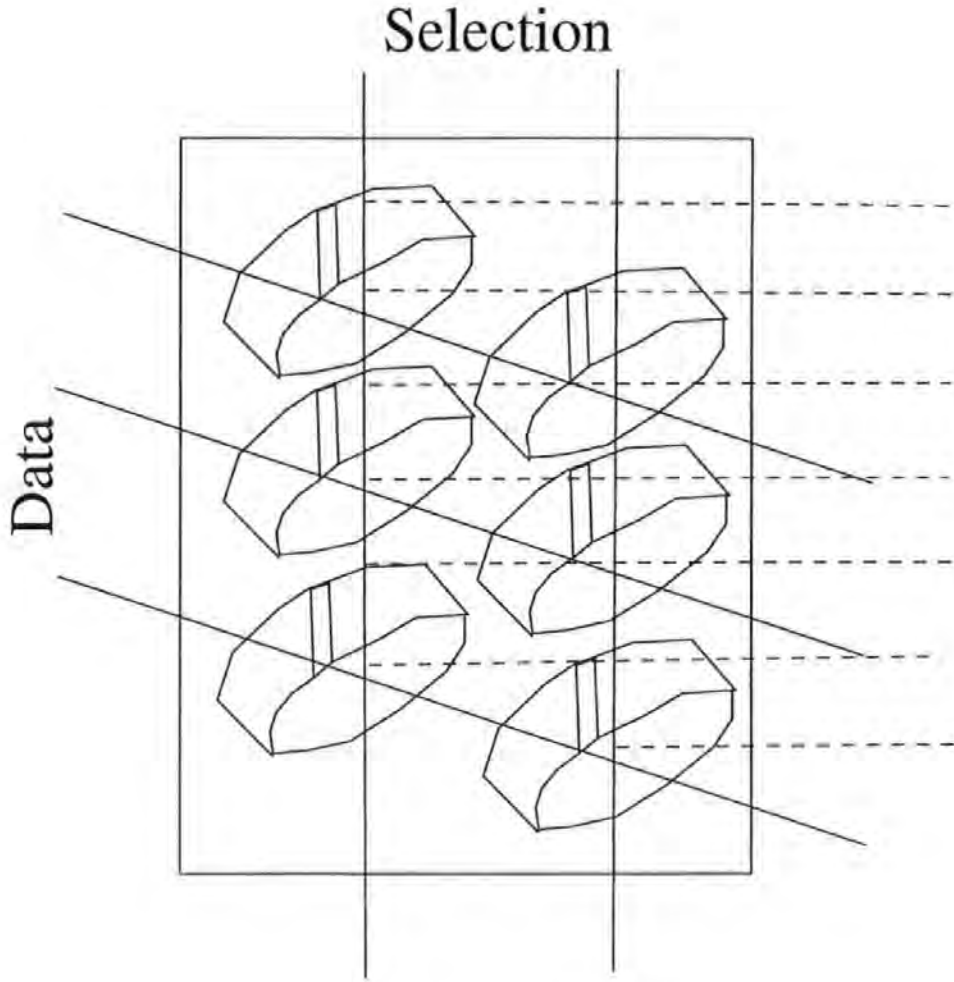


Figure 1.18: Recording gap layout of a 384 track fixed recording head in Coutellier's work.

elements. Multiplex-induced crosstalk was analyzed and was measured in the worst case to be below -23 dB, attributing to the grooved ferrite wafer structure. A raw bit error rate of 10^{-5} was measured for the complete channel, including a new readout component.

In 1996, Y. Murata, et al, Mitsubishi Corporation, Japan[21], developed a simple design method to analyze the crosstalk using the 3D Finite Element Method (FEM). In previous crosstalk theory, separating the erase head and the R/W head by the nonmagnetic layer was the main method to reduce crosstalk. However, this

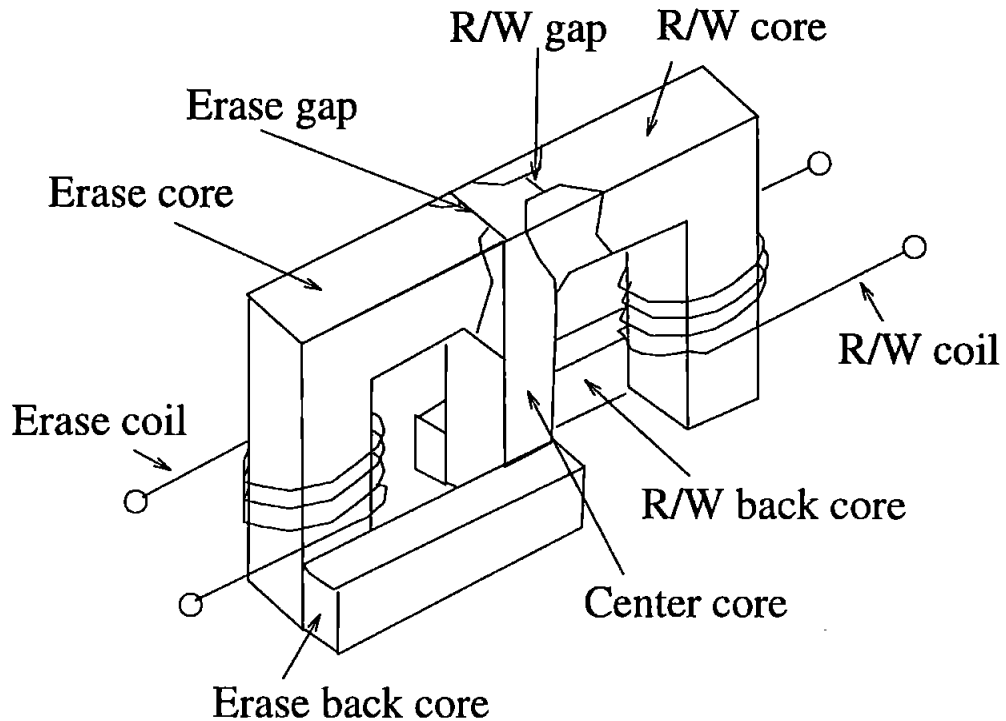


Figure 1.19: Structure of the 4 MB FDD head in Murata's work.

method reduced R/W efficiencies because the cross-sectional area of the center core was reduced. Murata, et al, found that there were two flux paths contributing to the crosstalk in the write/read process: one was the path through the ferrite cores, and another was the path once fringing through air and re-entering into the R/W core. By balancing the fluxes through those two paths, it was possible to realize both high efficiency and low crosstalk simultaneously. Murata's head assembly, as shown in Figure 1.19, was adopted for 4 MB flexible disk drives.

In 1998 J.J.M. Ruigrok, et al, Philips[3], developed an advanced tape storage system named DigaMaxTM. It was a new multitrack tape system which offered high storage capacity and high, variable data rates. It could reach up to 13 GB (uncompressed) on 300 m (1000 ft) of 8 mm wide 72 kA/m (900 Oe) tape using a track pitch of 37.5 μm and a minimum bit length of 0.35 μm . Eight-channel thin-film data heads, as shown in Figure 1.20, enabled data rates of 0.5-2 MB/s at a tape speed of

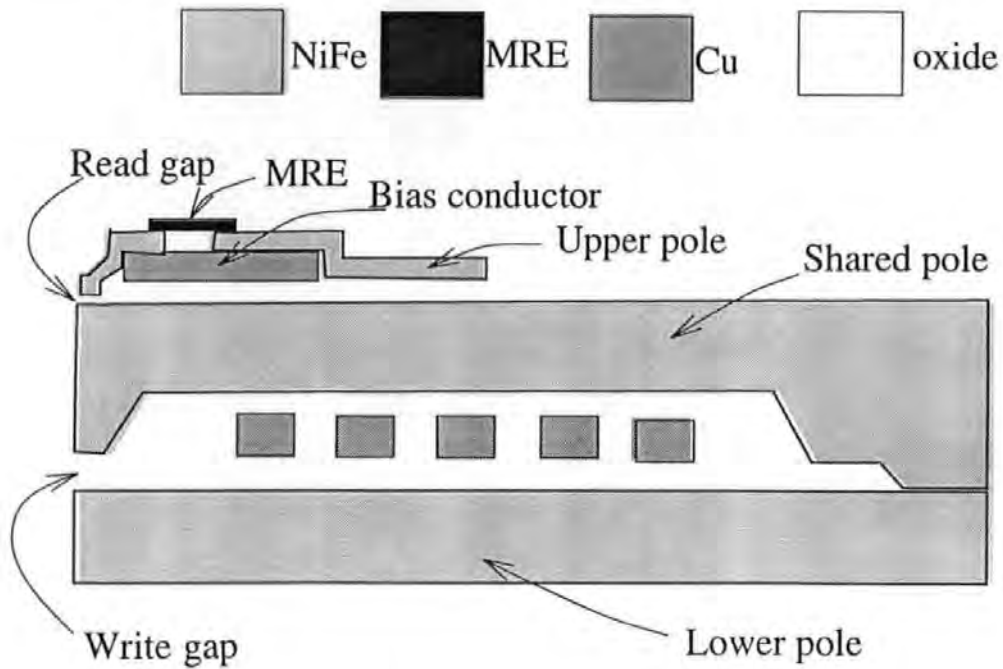


Figure 1.20: Cross-section of the read/write head in Ruigrok's work.

0.28-1.12 m/s (11-44 inch/s). These characteristics enabled, for example, real-time storage and play-back of 7 hours of high quality JPEG 2 video.

The eight-channel data head in Ruigrok's work, as shown in Figure 1.20, consisted of a yoke-type MagnetoResistive (MR) read head on top of a write head. Reading of the long wavelength servo signals by the data read head was possible by the use of yoke-type read heads. Shielded heads would have difficulty in detecting the servo tracks, since these heads are relatively insensitive to long wavelengths. The flux guides and the MR element were made of NiFe. The bottom writer flux guide had a width of $3\ \mu\text{m}$, while the reader was $24\ \mu\text{m}$ wide. Write and read gaps were $1.3\ \mu\text{m}$ and $0.25\ \mu\text{m}$, respectively. The relatively low number of windings on the data write head led to a very compact write head with a calculated efficiency better than 80%. Planarization steps made it possible to position the MR read head on top of the data write head. This enabled a reduction of the thickness of the separation oxide between the MR element and the reader flux guides from 0.6 to 0.3

μm , since the contacts to the MR element were no longer in between the MR element and the flux guides. Compared to earlier designs, the efficiency of the read heads was improved from 11 to 19 % by the reduction of the separation oxide thickness in combination with a reduction in die distance between the MR element and the tape bearing surface. This improvement in efficiency together with the absence of barber poles and a reduction of the MR element height and thickness led to a sensitivity improvement of a factor of 6. The improved sensitivity and small gap length of the DigaMaxTM read heads facilitated the detection of bit lengths as small as $0.35 \mu\text{m}$ in 72 kA/m tape. The gap field of the write head should have steep gradients on both sides of the gap to keep the transition length well below the minimum length of $0.35 \mu\text{m}$ for both directions of tape. Secondly, the data tracks should only be written in the surface part of the magnetic coating, leaving the bulk of these tracks unaffected. For this reason a current with an amplitude of 32 mA was applied to the 5-turn data write head. This small current induced a field that is optimum in recording of the smallest bits ($0.35 \mu\text{m}$) and was smaller than the coercive field of the tape at distances larger than $0.2 \mu\text{m}$.

1.7 Motivation

Traditionally, write-read crossfeed has been reduced in conventional heads by a variety of screening methods, but the effectiveness of these methods is very limited. On the other hand, the early theoretical investigations of the crossfeed problem, concentrating on the flux line pattern in front of a head structure based on a simplified model, may not be comprehensive. Today a growing number of magnetic recording equipment manufacturers employ thin-film technology to fabricate magnetic recording heads[1]. There are many advantages to this approach, with perhaps the most important being the ability to produce extremely narrow pole tips and recording gap widths in the thin-film process[22]. As a result, the size of the modern head is much smaller than that in the past. These narrow pole tips, in turn, permit the density of magnetic recording to be increased. In addition, employing magnetoresistive replay

heads is becoming more and more popular and this brings a tenfold increase in areal density[1]. Furthermore, keepered media has appeared as a potential technique with smoother transition, quieter replay and anti-thermal stability[23][24]. The increasing use of thin-film metallic magnetic materials for heads, along with the appearance of other new technologies, such as the MR reproductive mode and keepered media, has stimulated an increased understanding of the crossfeed problem by advanced analysis methods and a satisfactory practical solution to achieve the RWW operation.

The work described in this thesis to suppress the crossfeed field involves both a novel reproductive mode of Dual Magnetostrictive (DMR)[25][26] heads, which was originally designed to gain a large reproduce sensitivity at high linear recording densities exceeding 100 kFCI, playing the key role in suppressing the crossfeed, and several other compensation schemes, giving further suppression. Analytical and numerical methods of estimating crossfeed in single and multitrack thin-film/M-R heads under both DC and AC excitations can often help a head designer understand how the crossfeed field spreads and therefore how to suppress the crossfeed field from the standpoint of an overall head configuration. This work also assesses the scale of the crossfeed problem by making measurements on current and improved heads, thereby adapting the main contributors to crossfeed. Much of this work has either already been published or has been submitted for publication [27][28][29][30][31][32][33][34]. There have also been five conference presentations of the work.

1.8 Outline of This Work

This thesis will cover:

- Magnetostatics (Chapter 2)
- Magnetodynamics (Chapter 3)
- Experimental Assessment of Heads (Chapter 4)
- Conclusions (Chapter 5)

Chapter 2

Magnetostatics

2.1 Introduction

Chapter 2 describes an investigation of Read-While-Write (RWW) operation by magnetostatic analysis. Neither medium motion nor eddy current effects caused by conductive materials are considered in this chapter: it is presumed that all time scales are long compared to these phenomena. Time enters only through the constant head-to-medium relative speed, v , so that all temporal information is transformed immediately into the fundamental spatial recording process by $x=vt$ or $dx/dt=v$. The purpose of this chapter is to provide useful relations for the determination of crossfeed fields, both from traditional analytical models and modern Finite Element Method (FEM) models. In magnetic recording the track width is generally large with respect to dimensions in the nominal recording plane, which includes the head-to-tape motion direction and the direction perpendicular to the medium surface (thickness direction). Therefore, two-dimensional crossfeed field expressions are useful and will be given explicitly in Section 2.3. In two dimensions the analytical model acquires a particular simple form based on the arctangent and logarithm functions. Analysis of three-dimensional crossfeed fields, including using the 3D FEM, will be discussed in subsequent sections where it will be possible to consider more detailed contributors to crossfeed fields and various screening schemes for the reduction of these fields.

Thus, the framework will be provided for the determination of crossfeed fields in the case of single track (Section 2.3) and multiple track (Section 2.4) and contributions from different shielding schemes and different reproducing modes (Section 2.6 ~ 2.13). In particular, a novel dual-magneto-resistive (DMR) reproducing mode will be addressed in detail in Section 2.2. For direct correspondence with the magneto-resistive reproducing output the simple volume integral over the elements can be utilized.

2.2 Concepts of MR and DMR

Throughout this thesis two reproducing modes are considered : the traditional SAL (Soft Adjacent Layer) reproducing mode and the DMR (Dual-Magneto-Resistive) reproducing mode.

Ferromagnetic materials exhibit a variety of phenomena associated with changes in resistivity due to change of the state of magnetization. A magnetic field can rotate the direction of magnetization. The most useful effect is the anisotropic change in resistivity as the magnetization direction of a saturated specimen is rotated with respect to the direction of an applied current. Field sensors using the anisotropic MR effect can be fabricated into extremely small devices using thin film technology. The most common material utilized in MR transducers is the alloy NiFe with $\Delta\rho/\rho \sim 2\%$ and $\rho \sim 20 \mu\text{ohm-cm}$ for thin films with thicknesses $t \sim 200 \text{ \AA}$. At a composition near (81 %Ni, 19 %Fe), permalloy is nonmagnetostrictive and possesses a sufficiently low crystalline anisotropy and high saturation magnetization to yield a high intrinsic permeability.

The magnetoresistance effect was first utilized as an extremely efficient playback transducer in magnetic recording in 1975[1]. In the basic MR process a current is applied to a thin film along its long direction. As shown in Figure 2.1, an adjacent film, experiencing a field due to the sense current in the MR sensor, is used to bias

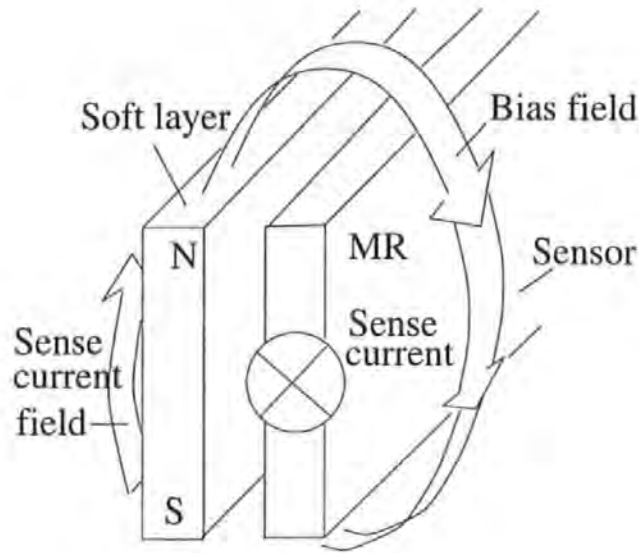


Figure 2.1: SAL (Soft Adjacent Layer) scheme.

the magnetization to a quiescent condition of optimum sensitivity and minimum distortion. For single domain operation, additional layers of 'exchange tabs' are often used to stabilize the film magnetization and define the active sensing width. Shield layers are often placed on either side of the element to enhance the spatial resolution.

A 2-terminal DMR head consists of two nominally identical, adjacent magnetoresistive stripes separated by a dielectric spacer (e.g. SiO_2 or Al_2O_3) in the active region but shorted at both ends (the contact regions underneath the leads and off-track wing regions) by conducting tabs (e.g. Au, but this might be replaced by a conducting permanent magnet or an exchange-coupled material) between the MR stripes. It is designed to combine simple fabrication with a large intrinsic sensitivity at high linear density[25][26].

In the DMR head[25][26], the magnetizations of the individual stripes are biased to a semi-saturation state by the sense current passing through the opposite stripe, as shown in Figure 2.2(a). This means that the magnetizations scissor from their nominal parallel position, one is at -45° , the other is at $+45^\circ$. The nominal parallel

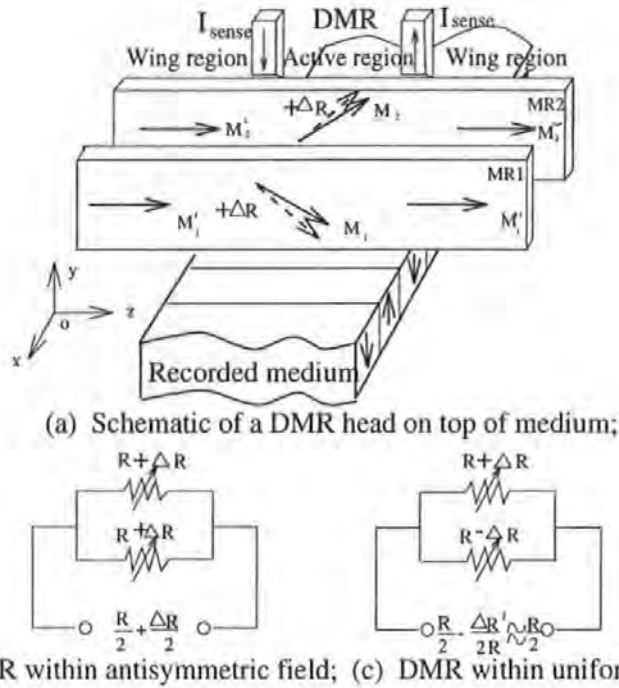


Figure 2.2: Schematic of a Dual MagnetoResistive head. DMR is a typical 2-terminal element because the two MR stripes are shorted at both ends.

magnetization configuration without sense current flowing is caused by permanent magnet tabs (e.g. Co alloy) or exchange-coupled tabs (e.g. FeMn or TbCo) placed in the contact regions and wing regions to control the magnetization orientation, thus avoiding multidomain formation within the soft films[7][10][8]. The DMR head is a typical 2-terminal element because the two MR stripes are shorted at both ends. In other words, these two MR stripes are connected in parallel electrically. In Figure 2.2 (a) and (b), the two MR stripes are exposed to the anti-symmetric field from a recorded bit and thus the DMR head produces an output(each of these two MR stripes within an anti-symmetric field has a resistance change with same change polarity). In Figure 2.2 (c), the two MR stripes are exposed to an uniform applied field and thus the DMR head produces almost null output(one MR stripe has a resistance increase, the other has a resistance decrease and they almost cancel each other with a parallel connection). In this regard, the DMR head is sensitive only to the spatially anti-symmetric component of the applied field. Most impor-

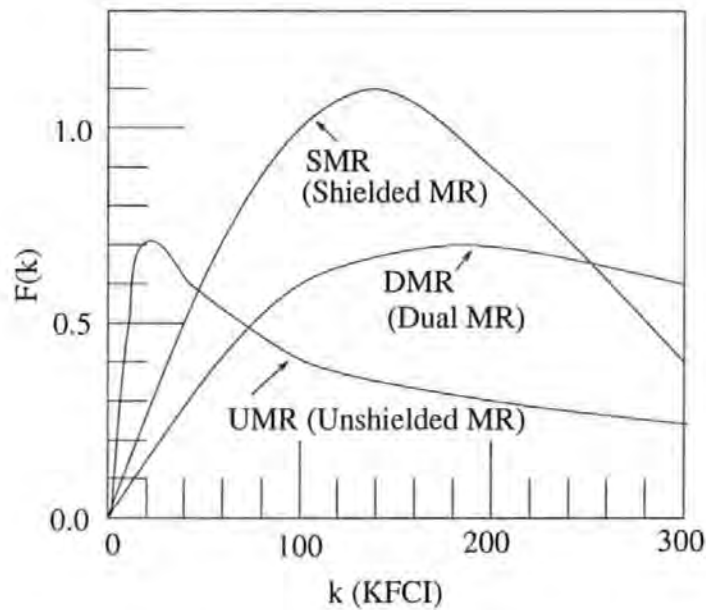


Figure 2.3: Normalized spectral response function, $F(k)$, for the UMR(Unshielded MR), SMR(Shielded MR) and DMR(Dual MR). The DMR has been shown to provide a large reproduce sensitivity at high linear recording densities exceeding 100 kFCI[25][26].

tantly, as shown in Figure 2.3, this DMR head promises excellent resolution when reading the high field gradients from extremely sharp magnetization transitions, e.g. those in good perpendicular media, due to the small separation of the elements in the device. These features are important for overcoming the limitations of present recording heads and achieving the high spatial resolution necessary for an ultra-high density perpendicular magnetic recording system. In this thesis, we will explore the possibility of crossfeed suppression by the DMR concept.

2.3 2D Analytical Model

Modeling plays an important role in the early phases of design. Head design, for example, focusing on fine detail, requires sophisticated programs that may be too slow for the needs of most users. For those interested in quickly seeing the

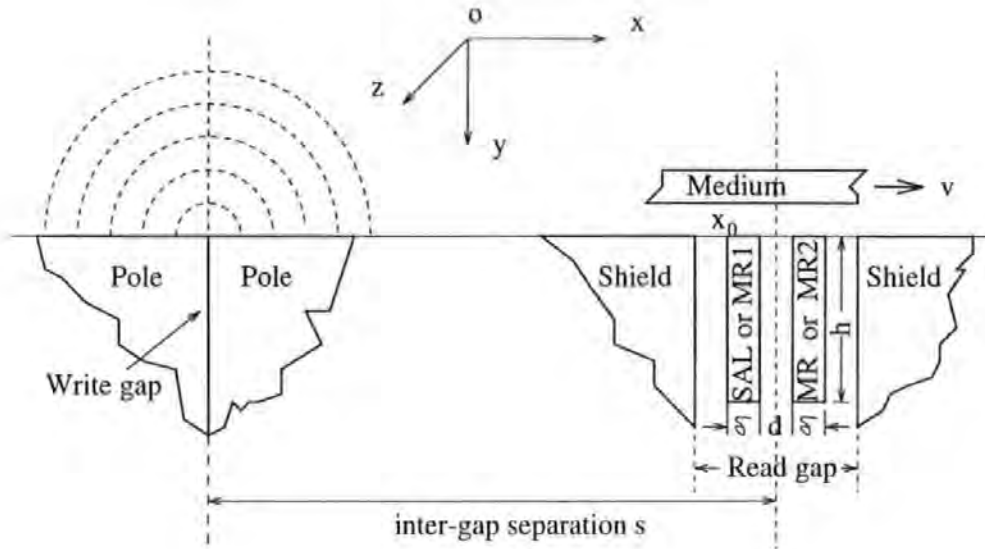


Figure 2.4: Idealized model of a RWW head. Two replay modes will be considered: the SAL mode (SAL and MR) and the DMR mode (MR1 and MR2).

consequences of design iteration, simplified analytical models are a welcome alternative. The simplified analytical models discussed in this section and the next section incorporate the essential details of the read and write processes while remaining computationally tractable[28][29].

The mathematical model is illustrated by Figure 2.4 which presents a cross-section perpendicular to the front face of the head structure and parallel to the direction of the medium motion indicated by an arrow. The recording field considered here is the component of the external field existing perpendicular to the direction of medium motion over an infinitesimal gap between pole pieces of infinite permeability[35]. Figure 2.4 shows the medium motion and gap direction referred to x, y coordinates existing parallel to the medium motion and perpendicular to the head-medium contact plane, respectively. The field (H) in SI units produced at a distance (R) from the gap by a recording current (i) in the winding of n turns around the head pole is given by

$$H(t) = \frac{1}{\pi} \frac{ni(t)}{R} \quad (2.1)$$

The component of this field parallel to the MR stripe depth is

$$H_y(t) = \frac{1}{\pi} \frac{ni(t)x}{x^2 + y^2} \quad (2.2)$$

The reproducing MR stripes will be sensitive to the H_y component only, due to a strong demagnetization effect through the film thickness direction. Two parallel soft magnetic stripes in read gap configuration have been used in the figure. As stated in Section 2.1, we will consider two replay cases: the SAL case and the DMR case. In the SAL case, the right stripe is assumed to be NiFe material for the MR sensor while the left stripe is assumed to be CoZrNb material for bias purposes. In the DMR case, both stripes are assumed to be NiFe material for the two MR sensors. The MR track width w is $22.9 \mu\text{m}$. The MR stripe thickness δ is 500 \AA . The thicknesses of the dielectric layers are 1000 \AA , 500 \AA and 1000 \AA , respectively. The inter-shield separation ($0.35 \mu\text{m}$) governs the linear resolution of readback processes in the SAL case whereas the inter-stripe separation ($0.05 \mu\text{m}$) governs that in the DMR case. The MR stripe depth h is $2.5 \mu\text{m}$. The inter-gap separation is denoted by s .

A rectangular-shaped thin-film magnetoresistor in a single domain state can be analysed by considering the various magnetic energy components that exist in the film. If an applied field is made up of a constant component, H_b , and a much smaller variable component, H_y , then, for a sense current I and initial resistance R_0 an output voltage e_j (1st order approximation, $j=1,2$) of a single MR stripe can be obtained by integrating over the device dimensions, i.e.

$$e_j = 2IR_0 \frac{\Delta\rho}{\rho_0} \frac{H_b}{[H_k + N_y M_s]^2} \int \int \int H_y(x, y, z) \frac{dx}{\delta} \frac{dy}{h} \frac{dz}{w} \quad (2.3)$$

Using the y component of the head field gives

$$e_j(t) \propto \frac{ni(t)}{\pi} \frac{1}{\delta h} \int \arctan\left(\frac{h}{x}\right) dx \quad (2.4)$$

$$= \frac{ni(t)}{\pi} \frac{1}{\delta h} \left[x \arctan\left(\frac{h}{x}\right) + \frac{h}{2} \ln\left(1 + \frac{x^2}{h^2}\right) \right]_{x_0}^{x_0+\delta} = f(x_0) \quad (2.5)$$

In the SAL case, we can simply take the volume integral over the right stripe as the crossfeed noise of the MR head, i.e.

$$\text{Crossfeed}_{\text{SAL}} \propto f\left(s + \frac{d}{2} + \delta\right) \quad (2.6)$$

However, in the DMR case we should subtract the integral over the left stripe from that over the right one then divide it by 2 as the approximate crossfeed response of the DMR head because of the parallel connection between the two magnetoresistive stripes in the DMR head, i.e.

$$\text{Crossfeed}_{\text{DMR}} \propto f\left(s - \frac{d}{2} - \delta\right) - f\left(s + \frac{d}{2} + \delta\right) \quad (2.7)$$

In order to evaluate fairly the proportion of the crossfeed within the effective signal, we define a Signal-Crossfeed-Ratio (SCR) as below:

$$\text{SCR} = 20 \log \frac{\text{Signal}}{\text{Crossfeed}} (\text{dB}) \quad (2.8)$$

The derivation of the reproducing head signal in the presence of a typical medium can be simply done by using the reciprocity principle[25][26]. The properties of the medium which go into the calculation are listed below: transition excitation $M_r t_m = 2.8 \text{ memu/cm}^2$ (remanent magnetization $M_r = 400 \text{ emu/cc}$, medium thickness $t_m = 0.07 \text{ } \mu\text{m}$), single step-functional transition without transition length, the head-medium spacing is $0.03 \text{ } \mu\text{m}$.

In Figure 2.5, the calculated SCR vs inter-gap-separation characteristics are depicted[36][37]. SCR increases as the gap-center separation increases. For efficient use of the available storage space a short distance between the head gaps is required, as mentioned in Section 1.3. Therefore, both heads must be fabricated on the same substrate. In the conventional combined head, the recording head is stacked on the playback head or vice versa. This stacking of heads results in poor mechanical

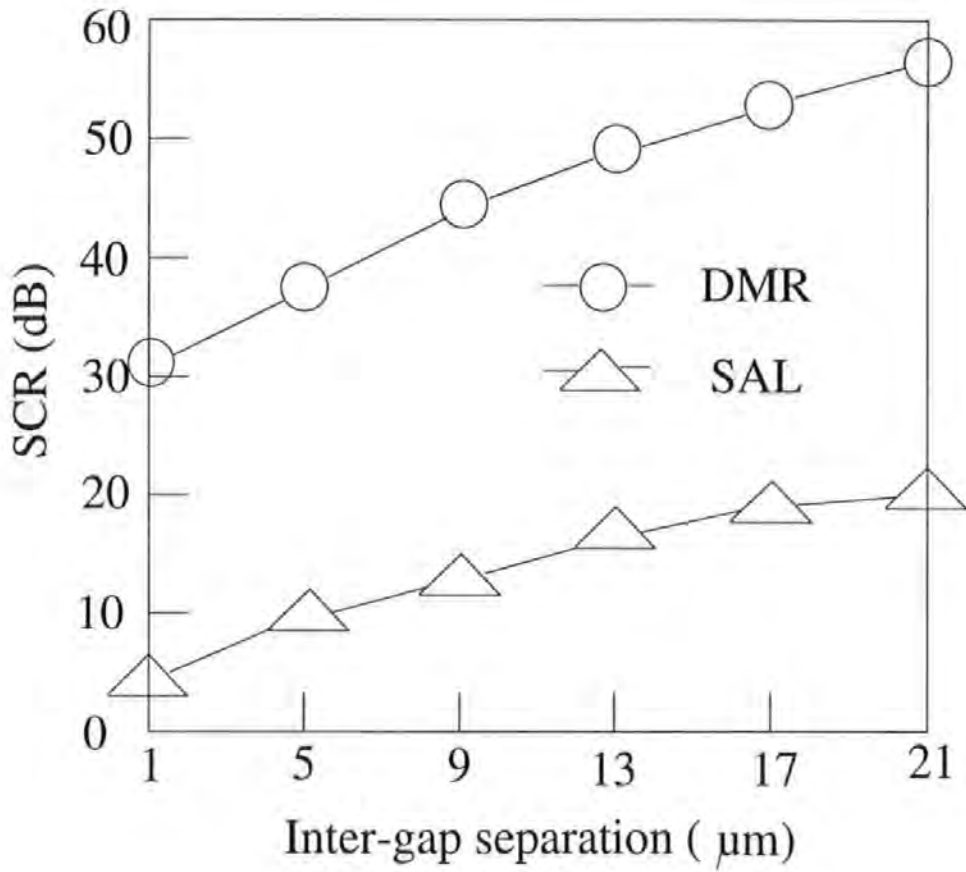


Figure 2.5: SCR-inter-gap-separation characteristics of RWW heads.

integrity because increasing the number and thickness of the layers increases the total stress. Furthermore, these stacking processes are very time-consuming and can degrade the properties of the MR element. An additional benefit from close write-to-read gap separation is fewer off-track errors due to the slope of the tape (and azimuth alignment of the head) as it passes over the head. In conclusion, it is found that the DMR reproducing method is very effective in reducing the crossfeed.

As shown in Figure 2.5, the SCR in the DMR design is generally 4-5 times higher than that in the SAL reproducing design. Such a high SCR in the DMR design is because the leakage flux from the medium goes upward in the right stripe and returns downward in the left stripe. This constitutes a closed magnetic circuit. Each MR stripe has a resistance change with same change polarity. Such anti-parallel field components will cause a signal output in the DMR head. In contrast, when considering crossfeed radiation from the write head, the field disturbance accepted by the two MR stripes is almost the same because these two stripes are located very close to each other with respect to the write gap. As a result, one MR stripe has a resistance increase, and the other has a resistance decrease. Obviously in the DMR case the output signals from these two stripes will cancel each other, as shown in Figure 2.2, thus causing an almost null final output.

2.4 3D Analytical Model: Multi-track Case

The work in this section involves the investigation of a range of important parameters related to noise-rejection and their optimisation to achieve a significant advance in the RWW performance of multi-track heads suitable for high data rates[29]. In the case of multi-track RWW heads, the individual crossfeed signals from different locations should be considered for a particular gap in the read array.

The analytical model, including three R/W channels, is illustrated by Figure 2.6. In this case, there needs to be a 3-dimensional system constructed to position

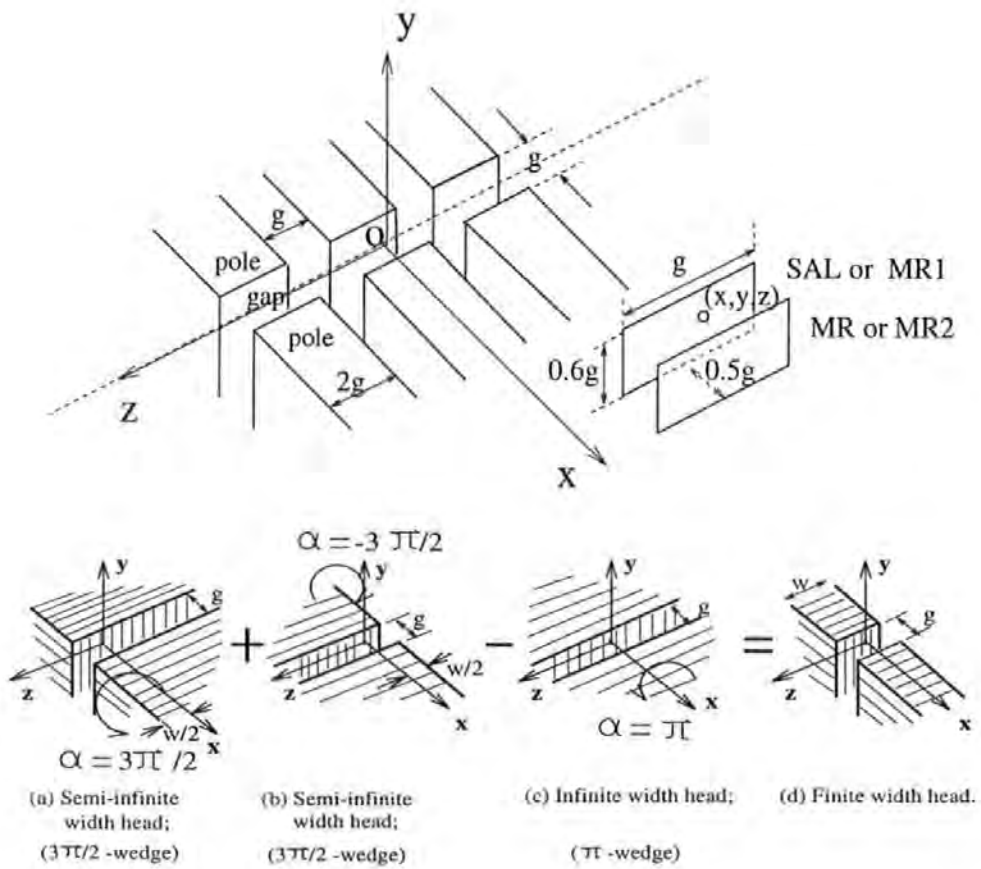


Figure 2.6: The higher: Idealized 3D model of a multi-track Read-While-Write (RWW) head. The recording gap length g is used as a size unit. Two replay modes will be considered: the SAL mode (SAL and MR) and the DMR mode (MR1 and MR2); The lower: Superposition of wedges to obtain finite gap, finite width head[38]. The excessive part should be removed by subtracting out a π -wedge (2d infinite track width Karlqvist head).

the heads accurately so that the individual crossfeed signals from different locations can be detected and summed. The x , y and z coordinates exist along the medium motion direction, perpendicular to the head-medium contact plane and along the trackwidth direction, respectively. The origin of the coordinate system is located in the center of the middle recording gap. The recording gap length is referred to g , which is used as the unit for all dimensions. An ultra-dense design is assumed here: the recording trackwidth is $2g$; the separation between recording poles is g . Two parallel soft magnetic stripes in read gap configuration have been used in the figure. As stated in Section 2.2, we will consider two replay cases: the SAL case and the DMR case. In the SAL case, the rear stripe MR is assumed to be NiFe material for the MR sensor while the front stripe is assumed to be CoZrNb material for bias purposes. In the DMR case both stripes, denoted by MR1 and MR2 respectively, are assumed to be NiFe material for the two MR sensors. The MR track width is g ; the MR stripe thickness is $0.2g$; the MR stripe depth is $0.6g$; the thickness of each dielectric layer is $0.5g$, which governs the linear resolution of readback processes in the DMR case. The spatial center of the two boundaries on the ABS (Air Bearing Surface) or TBS (Tape Bearing Surface) of the MR stripes is denoted by the coordinate (x, y, z) .

Closed form field solutions by Lindholm[38] are used for single finite gap heads with finite track width. In this method, several special cases are generated when the exterior angle α of the wedge[38] is a multiple of $\pi/2$, i.e. $\alpha = n \cdot (\pi/2)$. The multiple n will be used conveniently as a subscript to distinguish the different solutions to follow. When $n = 2$, the exterior angle is 180° and the geometry of this π -wedge is that of Karlqvist's 2-dimensional head. When $n = 3$, the exterior angle is 270° and the geometry of this $3\pi/2$ -wedge is that of a semi-infinite width head. The center-track head with finite track width as shown in Figure 2.6 is obtained by the superposition, also as shown in Figure 2.6, of π -wedge (Karlqvist's expression H_2), $3\pi/2$ -wedge (H_3) and another $3\pi/2$ -wedge (H'_3) with the field given by[38]

$$H = H_3(x, y, z - w/2) + H'_3(x, y, z + w/2) - H_2(x, y, z) \quad (2.9)$$

where the write head width $w = 2g$. This formula just represents the center-track write head. Contributions from end-track heads should also be summed.

As for the device used in the 2D analytical model, the magnetization is 45° biased in the rectangular-shaped thin-film magnetoresistor in a single domain state. Nevertheless, the 3-dimensional reproducing MR stripes will be sensitive to both the H_y and H_z components. H_x does not contribute to the output due to a strong demagnetization effect through the film thickness direction x . Considering the worst case, an approximate crossfeed response e_j ($j=1,2$) of a single MR stripe can be obtained by integrating over the device dimensions, i.e.

$$e_j \propto \left| \int \int \int H_y(x, y, z) dx dy dz \right| + \left| \int \int \int H_z(x, y, z) dx dy dz \right|. \quad (2.10)$$

To simplify the problem, we assume that the source magnetic flux in the MR films is from the ABS(TBS)-near boundaries and the injected flux into the MR films is uniform in the z direction.

In the SAL case, we can simply take the volume integral over the rear stripe as the crossfeed response. However in the DMR case, to get the crossfeed response, we should subtract the integral over the front stripe from that over the rear one and then divide it by two because of the parallel connection between the two stripes.

A convenient way to visualize the crossfeed response is by means of the perspective views, Figure 2.7 and Figure 2.8. Figure 2.7 depicts the calculated crossfeed response (absolute value) in arbitrary units of a SAL-MR head while 3 write heads are in operation simultaneously vs the MR head location (x, y, z) . Figure 2.8 is the similar case of Dual-MR. In the above cases, $y=0$ and x and z range from $-5g$ to $+5g$. It is noted that a series of peaks with different heights (due to superposition) are localized near the edge-ends of each write gap and the tallest peaks in the SAL-MR case are twice as tall as the tallest ones in the DMR case. Note that a central band

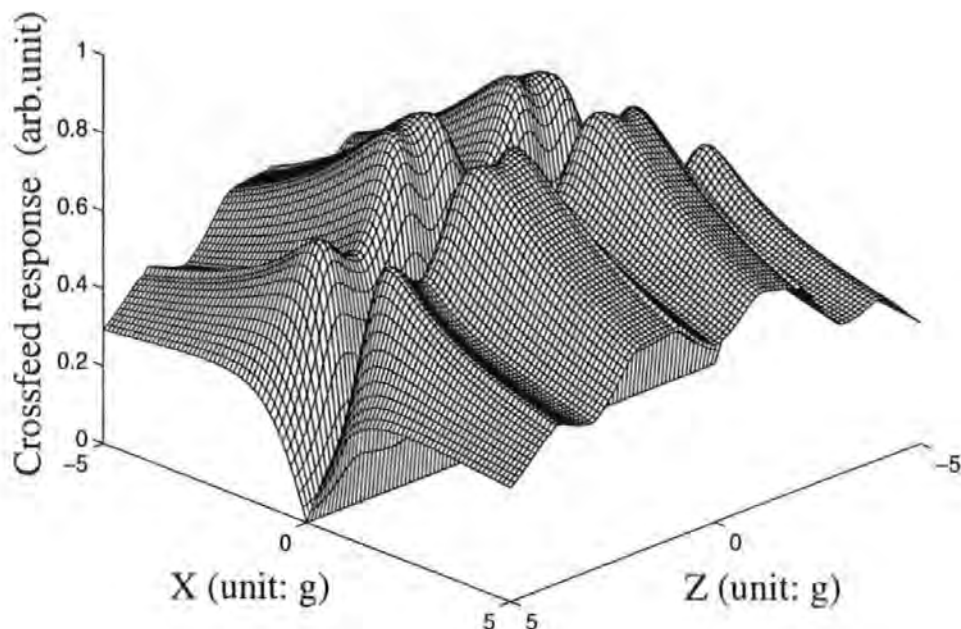


Figure 2.7: The calculated crossfeed response in arbitrary units of a SAL-MR head while 3 write heads are in operation simultaneously vs the MR head location (x,y,z) . In this case, $y=0$ and x and z range from $-5g$ to $+5g$.

around $-2.5g \leq x \leq +2.5g$ is a fictitious region because the MR heads cannot exist in this band, occupied by the write head array. The region of interest is beyond this band.

By cutting the views of Figure 2.7 and Figure 2.8 along certain planes, most of the information about the crossfeed noise response can be obtained. First, slicing parallel to the x -axis at a given z produces a plot of noise versus x with z as a parameter ($z=-3g, 0, +3g$), which shows the behavior of the noise as the track is traversed. Second, slicing parallel to the z -axis at a given x produces a plot of noise versus z with x as a parameter ($x \leq -2.5g$ or $x \geq +2.5g$), which shows the behavior of the noise as the trackwidth is traversed. Third, slicing parallel to the xz -plane at different noise levels produces contour plots of these noise levels in that plane.

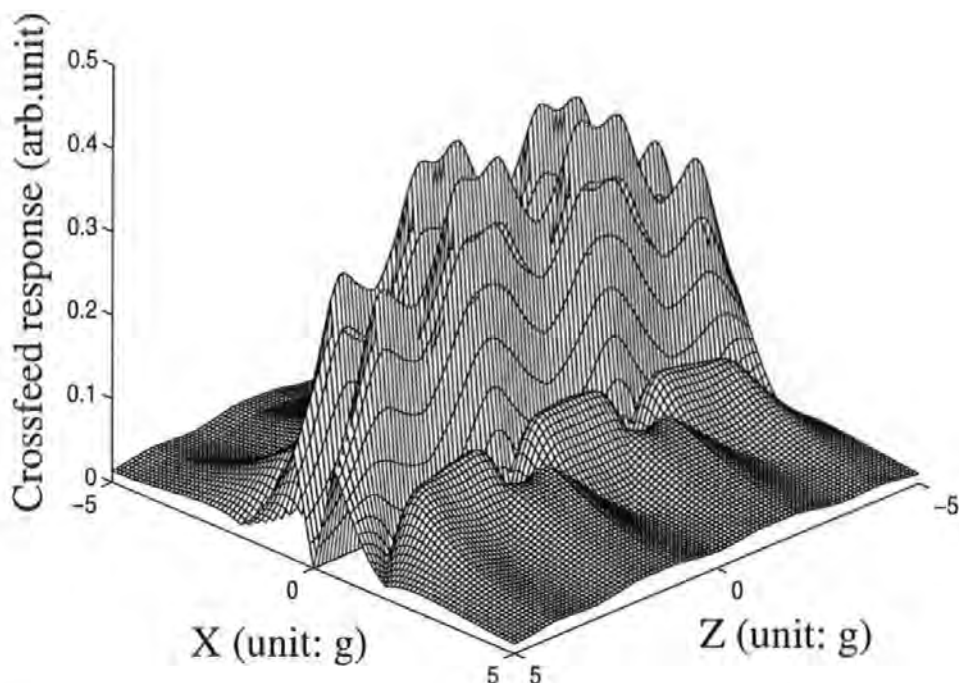


Figure 2.8: The calculated crossfeed response, in the same units as Figure 2.7, of a Dual-MR head while 3 write heads are in operation simultaneously vs the MR head location (x,y,z) . In this case, $y=0$ and x and z range from $-5g$ to $+5g$.

By studying Figure 2.7 and Figure 2.8 along these various cuts, the following conclusions can be drawn:

1. As shown in Figure 2.9, the crossfeed noise response decreases as the write-read-gap-center separation increases. For efficient use of the available storage space a short distance between the head gaps is required. An additional benefit from close write-to-read gap separation is fewer off-track errors due to the slope of the tape (and azimuth alignment of the head) as it passes over the head.
2. It is found that, as shown in Figure 2.9, the crossfeed noise in a DMR head

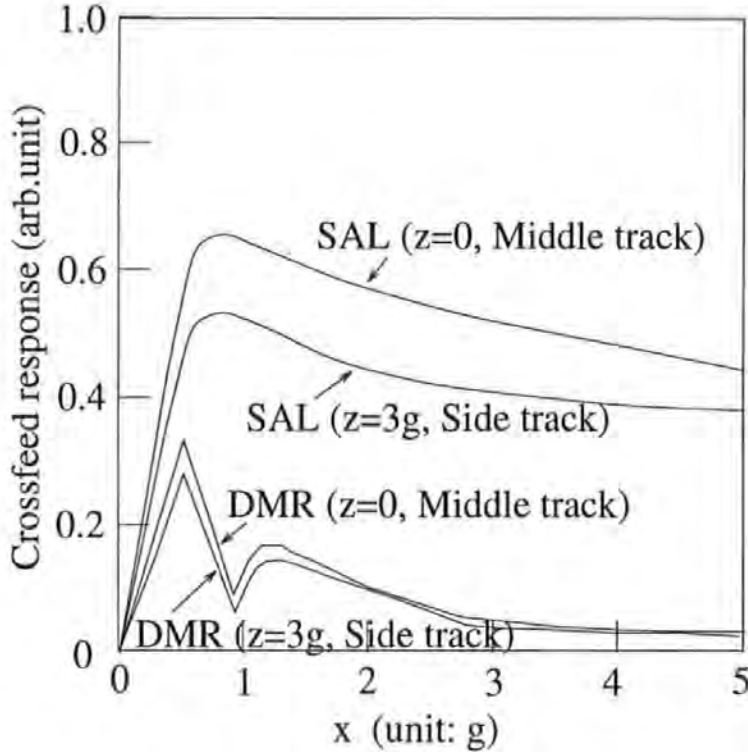


Figure 2.9: Crossfeed response 2D slices of Figure 2.7 and Figure 2.8. Three write heads are operative simultaneously.

decreases much more sharply than that in a SAL-MR head as the separation increases. For example, the crossfeed noise at a typical point ($x=\pm 4g$, $z=0$) in the DMR design is only 4.5% of that at the same point in the SAL. Such good crossfeed-noise-rejection in the DMR design is because the field disturbance accepted by the two MR stripes is almost the same since these two stripes are located very close to each other with respect to the write gap. As a result, one MR stripe has a resistance increase, and the other has a resistance decrease. Obviously in the DMR case the output signals from these two stripes will cancel each other due to the electrical parallel connection, thus causing an almost null final output.

3. A series of crossfeed response peaks with different heights, existing near the edge-ends of each write gap as mentioned above, leave their long tails far away from the write gap along the track direction. As a result, shown in Figure 2.10,

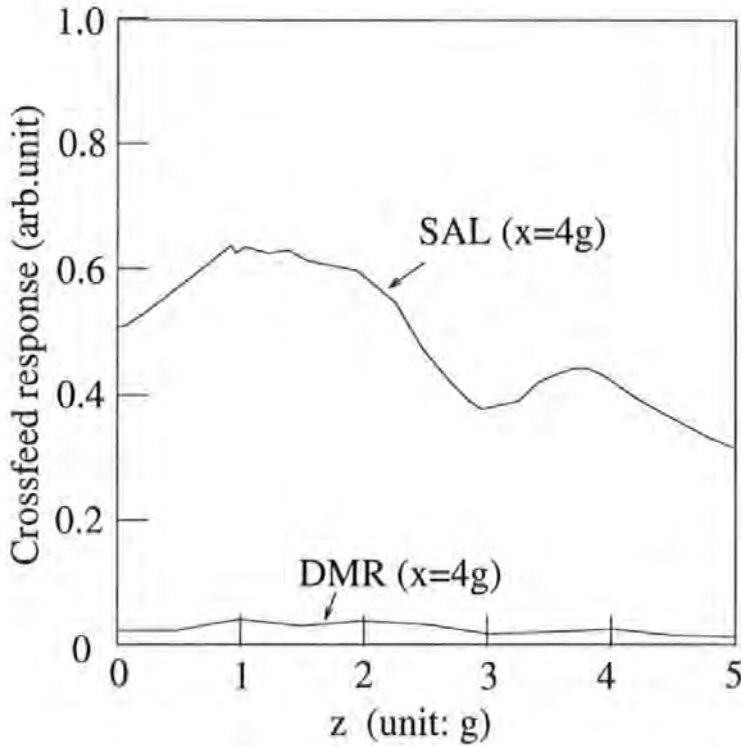


Figure 2.10: Crossfeed response 2D slices of Figure 2.7 and Figure 2.8. Three write heads are operative simultaneously.

the trackwidth-transverse direction is found to be very important with an array of read heads. The end-tracks have different crossfeed responses from the center-track. In the SAL-MR case, the center-track crossfeed response at $(x=\pm 4g, z=0)$ is 22.1% stronger than the end-track response at $(x=\pm 4g, z=\pm 3g)$. In the Dual-MR case, the center-track crossfeed response at $(x=\pm 4g, z=0)$ is just 3.2% stronger than the end-track response at $(x=\pm 4g, z=\pm 3g)$.

2.5 3D Finite Element Methodology (FEM)

OPERA-3d (an OPERating environment for Electromagnetic Research and Analysis) is the pre and post-processing system for well known electromagnetics analysis programs including TOSCA, ELEKTRA and VF/GFUN. The programs were developed at the Rutherford Appleton Laboratory in England. It represents the results of many years research, development and application experience.

The TOSCA 3-D Nonlinear Magnetic Field Simulation Package[39] (supplied by Vector Field Corp.) was used to study the crossfeed problem[31]. TOSCA can be used to compute magnetic or electrostatic fields including the effects of nonlinear media, in three dimensions. The program incorporates state of the art algorithms for the calculation of electromagnetic fields, advanced finite element and non-linear equation numerical analysis procedures.

Finite element discretization forms the basis of the methods used in these analysis programs[40]. This widely applicable technique for the solution of partial differential equations requires special enhancements to make it applicable to electromagnetic field calculations. Access to these features in TOSCA is supported by the OPERA-3d Pre-processor which provides facilities for the creation of finite element models, specification of complicated conductor geometry, definition of material characteristics including for example, non-linear and anisotropic descriptions and graphical displays for examination of the data. Similarly, the OPERA-3d post-processor provides facilities necessary for calculating electromagnetic fields. As well as displaying field quantities as graphs and contour maps, the OPERA-3d post-processor can calculate and display many derived quantities and can plot particle trajectories through the calculated fields.

The key steps in setting up a finite element model in TOSCA are now briefly discussed.

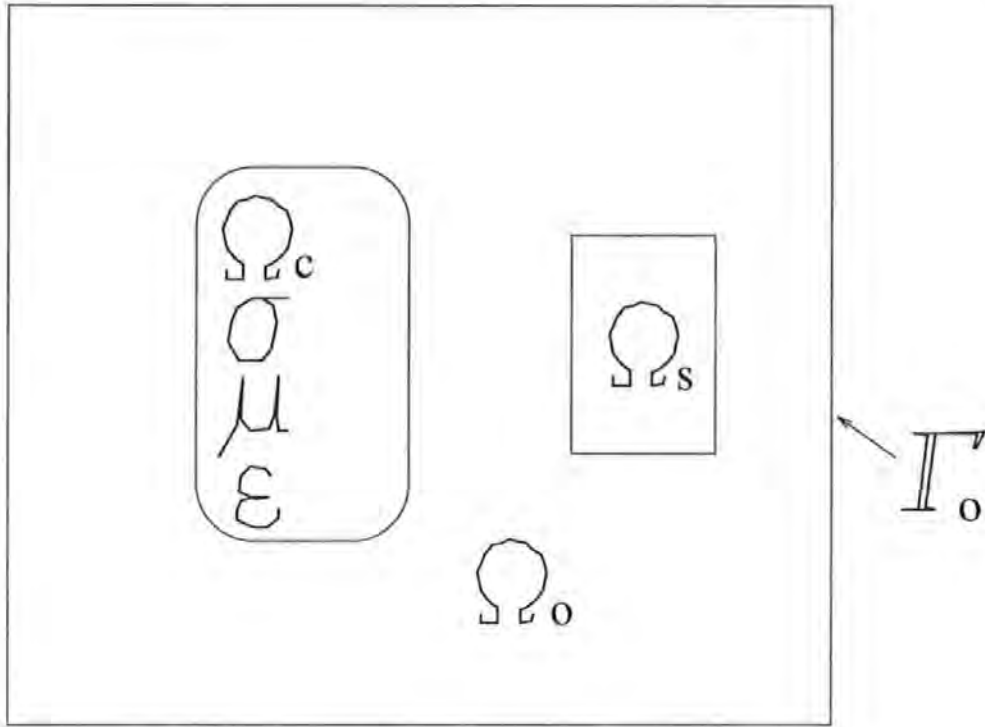


Figure 2.11: Regions of model space.

2.5.1 Model Space

Generally speaking, a typical model can be divided into a number of regions, each having particular physical characteristics, as illustrated in Figure 2.11.

- Ω_c - These are regions having non-zero conductivity σ , permeability μ and dielectric coefficient ϵ . Such regions would include ferromagnetic materials, eddy current regions and permanent magnets.
- Ω_s - These are regions contain field sources i.e. current carrying coils.
- Ω_o - Often the above regions are surrounded by air i.e. free space.
- Γ_o - For numerical modelling, the problem must be bounded. A suitable distant boundary is required to the problem.

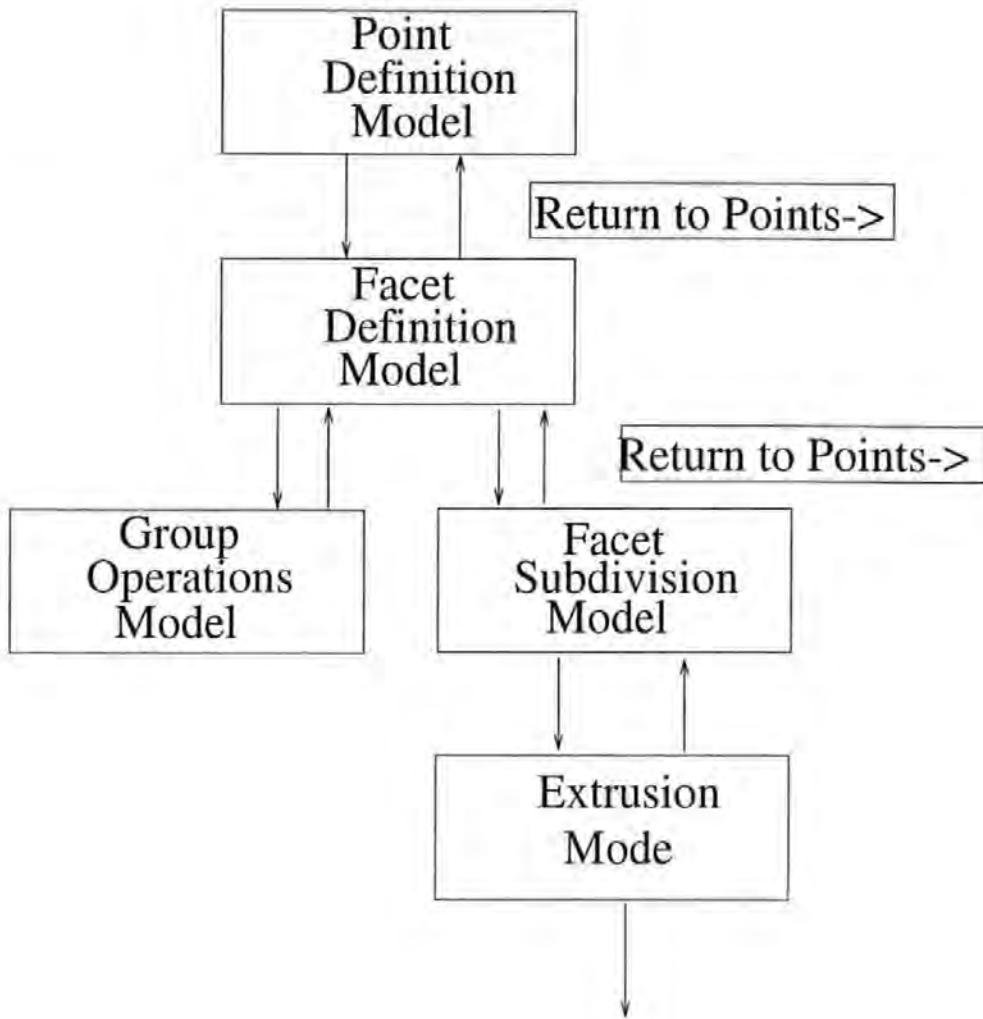


Figure 2.12: Moving between modes in the Pre-Processor.

2.5.2 Mesh Generation and Discretisation Strategy

The mesh generation stage is illustrated in Figure 2.12, showing the convenient method of defining a problem by the TOSCA 3D Pre-Processor. Each region of a model is divided into elements. The elements fit together to form a mesh. The solution potential is then calculated at each node in the mesh.

One of the advantages of TOSCA is that the finite element mesh does not have

to fit the shape of the coils. However it is important that the coil fields are accurately represented by the finite elements at the interface between reduced and total potential. The approach to distribute the elements to get best accuracy is

- Concentrate elements in the areas of interest
- Use quadratic elements in the areas of interest
- Use quadratic elements where field gradients are large
- Use sufficient elements to model the variation of permeability

A useful check may be made on the shape of the volumes in the Preprocessor to label the distorted elements, such as intersecting faces, mid-side points too close to corners, excessive curvature or distortion, too small volumes and negative volumes, etc.

2.5.3 Topology of the Potential Space

The magnetic steel should be total potential and the air containing the conductive coil should be reduced potential. The rest of the air should be total potential. Neither the reduced potential nor the vector potential should be surrounded by a total potential region completely with a net circulating loop, otherwise it violates the Ampere's law because the contour integral within the total potential region is non-zero. If a continuous magnetic "ring" exists, such a multiple connected problem can be overcome in two ways:

- Implied "cuts" with a discontinuity of potential in total potential regions. If the problem has a symmetry plane, a new boundary condition is needed such that difference in potential is equal to the enclosed current.
- Real "cuts" in total potential regions. If no symmetry exists, make a small reduced potential region cutting total potential but avoid the region of interest.

2.5.4 Magnetostatic Analysis

In the magnetostatic case, the magnetic field intensity \vec{H} and the flux density \vec{B} are required within the problem space.

By the electrostatic formulation, a magnetic scalar potential ψ is introduced such that:

$$\vec{H} = -\text{grad}\psi \quad (2.11)$$

where ψ is now the m.m.f.(magnetomotive force) and is called the (total) scalar potential.

In two dimensions the above equation reduces to

$$\vec{H}_x = -\frac{\partial\psi}{\partial x} \quad (2.12)$$

$$\vec{H}_y = -\frac{\partial\psi}{\partial y} \quad (2.13)$$

The permeability, μ , of a magnetic material is defined by the relationship:

$$\vec{B} = \mu\vec{H} \quad (2.14)$$

Here, μ may be field dependent giving a non-linear relationship between \vec{B} and \vec{H} . In case that \vec{B} and \vec{H} are not along the same direction, μ is a tensor with 9 components.

The formulation 2.11 relies on there being no source currents present, $I_s = 0$,

and Ampere's law can be written:

$$\text{rot}\vec{H} = \text{rot}(\text{grad}\psi) = I_s \equiv 0 \quad (2.15)$$

2.5.5 Source Currents in Three Dimensions

If a 3-D region contains source current density, I_s , then it is still possible to use a scalar potential approach. This relies on the current having a known value and distribution, i.e. there are predefined source currents.

A method of solving this problem is to partition the field into two parts. These parts relate to the magnetic field intensity due to sources, \vec{H}_s , and that due to material magnetization, \vec{H}_m :

$$\vec{H} = \vec{H}_s + \vec{H}_m \quad (2.16)$$

For a known source, the magnetic field intensity, due to that source, \vec{H}_s is known (from the Biot-Savart law). For a volume Ω containing currents, the field is given by

$$\vec{H}_s = \int_{\Omega} \frac{\vec{I} \times \vec{r}}{r^3} d\Omega \quad (2.17)$$

It is still necessary to determine \vec{H}_m . In a similar way to the total potential technique, since $\text{rot}\vec{H} = I_s = 0$, a scalar potential can be defined as

$$\vec{H}_m = -\text{grad}\phi \quad (2.18)$$

where ϕ is known as the (reduced) scalar potential.

This gives an expression for the total field of

$$\vec{H} = \vec{H}_s - \text{grad}\phi \quad (2.19)$$

This shows that finding ϕ (and knowing \vec{H}_s) allows the determination of \vec{H} and \vec{B} .

2.5.6 Boundary Conditions

The boundary conditions are an essential part of the mathematical model. The choice of conditions may significantly affect the solution obtained.

The boundary condition options available are:

- Set the potential, ϕ , on boundary to a specific value.

Setting $\phi = \text{constant}$ implies magnetic flux is normal to the boundary.

This is equivalent to setting: 'Normal Magnetic'(Dirichlet).

- Set the derivative of potential to a value.

Setting $\partial \phi / \partial n = \text{constant}$ implies magnetic flux is tangential to the boundary.

This is equivalent to setting: 'Tangential Magnetic'(Neumann).

- Note: If no condition is specified, 'Tangential Magnetic' is applied (default Neumann boundary condition).

2.5.7 Material Properties

TOSCA uses material characteristics to relate flux density and field intensity of all materials (except for air). These must be defined with the OPERA-3D Preprocessor and associated with the material names in the model.

- Soft magnetic materials

Characteristics should be defined in the first quadrant, with the first values of B and H both zero. The curve should not extend beyond saturation magnetization;

the program extrapolates correctly with $\partial B / \partial H = \mu_0$.

- Hard magnetic materials

The demagnetization curve in the second quadrant is used. The first value of B should be zero and H the coercive force.

- Permanent magnets

Two pieces of information are necessary to define a permanent magnet: 1. The coercive force. This is the first value of H in a BH curve. For this reason, BH files must be supplied even for linear (constant permeability) analysis. 2. The direction of the coercive force. This is supplied as 3 Euler angles defining the local Z' direction for a volume.

2.5.8 Laminations

Laminated materials can be solved by specifying each lamination or by giving information to enable the program to calculate the effect of the laminations using bulk laminated material properties.

To use laminated material anisotropy the following must be supplied:

1. The packing factor.

This is a number between 0 and 1 and defines the ratio of magnetic material thickness to total lamination thickness e.g. for a 0.049 inch thick plate with 0.01 inch thickness insulation.

If μ_{iron} is the permeability given by the BH data and p is the packing factor, then in directions parallel to the laminations, the program will use

$$\mu = p\mu_{iron} + (1 - p)\mu_0 \quad (2.20)$$

and normal to the laminations

$$\mu = \frac{\mu_0 \mu_{iron}}{p\mu_0 + (1-p)\mu_{iron}} \quad (2.21)$$

2. The direction normal to the plane of the laminations.
3. ANISotropic = LAMInated option must be switched on in the OPERA-3D Pre-processor.

2.5.9 Anisotropy

Different magnetic characteristics may be assigned to each of the local directions associated with each volume.

2.6 RWW Head Designs

The magnetostatic 3D model space containing a Read-While-Write head is considered. Due to symmetry, only half of the structure has been modelled here. Front, side, bottom and 3D perspective views are also shown in Figure 2.13 to Figure 2.16. The maximum element number used in the modelling was 45,000. For a write head, it is assumed that the permeability of the recording medium is the same as that of air and so in the write (crossfeed) process no medium will be taken into account. A default Neumann boundary was used in the model. To get best accuracy, quadratic elements are used around write and read gaps where field gradients are large. Newton-Raphson methods are used to solve the non-linear equations. The maximum number of the iteration is 15 and the convergence tolerance is 0.001.

All the dimensions are taken according to a new generation head TR5 produced by the Read-Rite company[41]. All the poles are 3.0 μm thick, and the throat height is 5 μm . The write head gap is 1.2 μm . The angle of the inclination of

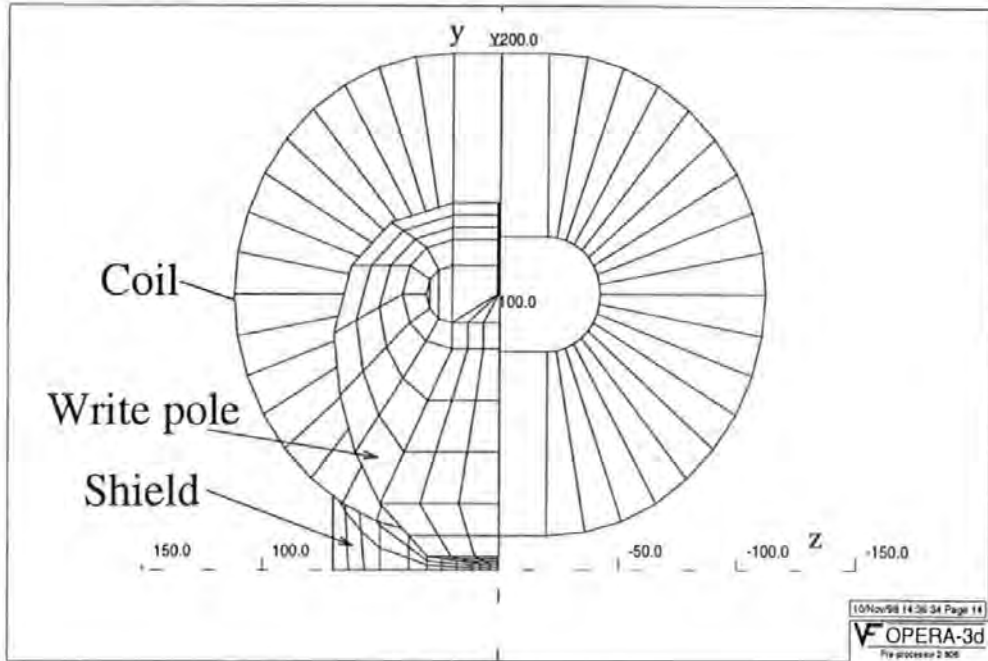


Figure 2.13: Front view with mesh elements. This is an example of the so-called separator design. The geometry and fields exhibit two-fold symmetry and hence only half of the structure, except for the coil, has been modelled here.

the left pole near the zero-throat point is 45° . The pole tip widths of the top pole (write pole), the bottom pole and the shielding pole are $61 \mu\text{m}$, $100 \mu\text{m}$ and $140 \mu\text{m}$, respectively. The top and bottom poles are $10 \mu\text{m}$ apart in the yoke region. Overall they are about $140 \mu\text{m}$ high and $140 \mu\text{m}$ wide. The head coils are assumed to be a single turn and the applied magnetomotive force is 0.60 A-turns. This is approximately equivalent to a write current of 40 mA for a 15-turn coil. In order to allow the head to potentially write the high coercivity (2000 Oersted or 160 kA/m) Metal Particle medium, the pole material is chosen to be a FeN based soft magnetic film with a saturation magnetization of 1.9 Tesla and an initial permeability of 6000.

In this investigation, we will consider two replay cases: the SAL (Soft Adjacent Layer)[1] case and the DMR (Dual-Magneto-Resistive) case. Two parallel soft magnetic stripes in read gap configuration have been used. In the SAL case, the right stripe near the write head is assumed to be NiFe material for the MR sensor while

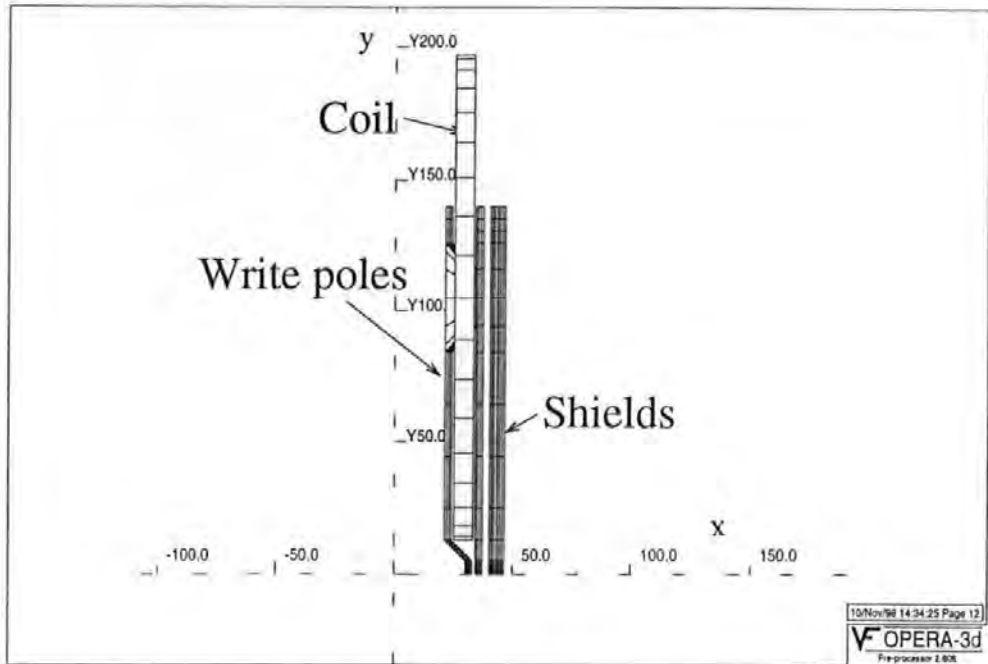


Figure 2.14: Side view with mesh elements. This is an example of the so-called separator design.

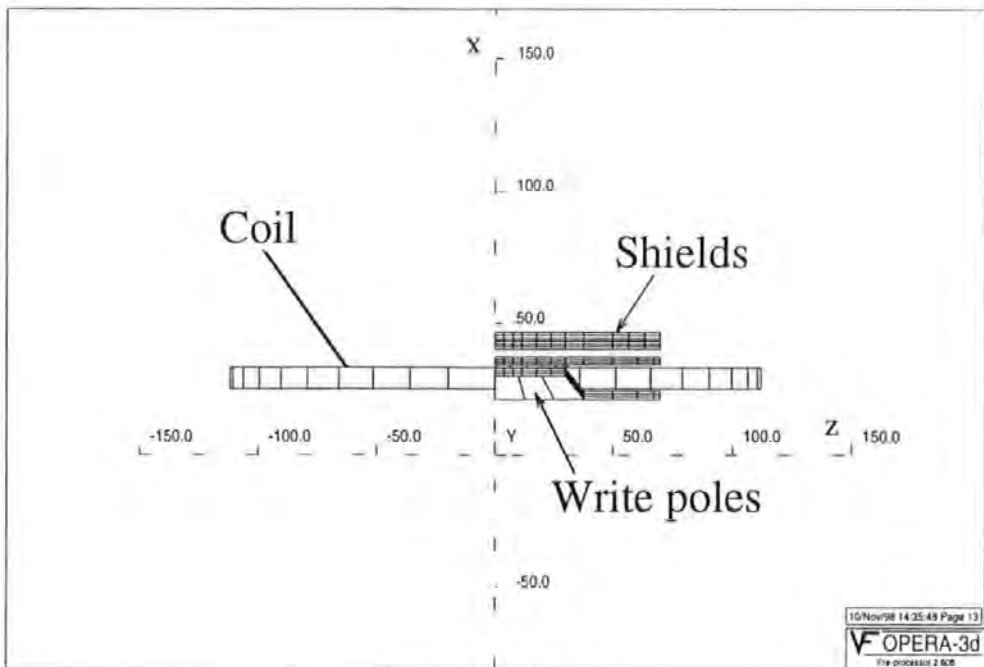


Figure 2.15: Bottom view with mesh elements. This is an example of the so-called separator design.

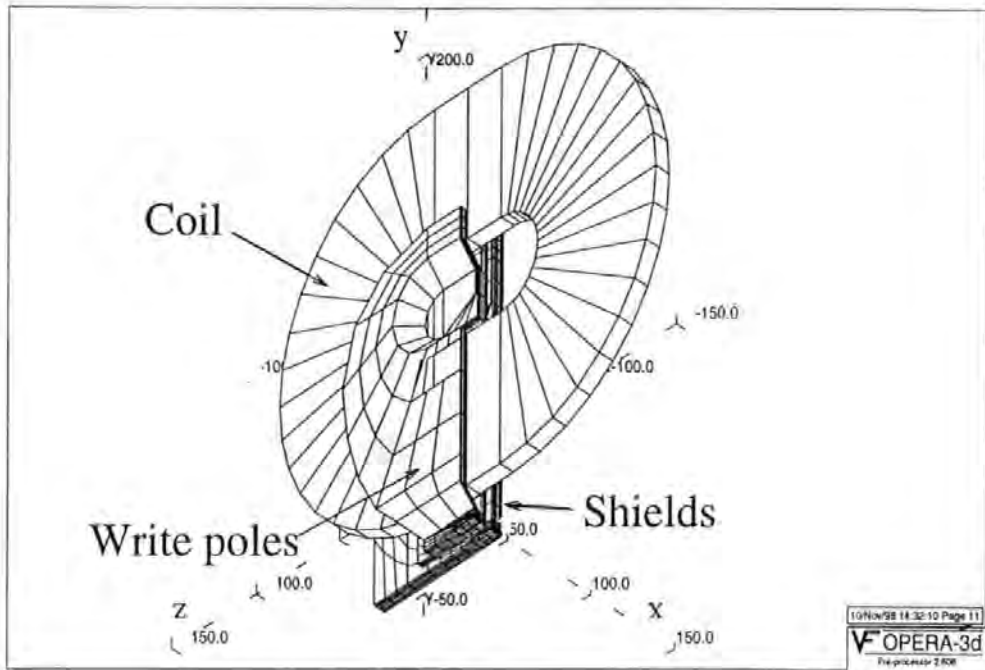


Figure 2.16: 3D perspective view with mesh elements. This is an example of the so-called separator design.

the left stripe is assumed to be CoZrNb material for bias purposes. In the DMR case, both stripes are assumed to be NiFe material for the two MR sensors. The MR track width is $22.9 \mu\text{m}$, less half of the write track width. The MR stripe thickness is 500 \AA . The thicknesses of the dielectric layers are 1000 \AA , 500 \AA and 1000 \AA , respectively. The inter-shield separation ($0.35 \mu\text{m}$) governs the linear resolution of readback processes in the SAL case whereas the inter-stripe separation ($0.05 \mu\text{m}$) governs that in the DMR case. The MR stripe depth is $2.5 \mu\text{m}$.

Three read-while-write tape head designs are considered in this chapter, as described below.

The reference head (conventional merged head design) is shown in Figure 2.17. It is based on a low-cost shared-pole sensor-in-gap head design (Figure 1.2 of Chapter 1). The bottom pole of the write head also simultaneously plays a shielding role for

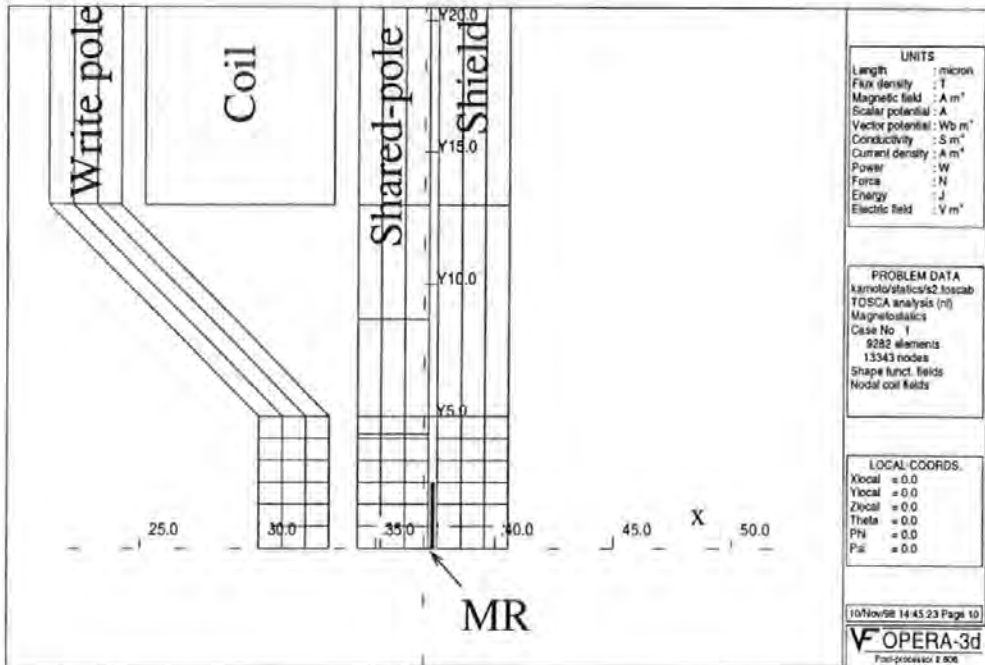


Figure 2.17: The reference shared-pole design.

MR sensor.

In order to eliminate the shared pole between the gaps, a so-called separator design has been proposed as shown in Figure 2.18. This is a slight variation of the reference head by an addition of a $3 \mu\text{m}$ non-magnetic separator between the two head elements. Separating the write element and the read element by a non-magnetic separator enables separate optimisation of write and read elements.

The third design considered in this investigation, called the laminated-separator design, is shown in Figure 2.19. In this case, an additional laminated-separator with $3 \mu\text{m}$ thickness is inserted between the two head elements. A laminated-separator will have not only high magnetic flux transport efficiency but also high mechanical intensity. It was hypothesized that the recording field would be confined to the left side of this laminated-separator. Laminated materials can be specified by the packing factor and the direction normal to the plane of the laminations. In this

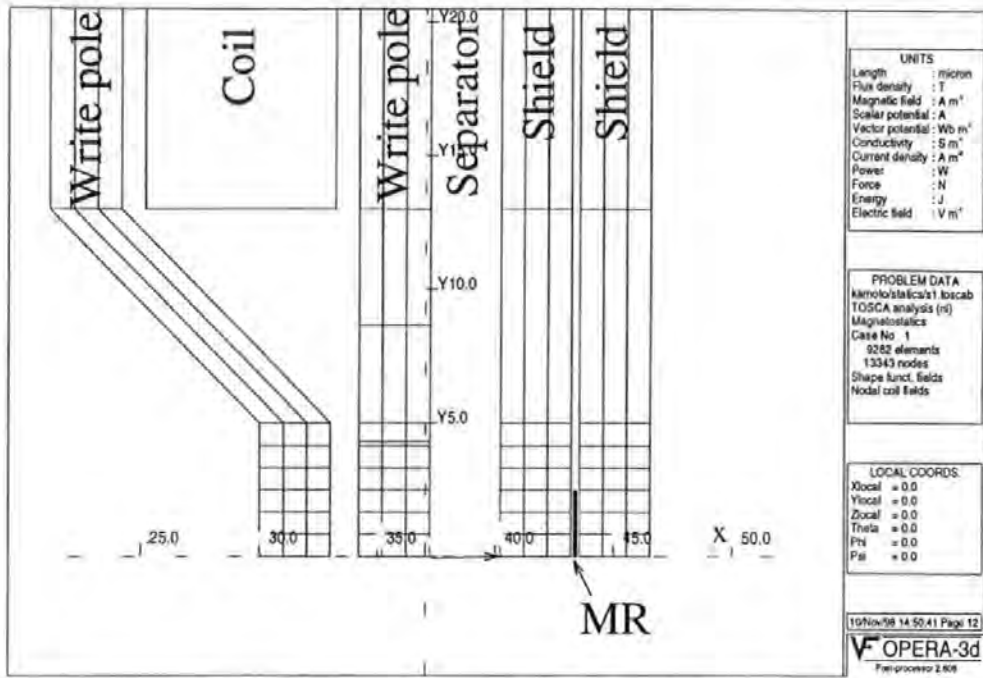


Figure 2.18: The improved (nonmagnetic) separator design.

investigation, the packing factor varies from 0.5 to 1.0. As the lamination is parallel to the head fabrication plane, the corresponding Euler angles for the lamination direction are set to be 90° , 90° and -90° , respectively.

The crossfeed response is evaluated by the output of the MR head. The output of the MR head is given by the volume integral of the vertical component of magnetic flux density within the MR stripe. In this case, an MR sensor is only sensitive to a vertical field because the transversal components cancel each other. The expression of the output V of a single MR stripe is:

$$V \propto \int \int \int B_y dx dy dz \quad (2.22)$$

The units for this volume integral are $T \cdot \mu\text{m}^3$. As mentioned above, we will consider both the SAL case and the DMR case for each head design. In the SAL case, we can simply take the volume integral over the right stripe as the final output of

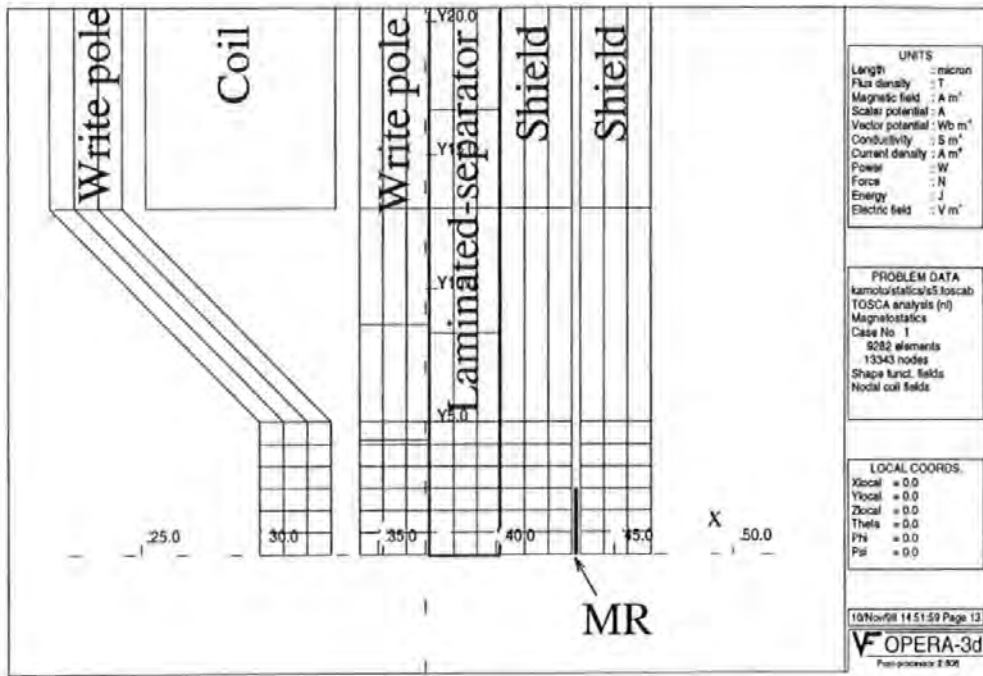


Figure 2.19: The improved laminated-separator design.

MR head. However, in the DMR case to set the final output of a DMR head, we should subtract out the integral over the right stripe from that over the left one and then divide it by 2 because of the parallel connection between the two MR stripes in a DMR head (See Section 2.2 for details.).

2.7 Different Coil Shapes

The crossfeed effect with different coil shapes is investigated. Two coil shapes are considered here: the well-used planar coil scheme (Figure 2.20) and the proposed tubular coil scheme (Figure 2.21). For a closed coil, two different sources of interference field can easily be distinguished, namely: (a) Positive-direction current carrying conductor (In abbreviation, positive conductor); (b) Negative-direction current carrying conductor (negative conductor).

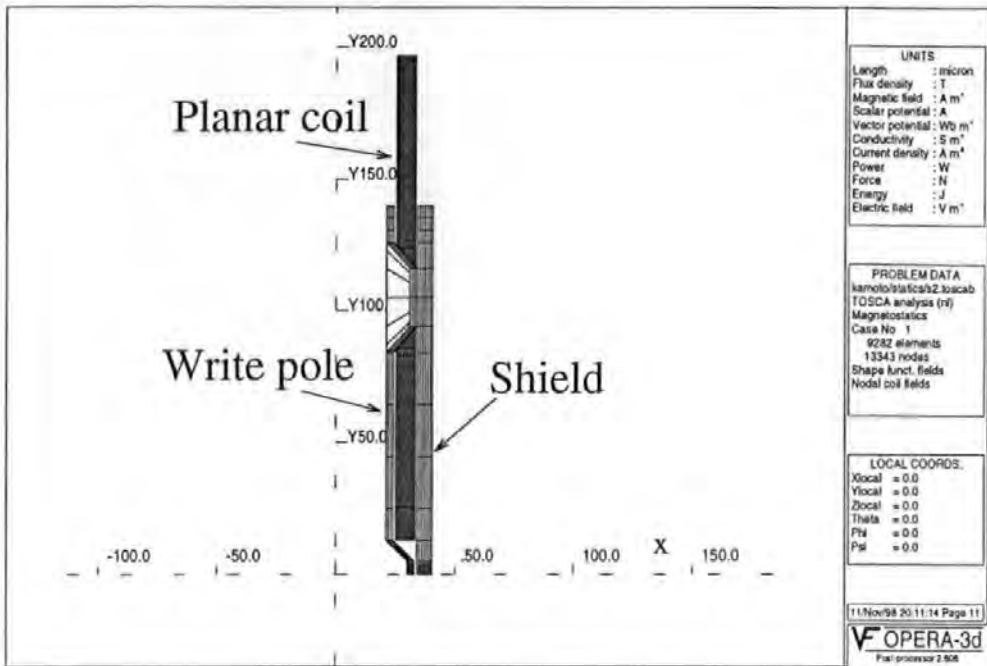


Figure 2.20: Traditional planar coil structure.

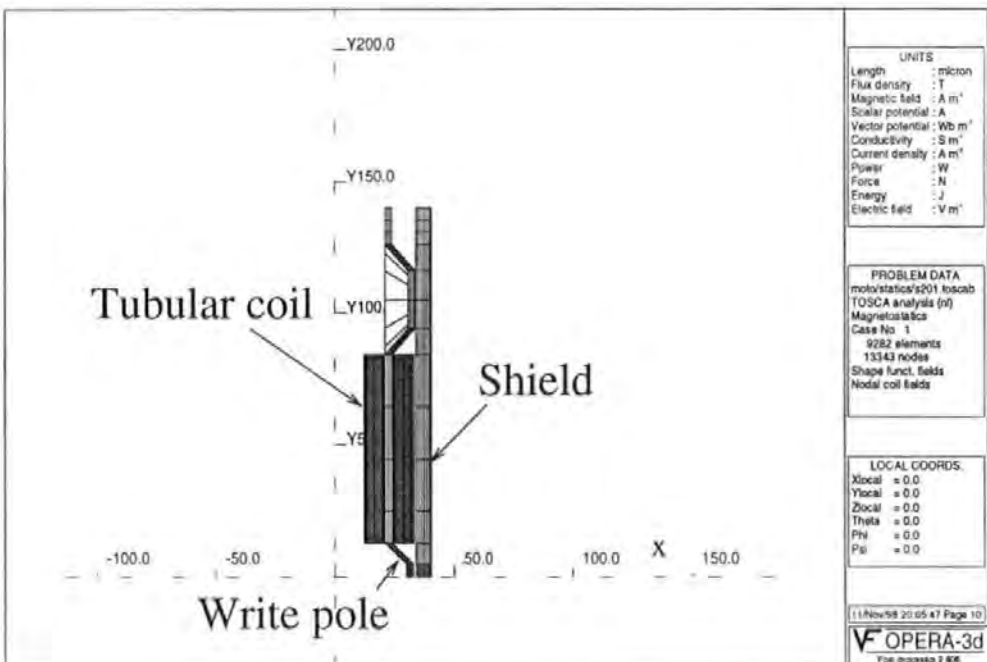


Figure 2.21: Proposed tubular coil structure.

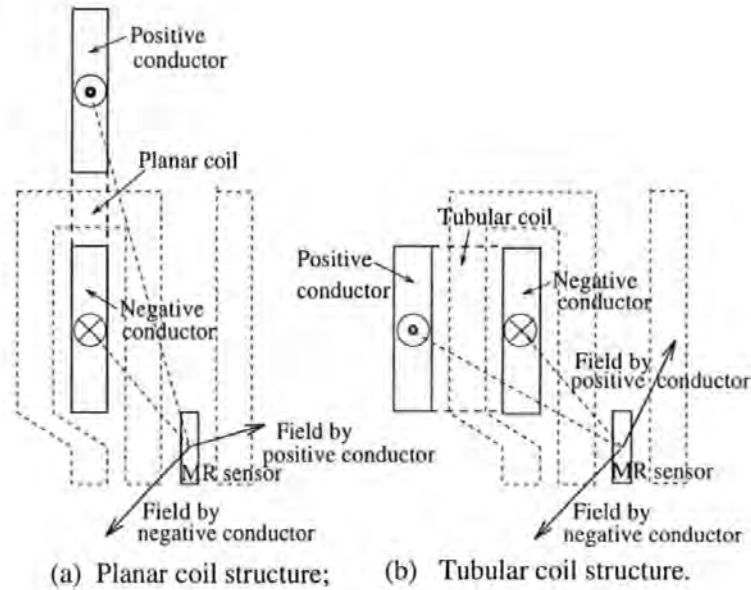


Figure 2.22: Fictitious field distribution comparison between planar coil structure and tubular coil structure. For a closed coil, two different sources of interference field can easily be distinguished, namely: (1) Positive-direction current carrying conductor (In abbreviation, positive conductor); (2) Negative-direction current carrying conductor (negative conductor). The primary motivation for the tubular coil scheme is to reduce the crossfeed by the property that the interference fields from the positive and negative conductors will cancel each other because they are so close to each other in the tubular coil scheme.

The primary motivation for the tubular coil scheme is to reduce the crossfeed by the property that the interference fields from the positive conductor and from the negative conductor will partially cancel each other because they are so close with respect to the MR sensor in the tubular coil scheme. Their fictitious field distributions are shown in Figure 2.22. Unfortunately, simulation result comparison between the tubular coil scheme, shown in Figure 2.23 (Figure 2.24), and the planar coil scheme, shown in Figure 2.27 later, displays no obvious different field distribution. This is because of the presence of magnetic poles with high permeability. In other words, the field distribution is mainly determined by the write gap between the write pole and the shared pole, not by the location of the conductors. Nevertheless, the planar coil is easier to manufacture than the tubular coil and so the rest investigations will be based on the planar coil design.

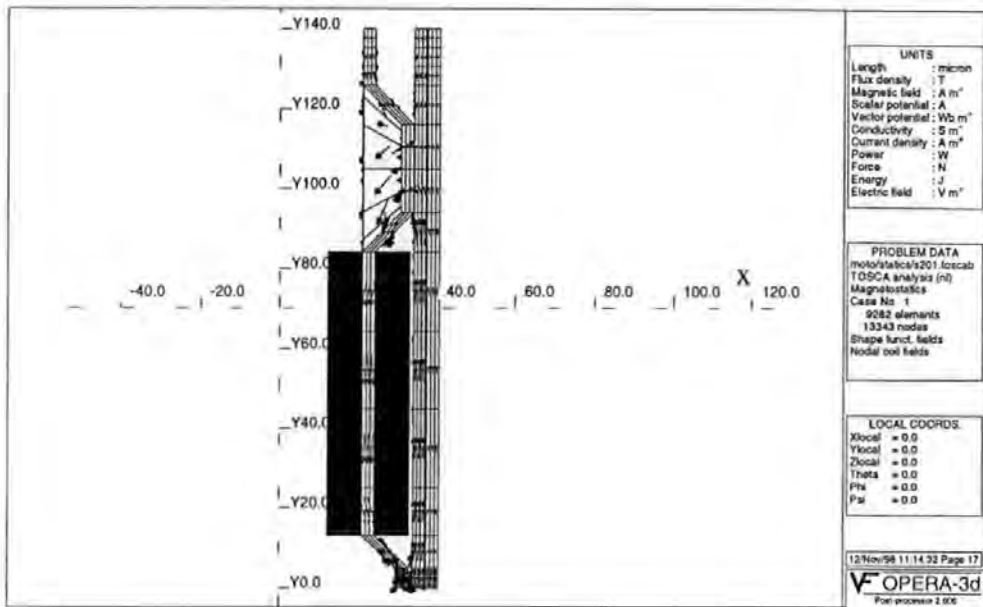


Figure 2.23: Flux density distribution in the mid-width plane ($z=0$) of magnetic materials for a tubular coil design at a selected applied magnetomotive force 0.60 AT.

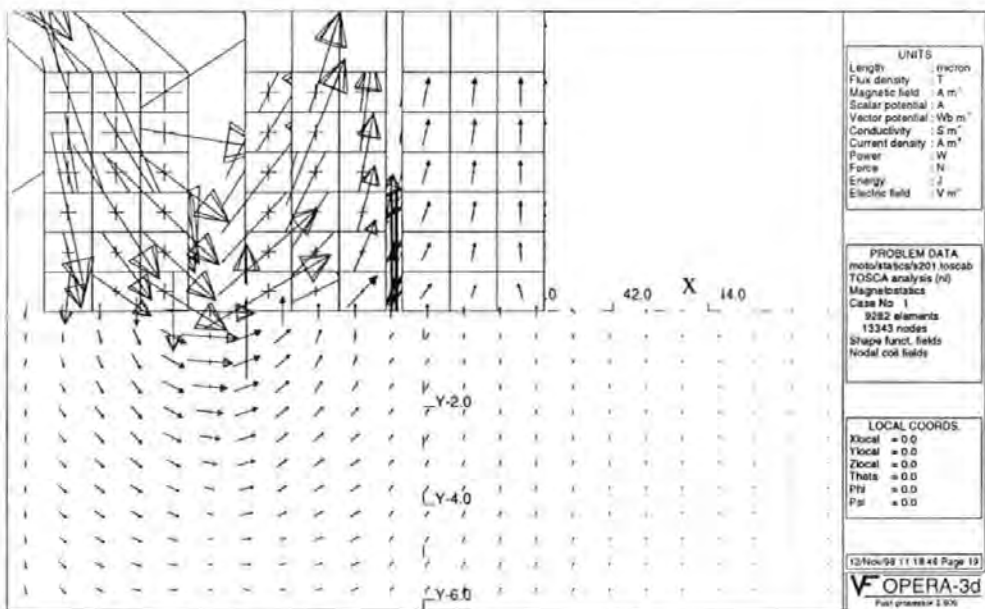


Figure 2.24: Magnified flux density distribution around the write gap for a tubular coil head design.

2.8 A By-product of Different Core Width Design

As described above, in our reference design, the pole tip widths of the write pole and the shared pole are $61 \mu\text{m}$ and $100 \mu\text{m}$, respectively. The primary motivation for this well-used merged head with different width poles is to reduce the magnetic flux resistance and for easy fabrication purposes (no aligning calibration is needed). The structure employed here, however, has another advantage that the magnetic flux leaking around the two sides of the shared pole will effectively be confined behind the pole. The write field distribution in the TBS of the MR stripe is shown in Figure 2.25. For comparison, the fictitious case of the head design with the same pole width is shown in Figure 2.26. In the present case with different pole widths, the SAL crossfeed is $0.1323 \text{ T}\cdot\mu\text{m}^3$ while the DMR crossfeed is $0.00291 \text{ T}\cdot\mu\text{m}^3$; in the fictitious case with same pole width, the SAL crossfeed is $0.1337 \text{ T}\cdot\mu\text{m}^3$ while the DMR crossfeed is $0.0336 \text{ T}\cdot\mu\text{m}^3$. That is to say, there is a reasonable reduction in crossfeed (1.1 % in SAL and 13.4 % in DMR) with a wider bottom (shield) pole, predicted by the above analysis.

2.9 Head Field Intensity

Recording of a tape or disk is accomplished when the media moves through the stray field from the gap in the write head. We need to know this field so we can determine the locations where the field intensity exceeds the coercive force of the individual particles, and hence may change their magnetization. The write flux distributions of the three designs at a selected applied magnetomotive force ($I = 0.60 \text{ AT}$) in the mid-width cut plane ($z=0$) are shown in Figure 2.27 to Figure 2.29. For clarity only the poles and the air region underneath the TBS are displayed with field arrows. The field intensity in the central point of the write gap is 3667 Oe , sufficient to allow that head to write both the low coercivity (900 Oersted) $\gamma\text{Fe}_2\text{O}_3$ and potentially

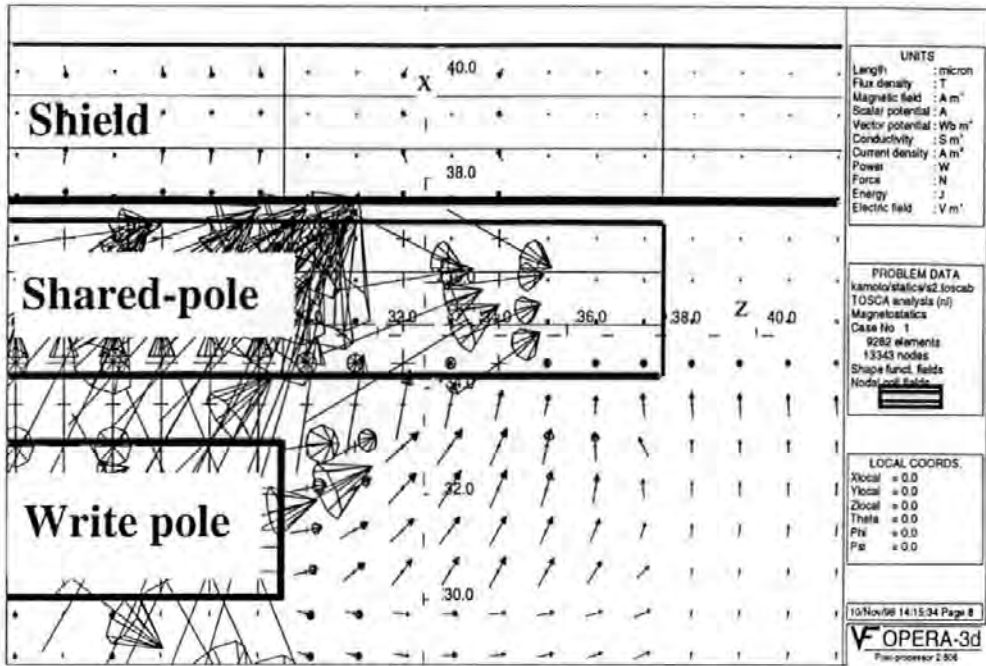


Figure 2.25: The write field distribution in the TBS ($y=0$) in the shared-pole design at a selected applied magnetomotive force 0.60 AT.

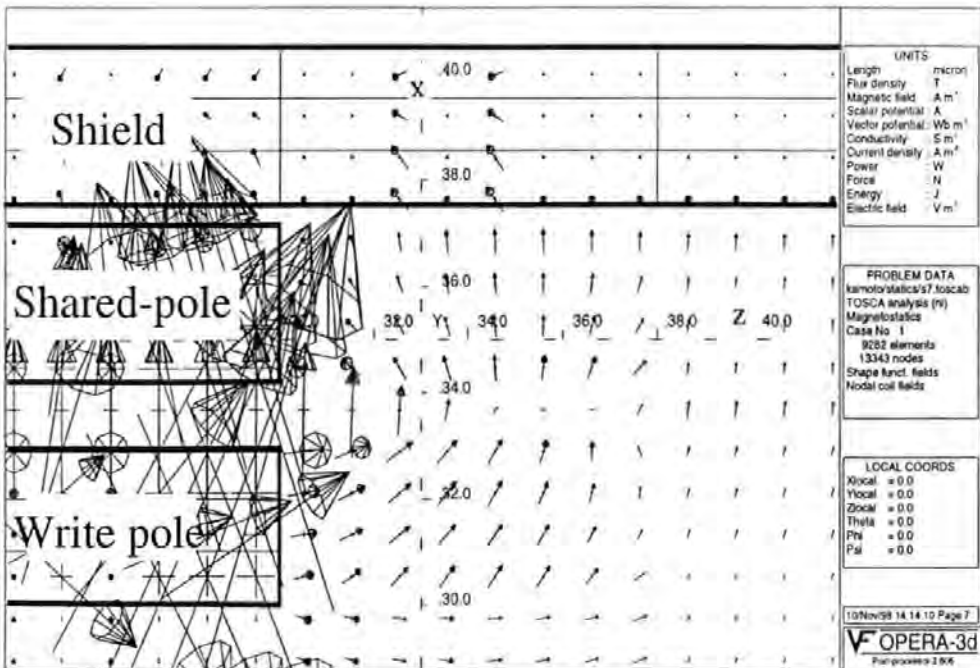


Figure 2.26: The fictitious write field distribution in the TBS ($y=0$) in the shared-pole design with same pole width at a selected applied magnetomotive force 0.60 AT.

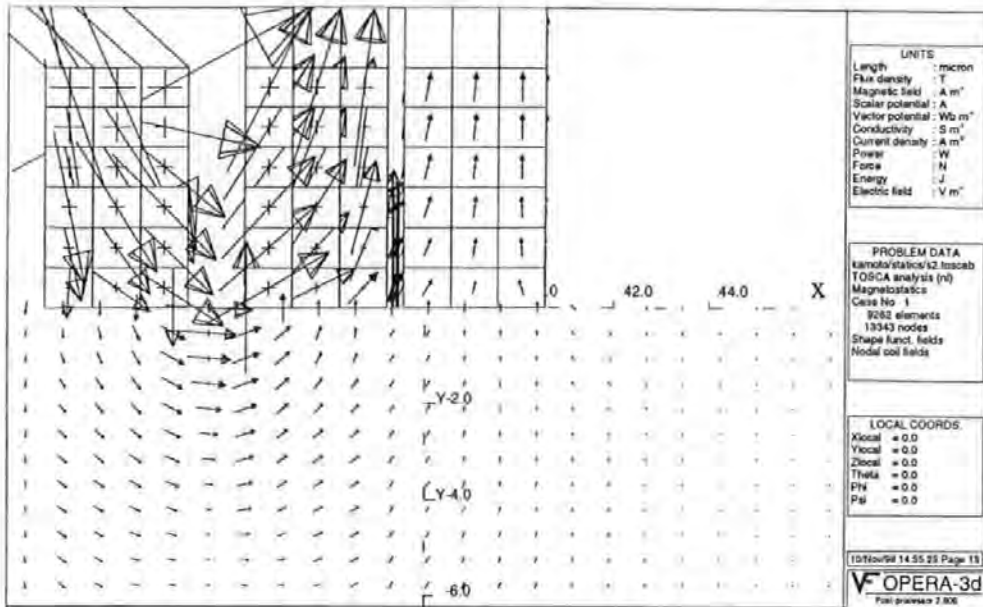


Figure 2.27: Flux density distribution in the mid-width plane ($z=0$) for a shared-pole design (with the planar coil) at a selected applied magnetomotive force 0.60 AT.

the higher (2000 Oersted) Metal Particle media[3].

Currently the highest output signal is obtained by advanced metal evaporated tape. This is due to the fact that the magnetic recording layer thickness has progressively decreased over the years to improve the recorded transition length, a , and the overwrite performance. The increase is mainly attributable to magnetic particles of higher remanent magnetization, M_r , and higher packing fractions. The downside to increasing the M_r indefinitely is that the recorded transition length, a , increases and may be approximated by[1]:

$$a = K \sqrt{\frac{M_r \delta d_{eff}}{H_c}} \quad (2.23)$$

where, δ is the magnetic layer thickness, d_{eff} is the effective head to medium spacing and K is a proportionality constant resulting from the write field and geometrical considerations. (The spacing loss was first described by Wallace and is generally

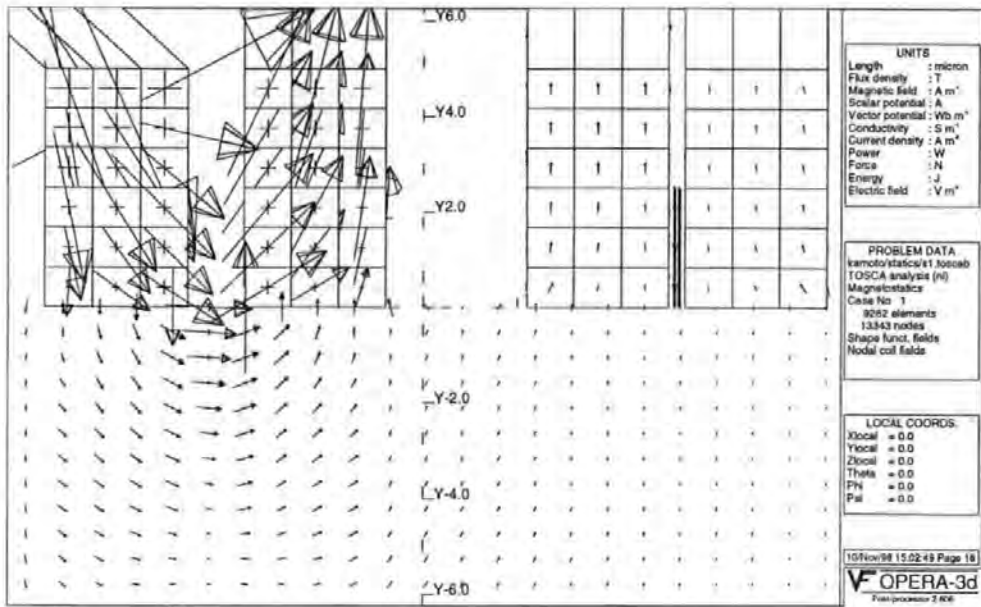


Figure 2.28: Flux density distribution in the mid-width plane ($z=0$) for a $3 \mu\text{m}$ non-magnetic separator design (with the planar coil) at a selected applied magnetomotive force 0.60 AT.

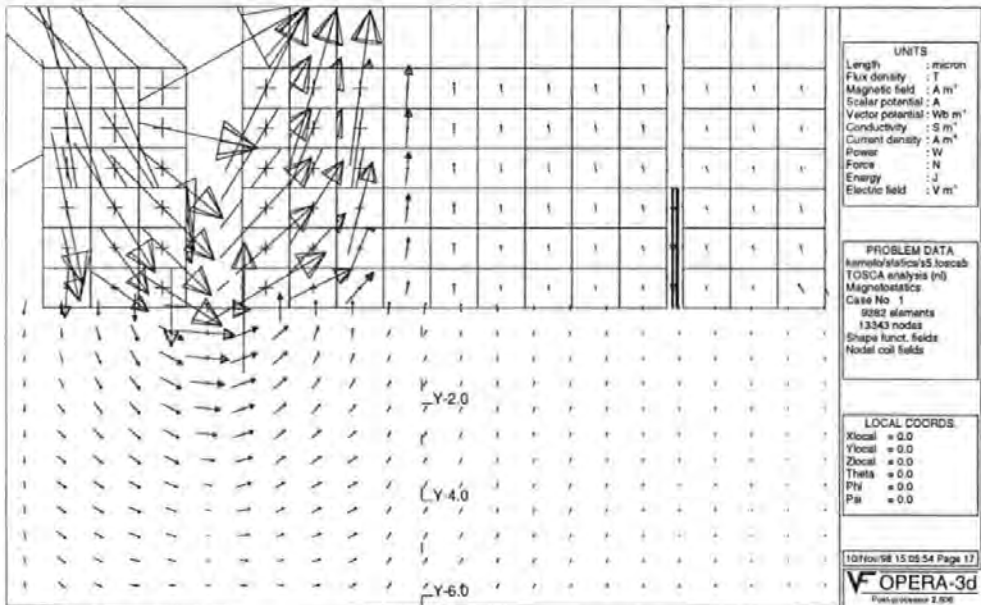


Figure 2.29: Flux density distribution in the mid-width plane ($z=0$) for a $3 \mu\text{m}$ laminated-separator (packing factor = 0.5) design (with the planar coil) at a selected applied magnetomotive force 0.60 AT.

referred to as the "Wallace Loss"[1]. The Wallace Loss assumes a coating $\mu=1$ but sometimes $\mu=2\sim 4$ will affect the sensing in a way that increases the spacing loss.) Thus, to prevent the transition length from reducing the maximum linear recording density appreciably the coercivity, H_c , is generally increased in line with M_r . The coercivity is limited in practice by the maximum write field that can be applied using inductive write heads. From the above we can see why the recent trends in magnetic recording have led to media with increased remanent magnetization and increased coercivity[42].

2.10 Crossfeed Response in Three Designs

By studying Figure 2.27 to Figure 2.29, it is found that the flux distribution is significantly asymmetric due to the existence of the read assembly. In particular, the 20 kA/m field arrow extends out about 10 μm towards the read gap side from the write gap. In contrast, it extends out only 2.5 μm on the opposite side. This implies that the MR reproductive element will receive serious interference from the write field.

Since the divergence of the flux density is always zero, the magnetic flux induced by a coil should constitute a closed loop. This has been justified in Figure 2.30 to Figure 2.32. As illustrated in Figure 2.33, the shields serve mainly to transport part of the flux from the write head back to the writing coil. During the RWW process, the coils of an inductive write element are energized with a current. A portion of the resulting magnetic leak flux is radiated to the read gap in front of the TBS and then transported through the high-permeability poles and shields in the head structure. The details of this flux, i.e. the transportation process and its overall efficiency (i.e., how much of the flux reaches the read gap), are determined by the head geometry and materials. For example, in the case of separator designs, the low permeability of the non-magnetic separator represents an increased reluctance (equivalent to air) to the crossfeed fields and this may cause the crossfeed fields to forcibly interfere

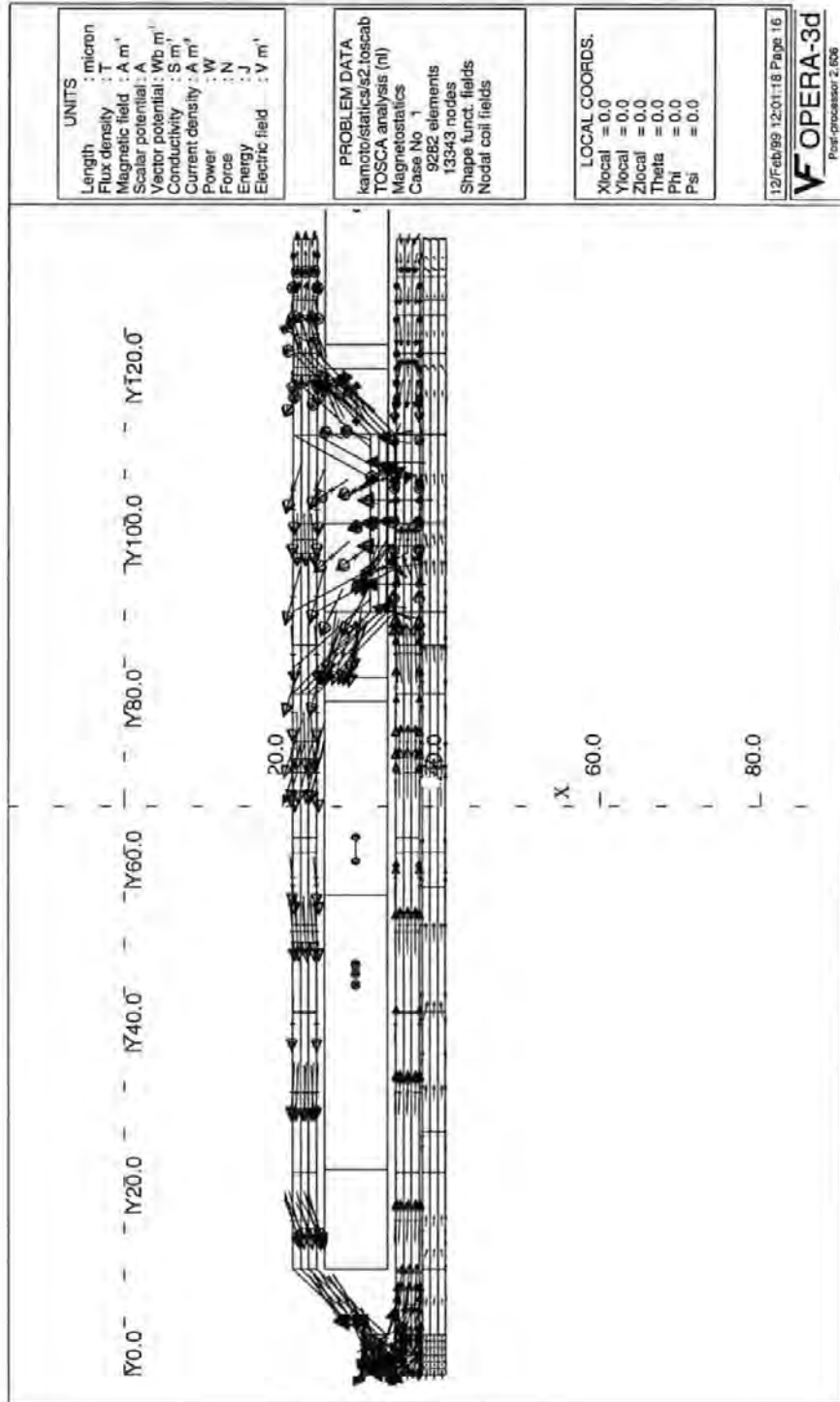


Figure 2.30: Flux density distribution in the mid-width plane ($z=0$) for a shared-pole design at a selected applied magnetomotive force 0.60 AT. The shield serves mainly to transport part of the flux from the write head back to the writing coil. The (planar) coil is also shown here.

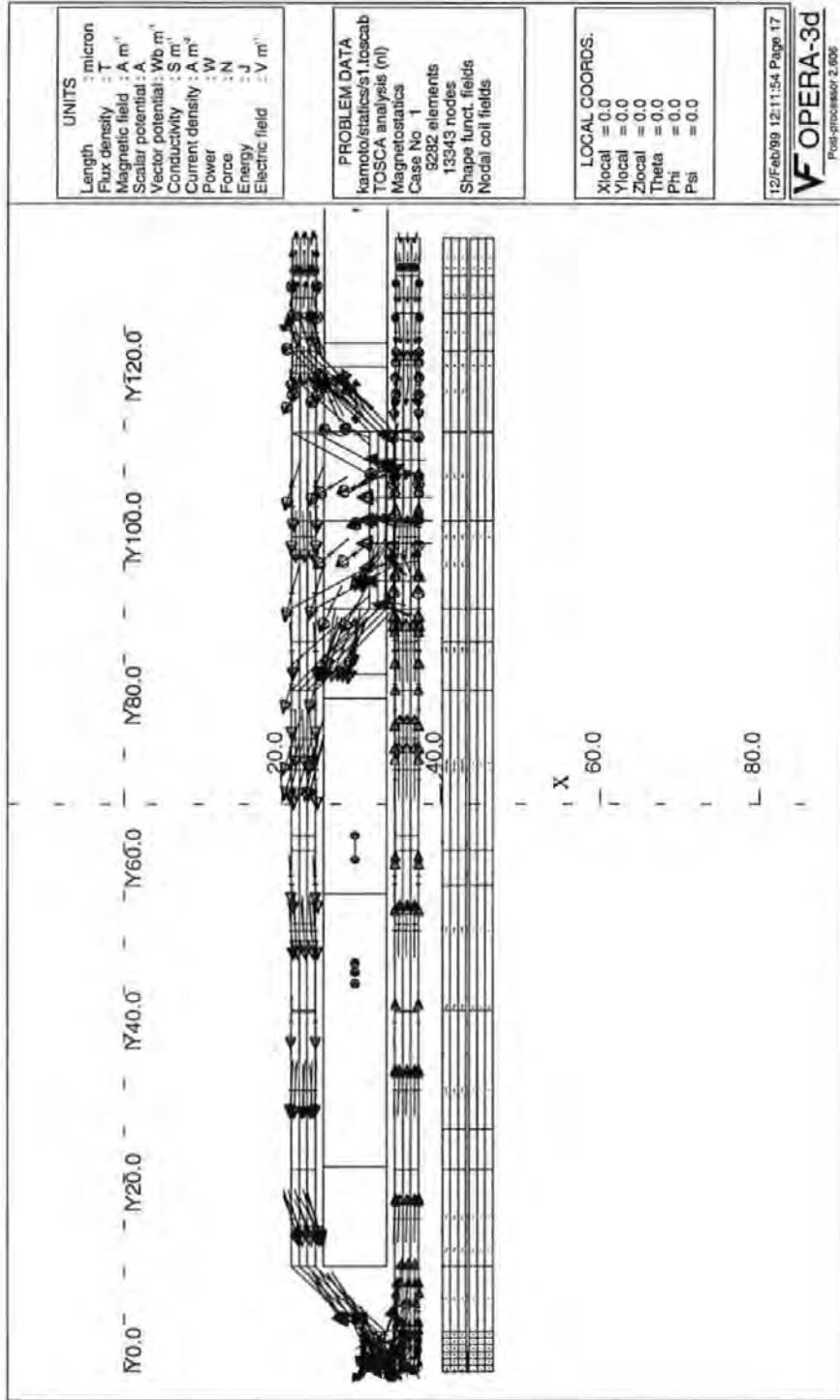


Figure 2.31: Flux density distribution in the mid-width plane ($z=0$) for a $3 \mu\text{m}$ separator design at a selected applied magnetomotive force 0.60 AT. The shield serves mainly to transport part of the flux from the write head back to the writing coil. The (planar) coil is also shown here.

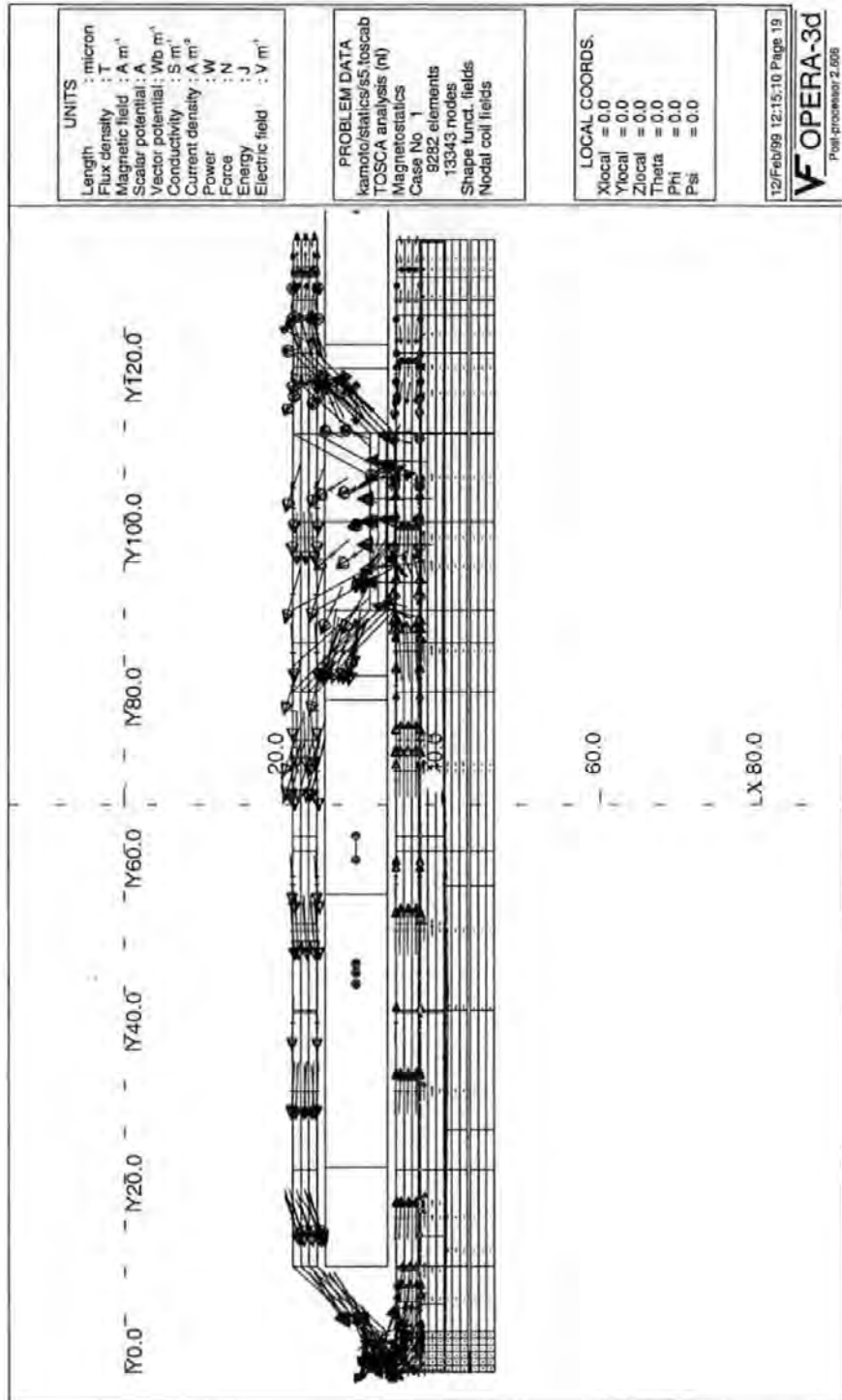


Figure 2.32: Flux density distribution in the mid-width plane ($z=0$) of magnetic materials for a $3 \mu\text{m}$ laminated-separator (laminating factor = 0.5) design at a selected applied magnetomotive force 0.60 AT. The laminated-separator and shield serve mainly to transport part of the flux from the write head back to the writing coil. The (planar) coil is also shown here.

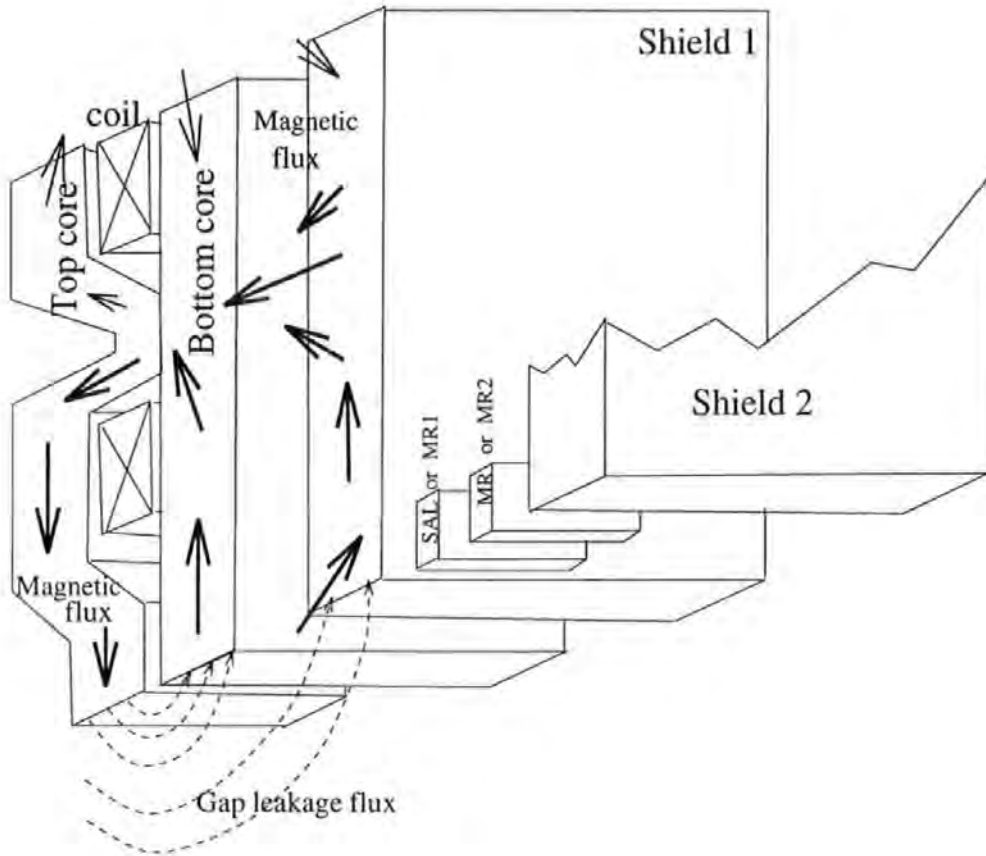


Figure 2.33: The shield serves mainly to transport part of the flux from the write head back to the writing coil. Here is example of separator design. During the RWW process, the coils of an inductive write element are energized with a current. A portion of the resulting magnetic leak flux is radiated to the read gap in front of the TBS and then transported through the high-permeability poles and shields in the head structure. The details of this flux — transportation process and its overall efficiency (i.e., how much of the flux reaches the read gap) are determined by the head geometry and materials.

with the MR element behind the shield. In this regard, the transporting efficiency is considerably improved when high permeability metallic magnetic materials are used as the separator. The higher the permeability, the more efficient the transportation becomes. The shields with a high permeability, e.g. CoZrNb, act more as alternative low-reluctance paths which divert the crossfeed fields away from the MR element.

We will discuss the above phenomena further by considering a vertical field mapping. A typical simulated one-dimensional field mapping of the vertical component in the TBS plane is shown in Figure 2.34 through Figure 2.36. We only take the vertical field into account because the MR sensor is only sensitive to the vertical component. A phenomenon deserving note is that some enhancements of the flux intensity exists in some regions, in agreement with electron beam tomography measurements on three components of the thin-film head field distribution[43]. In the case of the shared-pole design (Figure 2.34), the MR sensor is located near the 2nd positive peak of the vertical component. In the case of separator design (Figure 2.35), there are five separated positive peaks and the MR sensor is located near the 4th peak. In the case of laminated-separator (Figure 2.36), there are still five positive peaks and the MR sensor is still located near the 4th peak. Because the 4th peak is much lower than the 2nd one, the MR sensor senses little magnetic flux from the write head in the latter two cases. We conclude that in the separator (non-magnetic or laminated) head design the separator plays a very important role in reducing crossfeed from the write head to the MR sensor because it attracts and transports most of diverging flux (which is an enhancement!) from the write head. This is why some enhancements of the flux intensity exists in some regions. Therefore, the non-magnetic or laminated separator head is one preferred approach for achieving simultaneous operation of the read head and write head.

In principle the interference intensity depends on the different head structures and the exact calculation results are as follows:

In the case of shared-pole design (Figure 2.27), the SAL crossfeed is $0.1323 \text{ T} \cdot \mu\text{m}^3$

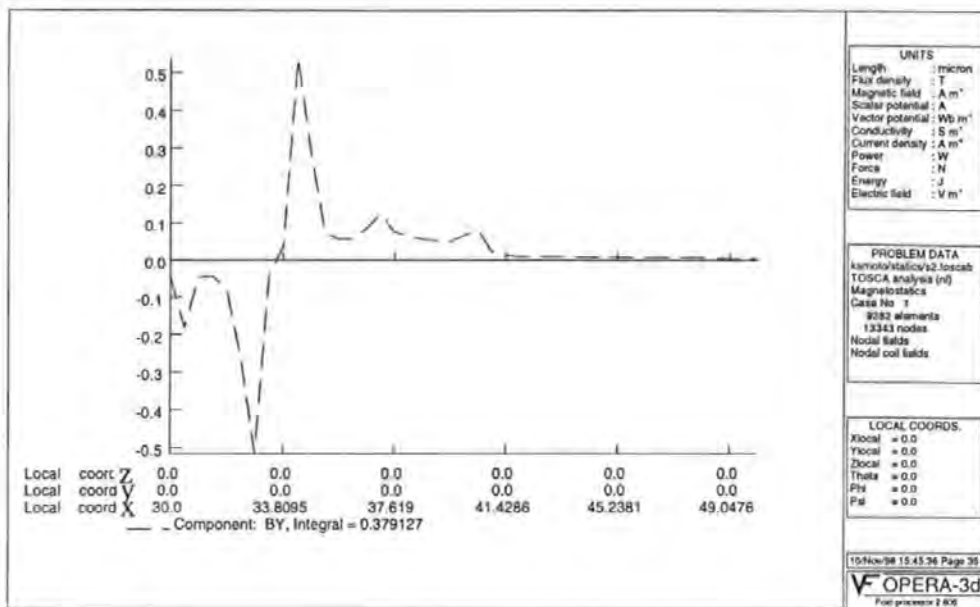


Figure 2.34: One-dimensional mapping of the vertical component B_y along the TBS (Tape Bearing Surface) ($z=0, y=0$) in a shared-pole design.

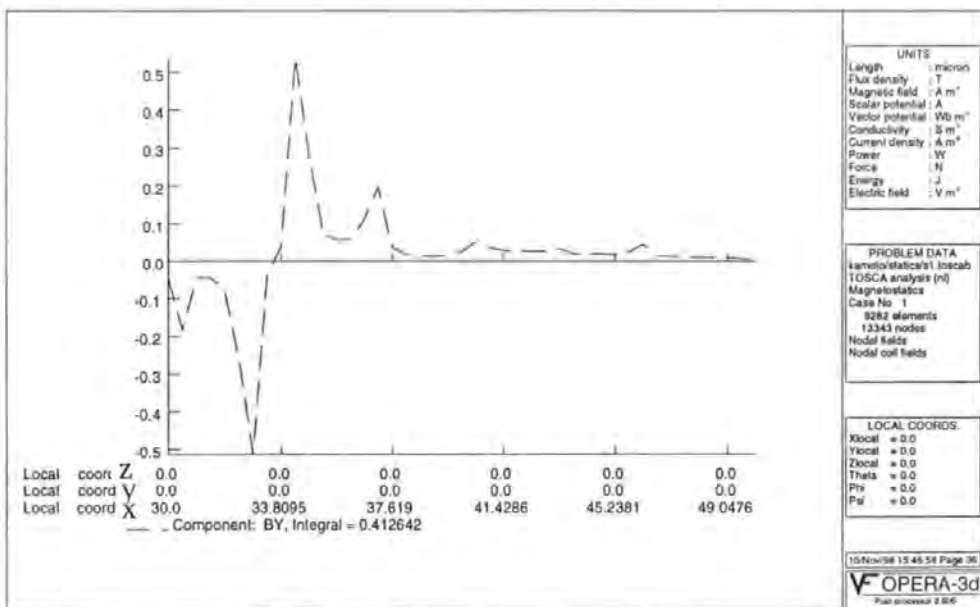


Figure 2.35: One-dimensional mapping of the vertical component B_y along the TBS ($z=0, y=0$) in a separator design.

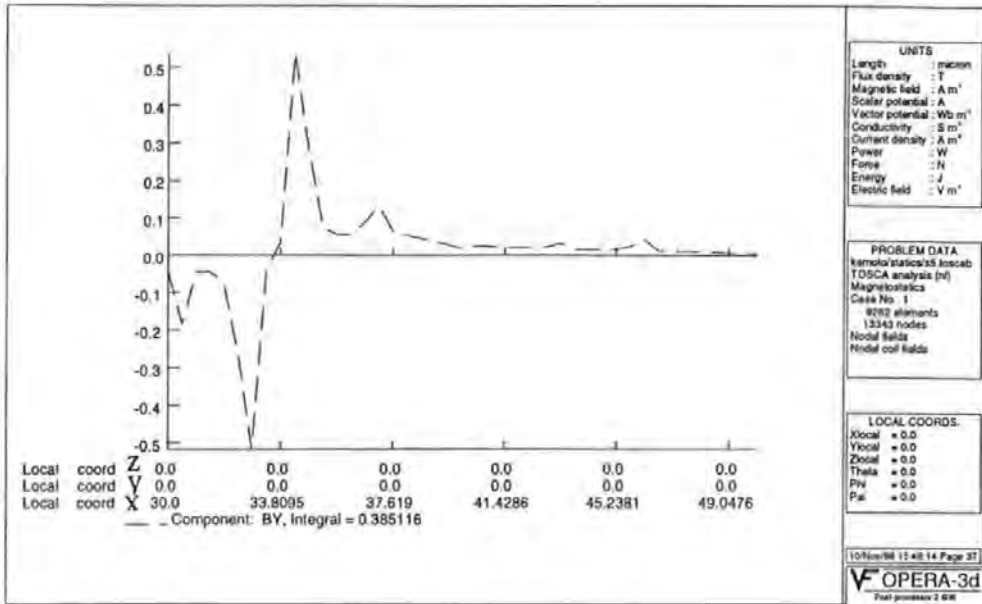


Figure 2.36: One-dimensional mapping of the vertical component B_y along the TBS ($z=0, y=0$) in a laminated-separator (packing factor = 0.5) design.

while the DMR crossfeed is $0.0291 \text{ T}\cdot\mu\text{m}^3$;

In the case of separator design (Figure 2.28), the SAL crossfeed is $0.0966 \text{ T}\cdot\mu\text{m}^3$ while the DMR crossfeed is $0.0145 \text{ T}\cdot\mu\text{m}^3$;

In the case of laminated-design (Figure 2.29) (the lamination packing factor is 0.5), the SAL crossfeed is $0.0825 \text{ T}\cdot\mu\text{m}^3$ while the DMR crossfeed is $0.0119 \text{ T}\cdot\mu\text{m}^3$.

From the above results, as summarized in Table 2.1, we see that shared-pole head design exhibits significant crossfeed from the write signals to the read sensor as a result of the shared pole and close proximity of the write element to the read sensor. Compared with the reference head, the crossfeed of the separator type head is reduced by 27% in the SAL case and by 50% in the DMR case. Compared with the reference head, the crossfeed of the laminated-separator (packing factor is 0.5) type head is reduced by 38% in the SAL case and by 59% in the DMR case. The main

<i>Head designs</i>	<i>Replay modes</i>	
	SAL	DMR
Shared-pole	0.1323	0.0291
Separator	0.0966	0.0145
Laminated-separator	0.0825	0.0119

Table 2.1: Crossfeed responses with three different RWW head designs. The thickness of the (non-magnetic) separator or the laminated-separator is $3 \mu\text{m}$. In the laminated-separator design, the packing factor is 0.5. The unit of response is $\text{T}\cdot\mu\text{m}^3$.

reason for such an improvement in the non-magnetic or laminated separator head design is that the enhancement of the flux intensity appears underneath the separator whereas the enhancement appears underneath the MR sensor in the shared-pole head design.

2.11 Laminating Effect

In order to investigate the laminating effect in detail, we also investigated two additional laminated-separator cases: when the packing factor is 0.75, the SAL crossfeed is $0.0745 \text{ T}\cdot\mu\text{m}^3$ while the DMR crossfeed is $0.0084 \text{ T}\cdot\mu\text{m}^3$; when the packing factor is 1.00, the SAL crossfeed is $0.0741 \text{ T}\cdot\mu\text{m}^3$ while the DMR crossfeed is $0.0074 \text{ T}\cdot\mu\text{m}^3$. As mentioned above, in the case of laminated-design (Figure 2.29) (the lamination packing factor is 0.5), the SAL crossfeed is $0.0825 \text{ T}\cdot\mu\text{m}^3$ while the DMR crossfeed is $0.0119 \text{ T}\cdot\mu\text{m}^3$. Compared with the packing factor of 0 (Figure 2.28), the crossfeed with a 0.5 packing factor is reduced by 14% in the SAL case and by 18% in the DMR case; the crossfeed with a 0.75 packing factor is reduced by 23% in the SAL case and by 42% in the DMR case; the crossfeed with a 1.00 packing factor is reduced by 23% in the SAL case and by 49% in the DMR case. Table 2.2 summarizes the above calculations.

As illustrated in Figure 2.33, the shields serve mainly to transport part of the flux

<i>Packing factor</i>	<i>Replay modes</i>	
	SAL	DMR
0	0.0966	0.0145
0.5	0.0825	0.0119
0.75	0.0745	0.0084
1.0	0.0741	0.0074

Table 2.2: Crossfeed responses in laminated-separator RWW head design with three different packing factors. The unit of response is $T \cdot \mu\text{m}^3$.

from the write head back to the writing coil in the RWW operation. From this standpoint, the transporting efficiency is considerably improved when laminated metallic magnetic materials with a high packing factor are used. The higher the lamination packing factor, the more efficient the transportation becomes. The shields with a high packing factor act more as alternative low-reluctance paths which divert the crossfeed fields away from the MR element.

2.12 Underpole and Underlayer Designs

We have also considered two other compensation schemes to give further reduction of crossfeed from the write head to the MR sensor. These two compensating methods have been well-used in magnetic tape units in the 1960's[14][15]. Figure 2.37 and Figure 2.38 show an under-pole scheme. In this scheme, a whole-plane shielding pole with a hole ($5 \mu\text{m}$ high) to let the tape go through is used to screen the diffusing magnetic flux from the reproductive element. It was hypothesized that this under-pole would attract most of the diverging flux and little write field would interfere with the MR sensor. Figure 2.39 and Figure 2.40 show an under-layer scheme. In this scheme, a thick soft magnetic underlayer with high permeability placed at a certain distance ($5 \mu\text{m}$) behind the tape, covers both the write head and the read head.

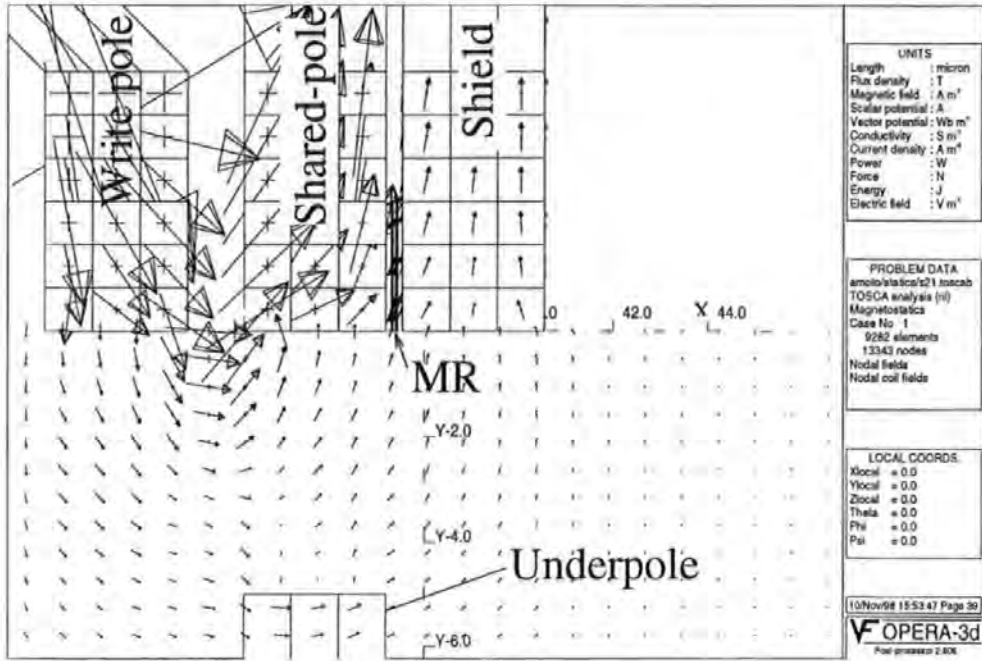


Figure 2.37: Write field distribution with an underpole. In this scheme, a whole-plane shielding pole with a hole (5 μm high) to let the tape go through is used.

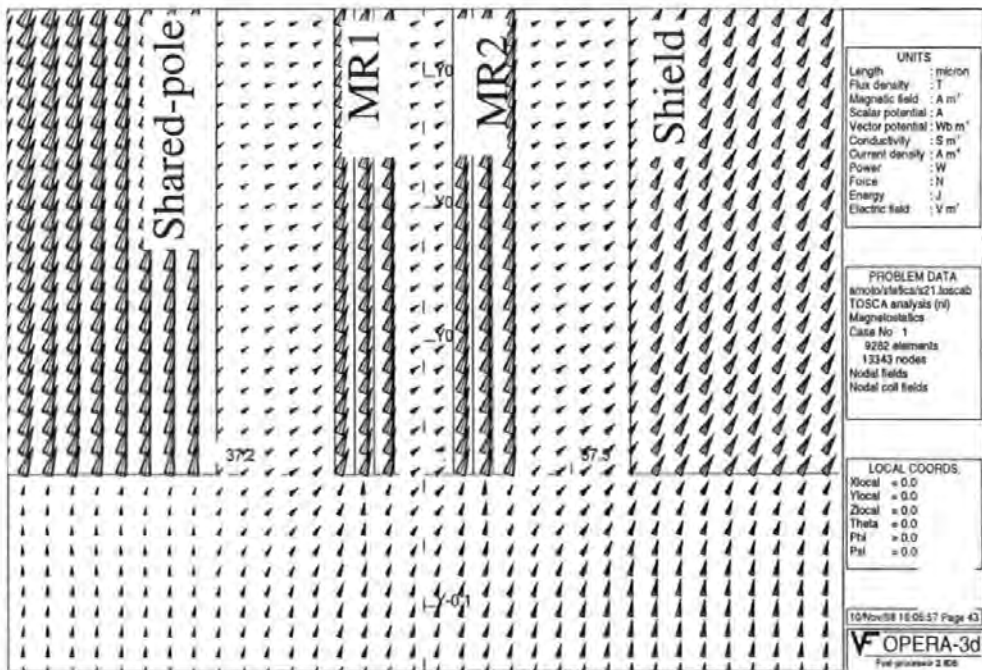


Figure 2.38: Field mappings of crossfeed situations around the read gap region in the under-pole design, with the 0.60 AT magnetomotive force through the writing coil.

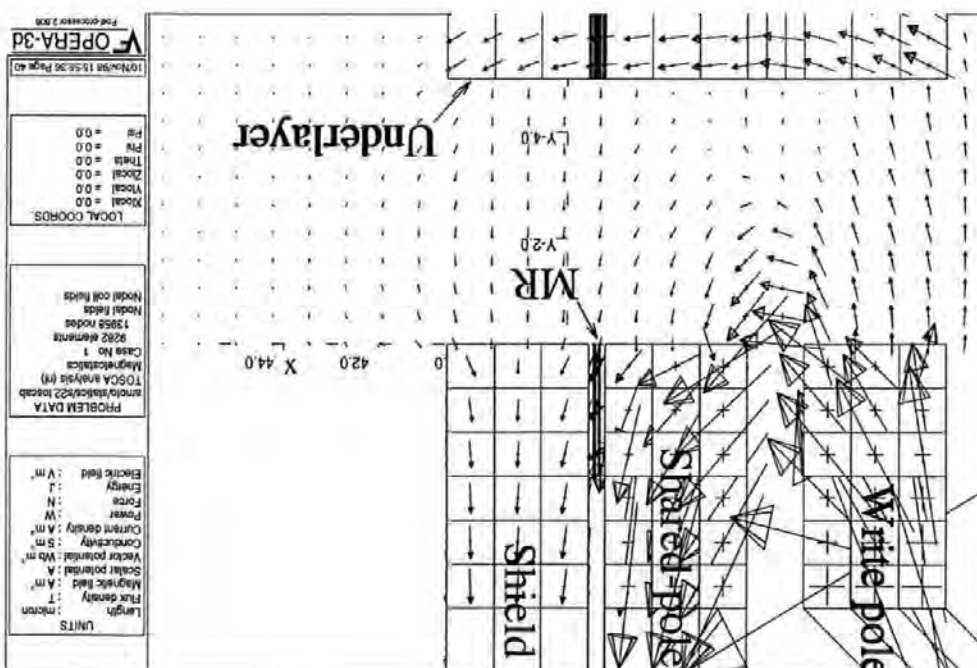


Figure 2.39: Write field distribution with an underlayer. In this scheme, a thick soft magnetic underlayer with high-permeability placed at a certain distance ($5 \mu\text{m}$) behind the tape covers both the write head and the read head.

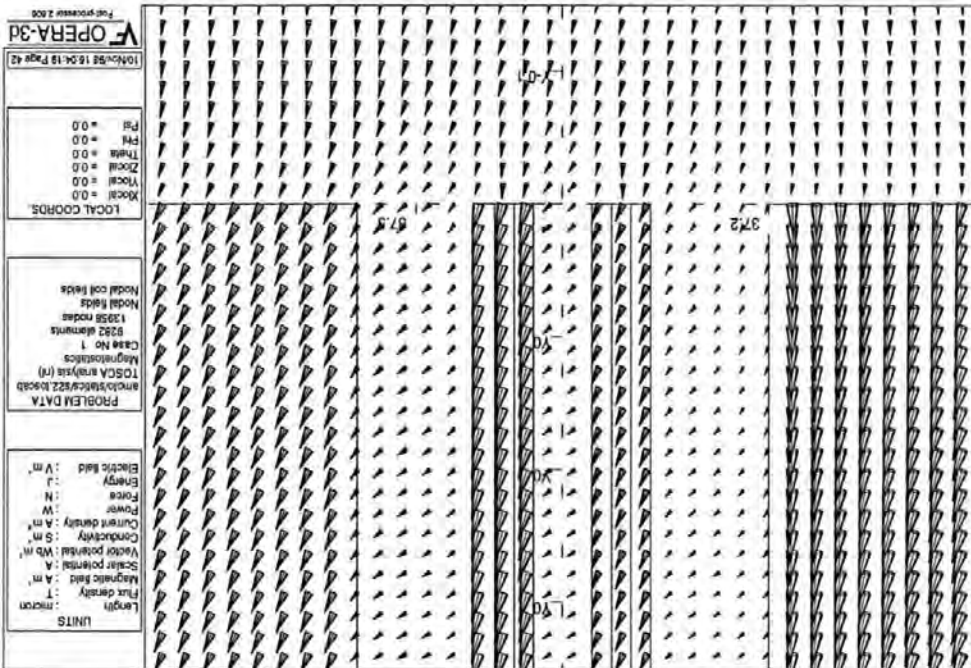


Figure 2.40: Field mappings of crossed situations around the read gap region in the under-layer design, with the 0.60 AT magnetomotive force through the writing coil.

<i>Head designs</i>	<i>Replay modes</i>	
	SAL	DMR
Shared-pole	0.1323	0.0291
Under-pole	0.1284	0.0283
Under-layer	0.1241	0.0267

Table 2.3: Crossfeed responses in shared-pole RWW head with two additional improved different designs. The response's unit is $T \cdot \mu m^3$.

Unfortunately, each of Figure 2.37 and Figure 2.39 shows no obvious different field distribution compared with the original one (Figure 2.27). In the case of the underpole design, the SAL crossfeed is $0.1284 T \cdot \mu m^3$ while the DMR crossfeed is $0.0283 T \cdot \mu m^3$; In the case of the underlayer design, the SAL crossfeed is $0.1241 T \cdot \mu m^3$ while the DMR crossfeed is $0.0267 T \cdot \mu m^3$. As a comparison, in the case of the standard shared-pole design, the SAL crossfeed is $0.1323 T \cdot \mu m^3$ while the DMR crossfeed is $0.0291 T \cdot \mu m^3$. Compared with the standard shared-pole design, the crossfeed in the underpole design is reduced by 3% in the SAL case and by 3% in the DMR case whereas the crossfeed in the underlayer design is reduced by 7% in the SAL case and by 8% in the DMR case. This is because the size of the modern head is much smaller than that in the past and we have to put an underlayer or underpole relatively far apart from the TBS of the head due to the limitation of the tape thickness. Thus, as summarized in Table 2.3, both underlayer and underpole have limited use for anti-interference purposes.

2.13 Replay Processes

The aim of a replay process simulation is to give the volume integral (i.e. equivalent signal) of the MR sensor in the presence of a typical medium, so we can compare the magnitude difference between this case and crossfeed case. In other words, we should give the proportion of the crossfeed within the effective signal. As mentioned above, we will consider both the SAL case and the DMR case for each head design.

The head structure and dimensions used in the replay simulation are the same as the crossfeed investigations except that, for the replay simulation, either a longitudinal recording medium or a perpendicular recording medium is included in the model. In order to reduce the size of the model, only a three recorded bit longitudinal recording medium and a two bit perpendicular medium right underneath the read gap were simulated. For the longitudinal medium, the central bit is magnetized in the left direction and the other two bits are magnetized in the right direction; the trackwidth of the three bits is $60 \mu\text{m}$; the bit length is $0.25 \mu\text{m}$ with transition length $0.05 \mu\text{m}$; the thickness of the medium is $0.07 \mu\text{m}$; the head-medium spacing is $0.03 \mu\text{m}$; the coercivity of the recording medium is 900 Oersted. Different magnetic characteristics may be assigned to each of the local directions associated with the anisotropic medium. For the perpendicular medium (Figure 2.41), the left bit is magnetized in the up direction and the right bit magnetized in the down direction. The parameters for the perpendicular medium are similar, but this case will not be considered as our standard output case.

Figure 2.42 is a computed three dimensional field mapping of the three recorded longitudinal bits in the mid-width cut plane ($z=0$), with the replay DMR head at the top of the medium. The direction of each arrow corresponds to the direction of the flux density and its thickness to the flux density magnitude. This figure illustrates the flux distribution around the read gap region. It can be seen from the figure that the leakage flux from the medium goes upward in the left stripe and returns downward in the right stripe. It constitutes a closed magnetic circuit. Obviously it will cause a signal output (not peak value at this location) due to differential output in the DMR head. The calculated maximum DMR output is $0.3925 \text{ T}\cdot\mu\text{m}^3$ for the longitudinal medium. This value will be used as standard output. We are now in a suitable position to compare advanced heads in a SCR manner. In the reference shared-pole head, the effective DMR signal is 13.5 times as large as the crossfeed (the SCR is 22.6 dB); in the separator head, the effective DMR signal is 27.1 times as large as the crossfeed (the SCR is 28.6 dB); in the laminated-separator head, the

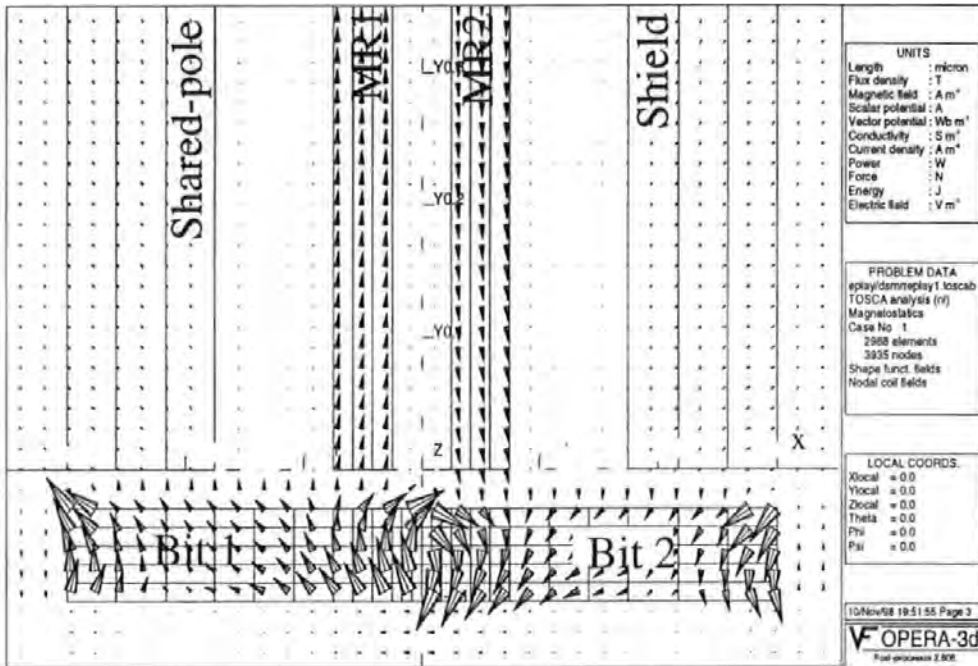


Figure 2.41: DMR (Dual Magnetoresistance) head replay processes. The figure illustrates the flux distribution of the 2-bit perpendicular recorded medium in the mid-width cut plane ($z=0$), with the replay DMR head located above the transition of those two bits.

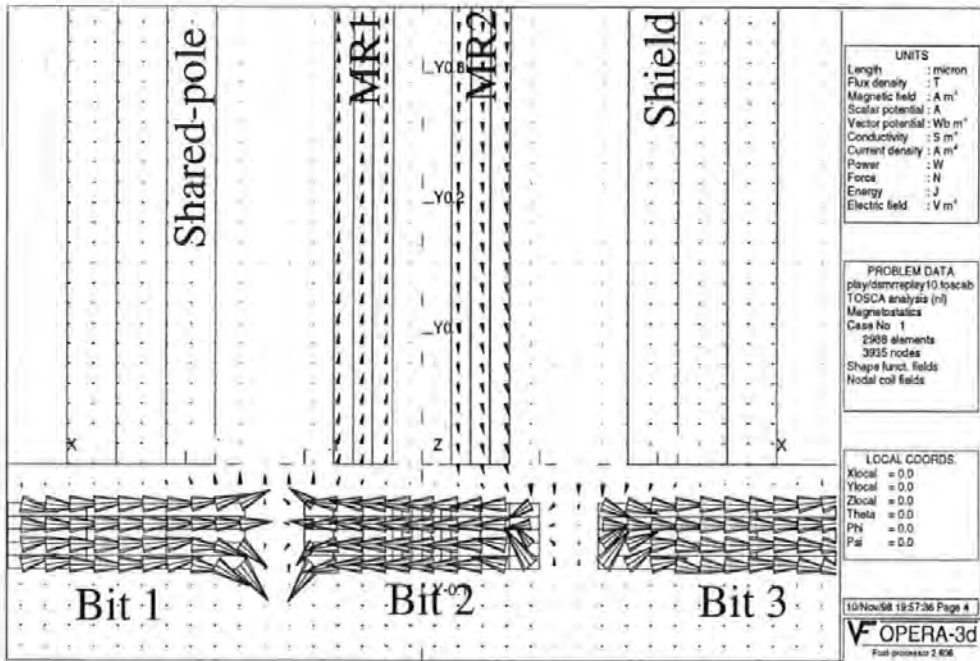


Figure 2.42: DMR (Dual Magnetoresistance) head replay processes. The figure illustrates the flux distribution of the 3-bit longitudinal recorded medium in the mid-width cut plane ($z=0$), with the replay DMR head located above the central bit.

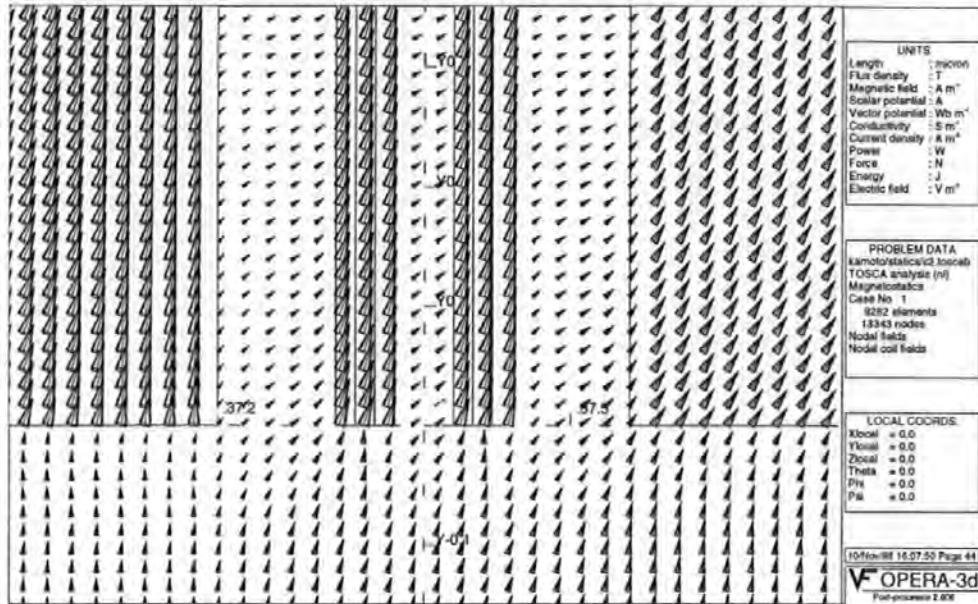


Figure 2.43: Field mappings of crossfeed situations around the read gap region in the shared-pole design, at a selected applied magnetomotive force 0.60 AT through the writing coil.

effective DMR signal is 33.0 times as large as the crossfeed (the SCR is 30.4 dB). In the other calculation, the maximum SAL output is found to be $0.3285 \text{ T}\cdot\mu\text{m}^3$ (also for the longitudinal medium). Therefore, in the SAL MR reproduction case, the SCR is: 7.9 dB (shared-pole case), 10.6 dB(separator case), 12.0 dB(laminated-separator case), respectively, for these three structures.

In contrast, we also computed three dimensional field mappings of crossfeed situations in the three head designs around the read gap region, at a selected applied magnetomotive force 0.60 AT through the writing coil. As shown in Figure 2.43 to Figure 2.45, the field distribution in the two MR stripes is almost the same because these two stripes are located so close with respect to the write gap. Obviously the output signals from these two stripes will cancel each other in the DMR case, thus an almost null final output will be caused (only $0.0119 \text{ T}\cdot\mu\text{m}^3$ for the laminated-separator RWW head design).

Figure 2.45: Field mappings of crossed situations around the read gap region in the laminated separator design, at a selected applied magnetomotive force 0.60 AT through the writing coil.

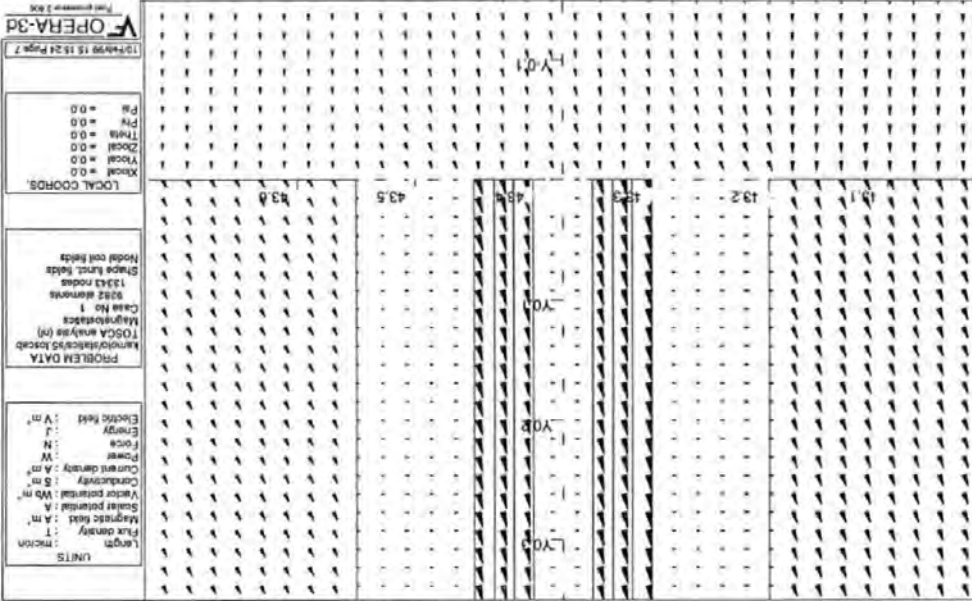
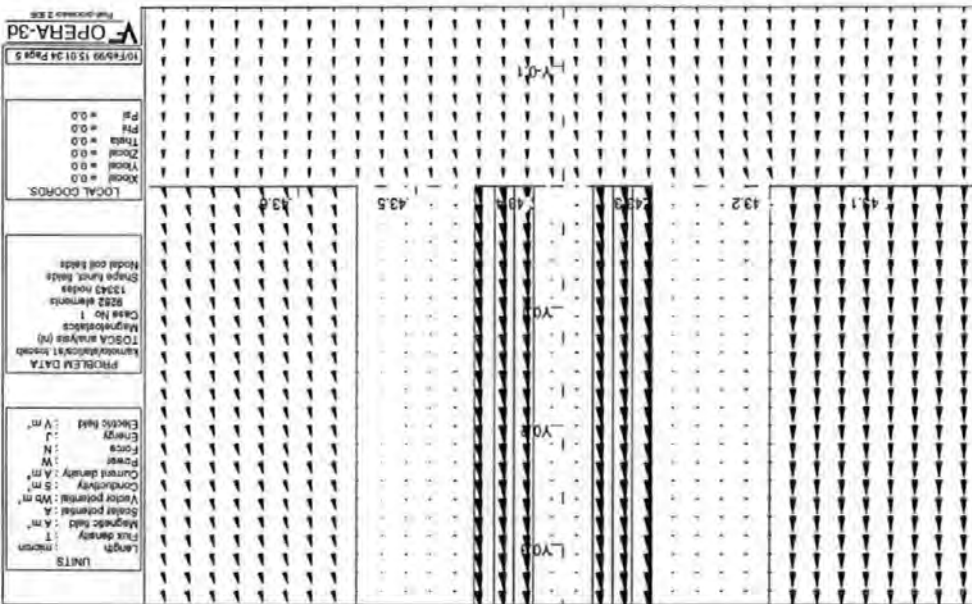


Figure 2.44: Field mappings of crossed situations around the read gap region in the non-magnetic separator design, at a selected applied magnetomotive force 0.60 AT through the writing coil.



2.14 Summary

Firstly in this chapter analytical models have been utilized to simulate the crossfeed problems in read-while-write (RWW) tape heads. The simplified analytical models discussed in this chapter incorporate the essential details of read and write processes while remaining computationally tractable. For those interested in quickly seeing the consequences of a design iteration, simplified analytical models can be extremely valuable. The most significant contributors, such as inter-shield spacing and reproductive mode, have been identified. A new Thin-Film Inductive/ Dual-Magneto-Resistive tape head design was found to reduce the crossfeed by about a factor of thirty, compared with the conventional shared-pole design, which is the most usual approach for achieving simultaneous read and write operations in both single-track and multi-track cases.

A 3D Finite Element Method (FEM), suited to study more detailed contributors (e.g., various screening schemes), was then used to give more exact results. The crossfeed performances over the surface of read-while-write (RWW) tape heads with several different screening schemes have been quantitatively simulated. The replay processes on a three (or two) bits medium have also been quantitatively simulated. In addition to the calculation mentioned above, we also considered two other examples to give a complete picture of crossfeed contributors: the separator type head with $9\ \mu\text{m}$ thickness and the laminated-separator type head with $9\ \mu\text{m}$ thickness (the packing factor is 0.5). In the case of $9\ \mu\text{m}$ separator, the SAL crossfeed is $0.0395\ \text{T}\cdot\mu\text{m}^3$ while the DMR crossfeed is $0.0063\ \text{T}\cdot\mu\text{m}^3$. In the case of $9\ \mu\text{m}$ laminated-separator (the packing factor is 0.5), the SAL crossfeed is $0.0267\ \text{T}\cdot\mu\text{m}^3$ while the DMR crossfeed is $0.0045\ \text{T}\cdot\mu\text{m}^3$. Table 2.4 summarizes the SCR of various head designs. Their SCR vs gap-separation characteristics are depicted in Figure 2.46.

In summary:

(a) The SCR increases as the gap-center separation increases. The (non-magnetic

Separation	Head structure					
	Shared-pole		Separator		Laminated	
	SAL	DMR	SAL	DMR	SAL	DMR
3.775 μm	7.9dB	22.6dB	7.9dB	22.6dB	7.9dB	22.6dB
9.775 μm			10.6dB	28.6dB	12.0dB	30.4dB
15.775 μm			18.4dB	35.9dB	21.8dB	38.8dB

Table 2.4: The SCR(Signal-Crossfeed-Ratio) of various head designs. In the separator design the material of the separator is non-magnetic. In the laminated-separator design, the packing factor is 0.5.

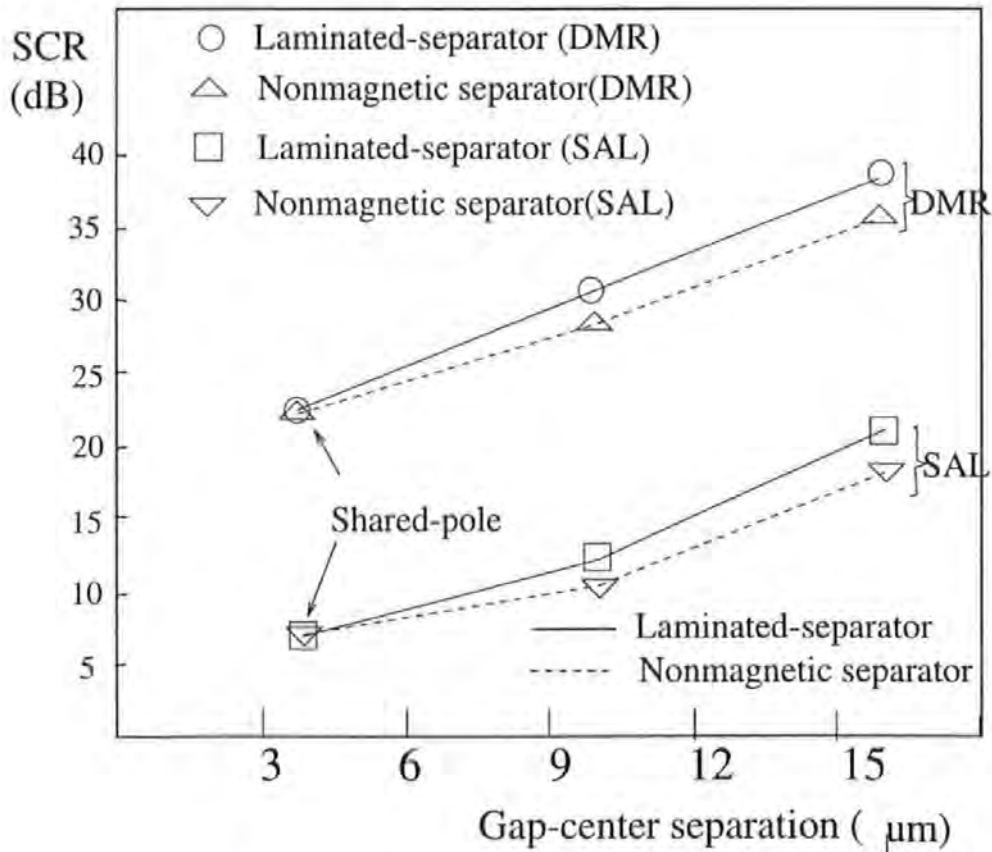


Figure 2.46: SCR vs. gap separation characteristics. Here the thickness of the laminated-separator is 3 μm and the packing factor for the laminated-separator design is 0.5.

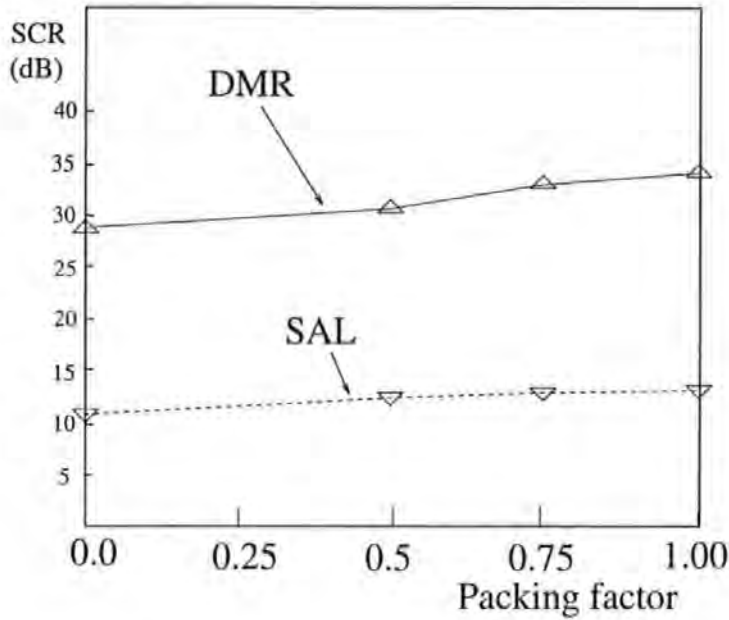


Figure 2.47: Lamination packing factor effect.

or laminated) separator plays a very important role in reducing crossfeed from the write head to the MR sensor. Generally the SCR in the separator design ($3 \mu\text{m}$ separator thickness) is 3-8 dB higher than that in the shared-pole design;

(b) The laminated-separator design is effective in reducing the crossfeed. Figure 2.47 shows the lamination packing factor effect. As illustrated earlier, the shields serve mainly to transport part of the flux from the write head back to the writing coil in the RWW operation. From this standpoint, the transporting efficiency is considerably improved when laminated metallic magnetic materials with a high packing factor are used. The higher the lamination packing factor, the more efficient the transportation becomes. The shields with a high packing factor act more as alternative low-reluctance paths which divert the crossfeed fields away from the MR element. But there is a saturation of increasing SCR when the packing factor approaches 1.00. Generally the SCR in the laminated-separator design is 2-3 dB higher than that in the (non-magnetic) separator design;

(c) The DMR reproductive method is effective in reducing the crossfeed. The SCR in the DMR designs is generally 15-18 dB higher than that in the SAL reproductive design.

In summary, the best scheme to suppress the crossfeed field from the write head in a RWW tape head is to employ the so-called laminated-separator head configuration and simultaneously employ a Dual-MR sensor instead of a traditional SAL MR sensor. The SCR is 28.6 dB for the head with 3 μm non-magnetic separator or 30.4 dB for the head with 3 μm laminated-separator beside the inserted pole (packing factor is 0.5). Obviously, the latter is more practical due to its high SCR together with high mechanical strength. To reduce the manufacture cost, the shared-pole DMR configuration is also acceptable. Its SCR is 22.6 dB.

Chapter 3

Magnetodynamics

3.1 Introduction

The aim of this chapter is to find a practical solution for the suppression of crossfeed field under Read-While-Write (RWW) operation at a high working frequency. For this reason, the effects of eddy currents in the conductive head yokes must be included. Optimally, a sudden reversal in the current direction would cause a sudden reversal of the head field (i.e., a fast rise time). But eddy currents in the head yokes would act like a choke to slow the reversal of the head field.

A growing number of magnetic recording equipment manufacturers employ thin-film technology to fabricate magnetic recording heads. A typical design for a thin-film-magnetoresistive head is shown in Figure 3.1. There are many advantages to this approach, with perhaps the most important being the ability to produce extremely narrow pole tips and recording gap widths in the thin-film process. These narrow pole tips, in turn, permit the density of magnetic recording to be increased. Unfortunately, the very feature of these heads which make them attractive for use in the recording process, namely, their small size, also makes thin-film heads difficult to study experimentally. In these circumstances, analytical and numerical methods of estimating crossfeed in single and multitrack thin-film/MR heads under both DC and AC excitations can often help a head designer understand how the crossfeed field spreads and therefore how to suppress the crossfeed field from the standpoint

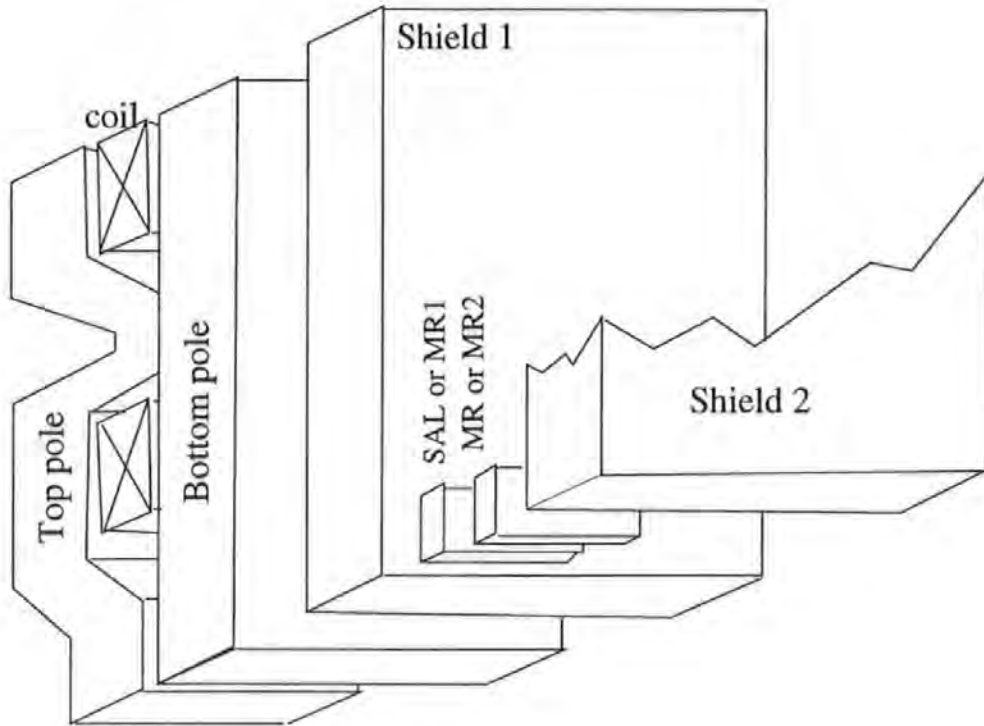


Figure 3.1: A typical thin-film-magneto-resistive head. This is the so-called separator design.

of an overall head configuration.

The increasing use of high frequencies in magnetic recording, along with the appearance of high-performance head materials, such as Sendust with finite conductivity and Ferrites with a complex permeability, has stimulated an increased interest in the magnetic fields of heads having solid pole tips made from these materials. Such dynamic field calculations are often too complicated by purely analytical methods. However, the availability of digital computers makes possible the numerical solution of the sinusoidally varying fields for heads with finite conductivity. Solutions can also be obtained for heads with complex permeability.

Currently, a high frequency response is required with increasing linear density and data transfer rate. That is to say, in order to realize a high data transfer rate,

high frequency write/read performance together with high movement velocity of medium and high recording density is necessary. Consider the examples of a hard disk drive[43]: in the case of 12 MB/s 1-7 code transformation the corresponding frequency is 36 MHz whereas in the case of 8/9 code transformation the corresponding frequency is 54 MHz. Furthermore, if 20 MB/s 1-7 code transformation is used, a high-frequency driving current of 90 MHz has to flow through the recording head. At such high frequencies, the effect of eddy current loss is significant, so precise understanding of the recording field and the crossfeed field is very important when designing high density and high speed data storage systems. Consider another example of a tape drive[1]: the rotary head systems used in the instrumentation and computing areas are based on either the VHS/8mm video format or the rotary head digital audio tape recorder (R-DAT) which has been developed for consumer application. The high tape/head velocity, plus the use of helical scan techniques can accommodate very high densities. The R-DAT cassette measures 7.3 cm \times 5.4 cm. An areal storage density of 176 kbits/mm² is typical, with total capacity amounting to 2 Gbytes. Data transfer rates as high as 12 MB per second are possible.

Previous analytical work on recording heads has almost exclusively dealt with magnetostatics and has ignored eddy current effects. In this chapter, we will use a 3D magnetodynamic computer package to compute the characteristics of thin-film heads over a range of frequencies and determine the magnetic field distribution produced by the heads under a variety of conditions. The RWW operation in the presence of a keepered medium will also be referred to in Section 3.8.

3.2 3D FEM Magnetodynamic Methodology

The ELEKTRA-3D Vector Fields Electromagnetics Analysis Package is used to compute electromagnetic fields including the effects of eddy currents, in three dimensions[34]. The program incorporates state of the art algorithms for the calculation of electromagnetic fields and advanced finite element numerical analysis procedures. The

approach is based on a combination of vector magnetic potentials in conducting media and scalar magnetic potentials in the rest of space to model time-varying electromagnetic fields. Finite element discretization forms the basis of the methods used in these analysis programs[44].

3.2.1 Vector Potential in Three Dimensions

The use of the (total) scalar potential is limited to cases where currents do not exist in the problem, otherwise Ampere's Law is violated. If a 3-D region contains source current density, I_s , then it is still possible to use a scalar potential approach by the introduction of the so-called reduced scalar potential. This relies on the current having a known value and distribution, i.e. there are predefined source currents. When eddy currents are induced in conductors, the current distribution is no longer known beforehand, so Biot-Savart integrals cannot be used. In this case, it is necessary to solve for the Magnetic Vector Potential, \vec{A} .

The relationship between electric field \vec{E} and magnetic flux density \vec{B} is given by Faraday's law[45]

$$\text{rot}\vec{E} = -\frac{\partial\vec{B}}{\partial t} \quad (3.1)$$

According to the definition of the magnetic vector potential \vec{A} : $\text{rot}\vec{A}=\vec{B}$ ($\text{div}(\text{rot}\vec{A})\equiv 0$), Formula 3.1 becomes

$$\text{rot}\vec{E} + \frac{\partial}{\partial t}\text{rot}\vec{A} = \text{rot}\left(\vec{E} + \frac{\partial\vec{A}}{\partial t}\right) = 0 \quad (3.2)$$

Since $\text{rot}(\text{grad } V) \equiv 0$, where V is any scalar potential, this shows that the potential V (either the total potential ψ or the reduced potential ϕ) must also be included in the analysis. That is

$$\vec{E} + \frac{\partial\vec{A}}{\partial t} = -\text{grad}V \quad (3.3)$$

The electric field \vec{E} results in

$$\vec{E} = -\frac{\partial \vec{A}}{\partial t} - \text{grad}V \quad (3.4)$$

The relationship between \vec{A} , \vec{J} (current density) and V is given by Ohm's law

$$\vec{J} = -\sigma \frac{\partial \vec{A}}{\partial t} - \sigma \text{grad}V \quad (3.5)$$

where σ is the electrical conductivity. So that, for example, the x-component of current density is

$$J_x = -\sigma \frac{\partial A_x}{\partial t} - \sigma \frac{\partial V}{\partial x} \quad (3.6)$$

3.2.2 Fields in Non-Conducting and Conducting Volumes

ELEKTRA can use a combination of vector and scalar magnetic potentials to model time varying electromagnetic fields. In time-varying fields the currents that are induced in conducting volumes are part of the unknowns in the system. Their fields cannot therefore be evaluated by simple performing an integration. Inside the conducting volumes the field representation must include a rotational component. The most elegant approach is to combine the efficient total and reduced scalar potential method for non-conducting volumes, as mentioned in the last section, with an algorithm that uses a vector potential (\vec{A}) in the conducting volumes.

3.2.3 Time Variation in ELEKTRA

In a low-frequency time-varying magnetic field when the dimensions of the objects in the space are small compared to the wavelengths of the fields, the magnetic and electric fields are related by the low frequency limit of Maxwell's equations. There are three ELEKTRA analysis modules which each solve a different form of time variation.

- ELEKTRA/SS calculates steady-state ac currents (the time harmonic form) where all fields and potentials are oscillating at the same frequency.
- ELEKTRA/TR calculates transient eddy currents induced by the fields of driving currents which change in time in a predetermined way, e.g. STEP, RAMP, SINE, COSine, PEAK, RISE or TABLE function.
- ELEKTRA/VL calculates eddy currents induced by motion which does not change the geometry of the problem.

3.2.4 Computational Effort

As mentioned above, the eddy current effects must be modelled with Vector Potential. However Vector Potential has 3 components and so the computational effort to solve such a problem is greater than for TOSCA. Sometimes, the number of elements will be reduced in the problem. With regard to the display of results, fields may be evaluated either from the shape function derivatives, or better still from the nodally averaged field.

As in TOSCA, it is necessary to change the potential type of some of the air, as conductors must be placed within a reduced potential volume in ELEKTRA. If this is not the case the model would be multiply-connected (The multiply-connected region is most easily described as being able to create a closed loop around the conductor through TOTAL potential regions only.) and this is in violation of the formulation.

3.2.5 An Eddy Current Example

An example is a conductive sheet with an exciting coil in its geometric center. This example model will be created in the OPERA-3D Preprocessor and analysed using

ELEKTRA/SS analysis modules. The results of this analysis will then be examined using the OPERA-3D Postprocessor.

Figure 3.2 and Figure 3.3 show how an AC magnetic field penetrates a sheet of conductive material. Because the field changes its value and direction all the time, circulating currents are induced inside the sheet, although the distribution is seriously distorted when the coil is shifted at its edge (Figure 3.3), in accordance with Lenz's law[45].

This law is similar to Le Chatelier's law[1], which states that all systems at rest will react to an outside change by an action that opposes the change. Lenz's law applies specifically to the induced currents, making them have direction so they create a field that is in opposition to the field that creates them.

If the AC field varies fast enough (higher frequency), then the induced fields may completely oppose the outside field, an effect used in shielding. The effectiveness of such shielding is not reduced by drilling a number of small holes in the sheet, since the circular currents still are operative. An example in daily life is the door of a microwave oven, where holes permit the user to look at the destruction of a good filet mignon, but the field cannot radiate out.

When the eddy currents are strong enough, no magnetic field goes through the center section of the sheet. Since the eddy currents increase with frequency, we will, with increasing frequency, have the flux concentrated at the edge of the sheet. It is then logical to talk about a surface flux that only penetrates into the sheet to a certain depth, the skin depth.

This skin depth is small for materials with high permeability μ_r and small resistivity ρ ; and it does decrease with higher frequencies. We could therefore, in our expression for the magnetic resistance of the pole (part of ΣR_m), substitute the area with an effective area, that decreases in size with increasing signal frequency.

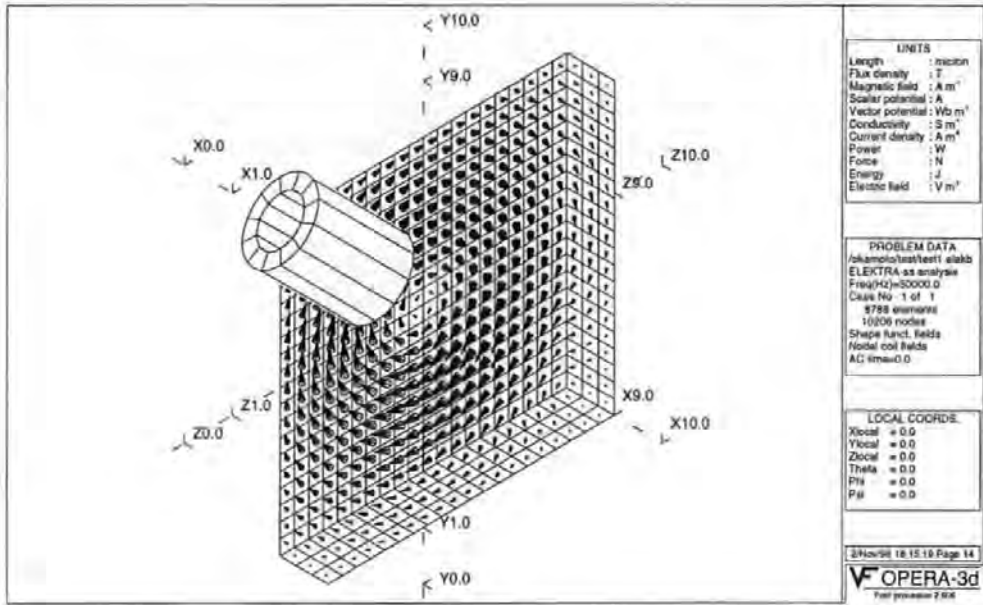


Figure 3.2: Eddy currents in a conductive sheet with an exciting coil in its geometric center. An applied field induces an eddy current that in turn produces a counteracting field. The two fields cancel at the center, but not at the edges (skin depth).

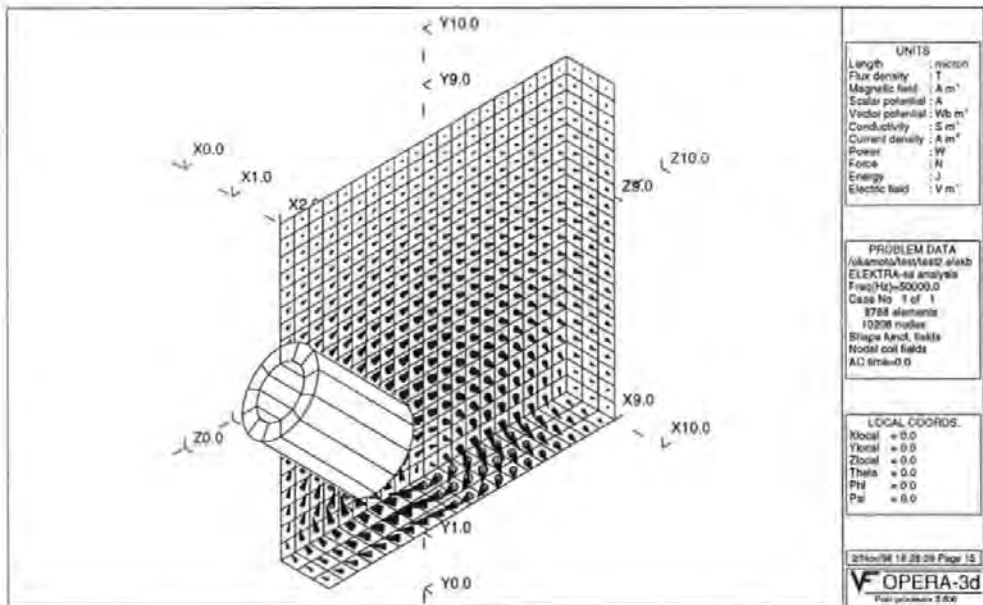


Figure 3.3: Eddy currents in a conductive sheet with an exciting coil at its edge. Induced circulating currents are still seen though they are seriously distorted when the coil is shifted at the edge of the sheet.

It is also intended to model the lamination arrangement for a typical write-read head to see how packing factor of the lamination pattern can be optimised. Electrically conducting and magnetically screening materials will need to be explored both simultaneously and separately in the model. The performance of such screens will vary with frequency depending on the frequency response of the head and the screens themselves. In this respect, bearing in mind that skin-depth is an important parameter in real heads, there will only be a limited extent to which the computer model can produce results identical to those found in practice. The computer model will be more accurate for this purpose. The skin depth can be calculated from[1]:

$$\delta = \left(\frac{1}{2}\pi\right) \cdot \sqrt{\rho/\mu_r f} \quad (3.7)$$

where

ρ = resistivity in $\mu\text{ohm}\cdot\text{cm}$

μ_r = relative permeability (at DC)

f = frequency in kHz.

This formula will allow the calculation of the area available for the flux, at each frequency we desire. The use of these values in the expressions for the efficiency and the inductance will indeed show a decrease in the value of each as we raise the frequency.

It will not provide an answer to the increase in resistance. Upon studying the literature we learn that a complex value for the permeability must be used[1]:

$$\mu = \mu' - j\mu'' \quad (3.8)$$

where j is the complex number $\sqrt{-1}$.

The complex permeability is not a true material constant — it depends not only

upon the material, but also its shape and the signal frequency.

3.3 Magnetodynamic RWW Head Model

In this chapter, we will choose the non-magnetic separator design to typify the RWW heads. A co-sinusoidal exciting current is applied through write coil and in most cases, except for special demonstration, only the results at time = 0 will be given.

The fabrication technique of a typical thin-film head has been borrowed from the semiconductor industry for fabrication of integrated circuits. Different layers are deposited onto an insulating substrate (silicon). The copper has been shaped into a multi-turn conductor and magnetic top and bottom poles are joined at the center of this conductor and there is no back gap. The front gap for an inductive head is controlled by a thin insulating layer. A Magneto-Resistive (MR) reproducing element is inserted between two shields. All the dimensions are taken according to a new generation head TR5 produced by the Read-Rite company[41], as used in Chapter 2. The poles are $3.0 \mu\text{m}$ thick. The optimum design of the pole thickness is very important in achieving high frequency recording with thin film heads. Increasing the pole thickness is believed to be an effective way to increase the maximum field intensity to prevent magnetization saturation of the pole tips. However, an increase in the pole thickness significantly degrades the frequency response. Considering the relatively low working frequency in magnetic tape units, here we adopted a relative large pole thickness. The throat height is $5 \mu\text{m}$. The write head gap is $1.20 \mu\text{m}$. The angle of the inclination of the top pole near the zero-throat point is 45° . The tip widths of the top pole, the bottom pole and the two shields are $61 \mu\text{m}$, $100 \mu\text{m}$ and $140 \mu\text{m}$, respectively. The top pole and the bottom pole are $10 \mu\text{m}$ apart in the yoke region. Overall they are about $140 \mu\text{m}$ high and $140 \mu\text{m}$ wide. The head coils are assumed to be a single turn, and the applied magnetomotive force is 0.60 A-turns. This is approximately equivalent to a write current of 40 mA 0-p for a 15-turn coil. The MR stripe track width is $22.9 \mu\text{m}$, the thickness 500 \AA and the

depth 2.5 μm .

3.4 Three Dimensional Dynamic Magnetic Field

As the linear recording density of magnetic storage systems increases, recording heads which can produce strong fields with steep field gradients are necessary in order to record the data patterns with sufficient overwrite characteristics on high coercivity media. Recording frequency, as well as linear recording density, must be increased to obtain higher data transfer rates. Currently, the highest data recording frequency is over 90 MHz in hard disk drives and 54 MHz in the rotary head digital audio tape recorder (R-DAT). At such high frequencies, the effect of eddy current loss is significant so precise understanding of the recording field is very important when designing high density, high speed data storage systems.

The dynamics of magnetization response in thin-film head yokes has been investigated. The three dimensional fringing fields of these heads are calculated. The magnetic poles are excited by a co-sinusoidal current (I_w) from 0 to 53.3 mA pp. Field intensity increases in proportion to I_w , and at $I_w = 40$ mA 0-p, the magnetic pole is almost saturated and the maximum value of 3667 Oe (DC, longitudinal field component) is reached, as shown in Figure 3.4. This figure reveals a clear dependence of frequency response on drive current: better response characteristics are obtained with higher drive currents. In the range of $I_w \leq 40$ mA 0-p, the intensity drops as the MMF decreases, while in the range of $I_w \geq 40$ mA 0-p, the intensity is almost a constant up to 10 MHz.

Field intensities and distributions are also calculated as a function of recording frequency. The maximum field intensities in the bit direction and phase angle are plotted as a function of recording frequency for each excitation, as shown in Figure 3.5. It is found that little difference due to recording frequency is observed between the results at 0.25 MHz and at 1 MHz for the 40 mA 0-p excitation. Frequency

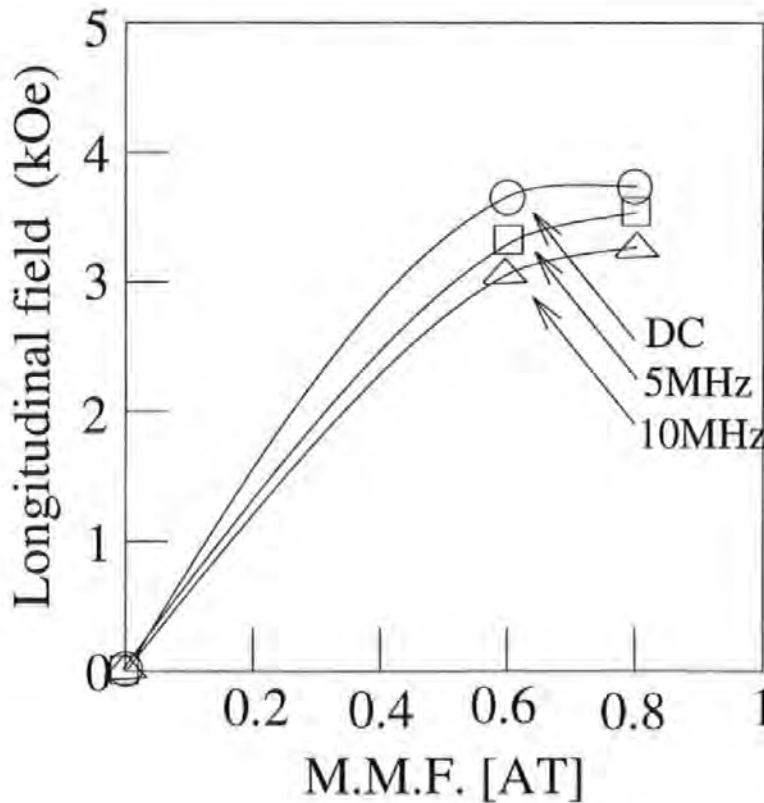


Figure 3.4: Field vs. MMF (Magneto-Motive Force).

responses are extremely degraded and field intensity begins to drop at frequencies higher than 1 MHz. The field intensity at 50 MHz decreases by about 15% at 40 mA 0-p excitation. Degradation of these frequency responses indicates the significant effect of the eddy current loss in the pole thickness direction.

Field response vs. cosinusoidally-varying write current at 50 MHz is shown in Figure 3.6. The value of the current (I_w) is 40 mA 0-p. There is approximately a 30 degrees phase shift between the write current and the peak field at the gap center. Such a phase shift is also due to the eddy current loss and it is equivalent that the resultant write field lags the original write current by about 2 ns at 50 MHz. This phase shift increases with the frequency's increasing and makes the recording pro-

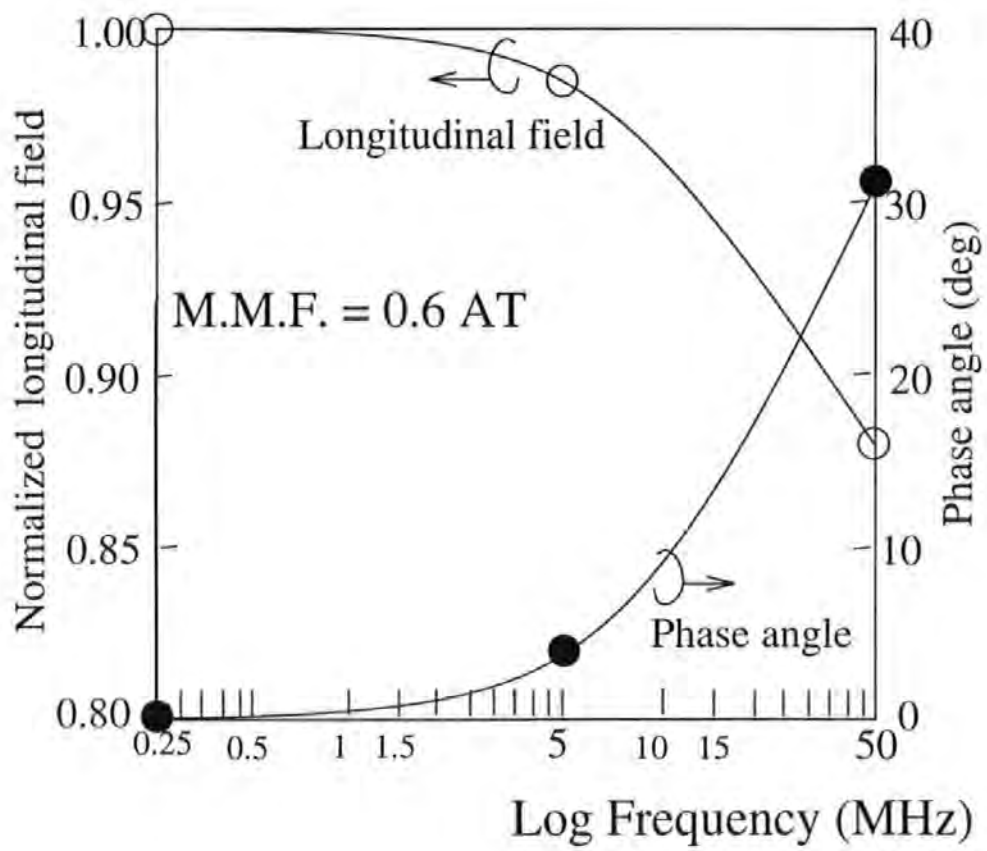


Figure 3.5: Frequency dependence of the normalized field intensity and phase angle.

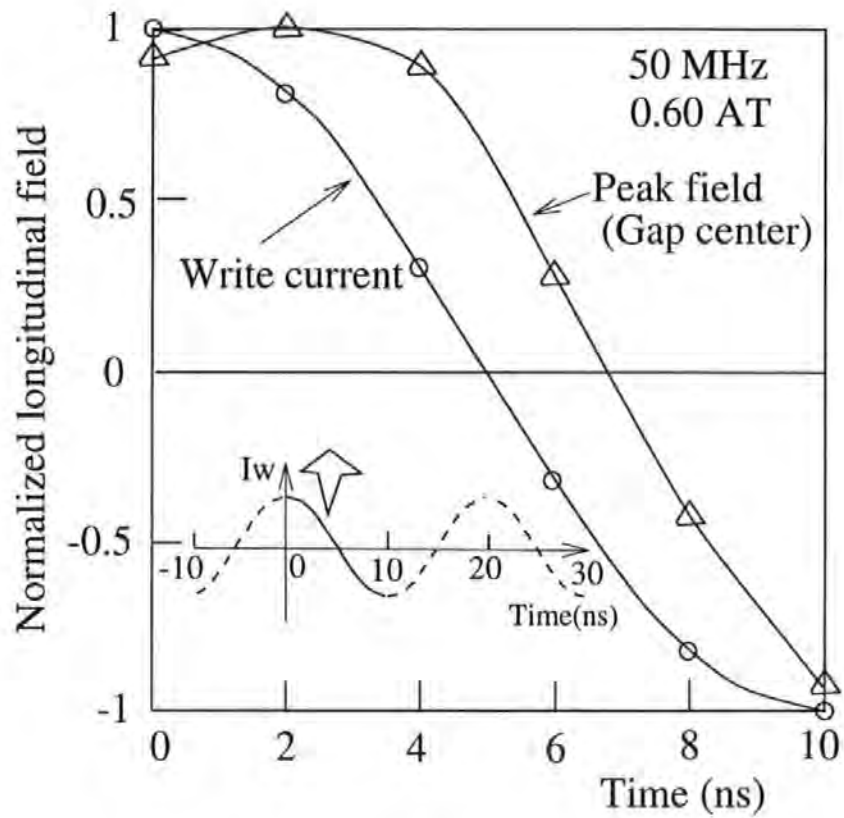


Figure 3.6: Field response vs. write current.

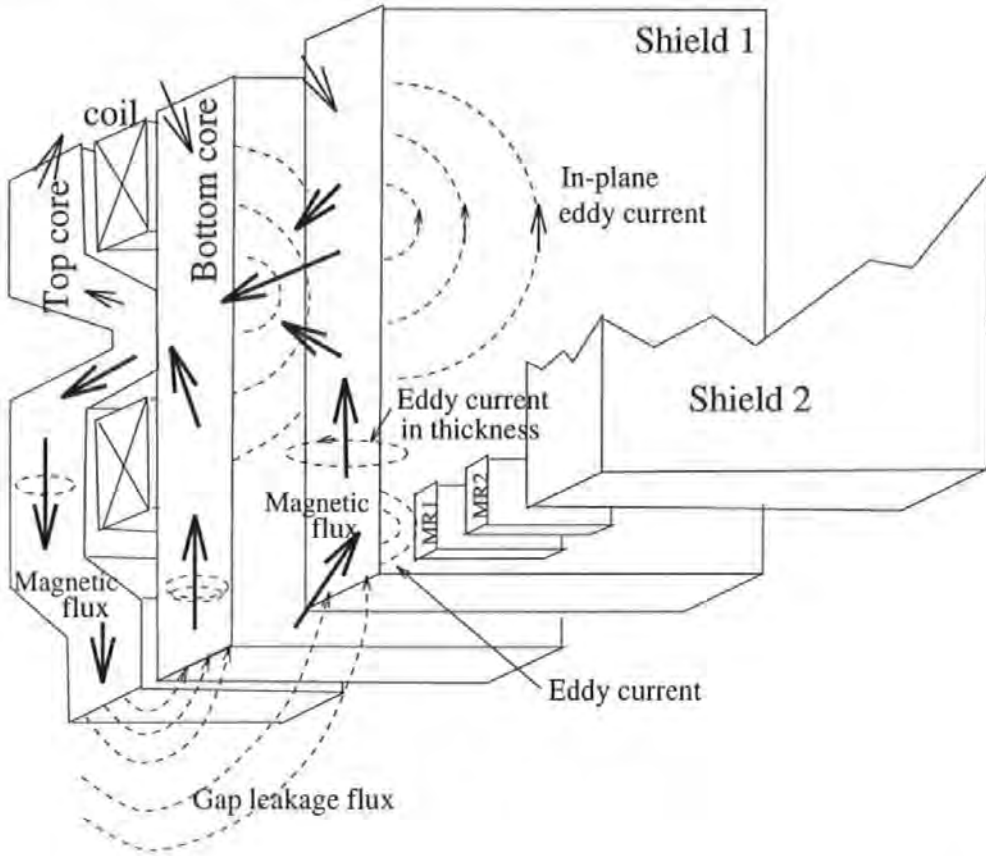


Figure 3.7: Magnetic flux and eddy current distribution in a typical RW head. Due to the high conductivity, the flux penetrating through the shield induces an in-plane eddy current that in turn produces a counteracting field to block the penetrating flux through the shield.

cess complicated at high linear density and transfer rates. Nevertheless, the phase shift may be ignored when analyzing RW operations since magnetic tape units normally operate at relatively low linear density and transfer rates.

3.5 Using Low Conductivity Materials

In the RW operation, the shields serve mainly to transport part of the flux from the write head back to the writing coil, as illustrated in Figure 3.7. The principle has also been illustrated in Chapter 2. Due to the high conductivity, the flux penetrating through the shield induces an in-plane eddy current that in turn pro-

<i>Materials</i>	<i>Properties</i>			
	Permeability	Coercivity(Oe)	Magnetization(T)	Conductivity(S/m)
Permalloy	2,000	0.05	0.9	6.25e6
Sendust	6,000	0.06	1	1.1e6
MnZn ferrite	4,000	0.1	0.55	0.7
FeSi	3,000		1.7	1e7
NiFeNb	2,000		1.0	1e7
CoTaZr	6,000	5	1.3	1.11e6
Fe-Al-O	800	1.5	0.95	2.86e4
FeN	6,000		1.9	1e7
(Cu)				6e7

Table 3.1: Properties of soft magnetic materials.

duces a counteracting field to block the penetrating flux through the shield. At the high frequencies encountered in digital recording, the high conductivity of metallic magnetic materials, e.g., FeN with a conductivity of 1×10^7 S/m, represents an increased reluctance (above air) due to the eddy-currents phenomenon, to the crossfeed fields. This causes the crossfeed fields to forcibly interfere with the MR element behind the shield.

In this regard, the transporting efficiency is considerably improved when magnetic materials with low conductivities are used. The shields with a low conductivity act more as alternative low-reluctance paths which divert the crossfeed fields away from the MR element. Recently, Fe-Al-O films with a nano-granular structure were successfully fabricated by RF magnetron sputtering[46]. These films exhibit good magnetic softness together with low electrical conductivity of 2.86×10^4 S/m. The amorphous CoTaZr head with 1.3 T saturation flux density B_s and zero magnetostriction shows superior frequency response, and constant field intensity is maintained up to 30 MHz, regardless of drive current. The use of higher saturation flux density films, such as Co-based amorphous films or Fe-based crystalline films has also been focused. Table 3.1 summarizes the properties of soft magnetic materials.

The ELEKTRA results, as shown in Figure 3.8 and Figure 3.9, confirm the in-plane eddy current distribution resulting from the flux transportation by the conductive magnetic shields. That is to say, the shielding efficiency depends partly on the flux transport in the magnetic shields. It is advantageous to use magnetic materials with a low conductivity to prevent eddy currents, as shown in Figure 3.10 and Figure 3.11. The eddy current intensity is drastically reduced by using low conductivity film for the poles and shields. This head exhibits a great improvement in suppressing crossfeed field. The corresponding crossfeed reduction is 7 % in the SAL case and 8 % in the DMR case when Fe-Al-O is used compared with conventional FeN material at a working frequency of 5MHz. Our interpretation of this result is that the eddy current loss is reduced because of the increased resistivity of the poles and shields (conductivity was decreased from 1×10^7 S/m to 2.86×10^4 S/m). In summary, the requirements below are needed for the selection of head pole and shield materials:

1. High permeability for high efficiency;
2. High saturation magnetization for high head field;
3. Low coercivity for low hysteresis;
4. Low conductivity for low eddy current losses.

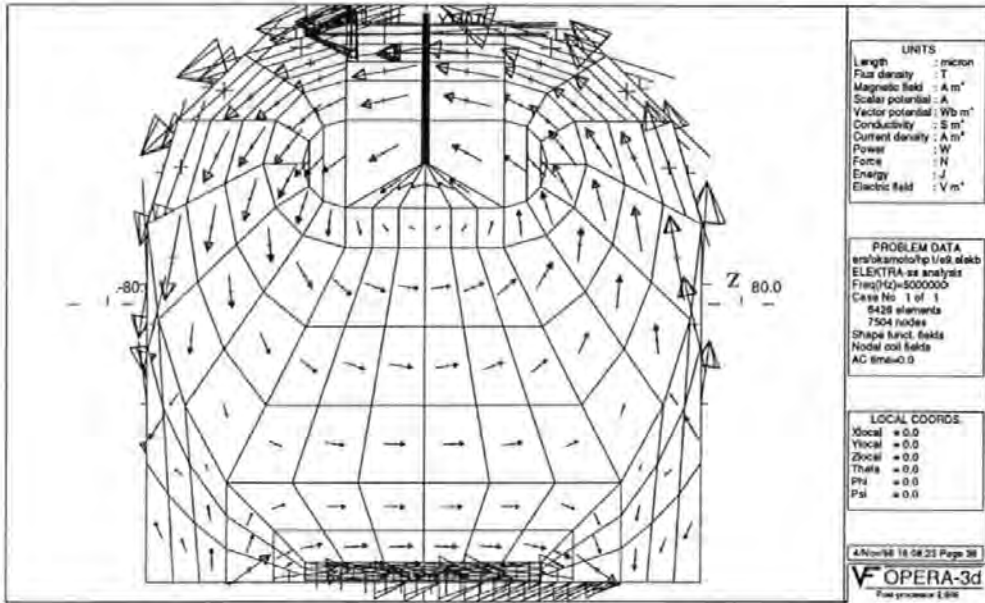


Figure 3.8: Eddy current distribution in the conventional shield (Shield 1 near the bottom pole) under a 5 MHz co-sinusoidal write current at time = 0. The material of the shields is FeN with a conductivity of 1×10^7 S/m. The finite-element mesh is also shown.

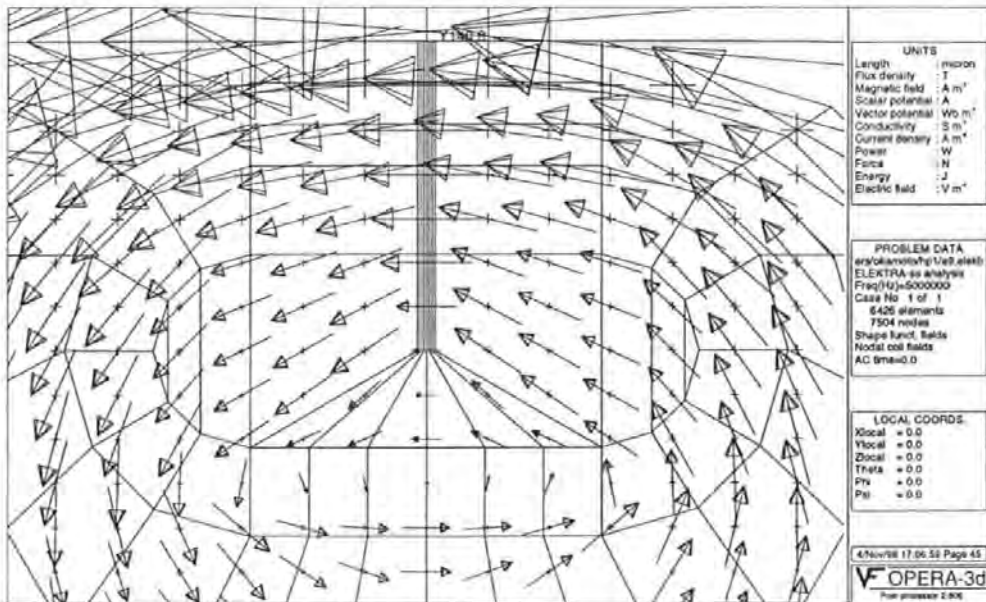


Figure 3.9: Magnified eddy current distribution in the conventional shield (Shield 1) at time = 0. The material of the shields is FeN with a conductivity of 1×10^7 S/m.

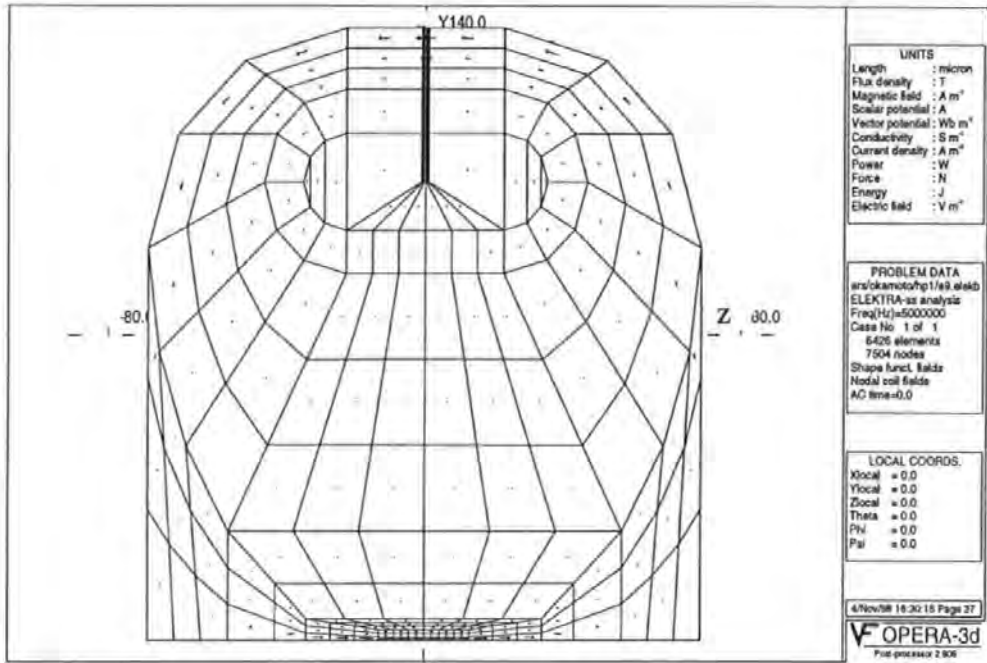


Figure 3.10: Eddy current distribution in the low-conductivity (2.86×10^4 S/m) shield (the top one near the bottom pole) under a 5 MHz co-sinusoidal write current at time = 0. The material of the shields is Fe-Al-O. The finite-element mesh is also shown.

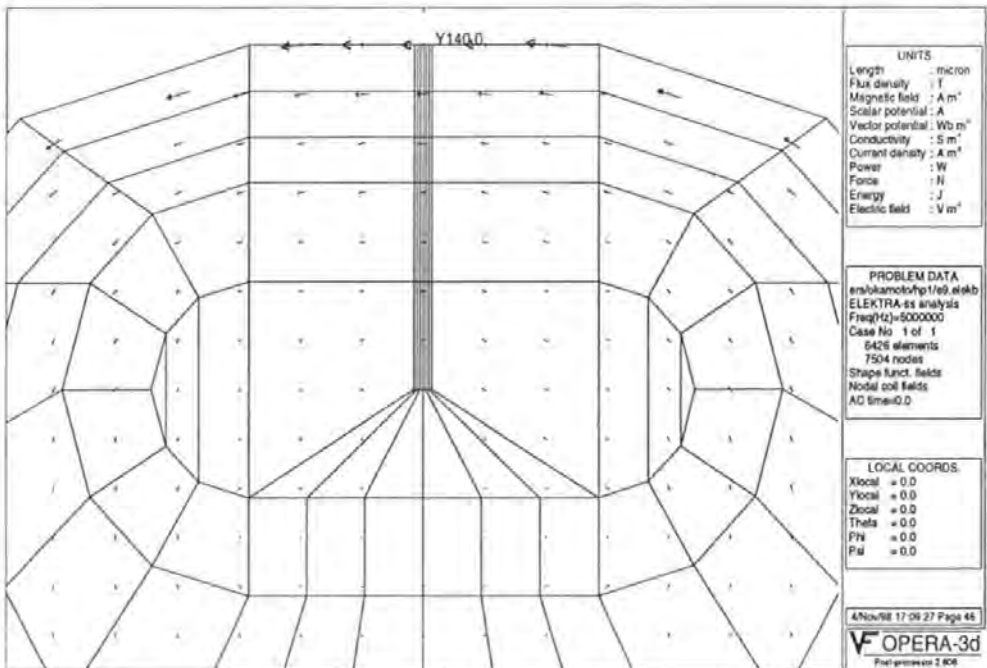


Figure 3.11: Magnified eddy current distribution in the low-conductivity Fe-Al-O shield (2.86×10^4 S/m) at time = 0.

3.6 Cutting a Slot

As mentioned in the last section, the shields with a low conductivity act more as alternative low-reluctance paths which divert the crossfeed fields away from the MR element. Nevertheless, in order to allow the head to write to the high coercivity (2000 Oe) metal particle medium, the pole material is still expected to be chosen as an excellent soft magnetic film FeN with a saturation magnetization of 1.9 Tesla, an initial permeability of 6000 and a conductivity of 1×10^7 S/m. Due to the high conductivity, the flux penetrating through the shield induces an in-plane eddy current (in Figure 3.8 and Figure 3.9) that in turn produces a counteracting field to block the penetrating flux through the shield.

We propose here a possible way to prevent these eddy currents by cutting a slot through the metallic magnetic bottom pole and shields[34]. The schematic of cutting a slot is illustrated in Figure 3.12. A slot with a depth of $35 \mu\text{m}$ and a width of $2 \mu\text{m}$, ending at the nominal center of the coil, has been cut. As can be clearly seen in Figure 3.13 and Figure 3.14, the in-plane eddy currents have been retarded and the strength of the in-plane eddy currents has been reduced to around half of that in the conventional case shown in Figure 3.8 and Figure 3.9. The corresponding crossfeed reduction is 3% in the SAL case and 5% in the DMR case when a slot is cut compared with the conventional case at a working frequency of 5MHz.

Eddy current distributions along the vertical symmetric line in the conventional top shield (Shield 1) and the improved top shield are shown in Figure 3.15 and Figure 3.16, respectively. A comparison of normalized crossfeed response vs. phase angle for heads with and without slot is shown in Figure 3.17. It has been shown in this section that it is advantageous to cut a slot through the metallic magnetic pole and shields to prevent eddy currents.

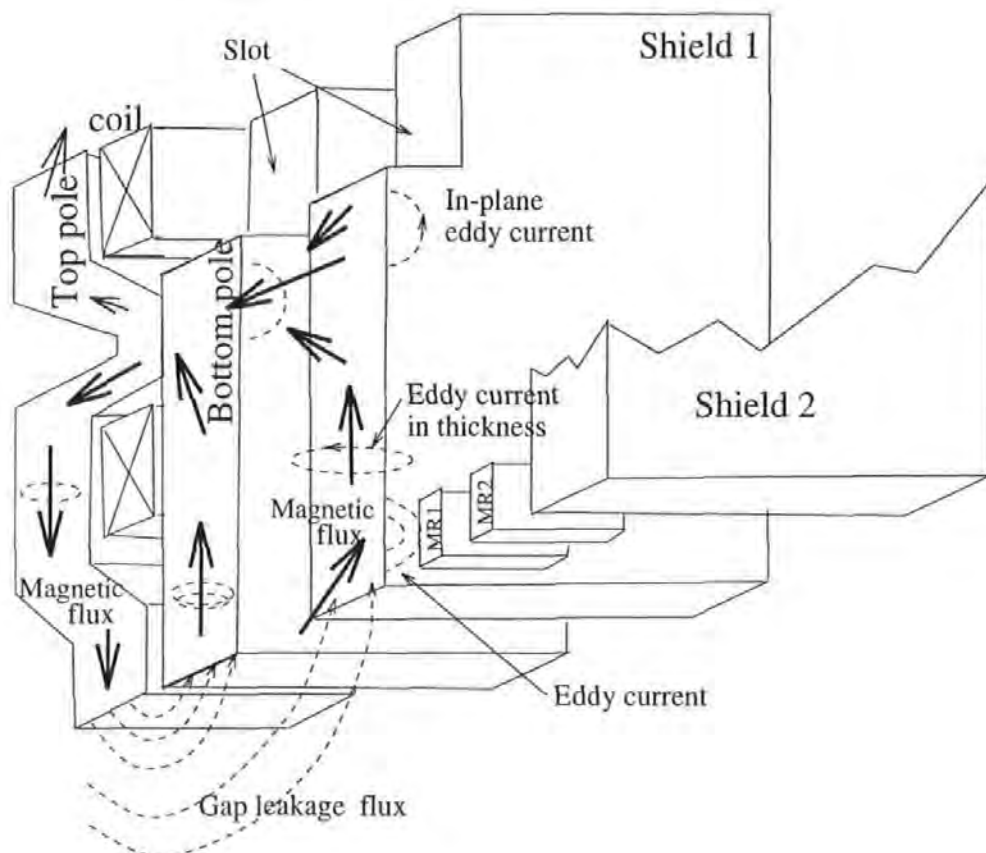


Figure 3.12: Magnetic flux and eddy current distribution for head with a slot. The in-plane eddy currents have been retarded by the slot.

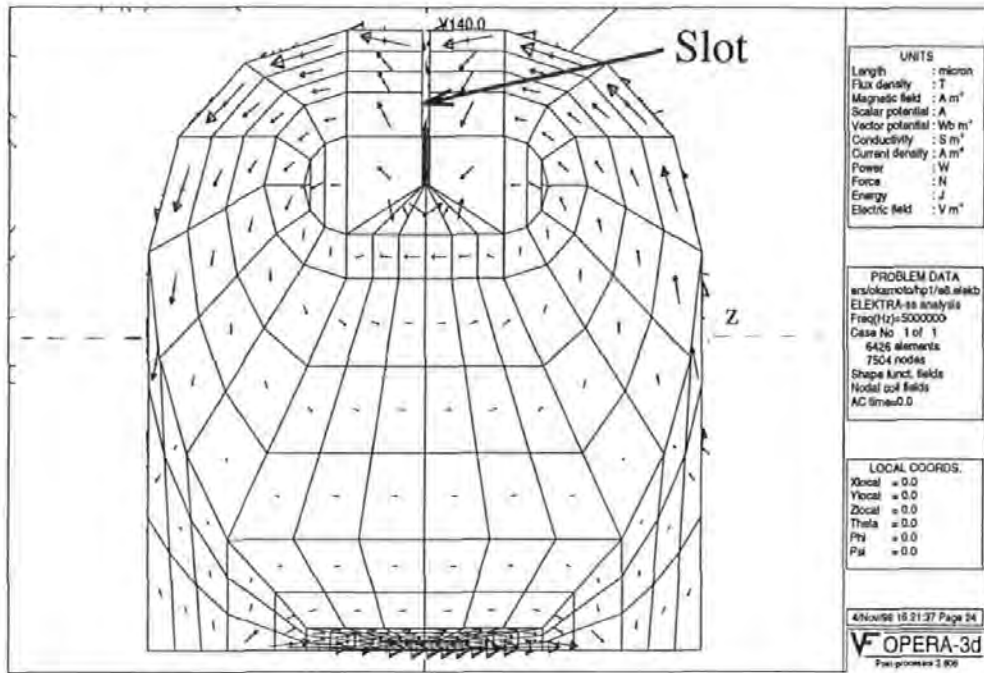


Figure 3.13: Eddy current distribution in the improved shield (Shield 1, FeN) with a slot, ending at the nominal center of the coil, under a 5 MHz co-sinusoidal write current at time = 0.

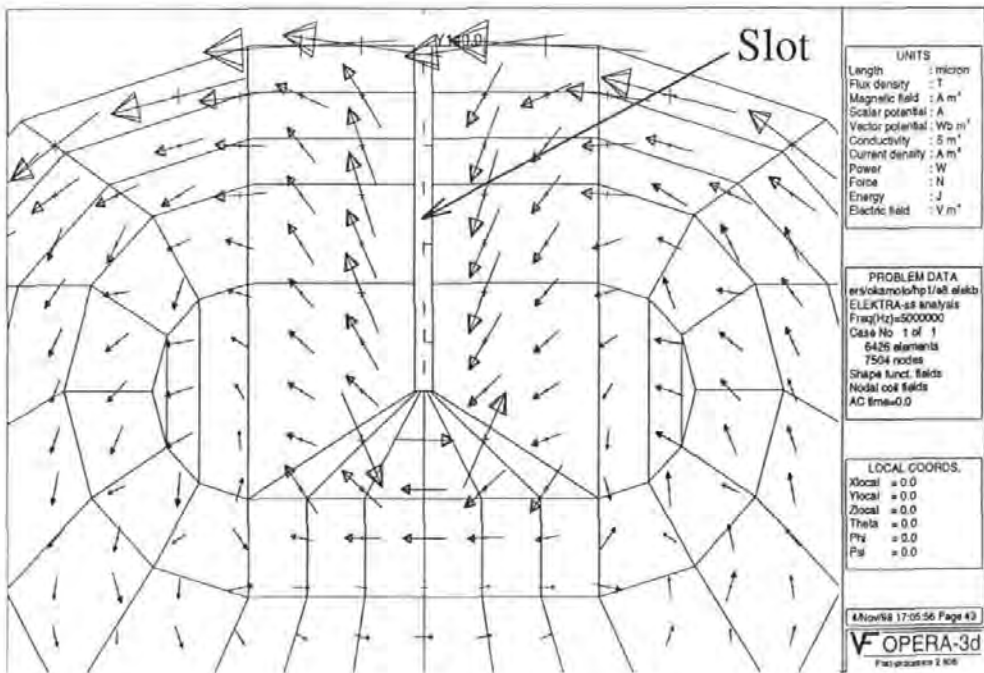


Figure 3.14: Magnified eddy current distribution around the slot in the improved shield (Shield 1) at time = 0.

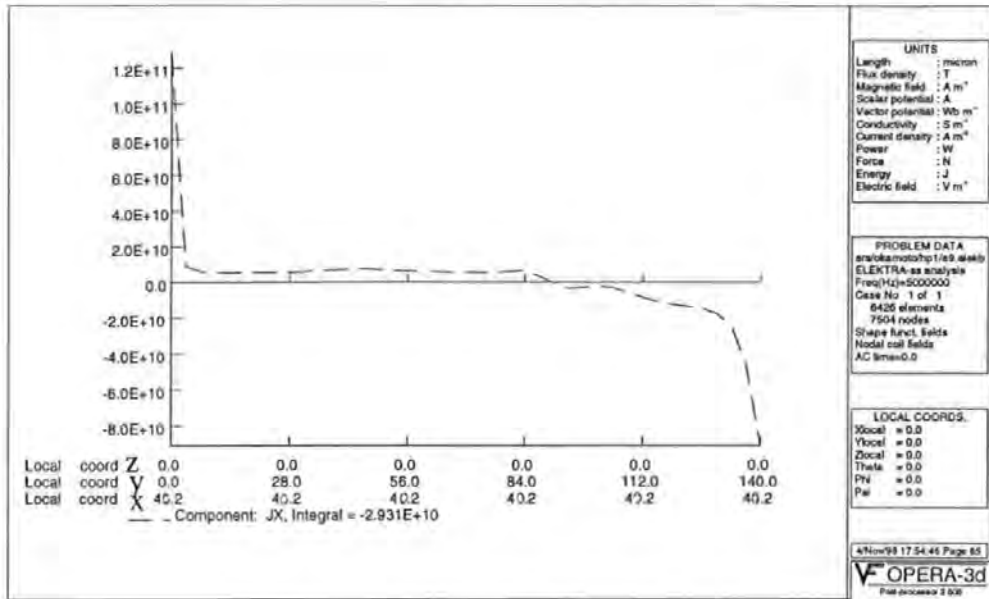


Figure 3.15: Eddy current distribution along the vertical symmetric line ($z=0$, $x=40.2$) in the conventional shield (shield 1) under a 5 MHz co-sinusoidal write current at time = 0.

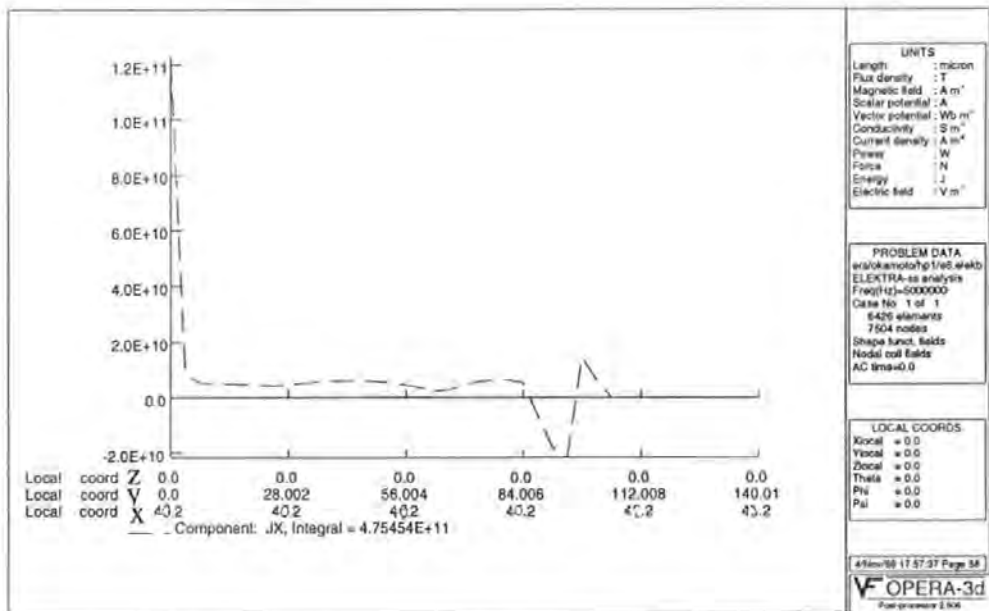


Figure 3.16: Eddy current distribution along the vertical symmetric line ($z=0$, $x=40.2$) in the improved shield (shield 1) under a 5 MHz co-sinusoidal write current at time = 0.

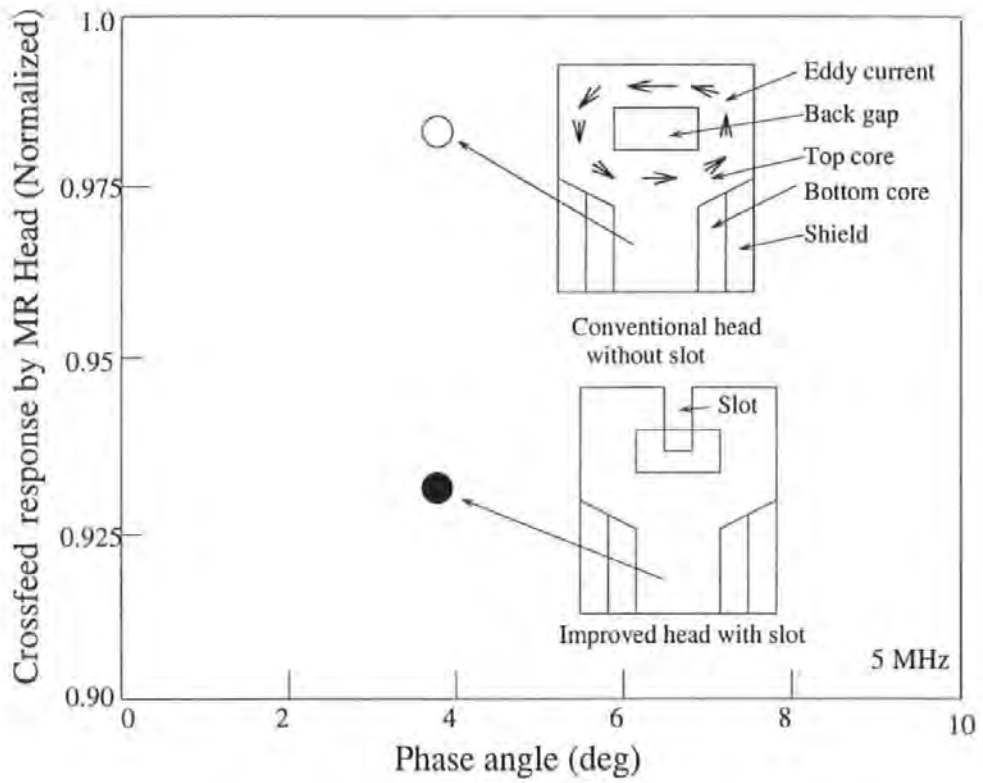


Figure 3.17: Comparison of normalized crossfeed response vs. phase angle for heads with and without slot.

3.7 Interconnecting Shields

In this section, we shall confine ourselves to crossfeed field suppression by interconnecting the metallic magnetic shields of the MR element to constitute a conductive ring. The schematic is shown in Figure 3.18. An applied crossfeed field H_a induces circulating eddy currents I_e that in turn produce a counteracting field H_e . The two fields cancel (partially) at the center, but not at edges. Therefore eddy currents I_e around the ring induced by incoming field H_a prevent the 'write' field flow through the interior of the 'read' ring, i.e. the MR element.

A read-while-write thin-film tape head is modelled. All the dimensions are taken according to a new generation head TR5 produced by the Read-Rite company, as used previously. Figure 3.19 gives bottom views of a shield-wing-interconnecting RWW head.

Figure 3.20 shows a circular eddy current distribution around the joint region of the two shields under a write field of 5 MHz. Because these eddy currents produce a counteracting field to block the penetrating flux through the shield ring, a corresponding crossfeed response of the MR element, $\iiint \text{By dx dy dz}$, has been reduced by a factor of 4 % in the SAL case and 5 % in the DMR case, respectively, compared with that of a traditional parallel-shield design. A further 3 % reduction can be obtained if copper overlay shields with a conductivity of $6.29 \times 10^7 \text{ S/m}$ are used. In addition, the frequency-dependent crossfeed response comparison between the improved shield-wing-interconnecting design and the traditional one has also been depicted in Figure 3.21.

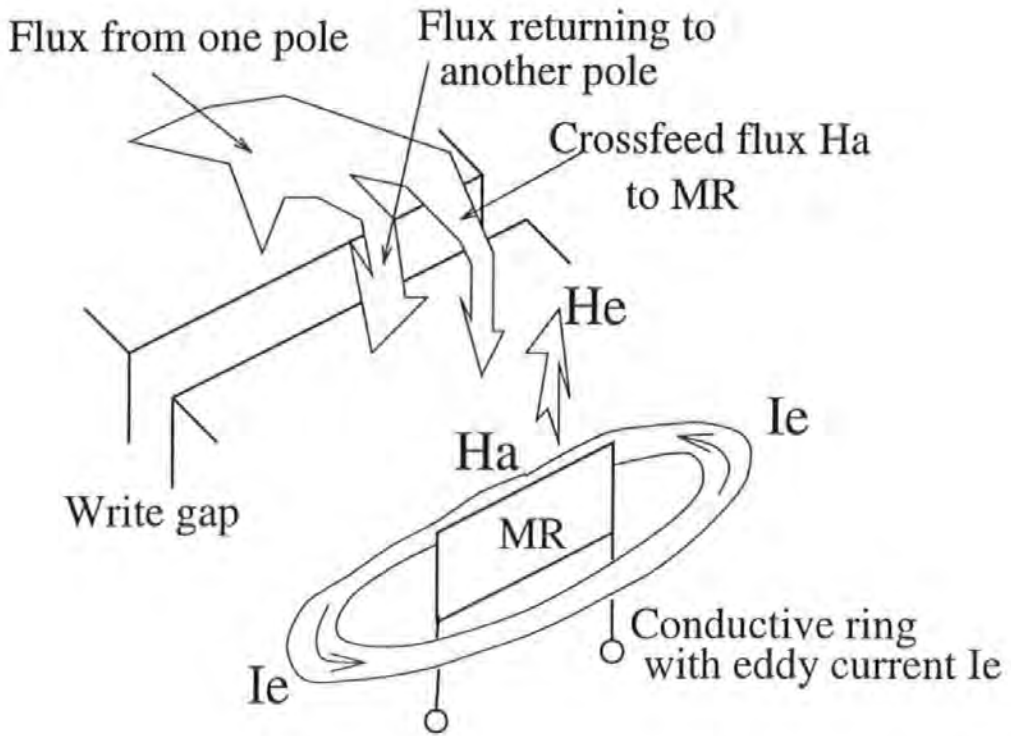


Figure 3.18: Schematic of suppression the so-called crossfeed field radiation from the write head by a conductive ring around the MR reproducing element.

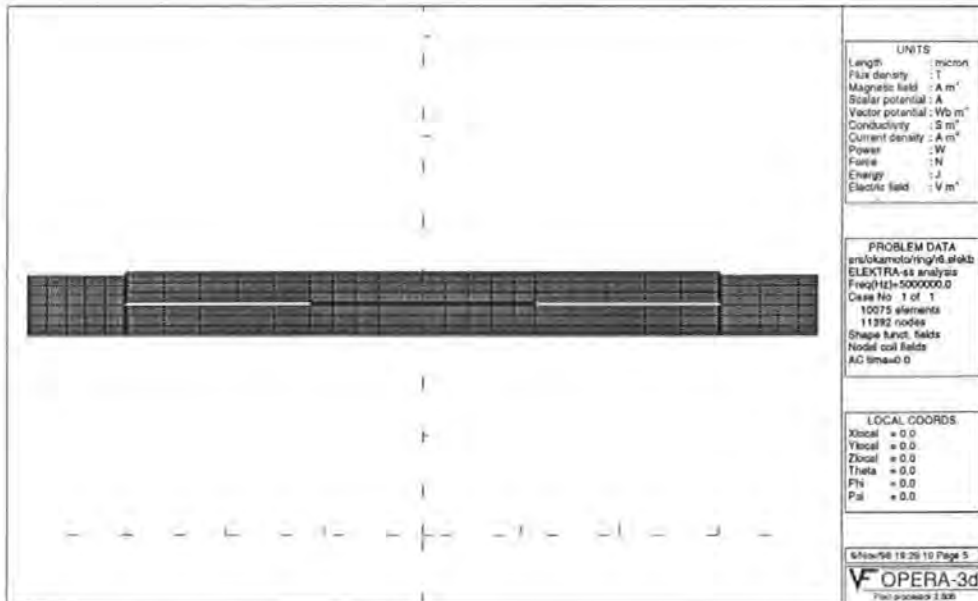


Figure 3.19: Bottom view of a shield-wing-interconnecting RWW head (Write poles are not shown here). Finite-element mesh is displayed.

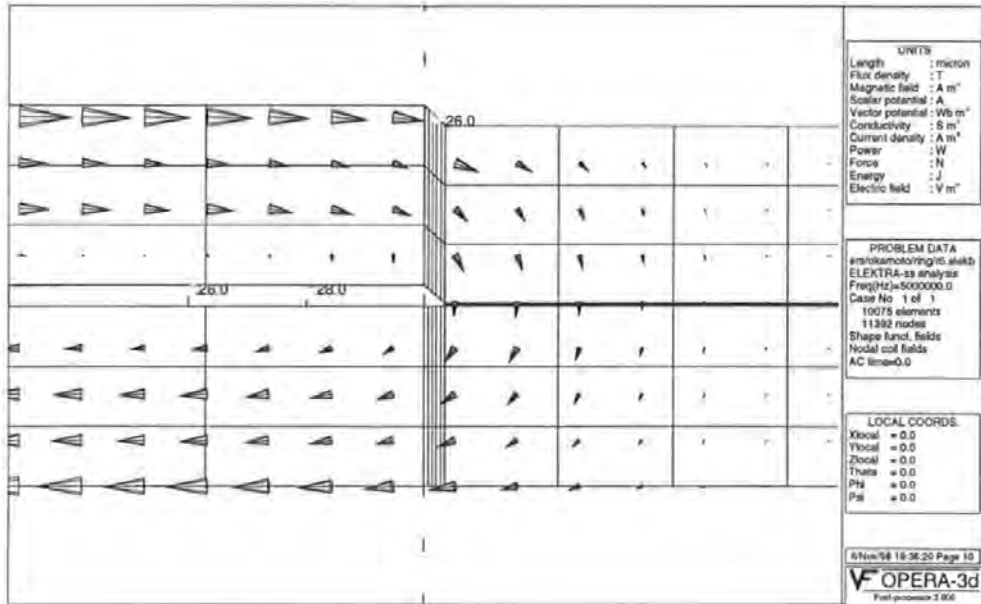


Figure 3.20: Magnified eddy current distribution in the TBS around the joint region of the two shields under a 5 MHz co-sinusoidal write current at time = 0.

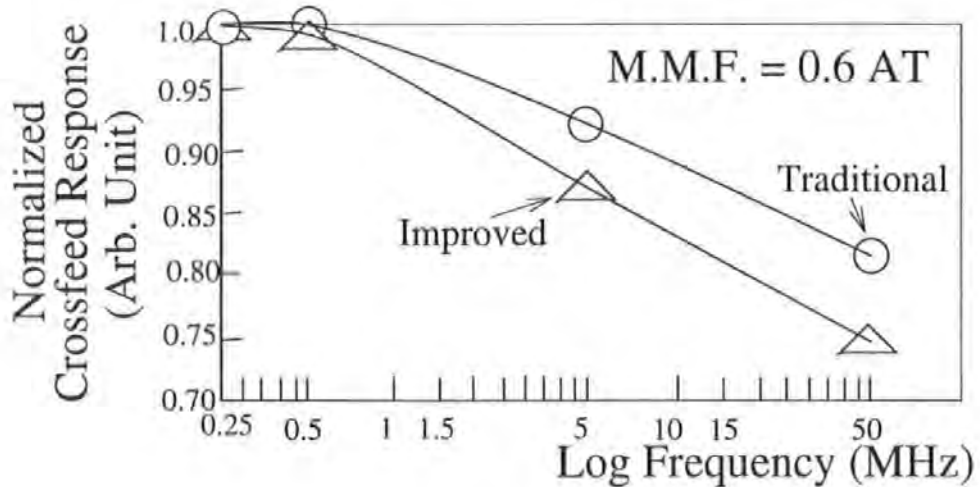


Figure 3.21: Crossfeed response vs. write field frequency. The improved stands for the shield-wing-interconnecting design and the traditional for the parallel-shield design.

3.8 RWW Operation in the Presence of Kepered Media

3.8.1 Background to Kepered Media

A soft-magnetic top keeper layer adjacent to the hard-magnetic storage layer can profoundly affect the recorded magnetic transitions in the media. The keeper layer reduces the demagnetization of the magnetic transition and hence the transition length, trims media noise, smoothes zigzag transitions, and significantly reduces the effects of finite head-pole width on the output. Magnetic Force Microscopy (MFM) imagings of the recorded tracks confirm that the track width associated with kepered media is not only narrowed by 5-10% than the tracks on unkepered media, but that there also are up to half as many erase bands on the sides of the written tracks. Smoother transitions imply a quieter medium, while narrower tracks and fewer erase bands make it easier to increase track density[23][24]. As a result, kepering not only boosts recording densities, but has the potential to stabilize recorded data against thermal demagnetization. In a typical perpendicular magnetic recording system, a soft-magnetic underlayer is used to enhance the read sensitivity. An improved perpendicular media design with both top and bottom soft-magnetic kepered layers is discussed here. The top soft-magnetic keeper layer will further stabilize recorded data against thermal demagnetization and improve read characteristics.

The key technique in designing a kepered media system is how to "open" the kepered layer. In other words, the kepered media system requires a small bias field during read operations. Work to date has been done with thin-film and metal-in-gap inductive heads together with kepered longitudinal media since it is relatively easier to produce a head-bias field by a ring head structure. In this section, we would propose a new concept of kepered-media reproduction with Dual MR heads and then discuss the corresponding requirements for RWW operation[32][30]. To simplify the problem, we will confine ourselves in this section to the separator RWW head design. It is believed that kepered media may offer a similar advantage with

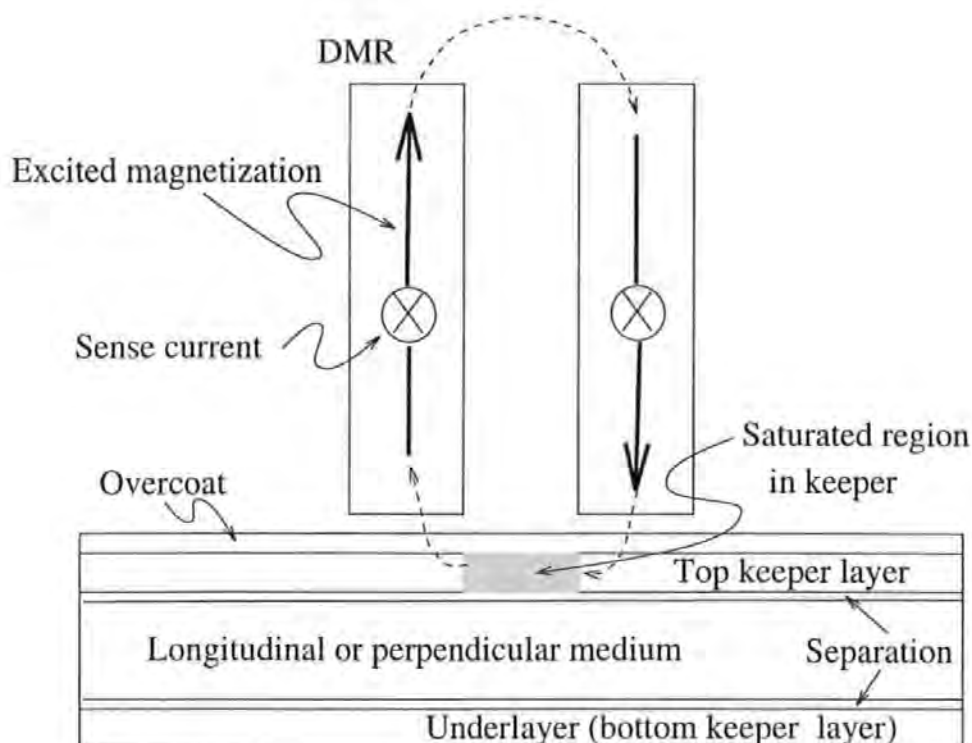


Figure 3.22: Media cross-section and flux path for a basic keptered-longitudinal(perpendicular)-medium reproduction with a Dual MR head. A soft-magnetic keeper film is deposited on top of the medium layer and below the lubricating overcoat. During a write operation, flux from the recording head saturates the keeper above the medium region. The keeper layer could be biased by the stray flux from dual MR sensors during a read operation.

MR heads due to the high performance gains of MR heads.

3.8.2 Reproductive Principle

The principle of keptered-media reproduction with Dual MR heads is illustrated in Figure 3.22. The medium cross-section and the flux path for basic keptered-longitudinal(perpendicular)-medium reproduction with a Dual MR head are shown. A soft-magnetic top keeper film is deposited on the medium layer and below the lubricating overcoat. During a write operation, flux from a recording head[47](not shown in the figure) saturates the keeper above the medium region. The keeper layer

could be biased by the stray flux from dual MR sensors during a read operation.

The aim of a replay process simulation is to verify the feasibility of keepered-medium reproduction with DMR heads. After obtaining the volume integral (i.e. effective signal) of the DMR sensor in the presence of a typical perpendicular medium, we can compare the magnitude difference between the releasing (or reproductive) case and the shunting case. In other words, we should give the proportion of the unexpected signal without a sense current flowing within the effective reproductive signal with a sense current flowing. In order to simplify the problem, only a two-bit perpendicular medium right underneath the read gap was simulated. The left bit is magnetized in the down direction and the right bit magnetized in the up direction. The trackwidth of the two-bit medium is $60\ \mu\text{m}$; the bit length is $0.2\ \mu\text{m}$ with no transition length; the thickness of the medium is $0.07\ \mu\text{m}$; the head-medium spacing is $0.012\ \mu\text{m}$; the coercivity of the perpendicular recording medium is 900 Oe; the keeper layer thickness is nominally $200\ \text{\AA}$, with a coercivity of 15 Oe and a saturation magnetization of about 0.6 Tesla; the thickness of the keeper/record layer separation is $25\ \text{\AA}$; the thickness of the C+ lubricating layer is $25\ \text{\AA}$. The DMR head structure and dimensions used in the replay simulation are listed below: the shield material is chosen to be a FeN based soft magnetic film with a saturation magnetization of 1.9 Tesla and an initial permeability of 6000; two parallel soft magnetic stripes in gap configuration have been used; both these stripes are assumed to be NiFe material for the two MR sensors; the MR track width is $22.9\ \mu\text{m}$; the MR stripe depth is $2.5\ \mu\text{m}$; the MR stripe thickness is $500\ \text{\AA}$; the thicknesses of the dielectric layers are $1000\ \text{\AA}$, $500\ \text{\AA}$ and $1000\ \text{\AA}$, respectively; the stripe-stripe separation, $500\ \text{\AA}$, governs the linear resolution of the readback processes.

In 2 terminal DMR heads, sense current of the same magnitude and direction is sent through both elements producing opposing bias fields in each sensor. The stray field distribution of the DMR in the presence of a top keeper layer (without a recording layer) at a selected sense current $I = 10\ \text{mA}$ in the mid-width cut plane ($z=0$) is shown in Figure 3.23. The field distribution is significantly up-down asymmetric

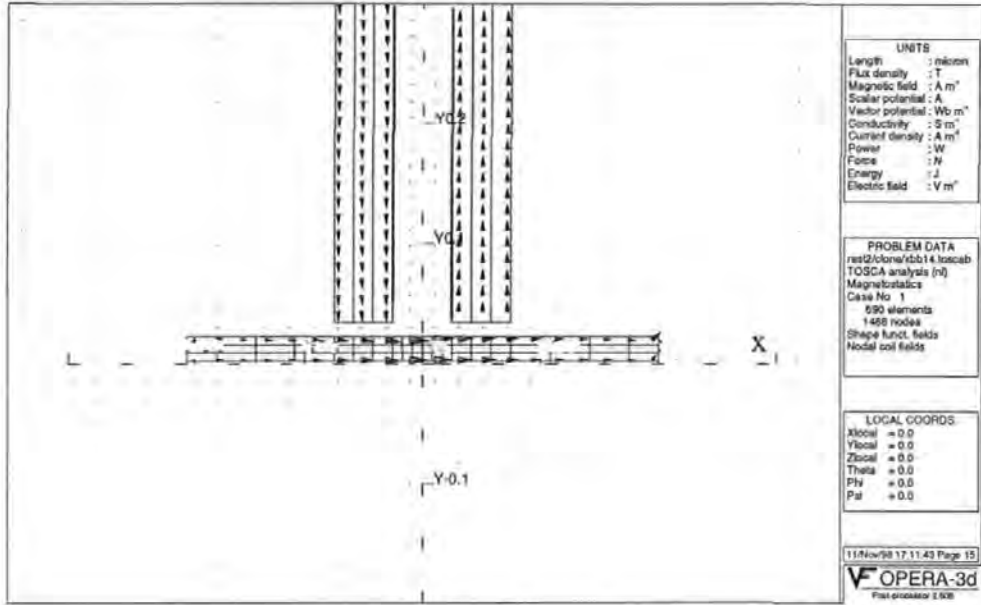


Figure 3.23: The stray flux density distribution of the DMR in the presence of a top keeper layer (without recording layer) at a selected sense current $I = 10$ mA. Sense current of the same magnitude and direction is sent through both elements producing opposing semi-saturated state in each sensor. The resulting bias field in front of the stripe-stripe gap saturates a small region of the keeper layer underneath the gap.

due to the existence of the keeper layer. A strong field has been produced in front of the ring-head-like stripe-stripe gap. This figure also illustrates the magnetization depth distribution around the read gap region. In particular, from the figure, the resulting bias field in front of the stripe-stripe gap saturates a small region of the keeper layer. In a simple word, a "window" has been opened in the keeper layer. In contrast, the two MR stripes are only semi-saturated, i.e. 45° biased, just suitable for signal reproduction.

Figure 3.24 shows a computed three dimensional flux distribution of the recorded bits in the mid-width cut plane ($z=0$), with the replay DMR head with an optimum sense current $I = 10$ mA at the top of the medium. The direction of each arrow corresponds to the direction of the flux density and its thickness to the flux density magnitude. From the figure, it is found that the small saturated region in the top

keeper layer, which is created by the resulting bias field in front of the stripe-stripe-gap, cuts off the return path of the medium transition flux through the top keepered layer due to the low permeability of the saturated region. The medium transition flux is therefore forcibly released from the shunting in the keeper layer, which allows flux transitions to be picked up by the reproductive DMR head. For this reason, Figure 3.24 shows a "releasing state". The leakage flux from the medium goes upward in the right stripe and returns downward in the left stripe. Obviously the anti-symmetrically-distributed flux density components will cause a signal output (not peak value at this location) for 2 stripes shorted at both ends in the DMR head. The calculated maximum DMR output is $0.5298 \text{ T}\cdot\mu\text{m}^3$.

In contrast, we also computed the three dimensional flux distribution in the shunting state, without sense current flowing through the MR stripes. As shown in Figure 3.25, the flux distribution from the perpendicular recording layer is well restrained beneath the top keeper layer and above the bottom keeper layer (under-layer). In a similarly simple word, the "window" has been closed in the keeper layer. Almost no stray flux from the medium enters the MR stripes to be picked up by the reproductive DMR head. In this case, only $0.0251 \text{ T}\cdot\mu\text{m}^3$ is caused in the maximum output of the DMR head. This value is fictitious because an MR sensor cannot work without sense current flowing through the stripes.

In order to evaluate fairly the proportion of the contributions to the MR output between the shunting case and the releasing case, we define a Shunting-Releasing Ratio (SRR) as below:

$$SRR = 20 \log \frac{\text{Signal without sense current}}{\text{Signal with sense current}} (dB) \quad (3.9)$$

In our investigation, the signal with a sense current (releasing case) is $0.5298 \text{ T}\cdot\mu\text{m}^3 / 0.0251 \text{ T}\cdot\mu\text{m}^3 = 21.11$ times as large as the signal without a sense current (shunting case), so the SRR is - 26.5 dB. Therefore the designed top keepered layer plays a reasonable role in shunting and releasing the medium transition flux.

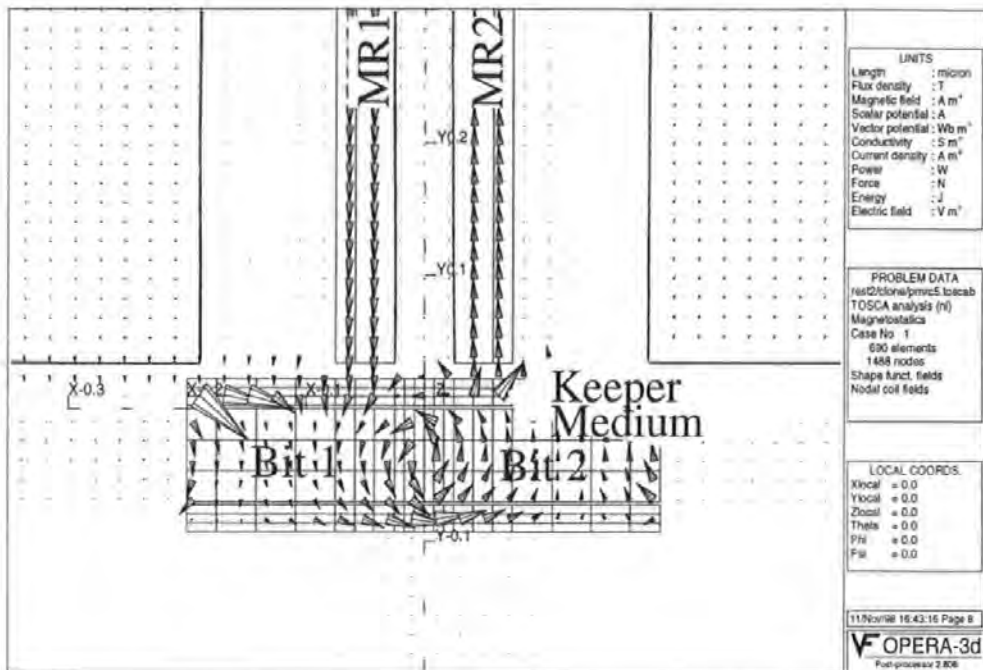


Figure 3.24: Releasing state. Flux distribution of the recorded bits (not including the contribution from the MR sense currents) in the mid-width cut plane ($z=0$), with the replay DMR head with an optimum sense current $I = 10$ mA at the top of the medium, is shown. The small saturated region in the top keepered layer, which is created by the resulting bias field in front of the stripe-stripe-gap, cuts off the return path of the medium transition flux through the top keepered layer due to saturated region's low permeability. The medium transition flux is therefore forcibly released from the shunting in the top keeper layer, which allows flux transitions to be picked up by the reproductive DMR head.

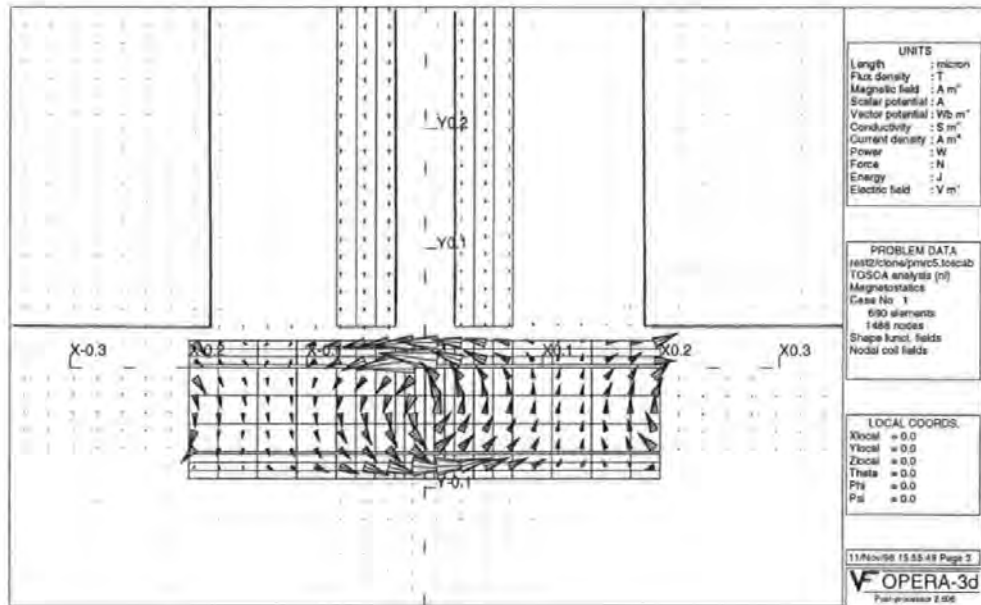


Figure 3.25: Shunting state. Flux distribution of the recorded bits in the mid-width cut plane ($z=0$), with the replay DMR head without any sense current is shown. The flux distribution from the perpendicular recording layer is well restrained beneath the top keeper layer and above the bottom keeper layer (underlayer).

3.8.3 Crossfeed Analysis

In the RWW operation, the shields, including the bottom pole of the write head, serve mainly to transport part of the flux from the write head back to the writing coil, as mentioned above. When an AC magnetic field penetrates a sheet of conductive keeper, circulating currents are induced inside the sheet because the field changes its value and direction all the time. If the AC field varies fast enough (higher frequency), then the induced fields may completely oppose the outside field.

Figure 3.26 and Figure 3.27 give the details of the crossfeed field distribution. From the write field distribution around the write gap in the presence of a keepered medium (Figure 3.26), the write field is seen to be so strong that it saturates both the top and bottom keepers completely. However, the keepers underneath the write

head still contribute to the crossfeed suppression owing to the existence of in-plane eddy currents. In comparison, the keeper underneath the read gap represents a natural shielding against the crossfeed field from the crossfeed situation around the read gap region of Figure 3.27. Furthermore, Figure 3.28 gives the eddy current distribution in the conductive keeper due to the penetrating stray flux through the keeper under a 5 MHz co-sinusoidal write current at time = 0. In Figure 3.28, two in-plane eddy current loops may be seen: the small loop, located underneath the top pole, is induced by the oncoming flux from the top pole; the big loop, located underneath the bottom pole, shield 1, MR1, MR2 and shield 2, is induced by the returning flux. Approximately, the bottom pole, shield 1, MR1, MR2 and shield 2 as a whole provides a returning path of the write flux, gushing from the top pole. These two loops are countercurrent to each other at any time and thus there is an enhancement of the eddy currents underneath the write gap. The corresponding schematic is illustrated in Figure 3.29. Obviously both loops may retard the penetrating write flux to interfere with the MR stripes, i.e. the conductive keeper plays a positive role of "shielding". In this regard, the crossfeed situation is considerably improved when magnetic conductive keepers are used.

In order to evaluate shielding efficiency we give the crossfeed responses (the volume integral of the vertical component of magnetic flux in the MR stripes) in the cases without and with a keepered medium. In the case of without a keepered medium, the crossfeed response is $0.0145 \text{ T}\cdot\mu\text{m}^3$. In the case of with a keepered medium, the crossfeed response is $0.0129 \text{ T}\cdot\mu\text{m}^3$. There is an 11 % reduction with the aid of a keeper layer. Most importantly, the principle of using a dual MR head to suppress the crossfeed field also applies to keepered media reproduction.

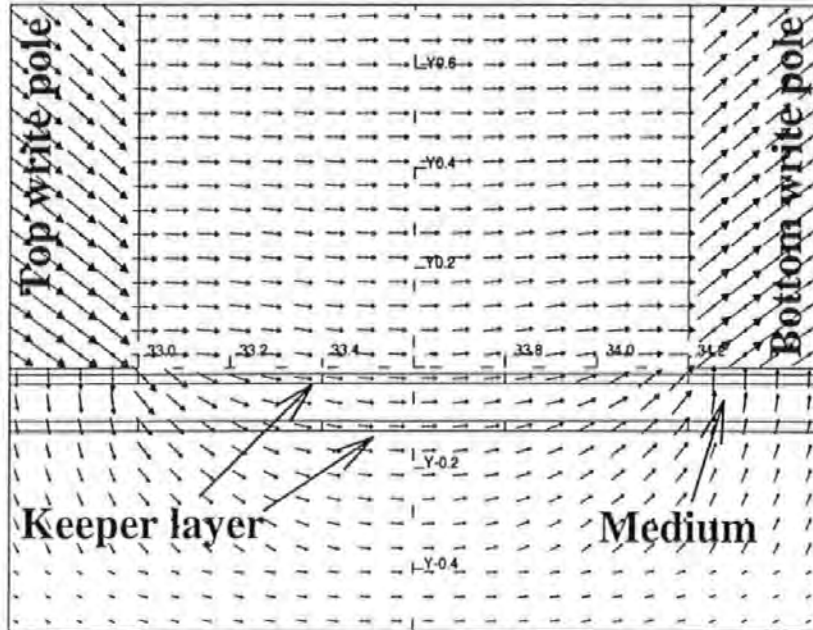


Figure 3.26: Magnified write field distribution under a 5 MHz co-sinusoidal write current at time = 0 around the write gap in the presence of keptered medium.

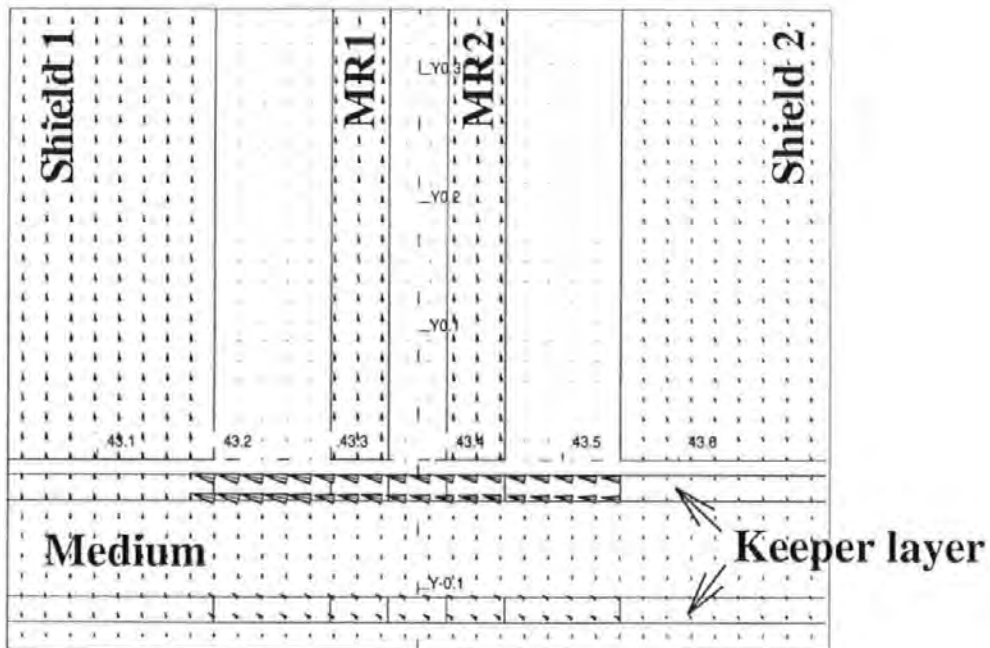


Figure 3.27: Field mapping of crossfeed situation around the read gap region in the presence of keptered medium, under a 5 MHz co-sinusoidal write current at time = 0.

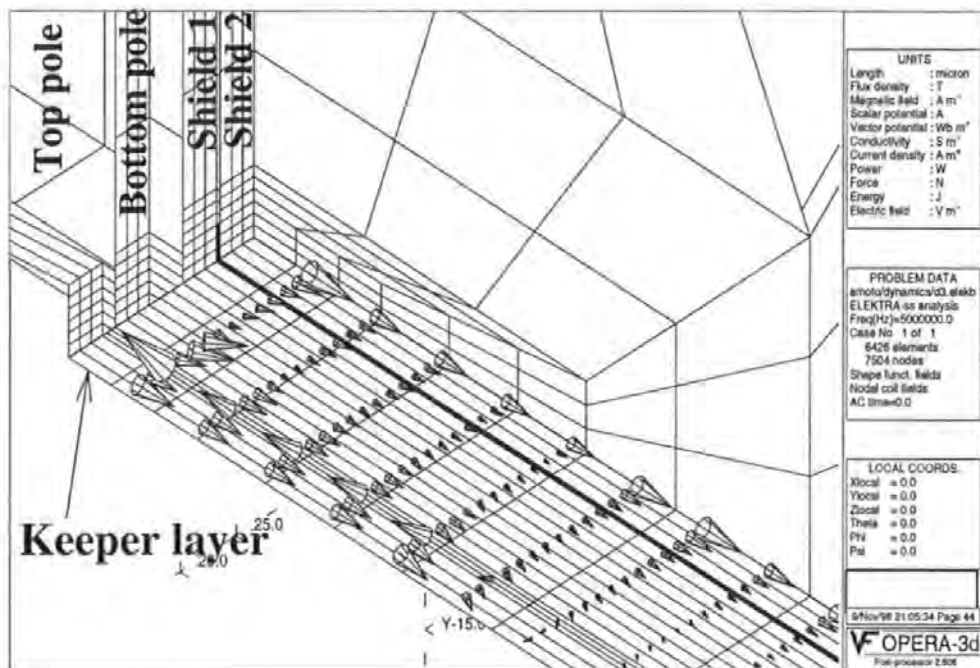


Figure 3.28: Eddy current distribution in the keeper layer under a 5 MHz co-sinusoidal write current at time = 0.

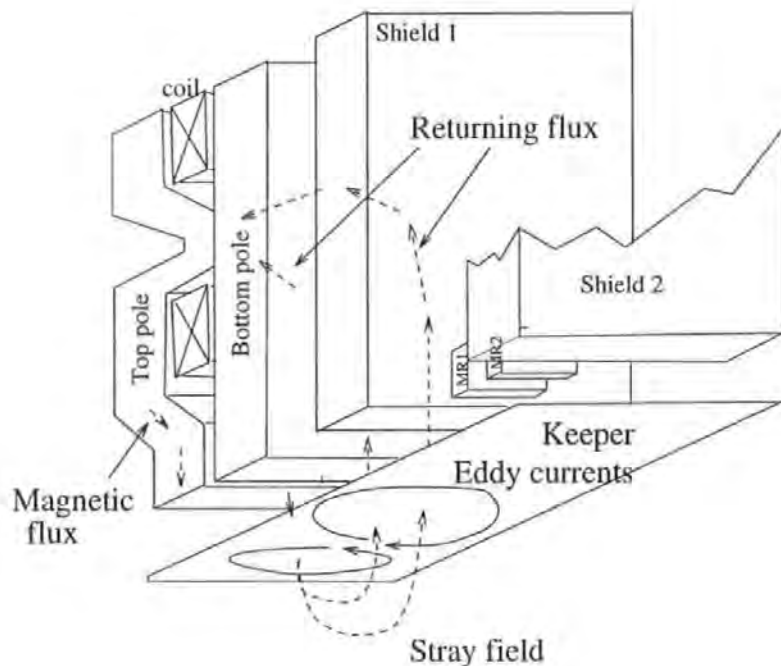


Figure 3.29: Schematic of eddy current in a conductive keeper due to the penetrating stray flux through the keeper layer.

3.8.4 Summary of RWW in the Presence of a Keeperead Medium

In this section, we proposed a new concept of keeperead-media-reproduction with Dual MR heads. As a result, the keeper layer could be biased by the stray flux from DMR sensors. A so-called "shunting-releasing ratio" between reproductive signals without and with a sense current is found to be -26.5 dB. This double-keeperead perpendicular medium is a completely-stable system against thermal demagnetization. It is believed that keeperead media may offer an advantage with MR heads and potentially allow magnetics to break the over 10 Gb/in² areal density barrier due to the high performance gains of MR heads.

The crossfeed situation is considerably improved in the presence of keeperead medium since the conductive keeper plays a positive role of "shielding". There is an 11 % reduction with the aid of a keeper layer. Most importantly, the principle of using a dual MR head to suppress the crossfeed field also applies to a keeperead medium magnetic recording system.

In addition, the principle stated here is also applicable to longitudinal media systems although only a perpendicular medium has been included in this investigation.

3.9 Summary

A growing number of magnetic recording equipment manufacturers employ thin-film technology to fabricate magnetic recording heads. There are many advantages to this approach, with perhaps the most important being the ability to produce extremely narrow pole tips and recording gap widths in the thin-film process. These narrow pole tips, in turn, permit the density of magnetic recording to be increased. Currently, the high frequency response is required with increasing linear density and data transfer rates. That is to say, in order to realize high data transfer rates, high

frequency write/read performance together with high movement velocity of medium and high recording density is necessary. For this reason, the effects of eddy currents in the conductive head yokes must be included. The availability of digital computers makes possible the numerical solution of the sinusoidally varying fields for heads with finite conductivity.

The ELEKTRA-3D Vector Fields Electromagnetics Analysis Package is used to compute electromagnetic fields including the effects of eddy currents, in three dimensions. ELEKTRA can use a combination of vector and scalar magnetic potentials to model time varying electromagnetic fields. The ELEKTRA analysis confirms that the work to suppress the crossfeed field involves both a novel reproductive mode, stated mainly in Chapter 2, playing the key role in suppressing the crossfeed, and several other compensating schemes, stated mainly in this chapter, giving further suppression.

The thrust of this chapter is to find a practical solution for the suppression of crossfeed field under Read-While-Write (RWW) operation at high working frequency. In summary:

1. It is advantageous to use magnetic materials with a low conductivity to prevent eddy currents. The corresponding crossfeed reduction is 7% in the SAL case and 8% in the DMR case when Fe-Al-O is used compared with conventional FeN material at a working frequency of 5MHz.
2. It is advantageous to cut a slot through the metallic magnetic pole and shields to retard the in-plane eddy currents. The corresponding crossfeed reduction is 3% in the SAL case and 5% in the DMR case compared with the conventional case at a working frequency of 5MHz.
3. An improved shield-wing-interconnecting design can reduce the crossfeed field by a factor of 4% in the SAL case and 5% in the DMR case compared with that

of a traditional parallel-shield design. The eddy currents around the constituted conductive loop produce a counteracting field to block the penetrating flux.

4. Kepered media is a potential technique with smoother transition, quieter replay and anti-thermal stability. Here we propose a new concept of kepered-media-reproduction with Dual MR heads. Most interestingly, the principle of using dual MR stripe to suppress the crossfeed field harmonizes the kepered media reproduction with DMR heads. The conductive keeper plays a positive role in suppressing crossfeed field. There is an 11% reduction with the use of a conductive keeper layer.

In principle, the above measures can be combined to get further suppression of crossfeed field. For example, combining measures 2 and 3 gives around 10% reduction of crossfeed field. Whichever measure 1 through 3 is used, a further automatic 11% improvement can be expected in the presence of a kepered medium.

Chapter 4

Experimental Assessment of Heads

4.1 Introduction

This chapter assesses the main contributors to crossfeed by making measurements on current and improved heads. The primary components can (usually) be separated out into electrostatic and electromagnetic crossfeed. Electrostatic crossfeed is important because it can lead to large transients in the feedthrough waveform. It is usually reduced by grounding the metallic parts of the head or introducing grounded planes in key positions. Inter-lead coupling is also a source of electrostatic crossfeed[48]. Electromagnetic crossfeed usually has a different waveform and is suppressed using different techniques. In this work, we have succeeded in designing and developing an experimental apparatus for crossfeed and other measurements. The most relevant constraint in this project has been the availability of heads. Three different heads were used for crossfeed measurements: TR5 heads for basic crossfeed measurements, DSMR heads for comparison between single MR and DMR heads, and DCC multi-channel heads for multi-track crossfeed measurements. The measurement results have also been compared with the corresponding simulation results of the previous chapters.

4.2 Experimental Apparatus

An experimental apparatus for the assessment of heads has been designed and fabricated[27]. The photograph in Figure 4.1 shows the computer-controlled system. The PC is used to control the stage motion through its interface RS232 as well as to acquire MR voltage through 8255[49][50]. To allow enough up-down room and manipulate the heads freely to yaw, pitch and roll, the heads were mounted on a holder with four degrees of freedom, as shown in Figure 4.2. A sample (either a hard disk platter or a magnetic tape coupon) is mounted on the center of a small stage with the aid of the four screws. This small stage is a one-body two-axial parallel-spring parallelogram, shown in Figure 4.2. The overall size of the stage is 105mm \times 95 mm \times 10mm(thickness). The stage is shaped by spark erosion. As can be seen in Figure 4.2, an "L" shaped peripheral supporting part with three screw holes is used as the basis of the whole stage. Two "parallelograms" in a body, one of which has 4 hinges, have been integrated into this stage. The sample-containing small parallelogram, responsible for y-axial movement, is inserted inside the large one for x-axial movement. A two-dimensional random-access of the sample is performed by inclining these two parallelograms with the aid of two multi-layer piezoelectric ceramic actuators[51].

The parallel-spring stage is mounted on a coarse stage, driven by two linear motors. The combined fine-positioning parallel-spring stage and coarse-positioning stage constitutes a two-stage positioning system. It can reach a centimeter order random-access range with nanometer resolution[27]. The slider is in physical contact with the sample. The velocity-independent-sensitivity of MR sensors make it possible to evaluate recording media and the MR head itself without causing thermal noise due to friction at room temperature[33].

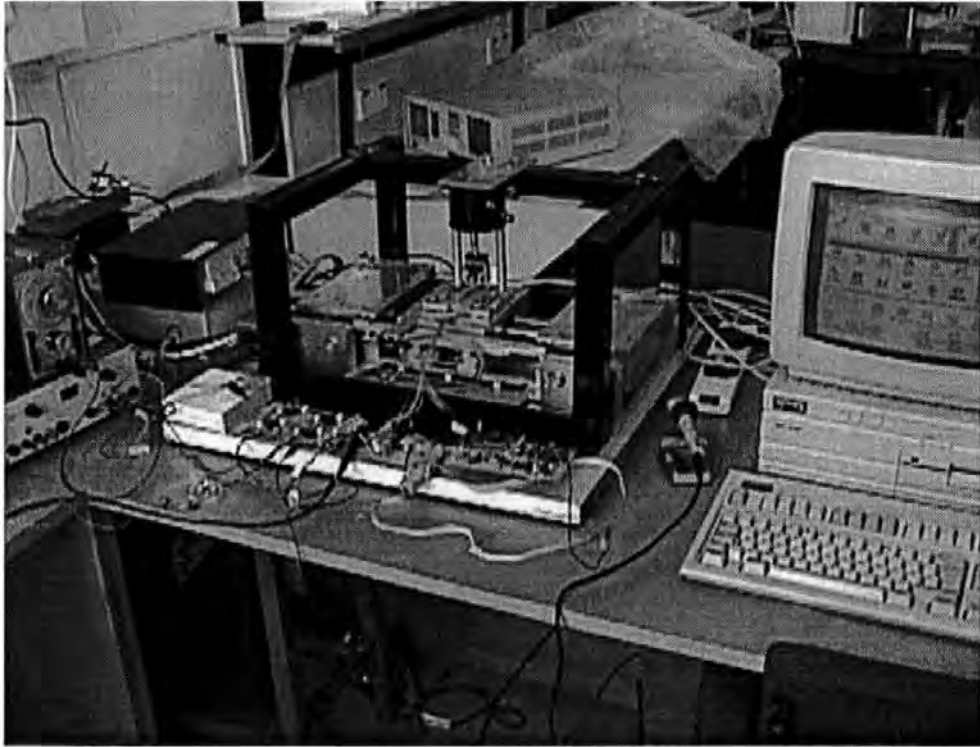


Figure 4.1: A computer-controlled experimental apparatus for the assessment of heads. IBM PC-386 computer (right), two-stage positioning system (centre), MR/inductive head with its holder (up centre), circuits for write amplifiers and read amplifiers (lower centre), voltage booster for piezoelectric actuators (left, black), linear motor controller (left, white, underneath booster), power supply (far left, white) and signal generator (far left, above supply).

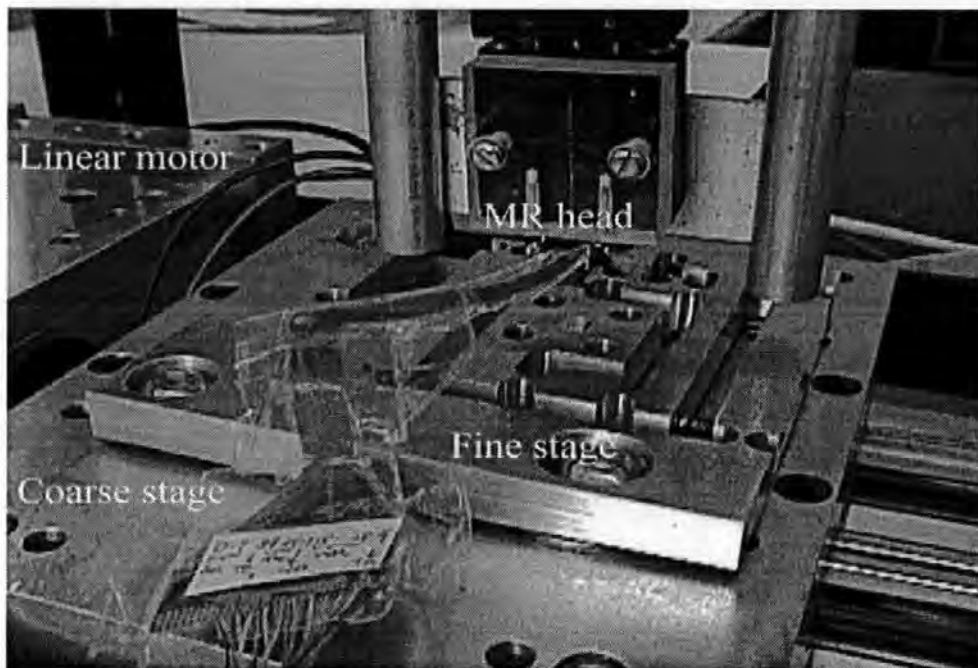


Figure 4.2: Magnified photograph near the heads.

4.3 Experimental Assessments

With the aid of the above developed system, measurements with MR/inductive heads have been done. The schematic illustration is shown in Figure 4.3. In the crossfeed measurements, the head assembly was put far away from the medium. When a squarely-varying or sinusoidally-varying recording current is flowing through the write coil, just as in the case of recording, we can observe the reproductive waveform from the MR sensor on the oscilloscope. Part of the crossfeed measurement system is shown in Figure 4.4. We can confirm if it is the crossfeed waveform from the write field by both frequency comparison and amplitude dependence on sense current.

The most relevant constraint in this project was the availability of heads. Three different heads were used for crossfeed measurements: TR5 heads (Read-Rite), DSMR heads (Read-Rite) and DCC multi-channel heads (Philips). Figure 4.5 shows

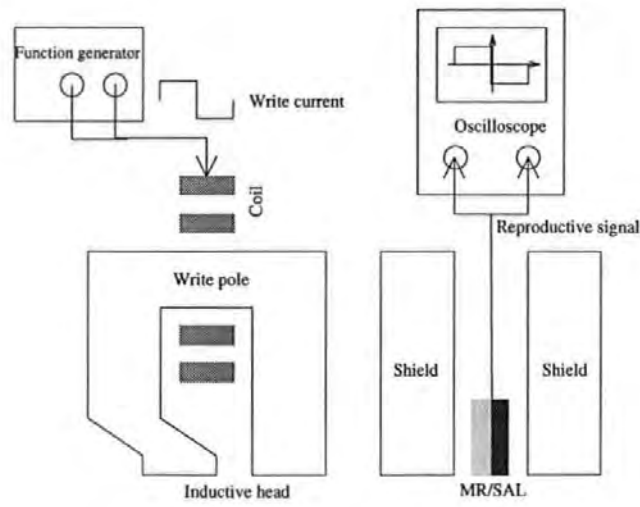


Figure 4.3: Schematic of experimental apparatus for measuring crossfeed on an MR/inductive head.

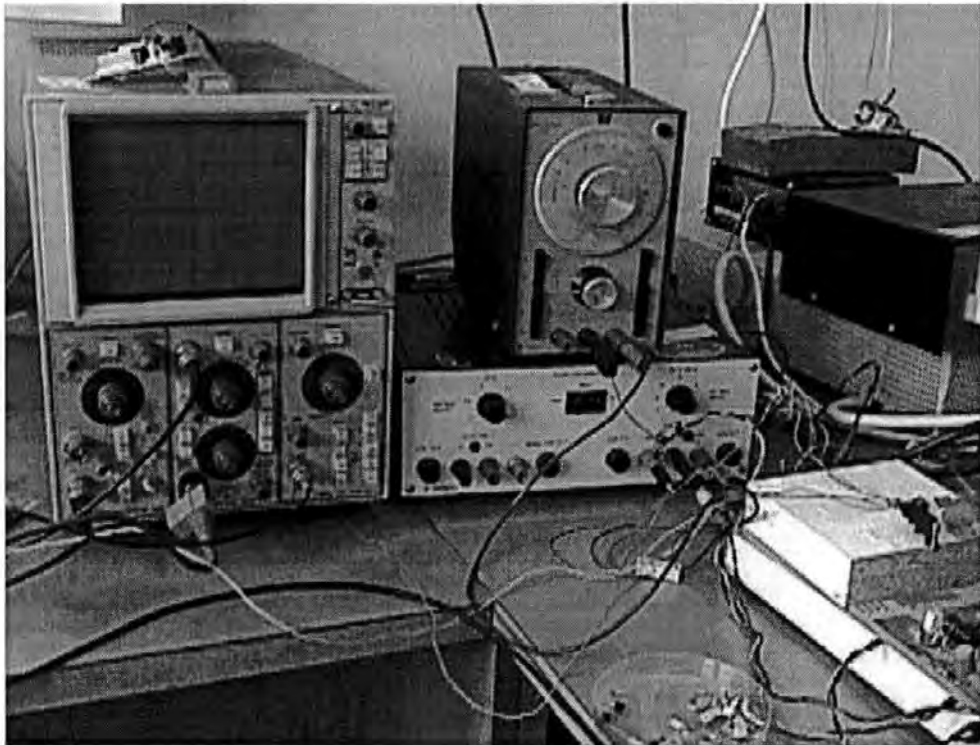


Figure 4.4: Part of the crossfeed measurement system.

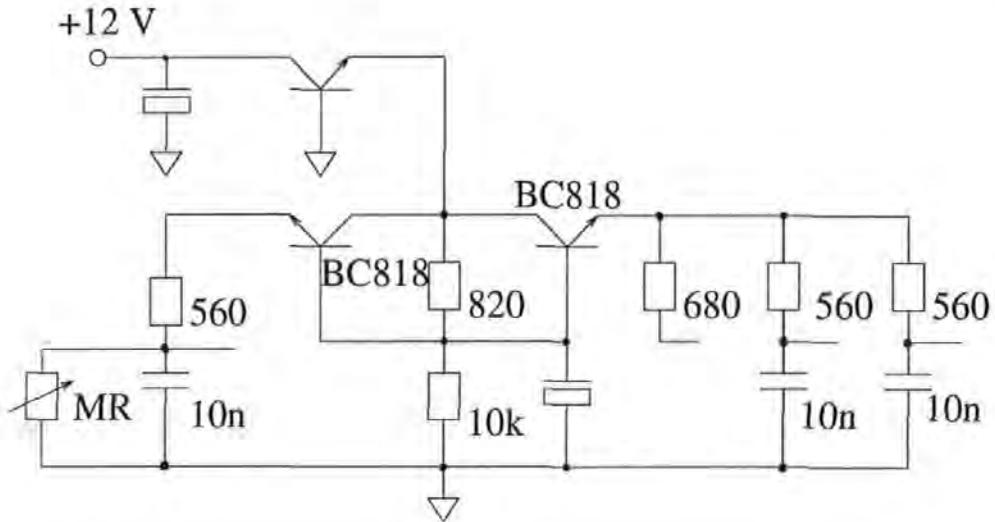


Figure 4.5: Part of analog and digital playback circuitry—sense current (analog and digital channels) and DC bias current (digital MR channels).

the sense current which is required for MR sensors.

4.3.1 Read-Rite TR5 Heads

TR5 is a new generation of thin-film MR tape head products (Figure 4.6). The shields and pole materials have been changed from NiFe (TR4) to allow the head to write the higher coercivity (1650 Oe) metal particle media. While TR5 remains a single channel architecture, it is expected that future generations will be multi-channel architectures with 4-8 parallel channels, to maximize the transfer rate while maintaining reasonable tape speeds, with channel-to-channel separation of 5-7 mils (1 mil = 1/1000 inch = 25.4 μm). Read track widths are expected to be 0.5 mils (1 mil = 25.4 μm). Multi-channel heads will have all the same feedthrough sources as the single channel versions of today but additionally will have channel-to-channel coupling. Figure 4.7 shows the arrangement of the poles and shields for a single channel head. The MR is a SAL biased design, Barkhausen noise is controlled through shape anisotropy. Most of the parameters of TR5 have been already used

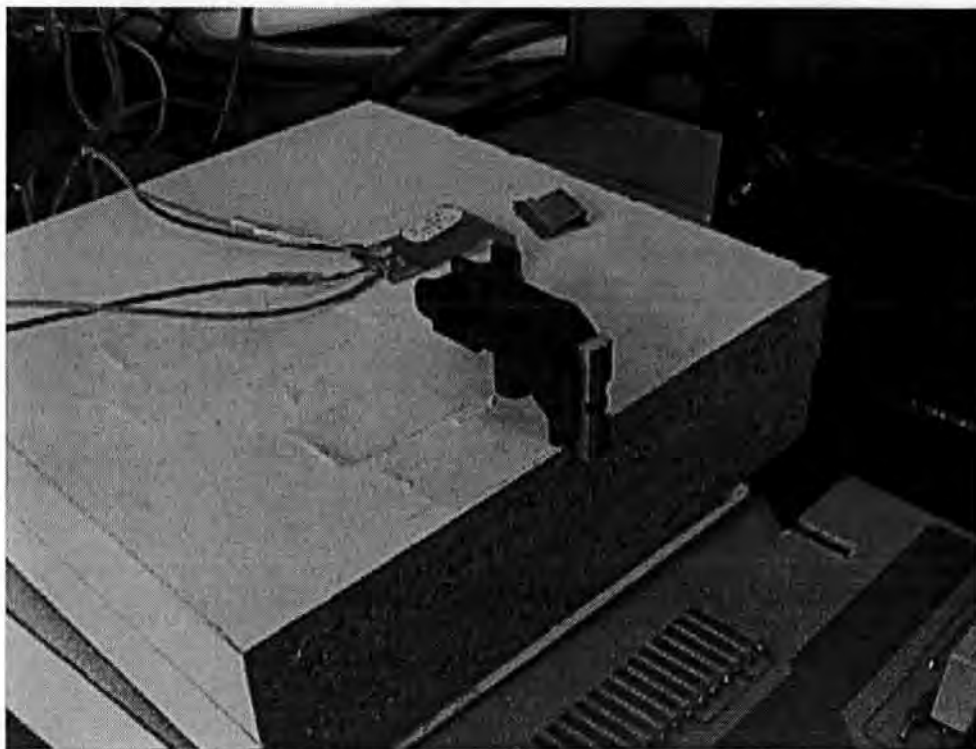


Figure 4.6: A new generation thin-film MR tape head product TR5 provided by Read-Rite.

in our computer models. The MR playback channel is $22.9 \mu\text{m}$ wide, the record channel is $61 \mu\text{m}$ wide. The write gap length is $1.2 \mu\text{m}$ and the read gap length is $0.35 \mu\text{m}$. The record channel is 15 turns.

First, we will prove the existence of the inductive coupling between write-read windings, as mentioned in Chapter 1. Flowing a 40 mA_{0-p} squarely-varying recording current (optimum recording current) through the write coil of the write head, we observed the reproducing waveform, as shown in Figure 4.8, from the MR sensor without any sense current. Sharp pulses appeared at the leading edges and trailing edges of the reproductive waveform because of the inductive coupling between write-read windings. With regard to the capacitive coupling from the writing to the reading bumps, which should be proportional to the writing voltage, there is no observation at the reading terminals in our measurements. In principle, it may

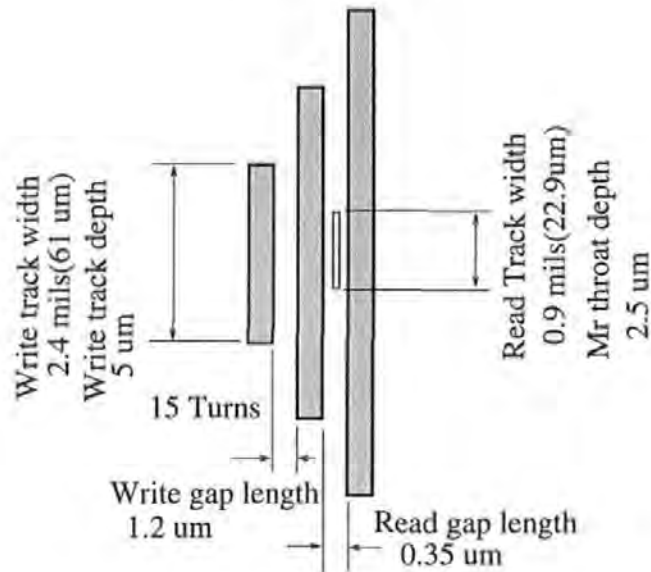


Figure 4.7: Arrangement of the poles and shields for the single channel head TR5.

be reduced to an altogether negligible quantity by earthing one of the electrically conducting layers of the screen.

Figure 4.9 to Figure 4.12 show the reproducing waveforms at different frequencies from the MR sensor, where a squarely-varying (this is the case of digital magnetic recording) recording current of 40 mA_{0-p} (optimum recording current) was flowing through the write coil of the write head and a sense current of 10 mA through the MR sensor. The crossfeed responses are 160 mV_{p-p} (after an amplifier) at 36.4 kHz , 176 mV_{p-p} at 364 kHz , 120 mV_{p-p} at 3.64 MHz and 0 mV at 36.4 MHz . Figure 4.13 summarizes this frequency response. This humped curve reveals a clear dependence of crossfeed response on frequency. In the range of frequency $\leq 364 \text{ kHz}$, the response rises as the frequency increases, while in the range of frequency $\geq 364 \text{ kHz}$, the response drops as the frequency increases and eventually declines to zero. The frequency response indicates the significant effect of the eddy current loss. Due to the high conductivity, the flux penetrating through the shield induces an in-plane eddy current that in turn produces a counteracting field to block the penetrating flux through the shield. This causes the crossfeed fields to forcibly interfere with the

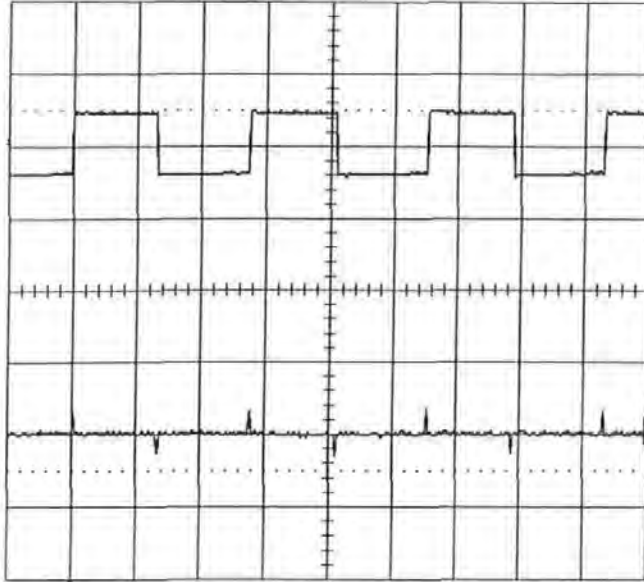


Figure 4.8: The reproducing waveform of TR5 (the lower) without any sense current through MR against a squarely-varying excitation (the higher) in the write coil at frequency of 36.4 kHz. The vertical scale is 50 mV/div and the horizontal scale is 10 μ s/div.

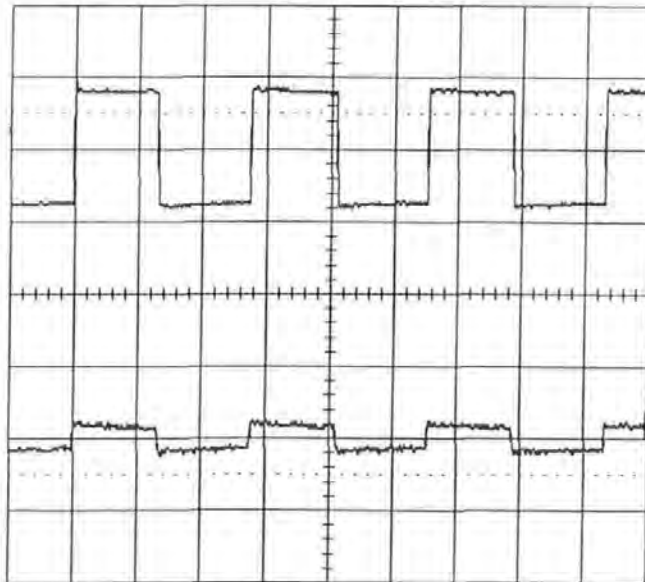


Figure 4.9: The reproducing waveform of TR5 (the lower) with a 10 mA sense current through MR against a squarely-varying excitation (the higher) in the write coil at frequency of 36.4 kHz. The vertical scale is 400 mV/div and the horizontal scale is 10 μ s/div.

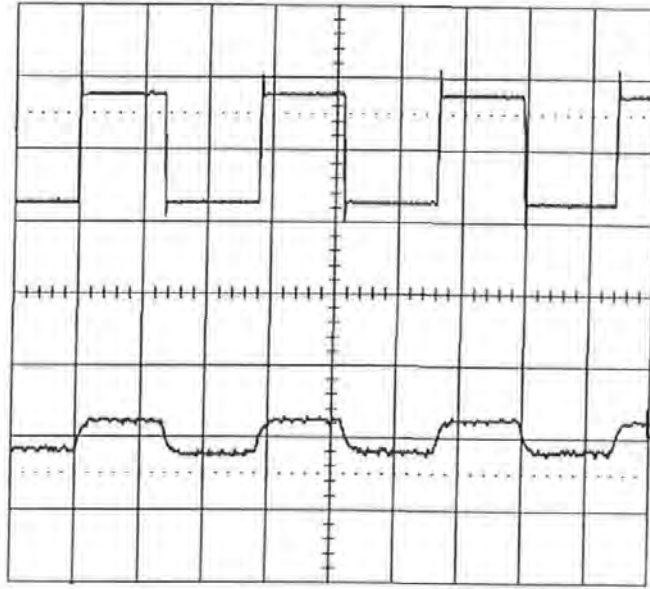


Figure 4.10: The reproducing waveform of TR5 (the lower) with a 10 mA sense current through MR against a squarely-varying excitation (the higher) in the write coil at frequency of 364 kHz. The vertical scale is 400 mV/div and the horizontal scale is 1 μ s/div.

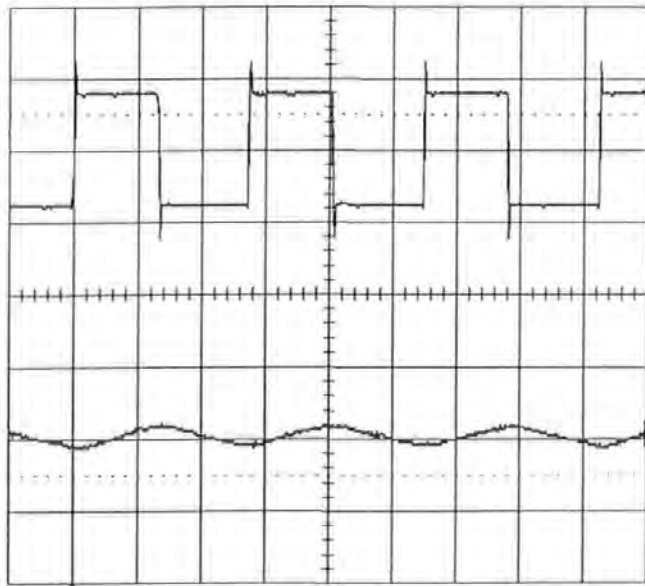


Figure 4.11: The reproducing waveform of TR5 (the lower) with a 10 mA sense current through MR against a squarely-varying excitation (the higher) in the write coil at frequency of 3.64 MHz. The vertical scale is 400 mV/div and the horizontal scale is 0.1 μ s/div.

MR element behind the shield resulting in increased crossfeed response. However, as the frequency increases further, the write field intensity decreases drastically due to the eddy current loss in the pole thickness direction and eventually no write field will be sensed.

TR5 heads have also been used with tapes to estimate the replay performance that is possible with respect to TDK Co- γ Fe₂O₃ 900 Oe coercivity tape. Sense current is set to 10 mA in the application circuit. The optimum bias current may be changed by the magnetization of the poles. Here, the optimum bias current was defined as that which produced minimum distortion in the MR response. Figure 4.14 shows the reproducing waveform in the MR sensor against a TDK magnetic tape coupon, pre-recorded by a 9.6 kHz sinusoidally-varying recording field. Figure 4.15 shows the reproducing waveform against a TDK magnetic tape coupon, pre-recorded by a 9.6 kHz squarely-varying recording field. The replay amplitudes of the head are 560 mV_{p-p} (after the same amplifier) in the case of sine-wave and 700 mV_{p-p} in the case of square-wave.

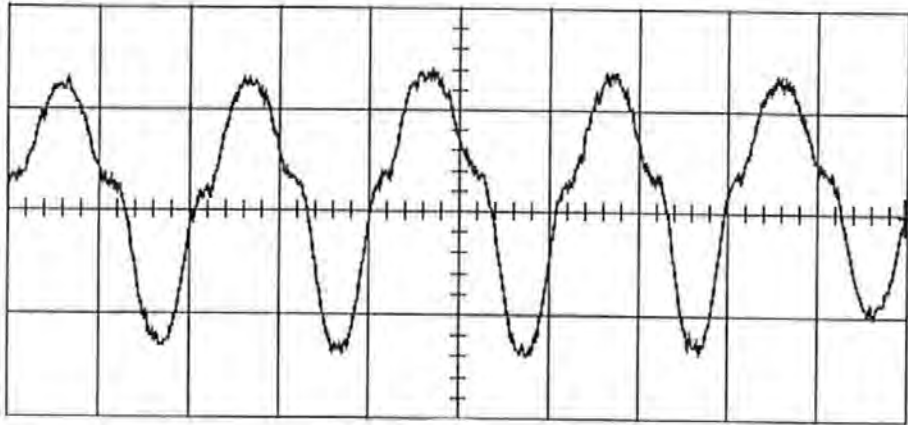


Figure 4.14: The reproducing waveform of TR5 against a TDK magnetic tape coupon, pre-recorded by a 9.6 kHz sinusoidally-varying recording field. The vertical scale is 200 mV/div and the horizontal scale is 1 ms/div.

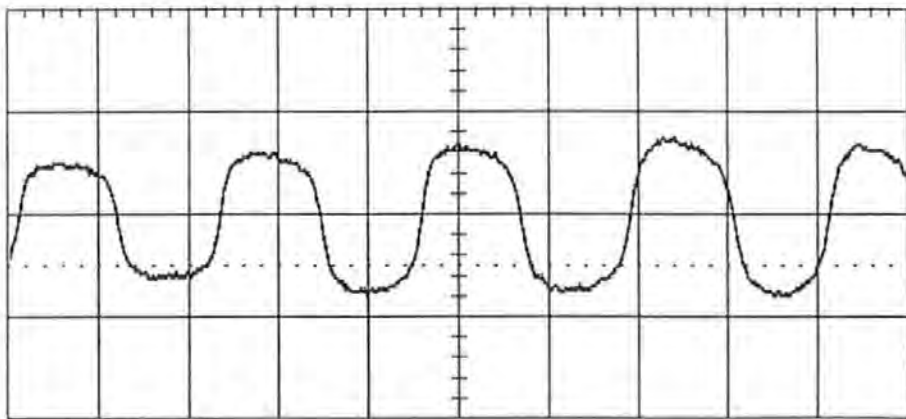


Figure 4.15: The reproducing waveform of TR5 against a TDK magnetic tape coupon, pre-recorded by a 9.6 kHz squarely-varying recording field. The vertical scale is 500 mV/div and the horizontal scale is 1 ms/div.

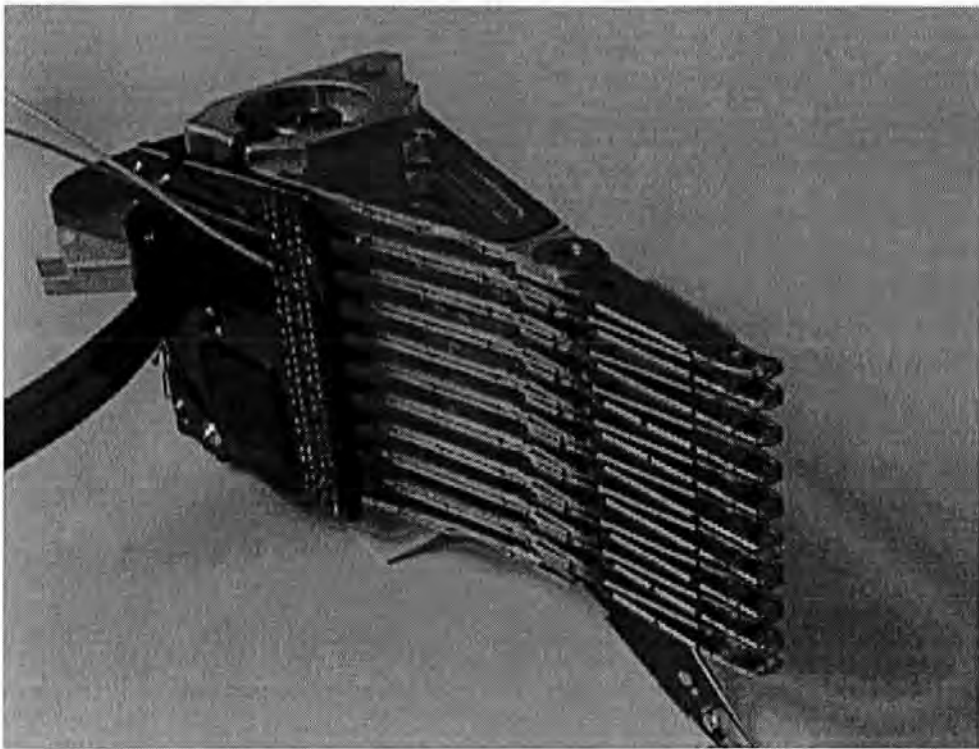


Figure 4.16: A Dual-Stripe Magnetoresistive (DSMR) head stack, provided by Read-Rite, were originally designed for hard disk drives.

4.3.2 Read-Rite DSMR Heads

Measurements with Dual-Stripe Magnetoresistive (DSMR) heads (Figure 4.16), provided by Read-Rite, were done. The magnetization configuration of 2-terminal DMR, mentioned in Section 2.2, is the same as 4-terminal DSMR, mentioned in Section 1.4, but their electrical connections are different. Based on this fact, by re-connecting the terminals of DSMR in a different way, we can get a single MR head sample (biased by the sense current passing through the opposite "dummy" stripe) and a DMR head sample, respectively.

As shown in Figure 4.17 and Figure 4.18, we observed the reproducing waveforms (crossfeed response) from the MR sensors at sense currents of 12 mA on the oscilloscope when a squarely-varying recording current of 50 mA_{0-p} (This is optimum recording current, but 70 mA_{0-p} is still safe.) was flowing through the write

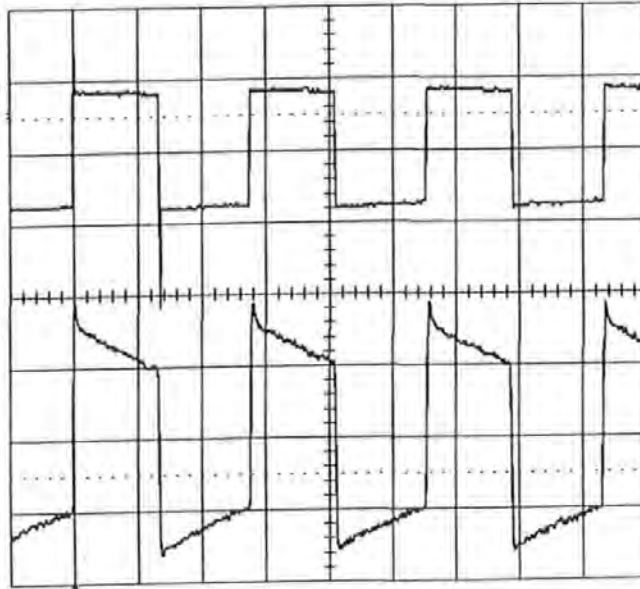


Figure 4.17: The reproducing waveform (the lower) with a 12 mA sense current through the single MR against a squarely-varying excitation (the higher) in the write coil. The vertical scale is 2.00 V/div and the horizontal scale is 0.1 ms/div.

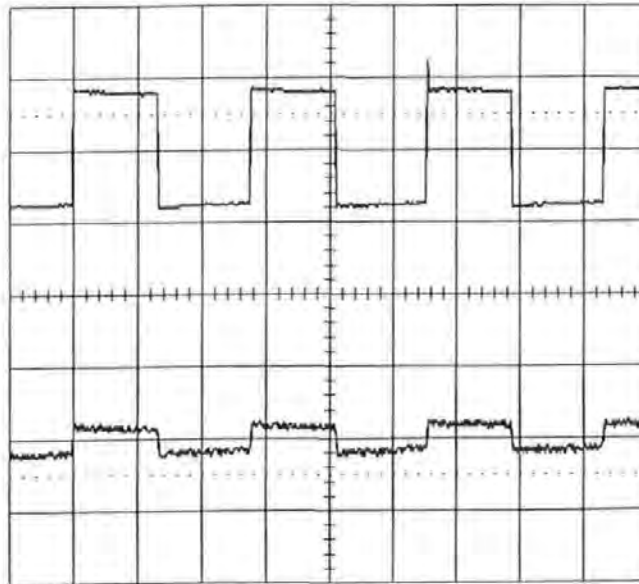


Figure 4.18: The reproducing waveform (the lower) with a 12 mA sense current through the DMR against a squarely-varying excitation (the higher) in the write coil.

coil of the write head. During the measurement, the head assembly was put far away from the medium to measure noise interference occurring between the write and read elements. The MR playback channel is $2.9 \mu\text{m}$ wide, the record channels is $3.6 \mu\text{m}$ wide. The write gap length is $0.35 \mu\text{m}$ and the read gap length is $0.28 \mu\text{m}$. The gap-center separation is $2.32 \mu\text{m}$. The record channel is 9 turns. We confirmed the crossfeed waveform from the write field by both frequency comparison and amplitude dependence on sense current. In the case of single MR (Figure 4.17), the crossfeed response is $6.8 V_{p-p}$ (after an amplifier); in the case of DMR (Figure 4.18), the crossfeed response is $0.8 V_{p-p}$ (after the same amplifier). It is clear that the DMR head receives much less crossfeed noise from the recording coil than the MR sensor.

4.3.3 Philips DCC Heads

In this part, we will carry out multi-track crossfeed measurements with Philips Digital Compact Cassette (DCC) magnetic tape heads (Figure 4.19). Digital recording and playback is achieved using 9 integrated recording (IR) channels and 9 magnetoresistive (MR) channels respectively, which serve 9 parallel digital tracks on tape. The layout of the different channels contained in the head is shown in Figure 4.20. The 9 digital playback channels are each $70 \mu\text{m}$ wide (with a pitch of $195 \mu\text{m}$), the 9 digital record channels are each $185 \mu\text{m}$ wide (the pitch is $195 \mu\text{m}$). Note that the DCC multi-track head has a very wide trackwidth and track pitch but at this stage it is the only head available to us. The record channel is a single turn, as shown in Figure 4.21, single coil device which differs in technology but not in principle from conventional record heads. Figure 4.21 shows how a thin film electrical conductor carrying a write current is enclosed by a magnetic loop formed by the magnetic flux guides. The magnetic field associated with the write current is picked up by the flux guides and transported to the tape. Starting from the tape track indicated in the figure, the magnetic flux is transported across the MR element via magnetic flux guide layers. With the aid of the barberpole, the output characteristic of the MR

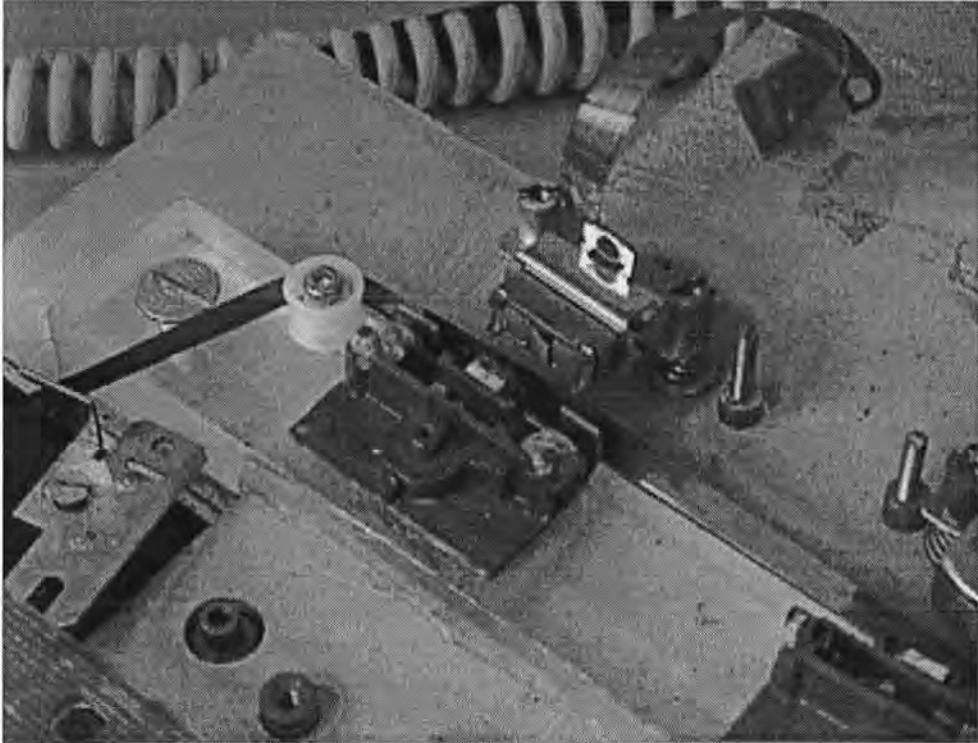


Figure 4.19: Philips Digital Compact Cassette (DCC) magnetic tape head, which serve 9 parallel digital tracks on tape.

element is linear (otherwise parabolic). Multi track recording is easily achieved by repeating this thin film structure in the head.

In the crossfeed measurement, the head assembly was put far away from the medium to measure noise interference occurring between the write and read elements. When a sine-wave recording current of 165 mA_{0-p} (optimum recording current) was flowing through the write coil of write head No.3 in the middle, we observed the reproducing waveform (crossfeed response) from MR sensor No.3 at a sense current of 10 mA on the oscilloscope, as shown in Figure 4.22. We confirmed the crossfeed waveform from the write field by both frequency comparison and amplitude dependence on sense current. The reproducing waveforms from MR sensors No.2 and No.4 are also pictured in Figure 4.22. Almost null signal can be seen on the screen. This is a design feature so that there would be fairly minimal inter-track crossfeed when

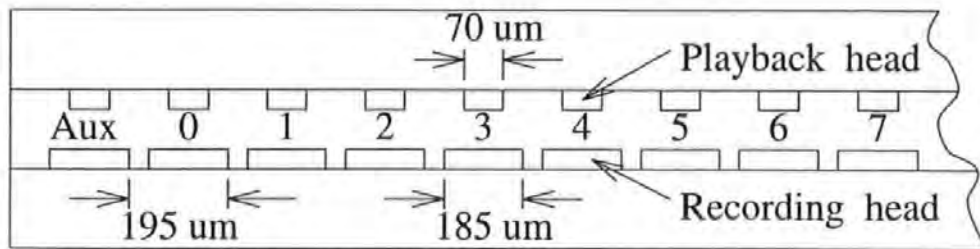


Figure 4.20: The Philips DCC head has a track pitch of 195 μm (130 tpi). The read elements are much smaller than the track pitch at 70 μm.

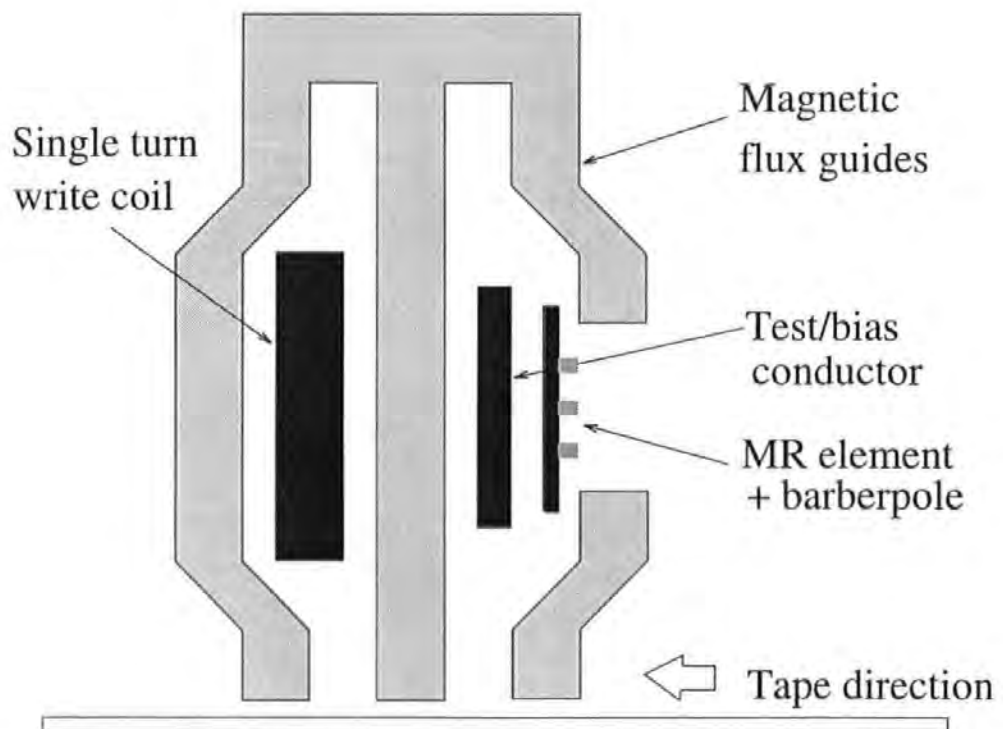


Figure 4.21: Schematic configuration of record and playback channels in the DCC head. Starting from the tape track indicated in the figure, the magnetic flux is transported across the MR element via magnetic flux guide layers. With the aid of the barberpole, the output characteristic of the MR element is linear (otherwise parabolic).

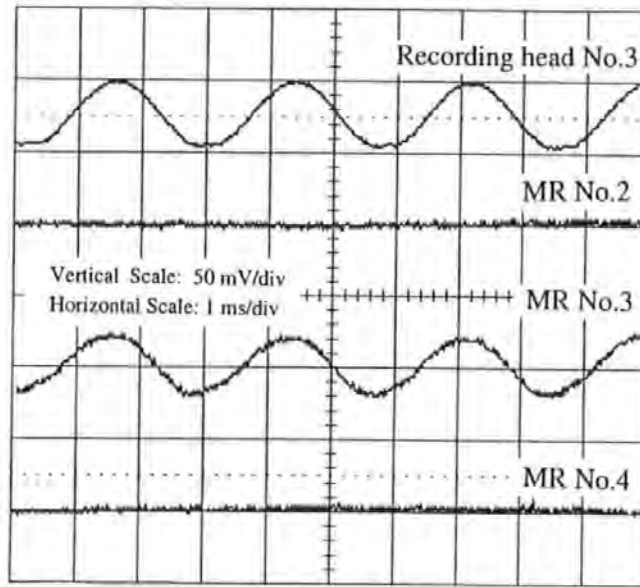


Figure 4.22: The crossfeed responses of the DCC head in MR sensor No.2, 3 and 4, respectively, against a squarely-varying excitation in write head No.3. The vertical scale is 50 mV/div and the horizontal scale is 1 ms/div.

used for digital tape recording.

4.4 Summary

This chapter assessed the scale of the crossfeed problem by making measurements on current and improved heads, thereby assessing the main contributors to crossfeed. For this purpose, we designed and developed an experimental apparatus for crossfeed and other measurements[5][33][27]. The most relevant constraint in this project was the availability of heads. Three different types of head were used for crossfeed measurements: TR5 heads for general crossfeed measurements, DSMR heads for comparison between single MR and DMR heads, and DCC heads for multi-track crossfeed measurements. In summary:

1. Electromagnetic coupling is important because it can lead to large transients in

the feedthrough waveform. Sharp pulses in the leading edges and trailing edges of the reproductive waveform have been confirmed, because of the inductive coupling between write-read windings. With regard to the capacitive coupling from the writing to the reading bumps, which should be proportional to the writing voltage, there was no observation at the reading terminals in our measurements. In principle, it may be reduced to an altogether negligible quantity by earthing one of the electrically conducting layers of the screen.

2. In the basic crossfeed measurements with TR5, whose configuration is very similar to our separator design, the peak-to-peak amplitude was found to be 176 mV at a sense current of 10 mA against an optimum recording current 40 mA_{0-p} through the write coil of the write head. On the other hand, the replay amplitude of this head was 700 mV_{p-p} over a longitudinal medium. We are now in a suitable position to compare results in a signal-noise-ratio manner. The crossfeed from the write head is about 25 % of the effective signal. We can compare these experimental results with our simulation results. In the simulation of the separator head, the SAL effective signal is $0.3285 \text{ T}\cdot\mu\text{m}^3$ while the SAL crossfeed is $0.0966 \text{ T}\cdot\mu\text{m}^3$. The crossfeed-signal ratio is $0.0966 \text{ T}\cdot\mu\text{m}^3 / 0.3285 \text{ T}\cdot\mu\text{m}^3 = 29 \%$. There is reasonably good agreement between simulation and experiment.

3. In the measurements with the DSMR heads, the MR crossfeed response is 6.8 V_{p-p} while the DMR crossfeed response is just 0.8 V_{p-p} , against the same write field. Hence, the DMR head receives much less crossfeed noise from the recording coil than the MR sensor. The best scheme to suppress the crossfeed field from the write head in a RWW tape head is to employ a Dual-MR sensor instead of a traditional (SAL) MR sensor.

4. The multi-track crossfeed measurement with DCC tape heads confirms a design feature that there would be fairly minimal inter-track crossfeed.

Chapter 5

Conclusions

5.1 Summary of This Work

A Read-While-Write (RWW) operation for tape and/or potentially disk applications is needed in the following three cases:

- 1. High reliability.** For information being recorded and verified continuously, this means that the read head and write head are operative simultaneously;
- 2. Data servo systems.** In traditional sector servo systems the servo signal is intermittent because data sectors and servo sectors are distributed alternately over the hard disk surface, thereby yielding a possible misregistration from the track when the head is passing through data sectors (inertia-dependent track following). A revolutionary track following method has been proposed, by which the position error signal (PES) of the head can be directly and continuously extracted from data sequences[4]. Another new concept of servoing with dual-strip MR (DSMR) heads uses the asymmetric microtrack profile of an MR element for estimating the data and providing servo information[5].
- 3. Buried servo systems.** A buried servo method can obtain a positioning signal continuously, in which servo and data share a medium layer by using the thin upper layer for data only and deeper layer for servo only. Both the data and the

servo signals are reproduced by an identical MR sensor.

For such continuous servo systems 2 and 3, these also mean that the read (servo) head and write head are in operation simultaneously. Consequently, RWW operation will require work to suppress the so-called crossfeed field radiation from the write head.

This research programme has been in three main parts. These relate to magnetostatics, magnetodynamics and experimental assessment of heads. A brief summary of the various components of this programme is now given in the following three sections.

5.2 Magnetostatics

A magnetostatic analysis of the head combination was first, a 2D model and then a 3D model. The TOSCA (Source: Vector Fields Ltd) software was run on a Hewlett Packard 9000-715 workstation, as shown in Figure 5.1. This is arguably the fastest and most user-friendly system available for running TOSCA.

For 2-D modelling, various sections were taken through the head, preferably along a plane of symmetry. This allowed a magnetic potential/flux-flow distribution to be produced for any MMF generator specified by some chosen boundary conditions. The flux through the MR or Dual Magnetoresistive (DMR) sensor was evaluated, leading to knowledge of the corresponding crossfeed field. The position of the MMF generator (e.g. writing coil) was varied together with the various critical dimensions in the head.

A variety of thin-film/M-R heads was studied so that new results and theory of general applicability might come out of the research, started by studying one basic configuration with sufficient flexibility in the design to allow it to be adapted for



Figure 5.1: The Hewlett Packard 9000-715 workstation. A TOSCA model is on screen.

various heads and different screening configurations. The following is a summary of the research results involving the computer model:

5.2.1 Writing Coils

The computer model took account of the effect of coil position in the head structure and its relationship to crossfeed. This was done by changing the shape of a single turn coil and using superposition to derive the result for a particular winding. The computer models were able to replicate real magnetic materials with non-linear and saturating characteristics. Two coil shapes were considered here: the commonly-used planar coil scheme and the improved tubular coil scheme. The primary motivation for the tubular coil scheme is to reduce the crossfeed using the property that the interference fields from the positive conductor and from the negative conductor will cancel each other because they are so close with respect to the MR sensor in the tubular coil scheme. Unfortunately, simulation results of the tubular coil scheme, for these two schemes, show no obvious different field distribution. This is because of the presence of magnetic poles with high permeability. In other words, the field distribution is mainly determined by the write gap between the write pole and the shared pole, not by the location of the current-carrying conductors. Nevertheless, the planar coil is easier to manufacture than the tubular coil and so all the investigations were based on the planar coil design.

5.2.2 Read and Write Gap Separation

Crossfeed in some cases is critically dependent on head dimensions, especially the read gaps (inter-shield spacing), which governs the linear resolution of readback processes and behaves just like a high-pass filter. For example, in the buried servo system, reading of the long wavelength servo signals by the data read head is enabled by the use of yoke-type read heads. Shielded heads have difficulty in detecting the servo tracks, since these heads are relatively insensitive to long wavelengths.

Read and write gap separation is another important parameter which needs to be addressed[28]. For efficient use of the available storage space a short separation is required. Therefore, both heads must be fabricated on the same substrate. In the conventional combined head, the recording head is stacked on the playback head or vice versa. This stacking of heads results in poor mechanical integrity because increasing the number and thickness of layers increases the total stress. Furthermore, these stacking processes are very time-consuming and can degrade the properties of the MR element. An additional benefit from tight write-to-read gap spacing is fewer off-track errors due to the slope of the tape (and azimuth alignment of the head) as it passes over the head. In modern thin-film/MR heads the write and read gaps can be very close together and in some cases head parts can be shared so write-read crossfeed can be unacceptable when both head functions are used at the same time.

The model was constructed with variable gap separation, each with different parameters. It is concluded that the (non-magnetic or laminated) separator plays a very important role in reducing crossfeed from the write head to the MR sensor. Generally the SCR in the separator design (3 μm separator thickness) is 3-8 dB higher than that in the shared-pole design. When the gap-center separation was more than 15 μm , the SCR (Signal-Crossfeed-Ratio) increased to larger than 20 dB. In practice, a SNR at this level hardly ever degrades the symbol error rate.

5.2.3 Screening Schemes

Different screening schemes were considered[31]. The laminated-separator design, e.g., NiFe/Cu multilayer screens, is effective in reducing the crossfeed. As illustrated in Chapter 2, the shields serve mainly to transport part of the flux from the write head back to the writing coil in the RWW operation. From this standpoint, the transporting efficiency is reasonably improved when laminated metallic magnetic materials with a high packing factor are used. The higher the lamination packing

factor, the more efficient the transportation becomes. Shields with a high packing factor act more as alternative low-reluctance paths which divert the crossfeed fields away from the MR element. Generally the SCR in the laminated-separator design is 2-3 dB higher than that in the non-magnetic separator design.

5.2.4 Other Compensation Schemes

We also considered two other compensation schemes to give further reduction of crossfeed from the write head to the MR sensor. These two compensating methods have been well-used in magnetic tape units in 1960's[14][15]. In the so-called underlayer scheme, a thick soft magnetic underlayer with high-permeability placed at a certain distance ($5\ \mu\text{m}$) behind the tape covers both the write head and the read head. It was hypothesized that this underlayer would attract most of the diverging flux and allow little write field to reach the MR sensor. In the so-called underpole scheme, a whole-plane shielding pole with a hole ($5\ \mu\text{m}$ high) to let the tape go through is used to screen the diffusing magnetic flux from the reproductive element. Unfortunately, the results show no obvious different field distribution compared with the original ones. This is because the size of the modern head is much smaller than that in the past and we have to put an underlayer or underpole relatively far apart from the TBS (Tape Bearing Surface) of the head due to the limitation of the tape thickness. Thus, both underlayer and underpole have limited use for anti-interference purposes.

5.2.5 MR Sensor

MR sensors have a variety of configurations and the model is sufficiently flexible to accommodate more than one design. The height and thickness of the sensor are especially important as well as the position between any shields. An asymmetrically positioned head in the on-track direction was catered for. It was possible, also, to allow for some MR biasing since this was especially important in crossfeed. It was

found that a biased film (a SAL), was a collector of crossfeed signals and transferred these to the MR stripe.

5.2.6 Dual-Magneto-Resistive (DMR) Sensor

Utilisation of two MR elements in a differential mode[52]citeHempstead is attractive and has led to different head designs: dual MR (DMR)[25][26], gradiometer[54], and dual stripe MR (DSMR)[6][12]. The 2-terminal DMR heads are spatially sensitive in unshielded format, while shielded DSMR heads can provide twice the output of single element structures. In a replay process using a DMR head, as shown in Figure 5.2, the leakage flux from the medium goes upward in the left stripe and returns downward in the right stripe. It constitutes a closed magnetic circuit. Obviously it causes an adequate signal output due to the parallel connection in the DMR head.

We have proposed a new Thin-Film Inductive/ Dual-Stripe-Magneto-Resistive tape head design, which is the most preferred approach for achieving simultaneous operation of the read head and write tape head. We also computed three dimensional field mappings of crossfeed situations in the case of DMR reproduction around the read gap region, at a selected applied magnetomotive force 0.60 AT through the writing coil, as shown Figure 5.3. The field distribution in the two MR stripes is almost the same because these two stripes are located so close with respect to the write gap. Obviously the output signals from these two stripes will cancel each other in the DMR case, thus an almost null final output will be caused. Generally, the SCR in the DMR designs is 15-18 dB higher than that in the SAL-MR reproductive design.

In summary, the best scheme to suppress the crossfeed field from the write head in a RWW tape head is to employ the so-called laminated-separator head configuration and simultaneously employ a Dual-MR sensor instead of a traditional SAL-MR sensor. The SCR is 28.6 dB for the head with 3 μm non-magnetic separator or 30.4

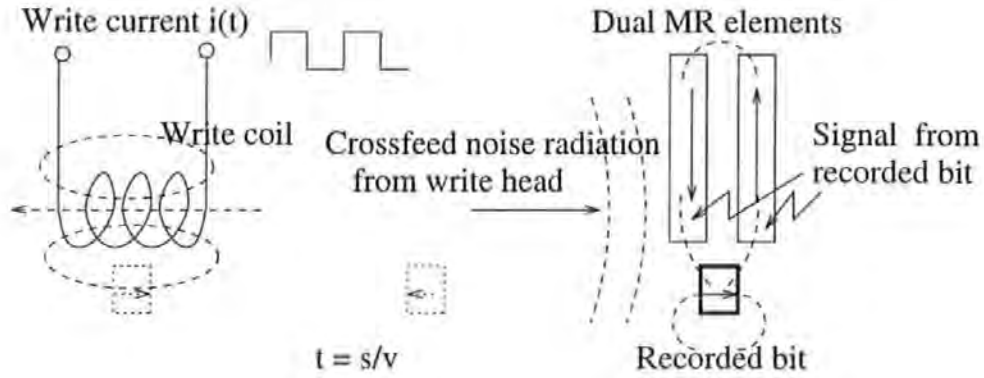


Figure 5.2: A recorded bit is being picked up by a DMR head. The leakage flux from the medium goes upward in the left stripe and returns downward in the right stripe. It constitutes a closed magnetic circuit. Obviously it causes an adequate signal output due to electrically parallel connection in the DMR head.

dB for the head with 3 μm laminated-separator beside the inserted pole (packing factor is 0.5). To reduce the manufacture cost, the shared-pole DMR configuration, whose SCR is 22.6 dB, is also acceptable.

5.2.7 Track Arrangement

This allowed for a relative variation of writing and reading track widths, for example, in a write-wide, read-narrow structure. The 3D computer model replicated the model and used superposition to study the effect of several heads writing and reading simultaneously. In Figure 5.4 there was an XYZ coordinate to position the head so that the individual crossfeed signals from different locations could be detected and summed. When an MR head is biased, the magnetic vector is placed approximately at 45 degrees to the current flow direction. To reduce Barkhausen noise a transverse field component was sometimes used. The field from the tape also has transverse components in it, especially if the track is narrow. It is found that, the crossfeed noise in DMR decreases much more sharply than that in SAL-MR as the separation increases. For example, the crossfeed noise at a typical point ($x=\pm 4g, z=0$) in the DMR design is only 4.5 % of that at the same point in the SAL.

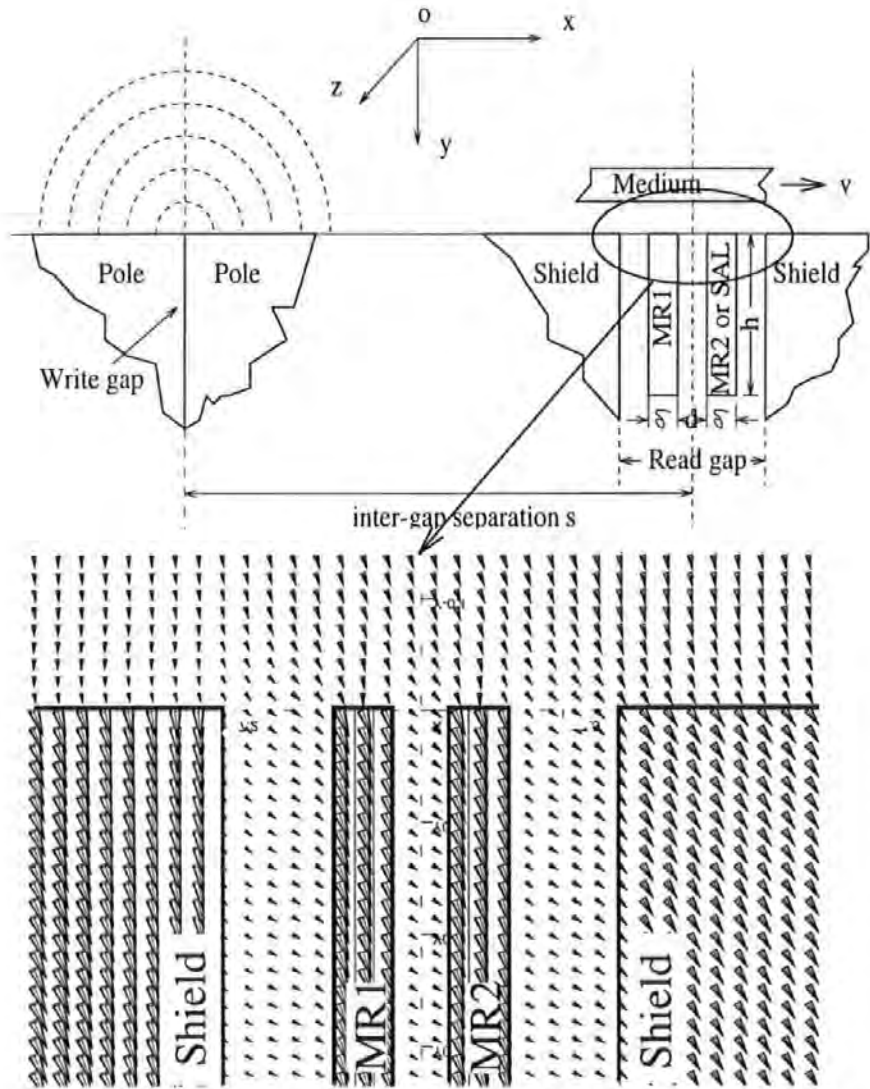


Figure 5.3: Resultant crossfeed field suppression by using a Dual MagnetoResistive head. Here the contribution from the medium is not included in the magnified flux density distribution.

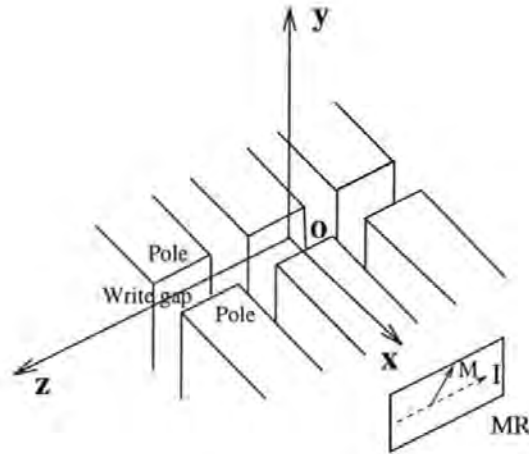


Figure 5.4: A multi-track Read-While-Write (RWW) head. When an MR head is biased, the magnetic vector is placed approximately at 45 degrees to the current flow direction. To reduce Barkhausen noise a transverse field component is sometimes used. The field from the tape also has transverse components in it, especially if the track is narrow. For these reasons it is important to consider the cross-track direction for crossfeed within a combination head.

In the case of multitrack heads (Figure 5.4), the transverse direction is very important, with an array of read heads. The gaps are not in the same lines relative to each other and the angles of the fields change with the track number. Also, the end tracks have a different crossfeed response from the tracks in the middle of the head. The individual crossfeed signals from different locations should be considered for a particular gap in the read array. In the SAL-MR case, the center-track crossfeed response at $(x=\pm 4g, z=0)$ is 22.1% stronger than the end-track response at $(x=\pm 4g, z=\pm 3g)$. In the Dual-MR case, the center-track crossfeed response at $(x=\pm 4g, z=0)$ is just 3.2% stronger than the end-track response at $(x=\pm 4g, z=\pm 3g)$ [29].

5.3 Magnetodynamics

At high frequency, the copper screens are activated by eddy-currents and represent increased reluctance (above air) to the crossfeed fields. The permalloy screens act more as alternative low-reluctance paths which divert the crossfeed fields away from the reading heads. It has been found possible in multitrack heads to adjust eddy-current and magnetic screens in such a way as to produce near zero crossfeed fields in arrays of reading heads when an array of writing heads are simultaneously writing. It was proposed to explore such ideas within this project bearing in mind that the eddy-current shielding imposes a phase-shift on the crossfeed fields at high frequencies. To model crossfeed at high frequency requires calculation of eddy-current effects in head components and screens since there are not only amplitude effects but also phase effects which need to be considered. For this we used a high-frequency simulation software package, ELECTRA, running on a Hewlett Packard 9000-715 workstation, as shown in Figure 5.1.

It is concluded that:

1. It is advantageous to use magnetic materials with a low conductivity to prevent eddy currents. The corresponding crossfeed reduction is 7% in the SAL case and 8% in the DMR case, when Fe-Al-O is used compared with conventional FeN material at a working frequency of 5MHz.
2. It is advantageous to cut a slot through the metallic magnetic pole and shields to retard the in-plane eddy currents[34]. The corresponding crossfeed reduction is 3% in the SAL case and 5% in the DMR case, compared with the conventional case at a working frequency of 5MHz.
3. An improved shield-wing-interconnecting design can reduce the crossfeed field by a factor of 4% in the the SAL case and 5% in the DMR case, compared with that of a traditional parallel-shield design. The eddy currents around the constituted

conductive loop produce a counteracting field to block the penetrating flux.

4. Keep-ered media is a potential technique with smoother transition, quieter replay and anti-thermal stability[32][30]. Here we propose a new concept of keep-ered-medium-reproduction with Dual MR heads. Most interestingly, the principle of using dual MR stripe to suppress the crossfeed field is in harmony with the keep-ered media reproduction with DMR heads. The conductive keeper plays a positive role in suppressing crossfeed field. There is an automatic 11% reduction with the use of a conductive keeper layer.

In addition, as mentioned in Chapter 1, the early theoretical investigations of the crossfeed problem concentrating on the flux line pattern in front of a head structure based on a simplified model, may not be comprehensive. In this thesis, in order to find a satisfactory practical solution to achieve the RWW operation, we have built an overall head configuration model, including as many contributors to crossfeed as possible. The primary beneficiary of this comprehensive model is the idea of cutting a slot through the metallic magnetic pole and shields to retard the in-plane eddy currents. The geometric location of this slot is so far away from the TBS that this solution would not be found by a simplified model concentrating on the flux line pattern in front of a head structure.

5.4 Experimental Assessment of Heads

The last step was to assess experimentally the scale of the crossfeed problem by making measurements on current and improved heads, thereby assessing the main contributors to crossfeed. The primary components can (usually) be separated out into electrostatic and electromagnetic crossfeed. Electrostatic crossfeed is important because it can lead to large transients in the feedthrough waveform. It is usually reduced by grounding the metallic parts of the head or introducing grounded planes in key positions. Inter-lead coupling is also a source of electrostatic crossfeed[48].

Electromagnetic crossfeed usually has a different waveform and is suppressed using different techniques.

The most relevant constraint in this project was the availability of heads. Three different heads were used for crossfeed measurements: TR5 heads for basic crossfeed measurements, DSMR (Dual Stripe Magneto-Resistive) heads for comparison between single MR and DMR heads, and DCC heads for multi-track crossfeed measurements. It is concluded that:

1. Electromagnetic coupling is important because it can lead to large transients in the feedthrough waveform. Sharp pulses in the leading edges and trailing edges of the reproductive waveform have been confirmed, because of the inductive coupling between write-read windings. With regard to the capacitive coupling from the writing to the reading bumps, which should be proportional to the writing voltage, there was no observation at the reading terminals in our measurements. In principle, it may be reduced to an altogether negligible quantity by earthing one of the electrically conducting layers of the screen.

2. In the basic crossfeed measurements with TR5, whose configuration is very similar to our separator design, the peak-to-peak amplitude was found to be 176 mV at a sense current of 10 mA against an optimum recording current 40 mA_{0-p} through the write coil of the write head. On the other hand, the replay amplitude of this head was 700 mV_{p-p} over a longitudinal medium. Therefore, the crossfeed from the write head is about 25 % of the effective signal. We can compare these experimental results with our simulation results. In the simulation of the (non-magnetic) separator head with 3 μm separator thickness, the SAL effective signal is 0.3285 T·μm³ while the SAL crossfeed is 0.0966 T·μm³. The crossfeed-signal ratio is 0.0966 T·μm³ / 0.3285 T·μm³ = 29 %. There is reasonably good agreement between simulation and experiment.

3. In the measurements with the DSMR/indexDSMR (Dual Stripe Magneto-Resistive)

heads, the MR crossfeed response is $6.8 V_{p-p}$ while the DMR crossfeed response is just $0.8 V_{p-p}$, against the same write field. Hence, the DMR head receives much less crossfeed noise from the recording coil than the MR sensor. The preferred scheme to suppress the crossfeed field from the write head in a tape head is to employ a Dual- MR sensor instead of a traditional (SAL) MR sensor.

4. The multi-track crossfeed measurement with DCC heads confirms a design feature that there would be fairly minimal inter-track crossfeed when used for digital tape recording.

5.5 Scientific/Technological Relevance

The relevance of this work to the computer industry is clear for achieving simultaneous operation of the read head and write head. The primary beneficiaries of this research are manufacturers of tape back-up systems for computers and data recorders which need to operate at high data rates with verification. To a lesser extent, the beneficiaries will include manufacturers of tape heads. Computer manufacturers will also benefit. More generally, all manufacturers of high-performance data storage systems could benefit, especially those using thin-film tape heads. This is because computer data rates must increase to meet the demands of storing more and more information in less time as computer graphics packages become more sophisticated. Present systems can operate at much higher data rates if the read head and write head are in operation at the same time. This is especially true of tape units where it is necessary to verify the written information on a tape by reading it with a read head a short time later.

5.6 Future Work

The work in this thesis is limited to head structure optimization. However, from the viewpoint of signal processing, the crossfeed field from a magnetic recording head field is a specific kind of noise. In other words, it is not a random noise, compared with other noise, because it is determined by what was written on the tape. Therefore, there exists one possibility to reduce the crossfeed field from the effective signal by designing a new demodulation circuit, in which a "pick-up coil" in the write head side would be used to sense the recorded data for comparison purposes and then this picked signal would be feedback to the reading terminals to remove away the excessive part of the crossfeed. So a high Signal-to-Crossfeed-Ratio (SCR) may not be required for signal processing, while with real noise at least 20 dB Signal-to-Noise-Ratio (SNR) is required. In practice, a SNR at this level hardly ever degrades the symbol error rate. Normally, a high SCR design results in high head manufacturing cost due to the complicated structure. It should be possible for head designers to divert some of the difficulties of crossfeed reduction to signal processing, but in order to solve the crossfeed problems satisfactorily in practical applications, a good balance between head design and signal processing will be needed, but this is beyond the scope of this thesis.

References

- [1] Finn Jorgensen, *The Complete Handbook of Magnetic Recording*, 3rd edition, Blue Ridge Summit, PA, USA, 1979
- [2] John C. Mallinson, *Magneto-Resistive Heads (Fundamentals and Applications)*, Academic Press Inc., 1995
- [3] J.J.M.Ruigrok, H.W.van Kesteren, S.R.Cumpson, D.J.Adelerhof, S.B.Luitjens, E.A.Draaisma and A.Hoogendoorn, "Multitrack thin film heads for the DigaMaxTM tape storage system", *IEEE Trans. Magn.*, Vol.34, No.4, pp.1459-1461, 1998.
- [4] L.He,N.Honda,K.Ouchi & S.Iwasaki, "A Novel Data Servo Method", *IEEE Trans. Magn.*, Vol.32, No.5, pp.3896-3898, 1996.
- [5] L.N.He, Z.G.Wang, Bin Liu, D.J.Mapps, P.Robinson, D.T.Wilton and Y.Nakamura, "Estimation of Track Misregistration by Using Dual-Stripe MR Heads", *IEEE Tran.Magn.*, Vol.34, No.4, pp.2348, 1998.
- [6] Voegel, Patent US 3860965
- [7] J.Zhu and D.J.O'Connor, "Impact of Microstructure on Stability of Permanent Magnet Biased Magnetoresistive Heads", *IEEE Trans. Magn.*, Vol. 32, No. 1, pp.54-60, 1996.
- [8] Y.Shen, W.Chen, W.Jensen, D.Ravipati, V.Retort, R.Rottmayer, S.Rudy, S.Tan and S.Yuan, "Comparative Study of MR Head Designs with Abutted vs. Overlaid Permanent Magnet Bias", *IEEE Trans. Magn.*, Vol. 32, No. 1, pp. 19-24, 1996.

- [9] N. H. Yeh, "Asymmetric Crosstalk of Magnetoresistive Head", *IEEE Trans. Magn.*, Vol. 18, No. 6, p.1155-1157, 1982.
- [10] F.B.Shelledy, J.L.Nix, "Magnetoresistive Heads for Magnetic Tape and Disk Recording", *IEEE Trans. Magn.*, Vol.28, No.5, p.2283-2288, 1992.
- [11] H.N.Bertram, *Theory of Magnetic Recording*, Cambridge University Press, 1994
- [12] Y.Hsu, C.C.Han, H.Chang, G.Ching, D.Hernandez, M.M.Chen, K.Ju, C.Che, J.Fitzpatrick, "Dual-Stripe MR Heads for One Gigabit per Inch Square Recording Density", *IEEE Trans.Magn.*, Vol.31, No.6, p.2621, 1995.
- [13] M. Mallary, S.Batra, and G.C.Rauch, paper EB-05, 37th MMM, 1992.
- [14] G.I.Walther, "Reduction of Crosstalk in Multiple-Head Structures for Digital Tape Units", *International Conference on Magnetic Recording (IEE)*, p.65, 1964.
- [15] J.A.Geurst, "Suppression of Cross-Talk Between Magnetic Heads in Magnetic Tape", *International Conference on Magnetic Recording (IEE)*, p.62, 1964.
- [16] H.N.Bertram, J.C.Mallinson, "A Theory of Eddy Current Limited Heads", *IEEE Trans. Magn.*, Vol.12, No.6, p.713, 1976.
- [17] D.Sansom, "Recording head design calculation", *IEEE Trans. Magn.*, Vol.12, No.3, pp.230-233, May 1976.
- [18] A.van Herk, "Analytical expressions for side fringing response and crosstalk with finite head and track widths", *IEEE Trans. Magn.*, Vol.13, No.6, pp.1764-1766, November 1977.
- [19] K.Tanaka, "Some considerations on crosstalk in multihead magnetic digital recording", *IEEE Trans. Magn.*, Vol.20, No.1, pp.160-165, January 1984.
- [20] J.M.Coutellier, H.Magna and X.Pirot, "A 384 track fixed recording head", *IEEE Trans. Magn.*, Vol.28, No.5, pp.2653-2655, September 1992.

- [21] Y.Murata, S.Tanabe, S.Handa and T.Ozeki, "A crosstalk model considering leakage fluxes and methods to reduce crosstalk between read/write head and pre-erase head", *IEEE Trans. Magn.*, Vol.32, No.6, pp.5271-5276, November 1996.
- [22] S.B.Luitjens, A.V.Herk, "A Discussion on the Crosstalk in Longitudinal and Perpendicular Recording", *IEEE Trans. Magn.*, Vol. 18, No.6, p.1804, 1982.
- [23] B.Gooch, R.Niedemeyer, R.Wood and R.Pisharody, *IEEE Trans.*, MAG-27, No.6, p.4549, 1991
- [24] W.Reed, U.Cohen, D.Hollars, B.Zubeck, AB-10, Intermag'96
- [25] N.Smith, J.Freeman, P.Koeppel, and T.Carr, "Dual Magnetoresistive Head for Very High Density Recording", *IEEE Trans. Magn.*, Vol. 28, No. 5, pp. 2292-2294, 1992.
- [26] N.Smith, D.R.Smith, and S.Shtrikman, "Analysis of a Dual Magnetoresistive Head", *IEEE Trans. Magn.*, Vol. 28, No. 5, pp. 2295-2297, 1992.
- [27] L.N. He, Z.G. Wang, D.J. Mapps, P. Robinson, D. Jenkins and W.W. Clegg, "Nano-Scale Positioning for Magnetic Recording", in press, *Sensors and Actuators A: Physical*, 1999
- [28] Z.G.Wang, D.J.Mapps, D.T.Wilton, L.N.He, "Read-While-Write Operation in Magnetic Recording", in press, *J. Magn. Magn. Mater.*, 1999
- [29] Z.G. Wang, L.N.He, D.J. Mapps, D.T.Wilton and W.W. Clegg, "Crossfeed Response of DMR vs. SAL Multitrack Heads", *IEEE Trans. Magn.*, Vol.34, No.4, pp.1456-1458, July 1998
- [30] Z.G. Wang, L.N. He, D.J. Mapps, D.T. Wilton and W.W. Clegg, "Kepered Media Reproduction with Dual MR Heads", *IEEE Trans. Magn.*, Vol.34, No.4, pp.1982-1984, July 1998

- [31] Z.G. Wang, D.J. Mapps, D.T. Wilton, L.N. He, "Crossfeed problems in read-while-write inductive/MR tape head", *IEEE Trans. Magn.*, Vol.33, No.4, p.2531-2537, July 1997
- [32] L.N. He, Z.G. Wang, D.J. Mapps, W.W. Clegg and D.T. Wilton, , "Perpendicular Kepered Media Reproduction with Dual MR Heads", *Journal of the Magnetics Society of Japan*, Vol.21, No.S2, pp.273-276, 1997
- [33] L.N.He, Z.G.Wang, D.J.Mapps, "Direct-access probe data storage", 7th International Conference on Magnetic Recording Media, Maastricht, The Netherlands, 1998
- [34] D.J.Mapps, Z.G.Wang, D.T.Wilton, L.N.He and W.W.Clegg, "Suppression of Cross-Feed Field for Magnetic Recording", accepted by *J. Magn. Magn. Mater.*, 1999
- [35] C.D.Mee, *The Physics of Magnetic Recording*, North-Holland Personal Library, (1986)
- [36] C and C++ SoftBench User's Guide, HP LaserROM HP UX 9.0, June 1995
- [37] MATLAB version 4.2c for Microsoft Windows, Copyright 1994, MathWorks Inc.
- [38] D.A.Lindholm, "Magnetic Fields of Finite Track Width Heads", *IEEE Trans. Magn.*, Vol.13, No.5, pp.1460(1977)
- [39] TOSCA Reference Manual, Vector Field Ltd., Oxford, United Kingdom, 1992.
- [40] S.X.Wang, P.R.Webb, "Modeling of Submicron Trackwidth Inductive Write Head Designs", *IEEE Tran. Magn.*, Vol.31, No.6, p.2687, 1995.
- [41] TR5 Manual, personal communication with Read-Rite company
- [42] E.A. Draaisma, S.R.Cumpson, T.P.H.G.Jansen, P.Hidding and S.B.Luitjens, "Performance of advanced tapes with DigaMax thin film heads", *J. Magn. Magn. Mater.*, (in press), 1999.

- [43] H.Takano, H.Shinada, S.Seitou, S.Fukuhara, T.Ohnishi, S.Otomo, H.Todokoro and K.Shiiki, "A Study on the Field Distribution of Thin-Film Heads", *IEEE Tran. Magn.*, Vol.28, No.2, p.4001, 1992.
- [44] ELEKTRA Reference Manual, Vector Field Ltd., Oxford, United Kingdom, 1992.
- [45] M. Nelkon, *Electricity*, Edward Arnold Ltd., London, 1970
- [46] W.D.Li, O.Kitakami, Y.Shimada, K.Ishiyama and K.I.Arai, *Journal of the Magnetism Society of Japan*, Vol.20, No.2, pp. 461-464, 1996.
- [47] Y.Nakamura, "A Challenge to Terabit Perpendicular Spinic Storage", *J.Magn.Soc.Jpn.*, Vol.18, Supple.No.S1, pp161-170, 1994.
- [48] D.J.Mapps, M.L.Watson, D.T.Wilton, "Asymmetric Biasing Fields from Mismatched Current-Carrying Overlay Conductors on Magnetoresistive Replay Sensors", *J.Appl. Phys.*, Vol.57, No.1, p.3982, 1985.
- [49] T.L.Chow, *Classical Mechanics*, John Wiley and Sons, Inc., USA, 1995
- [50] K.Takata and T.Hasegawa, *Appl. Phys. Lett.*55(1989)1718
- [51] *Piezoelectric Multi-layer Actuators Technical Data Sheet*, Morgan Matroc Limited, 1997
- [52] D.J.Mapps, U.K. patent No. 2143071, 28/10/1987
- [53] R. Hempstead, "Analysis of Thermal Noise Spike Cancellation", *IEEE Trans. Magn.*, Vol.11, No.5, p.1224, 1975.
- [54] R.S.Indeck, J.H.Judy, and S.Iwasaki, "A Magnetoresistive Gradiometer", *IEEE Trans. Magn.*, Vol. 24, No.6, pp. 2617-2619, 1988.

Crossfeed Problems in Read-While-Write Tape Heads

Zhi Gang Wang, Desmond J. Mapps, David T. Wilton, and Lianna N. He

Abstract— Three-dimensional finite element models have been utilized to simulate the crossfeed problems in read-while-write (RWW) tape heads, and the results have been compared with experimental measurements. The most significant contributors, such as shield structure, intershield spacing, and reproductive mode, have been identified. A new thin-film inductive/dual-magneto-resistive tape head design was found to reduce the crossfeed by about a factor of 30, compared with the conventional shared-pole design, which is the most favored approach for achieving simultaneous operation of the READ head and WRITE head.

Index Terms—Dual magneto-resistive head, magnetic recording, magnetic tape head, read-while-write operation.

I. INTRODUCTION

IT IS NECESSARY in some recording systems to write information on tape and verify it by reading with a READ head a short time later. For example, defects in the tape material and in the contact between the head and tape may give rise to errors in the recorded information. In order to detect such "drop-outs," a reproducing head placed closely behind the recording head in each track is employed to check-read the information stored on the tape. For information being recorded and verified continuously, this means that the READ head and WRITE head are in operation simultaneously. The magnitude of the flux sensed by the READ head on the tape is of the order of pico-webers (i.e., very small). In contrast, the writing flux can be very large, especially if a high-coercivity medium is being used. This means that the READ head may receive a flux component from the WRITE head which is of significant magnitude compared with the signal flux it is detecting from the tape, and this is especially true if the WRITE head and READ head are close together—an essential design-aim if the "dead" tape at the end of a recorded block of information (the interblock gap) is to be minimized. In intermittent operation of the tape-unit, the tape stops when the end of the record passes the reproducing gaps. Unless the tape is spooled backward before the next recording takes place, an interrecord gap arises in this way, the length of which is determined by the distance between the recording and reproducing-transducer gap and by the starting and stopping time of the tape transport mechanism. For efficient use of the available storage space, a short distance between the head gaps is thus required. An additional benefit from tight write-to-read gap spacing is less off-track errors due to the slope of the tape (and azimuth alignment of the head) as

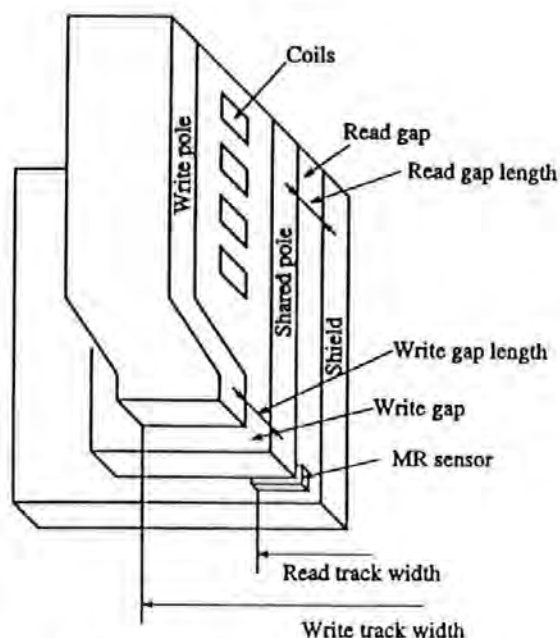


Fig. 1. A typical design for a thin-film-magneto-resistive tape head, based on a shared-pole sensor-in-gap structure.

it passes over the head. In modern thin-film/magneto-resistive (MR) heads the write and read gaps can be very close together (e.g., 10 μm) and in some cases, head parts can be shared, as shown in Fig. 1, so write-read crossfeed can be unacceptable when both head functions are used at the same time [1]–[4].

In principle, four different sources of crossfeed can easily be distinguished, namely:

- capacitance coupling from the writing to the reading bump;
- inductive coupling from the writing to the reading winding;
- magnetic flux leaking around the screens;
- magnetic flux penetrating through the screens.

In the inductive/MR tape head designs, the capacitive and inductive coupling between write-read bumps will result in sharp pulses in the leading edges and trailing edges of the reproductive waveform. Magnetic flux penetrating through the screens may be reduced to a negligible quantity by demagnetization and eddy current effects, especially in high-density recording. In this paper, we utilized a three-dimensional (3-D) finite element model to simulate the electromagnetic behavior in read-while-write (RWW). Analytical and numerical methods of calculating magnetic flux distributions and other problems can often help a head designer understand how the flux spreads and, therefore, how the head size for a given overall configuration is limited.

Manuscript received September 4, 1996; revised March 10, 1997.

Z. G. Wang, D. J. Mapps, and L. N. He are with the School of Electronic, Communication and Electrical Engineering, University of Plymouth, Drake Circus, Devon PL4 8AA, U.K. (e-mail: zwang@plymouth.ac.uk).

D. T. Wilton is with the School of Mathematics and Statics, University of Plymouth, Devon PL4 8AA, U.K.

Publisher Item Identifier S 0018-9464(97)04874-7.

II. READ-WHILE-WRITE TAPE HEAD DESIGNS

Three read-while-write tape head designs are considered in this paper, and their side views are shown in Fig. 2. The reference head (conventional merged head design) is shown in Fig. 2(a). It is based on a low-cost shared-pole sensor-in-gap head design (Fig. 1). All the three poles are $2.0\ \mu\text{m}$ thick, and the throat height is $10\ \mu\text{m}$. The WRITE head gap is $1.80\ \mu\text{m}$. The angle of the inclination of the left pole near the zero-throat point is 45° . The pole tip widths of the left pole (write pole), the shared pole, and the right pole (shielding layer) are $99.06\ \mu\text{m}$, $238\ \mu\text{m}$, and $344\ \mu\text{m}$, respectively. The left pole and shared pole are $10\ \mu\text{m}$ apart in the yoke region. Overall, they are about $240\ \mu\text{m}$ high. The head coils are assumed to be a single turn, and the applied magnetomotive force is $0.48\ \text{A}$ -turns. This is approximately equivalent to a write current of $60\ \text{mA}$ for an eight-turn coil. In order to allow the head to write the high coercivity ($130\ \text{kA/m}$) metal particle medium, the pole material is chosen to be a FeN-based soft magnetic film with a saturation magnetization of $2.1\ \text{T}$ and an initial permeability of 3500 . The read gap here is defined as the shield-to-shield separation, $0.35\ \mu\text{m}$, which governs the linear resolution of readback processes. Two parallel soft magnetic stripes in gap configuration have been used. For each head design, we will consider two replay cases: the soft adjacent layer (SAL) [5] case and the dual-magneto-resistive (DMR) case. In the SAL case, the left stripe is assumed to be NiFe material for the MR sensor while the right stripe is assumed to be CoZrNb material for bias purposes. In the DMR case, both stripes are assumed to be NiFe material for the two MR sensors. The DMR design has several advantages over the SAL approach, such as the simple fabrication and the large intrinsic sensitivity at high linear density [6], [7]. The primary motivation for our schemes is to make use of the high common-noise rejection ability to reduce crossfeed greatly. The MR track width is $50.8\ \mu\text{m}$, about half of the write track width. The MR stripe thickness is $500\ \text{\AA}$. The thicknesses of the dielectric layers are $1000\ \text{\AA}$, $500\ \text{\AA}$, and $1000\ \text{\AA}$, respectively. The MR stripe depth is $5.0\ \mu\text{m}$. In order to enlarge the spacing between the gaps, we propose a so-called air-gap design as shown in Fig. 2(b). This is a slight variation of the reference head only between the write gap and read gap. It differs from the reference head by the elimination of a shared pole and an addition of a $3\ \mu\text{m}$ air gap between the two head elements. Separating write element and the read element by an air gap enables separate optimization of write and read elements. The third design considered in this paper, called the inserted-pole design, is shown in Fig. 2(c). In this case, an additional pole with $2\ \mu\text{m}$ thickness is inserted between the two head elements. The two air gaps beside the inserted pole are the same thickness, $3\ \mu\text{m}$. It was hypothesized that the recording field would be confined on the left side of this inserted pole.

III. THE FINITE ELEMENT MODEL

The TOSCA 3-D Nonlinear Magnetic Field Simulation Package [8] (supplied by Vector Field Corp.) was used to study the crossfeed problems. Finite element discretization forms the basis of the methods used in these analysis programs

[9]. These programs provide facilities for the creation of finite element models, specification of complicated conductor geometry, definition of material characteristics including for example, nonlinear and anisotropic descriptions and graphical displays for examination of the data.

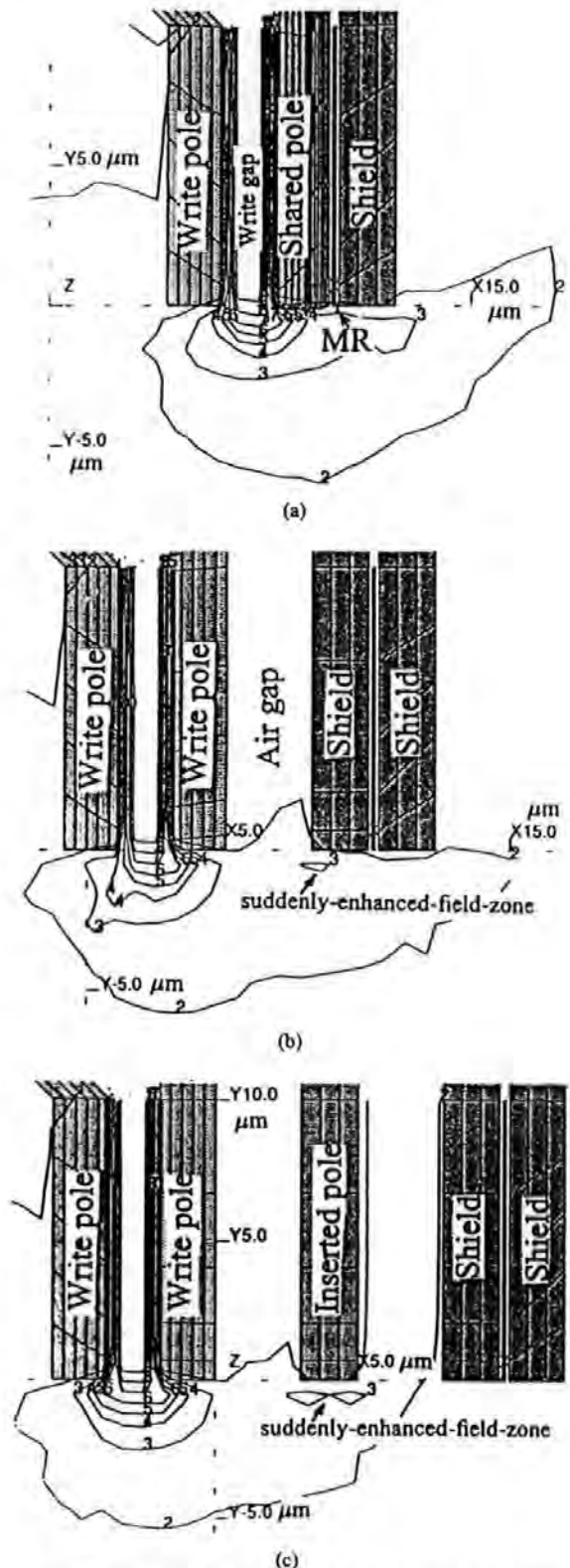


Fig. 2. Three RWW tape head designs and their write field contours at a selected applied current ($I = 0.48\ \text{A}$) in the mid-width cut plane. For clarity, only ten contour lines are shown and numbered from zero to nine.

Due to the symmetric structure of the heads, only half of the structure is needed for the simulation. The maximum element number used in the modeling was 45 000. For a WRITE head, it is assumed that the permeability of the recording medium is the same as that of air. An open boundary was used in the model. The effect of the open boundary condition on the accuracy of the solution was verified by comparing the solutions obtained by applying the potential and derivative boundary conditions to the open boundary, and the errors between the two were within 3.5%.

The output of the MR head was evaluated by the volume integral of magnetic flux density within the MR stripe. Its expression is as below

$$\text{Output of single MR stripe} \propto \iiint B_y dx dy dz.$$

The volume integral's unit is $T \cdot \mu\text{m}^3$.

As mentioned above, we will consider both the SAL case and the DMR case for each head design. In the SAL case, we can simply take the volume over the left stripe integral as the final output of MR head. However, in the DMR case, we should subtract the integral over the right stripe from that over the left one as the DMR is sensitive only to the antisymmetric components of magnetic flux.

IV. CROSSFEED SIMULATION RESULTS

As described above, in our reference design, the pole tip widths of the write pole and the shared pole are $99.06 \mu\text{m}$ and $238 \mu\text{m}$, respectively. The primary motivation for this well-used merged head with different width poles is to reduce the magnetic flux resistance. The structure employed here, however, has another advantage that the magnetic flux leaking around the two sides of the shared pole would effectively be confined behind the pole. The write field amplitude contours in the midheight cut plane of MR stripe are shown in Fig. 3. For comparison, the case of the head design with the same pole width is also shown in the same figure.

The write field amplitude contours of the three designs at a selected applied current ($I = 0.48 \text{ A}$) in the midwidth cut plane are shown in Fig. 2. For clarity, only ten contour lines are shown and numbered from zero to nine. The field contours are significantly asymmetric due to the existence of the read assembly. In particular, the 20 kA/m field contour (corresponding to line two) extends out about $10 \mu\text{m}$ toward the read gap side from the write gap. In contrast, it extends out only $2.5 \mu\text{m}$ in the inverse side. Another phenomenon deserving note is that so-called suddenly enhanced field zone exists in some regions, in agreement with an electron beam tomography measurements on three components of the thin-film head field distribution [10]. For example, in Fig. 2(b), the 40 kA/m field contour line (corresponding to line three) self closes underneath the shielding layer whereas in Fig. 2(c), the 40 kA/m field contour line (corresponding to line three) self closes underneath the inserted pole. These facts imply that the MR reproductive element will receive serious interference from the write field, but the interference strength depends on

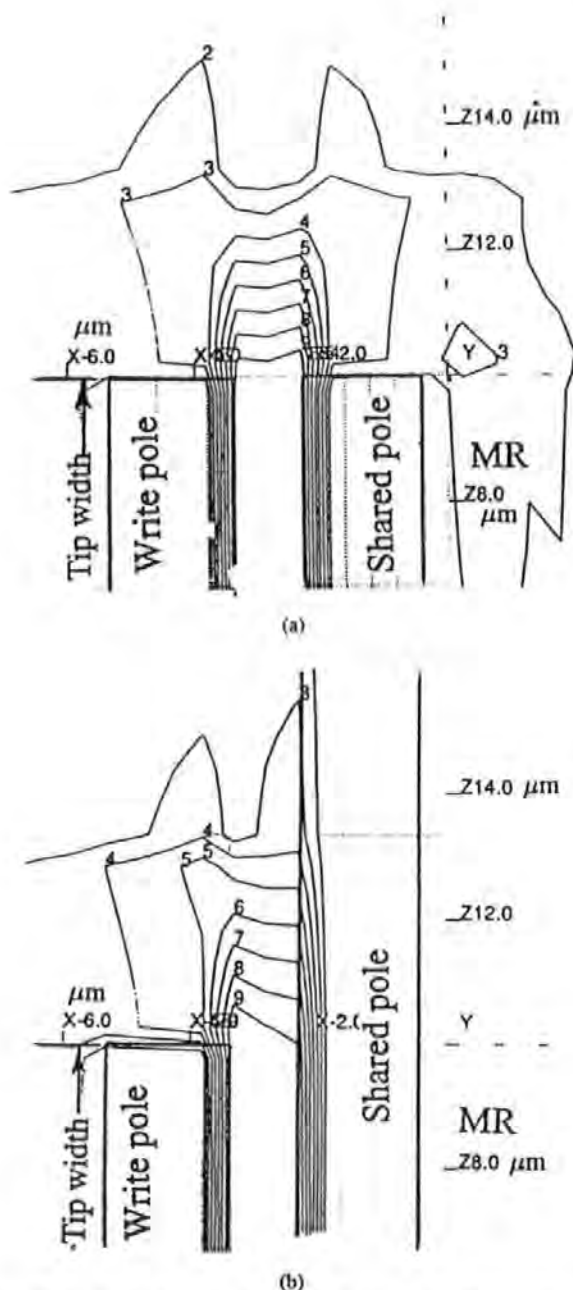


Fig. 3. The write field amplitude contours in the midheight cut plane of the MR stripe. The contour lines are numbered.

the different head structures. The exact calculation results are as follows:

Fig. 2(a) SAL crossfeed is $1.5425 T \cdot \mu\text{m}^3$ while the DMR crossfeed is $0.3425 T \cdot \mu\text{m}^3$;

Fig. 2(b) SAL crossfeed is $1.1313 T \cdot \mu\text{m}^3$ while the DMR crossfeed is $0.1706 T \cdot \mu\text{m}^3$;

Fig. 2(c) SAL crossfeed is $0.3180 T \cdot \mu\text{m}^3$ while the DMR crossfeed is $0.0740 T \cdot \mu\text{m}^3$.

From the above results, we see that shared-pole head design exhibits significant crossfeed from the write signals to read sensor as a result of the shared pole and close proximity of the write element to the read sensor. Although we cannot see an obvious improvement between (b) and (a), we can see an obvious improvement between (c) and (a). Compared

with the reference head, the crossfeed of the air-gap type head is reduced by 136% in the SAL case and 201% in the DMR case. Compared with the reference head, the crossfeed of the inserted pole type head is reduced by 484% in the SAL case and 462% in the DMR case. The main reason for such an obvious improvement in the inserted pole head design is that the suddenly-enhanced-field-zone appears underneath the inserted pole, whereas the suddenly-enhanced-field-zone appears underneath the MR sensor/shields in the air-gap head design.

We can confirm the above conclusion further by vertical field mapping. A typical simulated 3-D field mapping of the vertical component in the air bearing surface (ABS) plane is shown in Fig. 4. We only take the vertical field into account because the MR sensor is only sensitive to the vertical component. In Fig. 4(a), the MR sensor is located near the positive peak of the vertical component. In Fig. 4(b), there are two separated positive peaks, and the MR sensor is located in the second peak. In Fig. 4(c), there are three positive peaks, and the MR sensor is located in the third peak. Because the third peak is much lower than the other two, the MR sensor senses little magnetic flux from the write head. We conclude that in the inserted pole head design, the inserted pole plays a very important role in reducing crossfeed from the WRITE head to the MR sensor because it attracts most of diverging flux from the write head. Therefore, the inserted-pole head is a favored approach for achieving simultaneous operation of the READ head and WRITE head.

We also considered two other compensation schemes to give further reduction of crossfeed from the WRITE head to the MR sensor. These two compensating methods have been well-used in magnetic tape units [4]. Fig. 5 shows an underlayer scheme. In this scheme, a thick soft magnetic underlayer with high-permeability placed at a certain distance ($5 \mu\text{m}$) behind the tape covers both the WRITE head and the READ head. It was hypothesized that this underlayer would attract most of the diverging flux and little write field would interfere with the MR sensor. Fig. 6 shows an under-pole scheme. In this scheme, a whole-plane shielding pole with a hole ($5 \mu\text{m}$ high) to let the tape go through is used to screen the diffusing magnetic flux from the reproductive element. Unfortunately, Figs. 5 and 6 show no obvious different field distribution compared with the original one [Fig. 2(c)]. This is because the size of the modern head is much smaller than that in the past, and we have to put an underlayer or underpole relatively far apart from the ABS of the head due to the limitation of the tape thickness. Thus, neither underlayer nor underpole is workable for anti-interference purposes.

V. REPLAY SIMULATION RESULTS

The aim of a replay process simulation is to give the volume integral (i.e., effective signal) of the MR sensor in the presence of a typical medium, so we can compare the magnitude difference between this case and crossfeed case. In other words, we should give the proportion of the crossfeed within the effective signal. The head structure and dimensions used in the replay simulation are the same as the

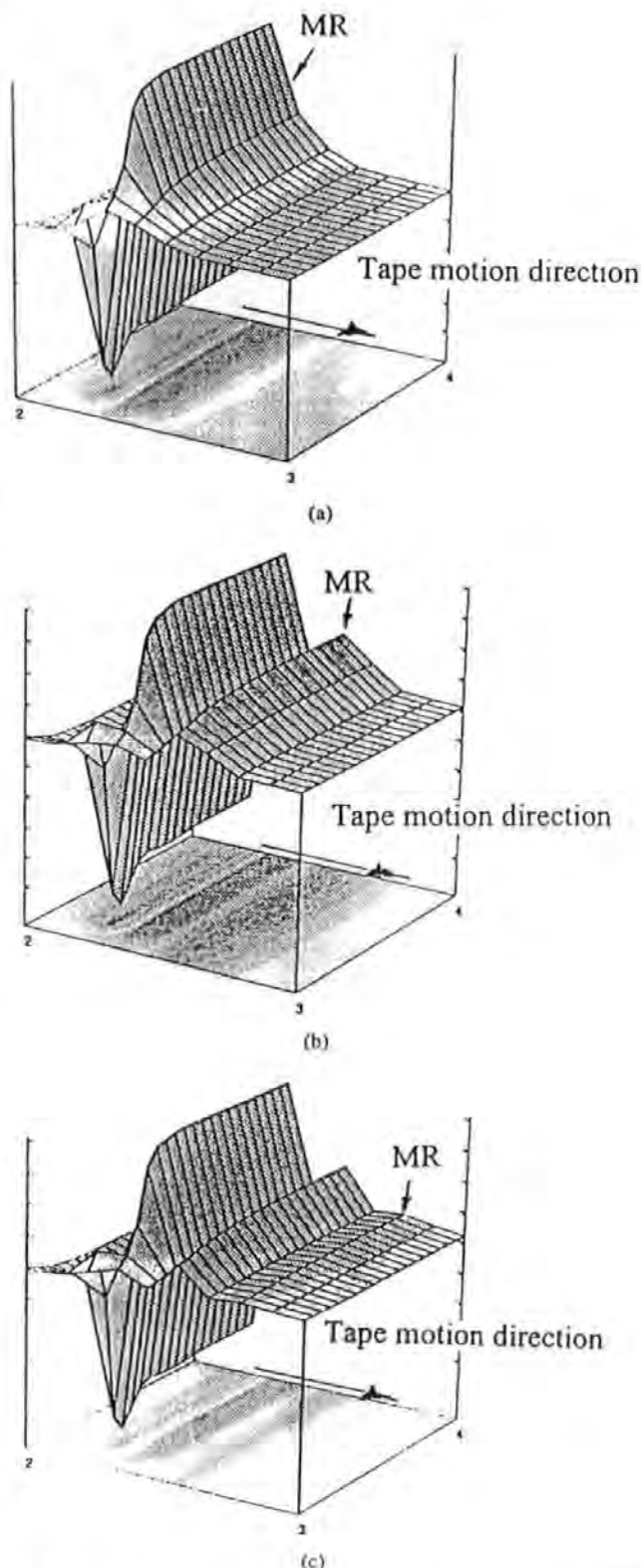


Fig. 4. Three-dimensional field mapping of vertical component in the ABS plane.

crossfeed investigations except that, for the replay simulation, a longitudinal recording medium and perpendicular medium are included in the model. In order to reduce the size of the model, only a three recorded bit longitudinal recording medium and a two-bit perpendicular medium right underneath

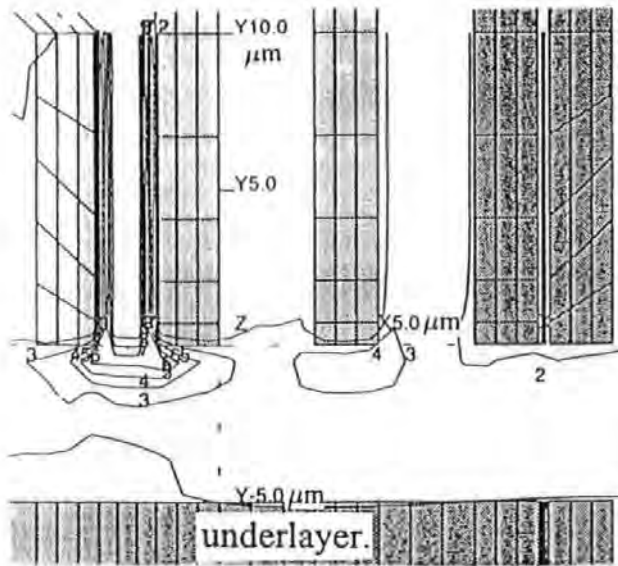


Fig. 5. Write field distribution with underlayer. In this scheme, a thick soft magnetic underlayer with high-permeability placed at a certain distance ($5 \mu\text{m}$) behind the tape covers both the WRITE head and the READ head.

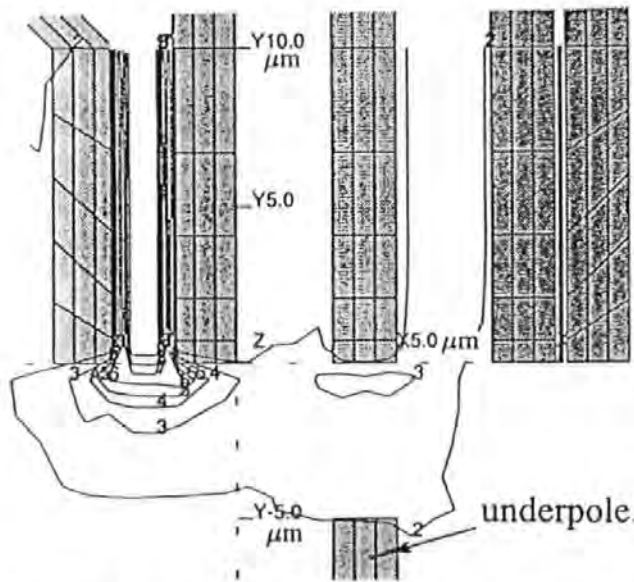


Fig. 6. Write field distribution with underpole. In this scheme, a whole-plane shielding pole with a hole ($5 \mu\text{m}$ high) to let the tape go through is used.

the read gap were simulated. For the longitudinal medium, the central bit is magnetized in the left direction and the other two bits magnetized in the right direction; the track width of the three bits is $99.06 \mu\text{m}$; the bit length is $0.25 \mu\text{m}$ with transition length $0.05 \mu\text{m}$; the thickness of the medium is $0.05 \mu\text{m}$; the head-medium spacing is $0.03 \mu\text{m}$; and the coercivity of the recording medium is 130 kA/m . For the perpendicular medium, the left bit is magnetized in the up direction and the right bit magnetized in the down direction. The parameters for the perpendicular medium are similar, but this case will not be considered as our standard reproductive output case. Note that the positions of the longitudinal medium and the perpendicular medium for maximum output signal will be different.

Fig. 7 is a computed 3-D field mapping of the recorded bits in the midwidth cut plane with the replay DMR head at the top

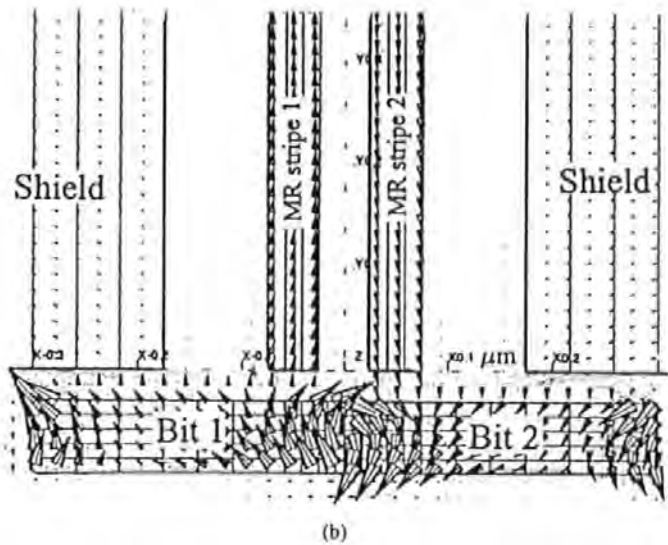
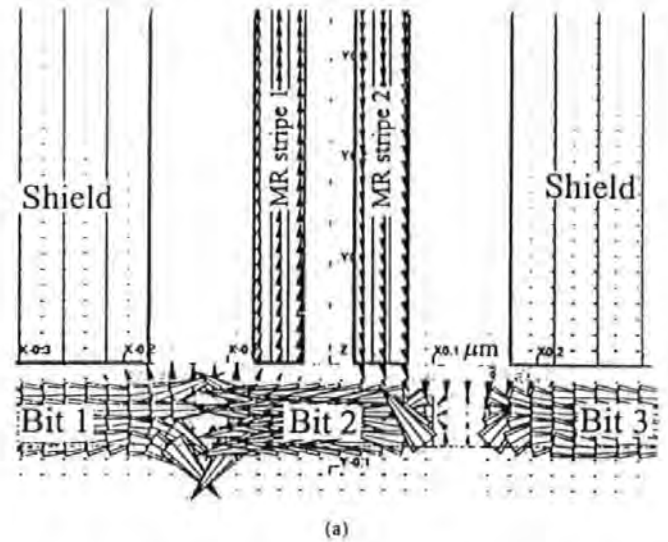


Fig. 7. DMR head replay processes. The figure illustrates the flux distribution of the recorded bits in the midwidth cut plane with the replay DMR head at the top of the medium.

of the medium. The direction of each arrow corresponds to the direction of the field and its thickness to the field magnitude. This figure illustrates the flux distribution around the read gap region. It can be seen from the figure that the leakage flux from the medium goes upward in the left stripe and returns downward in the right stripe. It constitutes a closed magnetic circuit. The calculated DMR output is $4.525 \text{ T} \cdot \mu\text{m}^3$ (for the longitudinal medium). Therefore, in the reference shared-pole head, the effective DMR signal is 13.21 times as large as the crossfeed [signal-crossfeed-ratio (SCR) is 22.4 dB]. In the air-gap head, the effective DMR signal is 26.52 times as large as the crossfeed (SCR is 28.4 dB). In the inserted-pole head, the effective DMR signal is 85.38 times as large as the crossfeed (SCR is 38.6 dB). In the other calculation, the SAL output is found to be $3.777 \text{ T} \cdot \mu\text{m}^3$ (also for the longitudinal medium). Therefore, in the SAL MR reproduction case, the SCR is: 7.8 dB (shared pole case), 10.4 dB (air gap case), 21.4 dB (inserted pole case), respectively, for these three structures.

In contrast, we also computed 3-D field mappings of cross-feed situations in the inserted-pole head case around the read

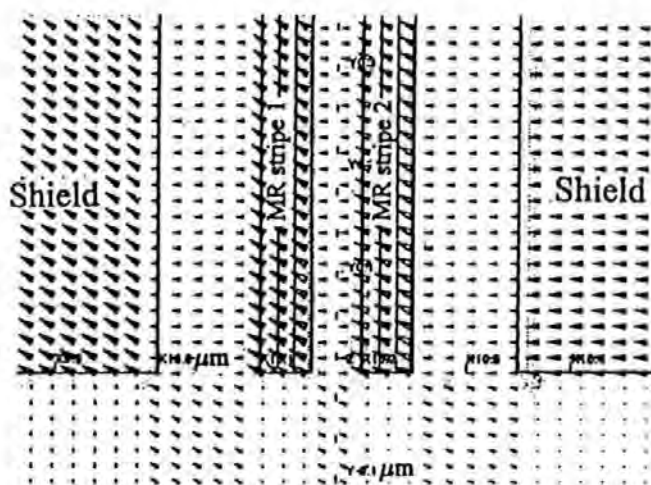


Fig. 8. Field mappings of crossfeed situations around the read gap region in the inserted-pole head case, with the 0.48 A writing current flowing through the writing coil.

gap region, with the 0.48 A writing current flowing through the writing coil. As shown in Fig. 8, the field distribution in the two MR stripes is almost the same because these two stripes are located so close with respect to the write gap. Obviously, the output signals from these two stripes will cancel each other in the DMR case, thus an almost null final output will be caused (only $0.0740 \text{ T} \cdot \mu\text{m}^3$).

VI. EXPERIMENTAL MEASUREMENTS

To verify these simulation results, measurements with MR/inductive head were done. The schematic illustration is shown in Fig. 9. A SAL type MR/inductive head was used. Its configuration is very similar to our air-gap design. In the experiment, the head assembly was put far away from the medium. When a 60 mA square-wave recording current is flowing through the write coil, just as in the case of recording, we observe the reproductive waveform from the MR sensor on the oscilloscope. We confirmed the crossfeed waveform from the write field by both frequency comparison and amplitude dependence on sense current. Sharp pulses appeared in the leading edges and trailing edges of the reproductive waveform because of the capacitive and inductive coupling between write-read bumps, as mentioned in the introduction section. From the measurements, the peak-to-peak amplitude was found to be $320 \mu\text{V}$ at a sense current of 15 mA. On the other hand, this head's replay amplitude was $900 \mu\text{Vp-p}$ over a single magnetization transition on a longitudinal medium. Therefore, the crossfeed from the WRITE head is just about 36% of the effective signal. We can compare these experimental results with our simulation results. In the simulation of the air-gap head, the SAL effective signal is $3.777 \text{ T} \cdot \mu\text{m}^3$, while the SAL crossfeed is $1.1313 \text{ T} \cdot \mu\text{m}^3$. The crossfeed-signal ratio is just $1.1313/3.777 = 30\%$. There is reasonably good agreement between simulation and experiment.

VII. CONCLUSION AND FURTHER DISCUSSIONS

The crossfeed performance over the surface in RWW tape heads and the replay process on a three (or two) bits medium

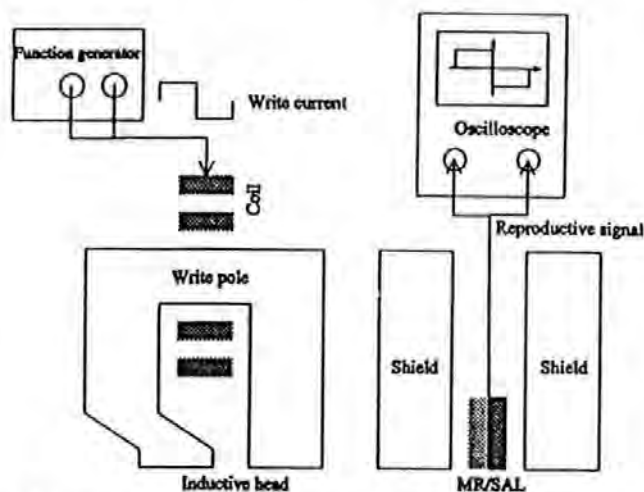


Fig. 9. Experimental apparatus for measuring crossfeed on a SAL type MR/inductive head. The head's configuration is very similar to our air-gap design.

have been quantitatively simulated by using a 3-D finite element method. Their SCR versus gap-separation characteristics are depicted in Fig. 10. In addition, we also considered two other examples: the air-gap type head with $9 \mu\text{m}$ air gap and the inserted-pole type head with $0.5 \mu\text{m}$ air gaps beside the inserted pole (Fig. 10). The Table I summarizes the SCR of various head designs. The following are concluded.

- The SCR increases with the gap-center separation's increasing.
- The inserted-pole design is effective to reduce the crossfeed. The SCR in the inserted-pole design is generally 2–3 dB higher than that in the air-gap design.
- The DMR reproductive method is effective to reduce the crossfeed. The SCR in the DMR designs is generally two to three times as high as that in the SAL reproductive design.

In a summary, the best scheme to suppress the crossfeed noise from the WRITE head in a RWW tape head is to employ the so-called inserted-pole head configuration and simultaneously employ a dual-MR sensor instead of a conventional SAL MR sensor. Its SCR is 38.6 dB (for the head with $3 \mu\text{m}$ air gaps beside the inserted pole) or 30.4 dB (for the head with $0.5 \mu\text{m}$ air gaps beside the inserted pole). Obviously, the latter is more practical due to its shorter gap separation ($8 \mu\text{m}$). To reduce the manufacture cost, the shared-pole DMR configuration is also acceptable. Its SCR is 22.4 dB.

Our work in this paper is limited to head optimization. However, from the viewpoint of signal processing, the crossfeed noise from a recording field is a special noise. In other words, we may say it is not a real noise compared with other real noise, because it is determined by what was written on the tape. Therefore, there exists a possibility to reduce significantly the crossfeed noise from the effective signal by designing a new demodulation circuit, in which a cache memory would be used to store the recorded data for comparison purposes. So a high SCR may not be required for signal processing, while with real noise at least 26 dB SNR is required. Normally, a high SCR design results in high head manufacturing cost

TABLE I
THE SCR OF VARIOUS HEAD DESIGNS

Structure Gap separation	Shared-pole type		Air-gap type		Inserted-pole type	
	SAL	DMR	SAL	DMR	SAL	DMR
3 μm	7.8 dB	22.4 dB			7.8 dB	22.4 dB
8 μm			10.4 dB	28.4 dB	14.2 dB	30.4 dB
13 μm			17.4 dB	35.8 dB	21.4 dB	38.6 dB

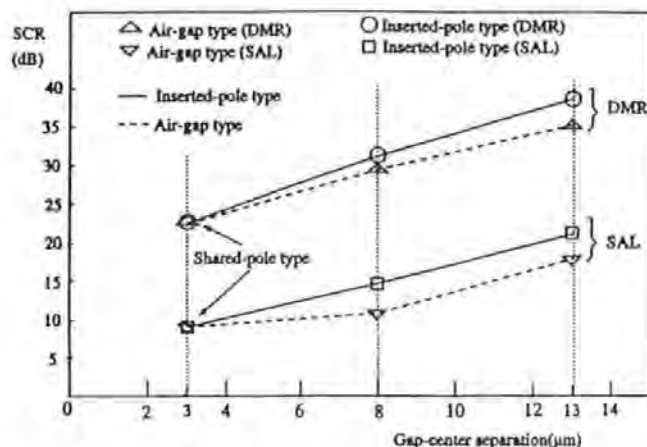


Fig. 10. SCR-gap-separation characteristics of RWW heads.

due to the complicated structure. It should be possible for head designers to divert some of the difficulties of crossfeed reduction to signal processing experts. In order to solve the crossfeed problems perfectly in practical applications, a good balance between head design and signal processing will be needed, but this is beyond the scope of this paper.

REFERENCES

- [1] H. N. Bertram and J. C. Mallinson, "A theory of eddy current limited heads," *IEEE Trans. Magn.*, vol. MAG-12, no. 6, pp. 713-715, 1976.
- [2] G. I. Walther, "Reduction of crosstalk in multiple-head structures for digital tape units," in *Int. Conf. Magnetic Recording (IEE)*, 1964, pp. 65-67.
- [3] S. B. Luitjens and A. V. Herk, "A discussion on the crosstalk in longitudinal and perpendicular recording," *IEEE Trans. Magn.*, vol. MAG-18, no. 6, pp. 1804-1812, 1982.
- [4] J. A. Geurst, "Suppression of cross-talk between magnetic heads in magnetic tape," in *Int. Conf. Magnetic Recording (IEE)*, 1964, pp. 62-64.
- [5] D. J. Mapps, M. L. Watson, and D. T. Wilton, "Asymmetric biasing fields from mismatched current-carrying overlay conductors on magneto-resistive replay sensors," *J. Appl. Phys.*, vol. 57, no. 1, pp. 3982-3984, 1985.
- [6] N. Smith, J. Freeman, P. Koeppel, and T. Carr, "Dual magnetoresistive head for very high density recording," *IEEE Trans. Mag.*, vol. 28, no. 5, pp. 2292-2294, 1992.
- [7] R. Hempstead, "Analysis of thermal noise spike cancellation," *IEEE Trans. Magn.*, vol. MAG-11, no. 5, pp. 1224-1226, 1975.
- [8] *TOSCA Reference Manual*, Vector Field Ltd., Oxford, U.K., 1992.
- [9] S. X. Wang and P. R. Webb, "Modeling of submicron track width inductive write head designs," *IEEE Trans. Magn.*, vol. 31, no. 6, pp. 2687-2689, 1995.
- [10] H. Takano, H. Shinada, S. Seitou, S. Fukuhara, T. Ohnishi, S. Otomo, H. Todokoro, and K. Shiiki, "A study on the field distribution of thin-film heads," *IEEE Trans. Magn.*, vol. 28, no. 2, pp. 1024-1030, 1992.

Zhi Gang Wang received the B.S. degree in computer science from Huazhong University of Science and Technology, Wuhan, China, in 1987 and the M.S. degree in condensed matter physics from East-China Research Institute of Computer Technology in 1990. He received an advanced training for English and Japanese at Northeast Pedagogical College, Changchun, from 1991 to 1992.

He started his research career with East-China Research Institute of Computer Technology, Shanghai, China, in 1987 and engaged in high density hard magnetic disk drive development. From 1990 to 1991, he was with Huazhong University of Science and Technology to develop a new servo method for ultra-high-density magnetic recording purposes. Then, he was with the Research Institute of Electrical Communication of Tohoku University, Sendai, Japan, as a Researcher. He joined what is now the University of Plymouth in 1996. Currently, he is with Centre for Research in Information Storage Technology, University of Plymouth, Plymouth, U.K., as a Research Assistant. He has worked in numerous areas in magnetics and electronics fields, including computer simulation of micromagnetic behavior, head, media, servo, and signal processing. He is the author or coauthor of more than 50 technical papers. He also obtained invention patents in the above areas. His present emphases focus on alternative storage devices using new mechanism.

Mr. Wang is a member of the American Association for the Advancement of Science, the New York Academy of Sciences, the U.K. Institute of Physics, the U.K. Institute of Electrical Engineers, the Institute of Electronics and Communication Engineers of Japan, and the Applied Magnetics Society of Japan. Recently, for his contribution to magnetics, he has been included in the newest edition of *Who's Who in the World*.

Desmond J. Mapps received the B.Eng. degree in electrical engineering and the Ph.D. degree in magnetics from the University of Wales, Cardiff, U.K., in 1966 and 1969, respectively.

From 1969 to 1973, he researched computer memories in industry before joining what is now the University of Plymouth. He is now SONY Professor of Electronic Engineering and Head of the Centre for Research in Information Storage Technology, University of Plymouth, Plymouth, U.K. He has published 53 journal papers and one book chapter (on magnetoresistance) in magnetics related subjects with most papers in the area of thin-film (heads and disks) for magnetic recording. He has obtained seven patents, published 57 reports for industry, and supervised 17 Ph.D. students. He has given 42 papers at international conferences and an additional 26 papers at other meetings in the U.K., U.S., and Japan.

Dr. Mapps is a Fellow of the U.K. Institute of Physics and a Fellow of the Institute of Electrical Engineers.

David T. Wilton received the B.A. degree in mathematics from the University of York, U.K., in 1969 and the D.Phil. degree in numerical analysis from the University of Oxford, U.K., in 1974.

He spent three years at the University of Dundee, Scotland, and then three years with the Ministry of Defence working on dynamic fluid-structure interaction problems in underwater acoustics. Since 1978, he has been Principal Lecturer in mathematics at what is now the University of Plymouth, Plymouth, U.K. From 1987 to 1989, he was at the City Polytechnic of Hong Kong. His main research interests are in numerical analysis and applied mathematics in the areas of acoustics and electromagnetics.

Lianna N. He received the B.S. degree in computer science and the Ph.D. degree in magnetic recording, both from Huazhong University of Science and Technology, Wuhan, China, in 1987 and 1992, respectively.

In 1992, she joined the Akita Research Institute of Advanced Technology, Japan as a Post-Doctoral Fellow. During 1996 she was with Data Storage Institute, National University of Singapore, Singapore. She is now Research Assistant of Centre for Research in Information Storage Technology, University of Plymouth, Plymouth, U.K. She has been engaged in magnetic recording by both theoretical and experimental approaches, especially in high-density magnetic recording. Recent works include media, heads, signal processing, servo systems for ultra-high magnetic recording, and theoretical analyses of high-density magnetic recording and reproducing performances using computer simulation.

Crossfeed Response of DMR vs. SAL Multi-track Heads

Frank Z. Wang, Lian N. He, Desmond J. Mapps, David T. Wilton, Warwick W. Clegg and Paul Robinson

Centre for Research in Information Storage Technology,

School of Electronic, Communication and Electrical Engineering, University of Plymouth, Devon PL4 8AA, United Kingdom

Abstract—A new concept of Dual Magnetoresistive reproductive mode is applied to improve the design and operation of high-performance multi-track Read-While-Write (RWW) heads for tape and/or potential disk applications. RWW operation exists in some magnetic recording units in which verifying what was recorded is necessary. A new multi-track Inductive/Dual Magnetoresistive (DMR) head design is found to reduce the crossfeed noise radiation by about a factor of 20, compared with the conventional Soft-Adjacent-Layer (SAL) Magnetoresistive Heads design, which is the most favoured approach for achieving simultaneous read and write operations, especially in a multi-track head with ultra-narrow trackwidth. To verify these analysis results, measurements with $2.9 \mu\text{m}$ track width inductive/MR and inductive/DMR heads were done.

Index Terms: Read-While-Write operation, Dual Magnetoresistive head, magnetic recording, multi-track recording

I. INTRODUCTION

In digital applications the magnetic recording process has to fulfil high requirements as to its reliability. In such units with a plurality of gaps, one gap is employed for writing and a second one, adjusted to the same track and placed closely behind the first, for reading immediately afterwards to verify the written information and thus increase the reliability of the recording system. This means that the read head and write head are in operation simultaneously. When the heads are in use, noise interference usually occurs between the write and read elements. This type of coupling is called "crossfeed" noise and it is caused by radiation across the recording surface of the magnetic transducer head due to the electromagnetic field. The magnitude of the flux sensed by the read head on the medium is of the order of pico-webers (i.e. very small). In contrast, the writing flux can be very large, especially if a high-coercivity medium is being used. Since the writing level is several orders of magnitude higher than the reading level, it is clear that crossfeed from the recording to the reproducing head may seriously disturb the output signal of the latter [1][2]. Especially in the case of multi-track RWW heads, the individual crossfeed signals from different locations should be considered for a particular gap in the read array.

This work involves the investigation of a range of important parameters related to noise-rejection and the optimisa-

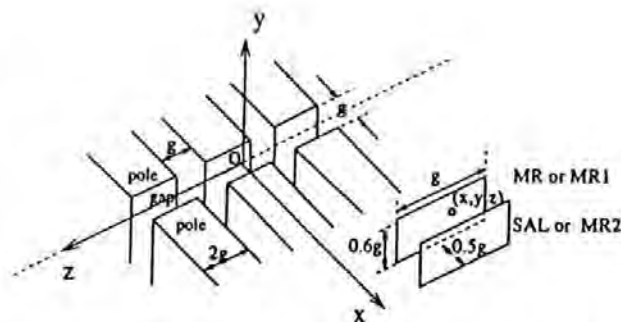


Fig. 1. Idealized 3D model of a multi-track Read-While-Write (RWW) head. The recording gap length g is used as a size unit.

tions to achieve a significant advance in RWW performance of multi-track heads suitable for high data rates. Two reproducing modes will be considered in this paper: the conventional Soft-Adjacent-Layer (SAL) reproducing mode and the Dual Magnetoresistive (DMR) reproducing mode. Utilisation of two MR elements in a differential mode [3] is attractive and has led to different head designs: DMR [4][5], gradiometer [6], and Dual Stripe MR (DSMR) [7]. The 2-terminal DMR heads, consisting of two nominally identical, adjacent magnetoresistive stripes shorted at both ends, is designed to combine the simpler fabrication with the larger intrinsic sensitivity at high linear density [4][5]. The possibility of continuous servoing with DMR heads has also been investigated [8]. The two MR stripes of DMR are connected in parallel electrically. In this regard, when the two MR stripes are exposed to a uniform applied field, the DMR head produces almost null output (one MR stripe has resistance increase, the other has resistance decrease and they cancel each other for parallel connection). In other words, the DMR is sensitive only to the spatially anti-symmetric component of the applied field.

II. MATHEMATICAL MODEL

The mathematical model, including three R/W channels, is illustrated by Fig. 1. In this case, there needs to be a 3-dimensional system constructed to position the heads accurately so that the individual crossfeed signals from different locations can be detected and summed. The x , y and z coordinates exist along the medium motion direction, perpendicular to the head-medium contact plane and along the trackwidth direction, respectively. The origin of the coordinate system is located in the center of the middle recording gap. The recording gap length is referred to g , which is used as a size unit. An

Manuscript completed 1 October, 1997, revised 12 January, 1998.
Corresponding author: Frank Z. Wang is with School of Elect., Communication & Elect. Eng., University of Plymouth, Drake Circus, Plymouth, Devon PL4 8AA, United Kingdom. FAX: +44-1752-232583, E-mail: wang@plymouth.ac.uk

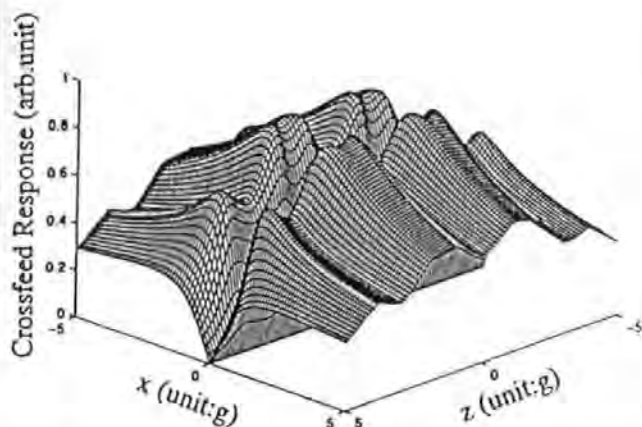


Fig. 2. The calculated crossfeed response in arbitrary units of a SAL-MR head while 3 write heads are in operation simultaneously vs the MR head location (x,y,z) . In this case, $y=0$ and x and z range from $-5g$ to $+5g$.

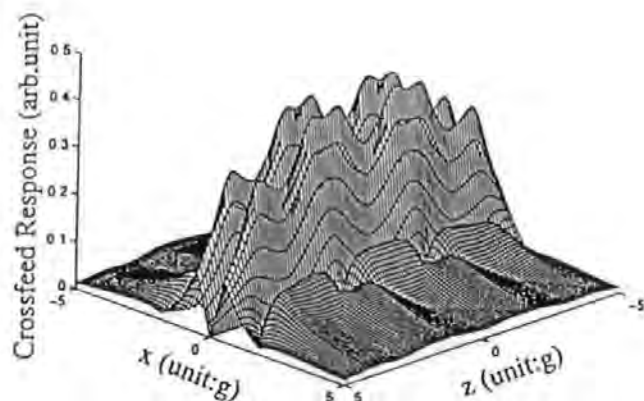


Fig. 3. The calculated crossfeed response, in the same units as Figure 2, of a Dual-MR head while 3 write heads are in operation simultaneously vs the MR head location (x,y,z) . In this case, $y=0$ and x and z range from $-5g$ to $+5g$.

ultra-dense design is assumed here: the recording trackwidth is $2g$; the separation between recording poles is g . Two parallel soft magnetic stripes in read gap configuration have been used in the figure. As stated in the Introduction section, we will consider two replay cases: the SAL case and the DMR case. In the SAL case, the rear stripe MR is assumed to be NiFe material for the MR sensor while the front stripe is assumed to be CoZrNb material for bias purposes. In the DMR case both stripes, denoted by MR1 and MR2 respectively, are assumed to be NiFe material for the two MR sensors. The MR track width is g ; the MR stripe thickness is $0.2g$; the MR stripe depth is $0.6g$; the thicknesses of the dielectric layers is $0.5g$, which governs the linear resolution of readback processes in the DMR case. The spatial center of the two boundaries near the ABS (Air Bearing Surface) of the MR stripes is denoted by the coordinate (x,y,z) .

Closed form field solutions by Lindholm[9] are used for single finite gap heads with finite track width. In this method, several special cases are generated when the exterior angle α of the wedge is a multiple of $\pi/2$, i.e. $\alpha = n \cdot (\pi/2)$. The multiple n will be used conveniently as a subscript to distinguish the different solutions to follow. When $n = 2$, the exterior angle is 180° and the geometry of this π -wedge is that of Karlqvist's 2-dimensional head. When $n = 3$, the exterior angle is 270° and the geometry of this $3\pi/2$ -wedge is that of a semi-infinite width head. The center-track head with finite track width as shown in Fig.1 is obtained by the superposition of π -wedge (Karlqvist's expression H_2), $3\pi/2$ -wedge (H_3) and another $3\pi/2$ -wedge (H'_3) with field given by[9]

$$H = H_3(x, y, z-w/2) + H'_3(x, y, z+w/2) - H_2(x, y, z) \quad (1)$$

where the write head width $w = 2g$. Formula (1) just represents the center-track write head. Contributions from end-track heads should also be summed.

The magnetization is 45° biased in the rectangular-shaped thin-film magnetoresistor in a single domain state. For this reason the 3-dimensional reproducing MR stripes will be sensitive to the H_y and H_x components. H_x does not contribute to the output due to a strong demagnetization effect through the

film thickness direction x . Considering the worst case, an approximate crossfeed response e_j ($j=1,2$) of a single MR stripe can be obtained by integrating over the device dimensions, i.e.

$$e_j \propto \left| \int \int \int H_y(x, y, z) dx dy dz \right| + \left| \int \int \int H_x(x, y, z) dx dy dz \right| \quad (2)$$

To simplify the problem, we assume that the source magnetic flux in the MR films is from the ABS-near boundaries and the injected flux into the MR films is uniform in the z direction.

In the SAL case, we can simply take the volume integral over the rear stripe as the crossfeed response. However in the DMR case we should subtract the integral over the front stripe from that over the rear one and then divide it by two as the crossfeed response because of the parallel connection between the two stripes.

III. ANALYSIS OF RESULTS

A convenient way to visualize the crossfeed response is by means of the perspective views, Fig.2 and 3. In Fig.2, the calculated crossfeed response (absolute value) in arbitrary units of a SAL-MR head while 3 write heads are in operation simultaneously vs the MR head location (x,y,z) is depicted. Fig.3 is the similar case of Dual-MR. In the above cases, $y=0$ and x and z range from $-5g$ to $+5g$. It is noted that a series of peaks with different heights (due to superposition) are localized near the edge-ends of each write gap and the tallest peaks in the SAL-MR case are twice as tall as the tallest ones in the DMR case. Bear in mind that a central band around $-2.5g \leq x \leq +2.5g$ is a fictitious region because the MR heads cannot exist in this band, occupied by the write head array. The region of interest is beyond this band.

By cutting the views of Fig.2 and 3 along certain planes, most of the information about the crossfeed noise response can

be obtained. First, slicing parallel to the x -axis at a given z produces a plot of noise versus x with z as a parameter ($z = -3g, 0, +3g$), which shows the behavior of the noise as the track is traversed. Second, slicing parallel to the z -axis at a given x produces a plot of noise versus z with x as a parameter ($x \leq -2.5g$ or $x \geq +2.5g$), which shows the behavior of the noise as the trackwidth is traversed. Third, slicing parallel to the xz -plane at different noise levels produces contour plots of these noise levels in that plane.

By studying Fig. 2 and 3 along these various cuts, the following conclusions can be drawn:

1. The crossfeed noise response decreases as the write-read-gap-center separation increases. For efficient use of the available storage space a short distance between the head gaps is required. An additional benefit from close write-to-read gap separation is fewer off-track errors due to the slope of the tape (and azimuth alignment of the head) as it passes over the head.

2. It is found that the crossfeed noise in DMR decreases much more sharply than that in SAL-MR with the separation's increasing. For example, the crossfeed noise at a typical point ($x = \pm 4g, z = 0$) in the DMR design is only 4.5% of that at the same point in the SAL. Such a good crossfeed-noise-rejection in the DMR design is because the field disturbance accepted by the two MR stripes is almost the same since these two stripes are located very close to each other with respect to the write gap. As a result, one MR stripe has resistance increase, and the other has resistance decrease. Obviously in the DMR case the output signals from these two stripes will cancel each other, thus causing an almost null final output.

3. A series of crossfeed response peaks with different heights, existing near the edge-ends of each write gap as mentioned above, leave their long tails far away from the write gap along the track direction. As a result, the trackwidth-transverse direction is found to be very important with an array of read heads. The end-tracks have different crossfeed responses from the center-track. In the SAL-MR case, the center-track crossfeed response at ($x = \pm 4g, z = 0$) is 22.1% stronger than the end-track response at ($x = \pm 4g, z = \pm 3g$). In the Dual-MR case, the center-track crossfeed response at ($x = \pm 4g, z = 0$) is just 3.2% stronger than the end-track response at ($x = \pm 4g, z = \pm 3g$).

IV. EXPERIMENTAL MEASUREMENTS

Measurements with Dual-Stripe Magnetoresistive (DSMR) heads were done. The magnetization configuration of DMR[4] is the same as DSMR[7] but their electrical connection are different. Based on this fact, by re-connecting the terminals of DSMR in a different way, we can get a MR head sample and a DMR head sample, respectively. Digital recording and playback is achieved using 1 integrated recording (IR) channel and 1 MR channel respectively, which serve 1 parallel digital track on medium. The digital playback channel is $2.9 \mu\text{m}$ wide, the digital record channels is $3.6 \mu\text{m}$ wide. The write gap length is $0.35 \mu\text{m}$ and the read gap length is $0.28 \mu\text{m}$. The gap-center separation is $2.32 \mu\text{m}$. (Note that this head has just one channel but at this stage it is the only head with a very narrow trackwidth available to us.) The record channel is 9 turns.

In the measurement, the head assembly was put far away

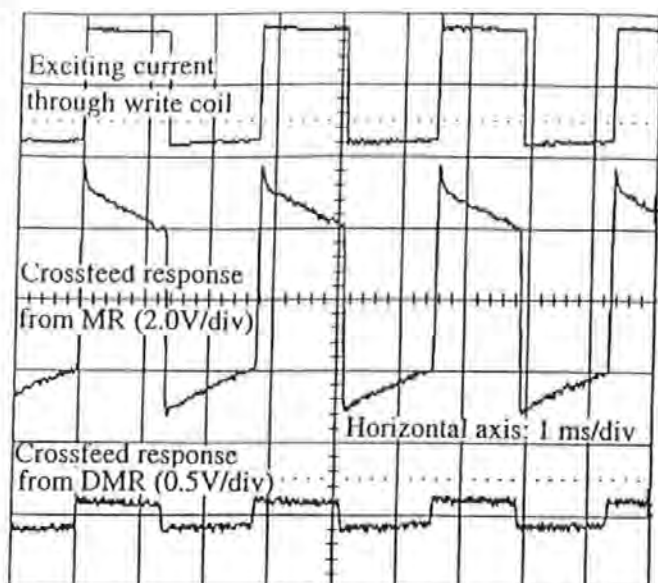


Fig. 4. The crossfeed responses against a square-wave excitation in the write coil. See text for detail.

from the medium to measure noise interference occurring between the write and read elements. When a 50 mA square-wave recording current (optimum recording current) was flowing through the write coil of the write head, we observed the reproducing waveform (crossfeed noise response) from the MR sensor at a sense current of 12 mA on the oscilloscope, as shown in Fig. 4. We confirmed the crossfeed waveform from the write field by both frequency comparison and amplitude dependence on sense current. The reproducing waveform from the DMR sensor is also pictured in Fig. 4. In the case of MR, the crossfeed response is 2.56 V (after a amplifier); in the case of DMR, the crossfeed response is just 62 mV (after the same amplifier). It is clear that the DMR head receives much little crossfeed noise from the recording coil than the MR sensor.

REFERENCES

- [1] H.N. Bertram and J.C. Mallinson, "A Theory of Eddy Current Limited Heads", *IEEE Trans. Magn.*, Vol. 12, No. 6, pp. 713 (1976).
- [2] Z.G. Wang, D.J. Mapps, D.T. Wilton and L.N. He, "Crossfeed Problems in Read-While-Write Tape Heads", *IEEE Trans. Magn.*, Vol. 33, No. 4, pp. 2531-2537 (1997).
- [3] D.J. Mapps, U.K. patent No. 2143071, 28/10/1987
- [4] N. Smith, J. Freeman, P. Koeppel, and T. Carr, "Dual Magnetoresistive Head for Very High Density Recording", *IEEE Trans. Magn.*, Vol. 28, No. 5, pp. 2292-2294, 1992.
- [5] N. Smith, D.R. Smith, and S. Shtrikman, "Analysis of a Dual Magnetoresistive Head", *IEEE Trans. Magn.*, Vol. 28, No. 5, pp. 2295-2297, 1992.
- [6] R.S. Indeck, J.H. Judy, and S. Iwasaki, "A Magnetoresistive Gradiometer", *IEEE Trans. Magn.*, Vol. 24, No. 6, pp. 2617-2619, 1988.
- [7] Voegel, Patent US 3860965
- [8] Z.G. Wang, L.N. He and D.J. Mapps, "Dual MR Elements Applied to a Read-While-Write Head", *Internmag*, ET-01, 1997
- [9] D.A. Lindholm, "Magnetic Fields of Finite Track Width Heads", *IEEE Trans. Magn.*, Vol. 13, No. 5, pp. 1460 (1977)

Keeped Media Reproduction with Dual MR Heads

Frank Z. Wang, Lian N. He, Desmond J. Mapps, David T. Wilton, Warwick W. Clegg and Paul Robinson

Centre for Research in Information Storage Technology,
School of Electronic, Communication and Electrical Engineering, University of Plymouth, Devon PL4 8AA, United Kingdom

Abstract—The key technique in applying keeped media system in a reproduction is how to "open" the keeper layer. In this paper we propose a new concept of keeped-media-reproduction with Dual Magneto-resistive (DMR) heads. The keeper layer may be biased by the stray flux from DMR sensors. The shunting-releasing ratio between reproduced signals without and with a sense current is found to be -26 dB. This media system is completely stable against thermal demagnetization. It is believed that keeped media may offer a similar advantage with MR heads and potentially allow magnetics to break the 10 Gb/in² areal density barrier with the aid of the high performance gains of MR heads.

Index Terms: keeped media, Dual Magneto-resistive head, magnetic recording

I. INTRODUCTION

As recording densities exceed 10 Gb/in² [1], recorded transitions may become unstable, causing magnetically recorded information to degrade over time. A top keeper layer adjacent to the hard-magnetic storage layer can profoundly affect the recorded magnetic transitions in the media. The recording process is similar to conventional recording—except there is an additional spacing loss due to the thickness of the keeper layer. As the head field moves away from the recorded transition, the keeper layer becomes unsaturated [2]. The keeper layer reduces the demagnetization of the magnetic transition and hence the transition length, smoothes zigzag transitions, and significantly reduces the effects of finite head-pole width on the output [2]. As a result, keeping not only boosts recording densities, but has the potential to stabilize recorded data against thermal demagnetization—which may become a significant issue when recording densities approach 10 Gb/in². The key problem in using a keeped media system is how to "open" the keeper layer. In other words, the keeped media system requires a small bias field during read operation. Work to date has been done with thin-film and metal-in-gap inductive heads together with keeped longitudinal media since it

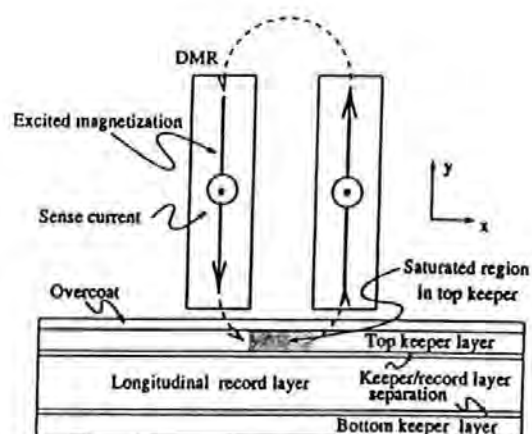


Fig. 1. The medium cross-section and flux path for basic keeped-media reproduction with a Dual MR head. A soft-magnetic keeper film is deposited on top of the storage layer and below the lubricating overcoat. During a write operation, flux from the recording head saturates the keeper above the storage layer. The keeper layer could be biased by the stray flux from dual MR sensors during a read operation.

is relatively easy to produce a head-bias field by the ring head structure [2][3][4]. In this paper, we propose a new concept of keeped-media reproduction with Dual MR heads. It is believed that keeped media may offer a similar advantage with MR heads due to the high performance gains of MR heads.

The 2-terminal DMR head [5], consisting of two nominally identical, adjacent magneto-resistive stripes separated by a dielectric spacer in the active region but shorted at both ends between MR stripes, is designed to combine simpler fabrication with larger intrinsic sensitivity at high linear density [5]. Most importantly, this DMR head promises excellent resolution when reading the high field gradients from extremely sharp magnetization transitions, due to the small separation of the elements in the device. These features are important for overcoming the limitations of present recording heads and achieving the high spatial resolution necessary for an ultra-high density magnetic recording system.

II. PRINCIPLE

The principle of keeped-media reproduction with Dual MR heads is illustrated in Fig. 1. The medium cross-section and

Manuscript completed 8 October, 1997, revised 18 January 1998.

Corresponding author: Frank Z. Wang is with School of Elect., Communication & Elect. Eng., University of Plymouth, Drake Circus, Plymouth, Devon PL4 8AA, United Kingdom. FAX: +44-1752-232583, E-mail: zwang@plymouth.ac.uk

flux path for basic keepered-media reproduction with a Dual MR head are shown. A soft-magnetic top keeper film is deposited on the storage layer and below the lubricating overcoat. Keeping will not occur for keeper layers that are relatively thin with respect to the hard recording layer unless there is a magnetic exchange breaking layer or spacing separating them. The reader is shown keeper/record layer separations in Fig. 1. During a write operation, flux from a submicron-trackwidth recording head (not shown in the figure) saturates the keeper above the storage layer. During a read operation, the keeper layer may be biased by the stray flux from dual MR sensors, as illustrated below.

In DMR heads, sense current of the same magnitude and direction is sent through both elements producing opposing bias fields in each sensor. A strong field will be produced in front of the ring-head-like stripe-stripe gap and this resulting bias field will saturate a small region of the top keeper layer. In this regard, a "window" has been opened in the keeper layer. In contrast, the two MR stripes are only semi-saturated, i.e. 45° biased, just suited for signal reproduction.

III. FINITE ELEMENT MODEL

The TOSCA 3-D FEM Nonlinear Electromagnetic Field Simulation Package (supplied by Vector Field Corp.) is used to study the playback behaviour in a keepered media system. Finite element discretization forms the basis of the methods used in these analysis programs. These programs provide facilities for the creation of finite element models, specification of complicated conductor geometries, definition of material characteristics including, for example, non-linear and anisotropic descriptions, and graphical displays for examination of the data.

Due to the symmetric structure of the heads, only half of the structure is needed for the simulation. The maximum element number used in the modelling was 45,000. An open boundary was used in the model. The effect of the open boundary condition on the accuracy of the solution was verified by comparing the solutions obtained by applying the potential and derivative boundary conditions to the open boundary. The error between the two was less than 3.5 %.

The output of the MR head was evaluated by the volume integral of magnetic flux density component B_y within the MR stripe,

$$\text{Output of single MR stripe} \propto \int \int \int B_y dx dy dz \quad (1)$$

The units of the volume integral are T- μm^3 . During a read operation, we should add the integral over the right stripe and that over the left one as the final output of the DMR head because within an anti-symmetric field both of these MR stripes, in parallel electrically in a DMR head, have a resistance change with

the same polarity change.

IV. ANALYSIS

The aim of a replay process simulation is to verify the feasibility of keepered-medium reproduction with DMR heads. After obtaining the volume integral (i.e. the effective signal) of the DMR sensor in the presence of a typical medium, we can compare the magnitude difference between the reproducing (or releasing) case and shunting case. In other words, we should give the ratio of the signal without sense current flowing to the effective reproduced signal with sense current flowing. In order to simplify the problem, only a three-bit longitudinal medium right underneath the read gap was simulated. The calculation provides an example of 10 Gb/in² areal density using very aggressive track density and somewhat conservative linear density. The trackwidth of the three-bit medium is 0.3 μm [6]; the bit length is 0.2 μm with transition length 0.025 μm ; the thickness of the medium is 0.07 μm ; the head-medium spacing is 0.012 μm ; the coercivity of the recording medium is 2500 Oe with an MrT of 1.0 memu/cm²; the keeper layer thickness is nominally 200 Å, with a coercivity of 15 Oe and a saturation magnetization of about 1.2 Tesla; the thickness of the keeper/record layer separation is 25 Å; the thickness of the C+ lubricating layer is 25 Å. The DMR head structure and dimensions used in the replay simulation are listed below: the shield material is chosen to be a FeN based soft magnetic film with a saturation magnetization of 2.1 Tesla and an initial permeability of 3500; the read gap here is defined as the shield-to-shield separation, 0.35 μm ; two parallel soft magnetic stripes in gap configuration have been used; both these stripes are assumed to be NiFe material for the two MR sensors; the MR track width is 0.28 μm ; the MR stripe depth is 0.25 μm ; the MR stripe thickness is 500 Å; the thicknesses of the dielectric layers are 1000 Å, 500 Å and 1000 Å, respectively; the stripe-stripe separation, 500 Å, governs the linear resolution of readback processes.

Figure 2 is a computed three dimensional flux distribution of the recorded bits in the mid-width cut plane, with the replay DMR head with an optimum sense current $I = 1.5$ mA at the top of the medium. The direction of each arrow corresponds to the direction of the field, and its thickness to the field magnitude. From the figure, it is found that the small saturated region in the top keeper layer, which is created by the resulting bias field in front of the stripe-stripe-gap, cuts off the return path of the medium transition flux through the top keeper layer due to low permeability of the saturated region. The medium transition flux is therefore forcibly released from the shunting in the keeper layer, which allows flux transitions to be picked up by the reproducing DMR head. For this reason, Fig.2 shows a "releasing state". The leakage flux from the medium goes upward in the left stripe and returns downward in the right stripe. Obviously the anti-symmetrically-distributed field components will cause a pronounced signal output for 2 stripes shorted at

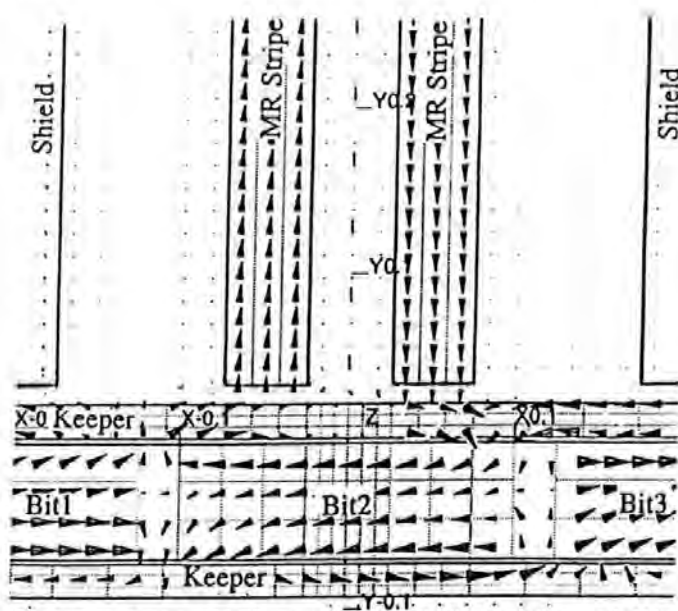


Fig. 2. Releasing state. Medium transition flux distribution of the recorded bits in the mid-width cut plane, with the replay DMR head with an optimum sense current $I = 1.5$ mA at the top of the medium, is shown. The small saturated region in the top keeper layer, which is created by the resulting bias field in front of the stripe-stripe-gap, cuts off the return path of the medium transition flux through the top keeper layer due to low permeability of the saturated region. The medium transition flux is therefore forcibly released from the shunting in the top keeper layer, which allows flux transitions to be picked up by the reproducing DMR head.

both ends in the DMR head. The calculated DMR output is $4.7 \times 10^{-19} \text{ T} \cdot \mu\text{m}^3$.

In contrast, we also computed the three dimensional flux distribution in the shunting state, without any sense current flowing through the MR stripes. As shown in Fig.3, the flux distribution from the recording layer is well restrained beneath the top keeper layer and above the bottom keeper layer. Effectively, the "window" has been closed in the keeper layer. Almost no stray flux from the medium enters the MR stripes to be picked up by the reproducing DMR head. In this case, only $2.5 \times 10^{-20} \text{ T} \cdot \mu\text{m}^3$ is sensed in the output of the DMR head. (This value is fictitious because an MR sensor cannot work without a sense current flowing through the stripes.)

In order to evaluate fairly the proportion of the contributions to the MR output between the shunting case and releasing case, we define a Shunting-Releasing Ratio (SRR) as below:

$$SRR = 20 \log \frac{\text{Signal without sense current}}{\text{Signal with sense current}} (\text{dB}) \quad (2)$$

In our investigation, the signal with sense current (the releasing case) is $4.7 \times 10^{-19} \text{ T} \cdot \mu\text{m}^3 / 2.5 \times 10^{-20} \text{ T} \cdot \mu\text{m}^3 = 18.8$ times as large as the signal without sense current (the shunting case), so the SRR is - 25.6 dB. Therefore the designed top keeper layer plays a reasonable role in shunting and releasing the medium transition flux.

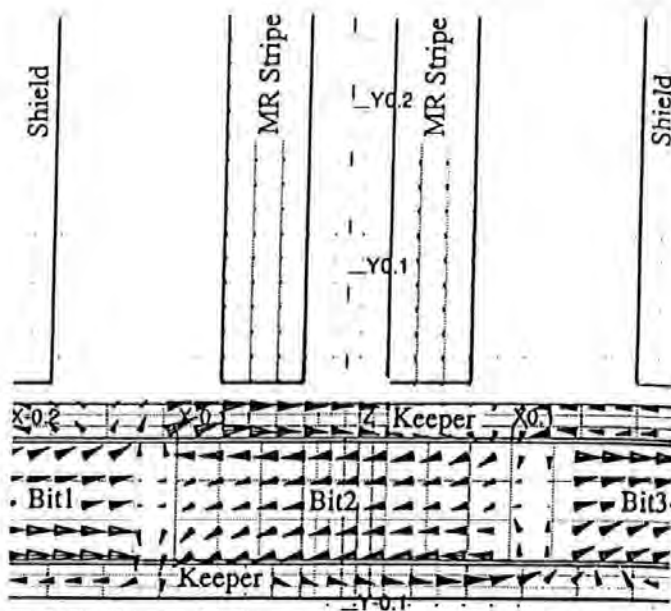


Fig. 3. Shunting state. Medium transition flux distribution of the recorded bits in the mid-width cut plane, with the replay DMR head without any sense current, is shown. The flux distribution from the recording layer is well restrained beneath the top keeper layer and above the bottom keeper layer (underlayer).

V. CONCLUSIONS

In this paper, we propose a new concept of keepered-media-reproduction with Dual MR heads. To verify its feasibility, a TOSCA 3-D FEM Nonlinear Electromagnetic Field Simulation Package is used. The keeper layer may be biased by the stray flux from DMR sensors. A so-called "shunting-releasing ratio" between reproduced signals without and with a sense current is found to be -26 dB. This media system is completely stable against thermal demagnetization. It is believed that keepered media may offer an advantage with MR heads and potentially allow magnetics to break the 10 Gb/in^2 areal density barrier due to the high performance gains of MR heads. In addition, the principle stated here is also applicable to perpendicular media systems [7] although only a longitudinal medium has been included in this investigation.

REFERENCES

- [1] E.S.Murdock, R.F.Simmons and R.Davidson, "Roadmap for 10 Gbit/in^2 media: Challenges", *IEEE Trans. Magn.*, Vol.28, No.5, pp.3078-3083, 1992
- [2] T.Coughlin, B.Gooch and B.Lairson, "Keepered media add more byte to magnetic recording heads", *Data Storage (Technology and Manufacture of Storage Devices)*, October, 1996
- [3] B.Gooch, R.Niedemeyer, R.Wood and R.Pisharody, "A high resolution flying magnetic disk recording system with zero reproduce spacing lost", *IEEE Trans. Magn.*, Vol.27, No.6, pp.4549-4554, 1991
- [4] W.Reed, U.Cohen, D.Hollars, B.Zubeck, AB-10, *Intermag'96*
- [5] N.Smith, J.Freeman, P.Koeppel, and T.Carr, "Dual Magnetoresistive Head for Very High Density Recording", *IEEE Trans. Magn.*, Vol.28, No.5, pp. 2292-2294, 1992.
- [6] Y.Nakamura, "A Challenge to Terabit Perpendicular Spinic Storage", *J.Magn.Soc.Jpn.*, Vol.18, Supple.No.S1, pp161-170, 1994.
- [7] L.N. He, Z.G. Wang, D.J. Mapps, D.D. Clegg and D.T. Wilton, "Perpendicular Keepered Media Reproduction with Dual MR Heads", *Journal of the Magnetics Society of Japan*, Vol.21, No.S2, 1997.



ELSEVIER

TYPESET FROM AUTHOR'S DISK

Journal of Magnetism and Magnetic Materials 000 (1998) 000-000

M Journal of
magnetism
and
magnetic
materials

Read-while-write operation in magnetic recording

Z.G. Wang*, L.N. He, D.J. Mapps, D.T. Wilton

Centre for Research in Information Storage Technology, School of Electronic, Communication and Electrical Engineering,
University of Plymouth, Drake Circus, Devon PL4 8AA, UK

Abstract

This investigation relates to magnetic transducing apparatus (magnetic tape units and potentially magnetic disk units) for use in read-while-write (RWW) mode. We shall confine ourselves here to the most important part of the noise, that resulting from field interaction. This type of coupling is called "crossfeed" noise and it is caused by radiation across the recording surface of the magnetic transducer head due to the electromagnetic field. As a result, a favoured scheme to suppress the crossfeed noise from the write head in a RWW head is to employ a dual-MR sensor instead of a conventional SAL MR sensor. The measured signal-crossfeed ratio (SCR) agrees reasonably with the theoretical predictions. © 1998 Elsevier Science B.V. All rights reserved.

Keywords: Magnetic recording; Read-while-write operation; Dual-magneto-resistive heads

1. Introduction

In digital applications the magnetic recording process has to fulfil high requirements as to its reliability. Magnetic-tape units used in combination with digital electronic computers contain therefore multiple-head structures in which the information written on the tape by means of a magnetic recording head is read out immediately afterwards by a magnetic reproducing head adjusted to the same track and placed closely behind the recording head. For information being recorded and verified continuously, this means that the read head and write head are in operation simultaneously, as shown in Fig. 1.

2. Model and results

As shown in Fig. 2, the field (H) produced at a distance (R) from an infinitesimal gap by a recording current (i) in

the winding of n turns around the head core is given by $H(t) = (1/\pi)ni(t)/R$ [2]. The reproducing MR stripes will be sensitive to the H_y component only, $H_y(t) = (1/\pi)ni(t)x/(x^2 + y^2)$. Two parallel soft magnetic stripes in read gap configuration have been used in the figure. We will consider two replay cases: the conventional (soft adjacent layer) SAL reproducing mode and the (dual-magneto-resistive) DMR reproducing mode [1]. The MR track width $\omega = 50.8 \mu\text{m}$; the MR stripe thickness $\delta = 500 \text{ \AA}$; the MR stripe depth $h = 5.0 \mu\text{m}$; the dielectric layer thicknesses $d = 500 \text{ \AA}$; the shield-to-shield separation is $0.35 \mu\text{m}$.

A rectangular-shaped thin-film magnetoresistor in a single domain state can be analysed by considering the various magnetic energy components that exist in the film. If an applied field is made up of a constant component, H_h , and a much smaller variable component, H_y , then, for a sense current I and initial resistance R_0 an output voltage e_j ($j = 1, 2$) of a single MR stripe can be obtained by integrating over the device dimensions, i.e.

$$e_j = 2IR_0 \frac{\Delta\rho}{\rho_0} \frac{H_h}{[H_h + N_y M_s]^2} \iiint H_y(x, y, z) \frac{dx dy dz}{\delta h \omega} \quad (1)$$

*Corresponding author. Tel.: 44-1752-232583; fax: +44-1752-232583; e-mail: zwang@plymouth.ac.uk

Combining with the y component of the head field gives

$$e_A(t) \propto \frac{ni(t)}{\pi \delta h} \int \arctan\left(\frac{h}{x}\right) dx$$

$$= \frac{ni(t)}{\pi \delta h} \left[x \arctan\left(\frac{h}{x}\right) + \frac{h}{2} \ln\left(1 + \frac{x^2}{h^2}\right) \right]_{x_0}^{x_0 + \delta} = f(x_0) \quad (2)$$

In the SAL case, we can simply take the volume inte-

gral over the left stripe as the crossfeed noise of the MR head, i.e.

$$\text{Crossfeed}_{\text{SAL}} \propto f\left(s - \frac{h}{2} - \frac{\delta}{2}\right) \quad (3)$$

However, in the DMR case, we should subtract the integral over the right stripe from that over the left one as the approximative crossfeed noise of DMR head because of the parallel connection between the two magnetoresistive stripes in the DMR heads, i.e.

$$\text{Crossfeed}_{\text{DMR}} \propto f\left(s - \frac{h}{2} - \frac{\delta}{2}\right) - f\left(s + \frac{h}{2} + \frac{\delta}{2}\right) \quad (4)$$

In order to evaluate fairly the proportion of the crossfeed within the effective signal, we define an SCR as below

$$\text{SCR} = 20 \log \frac{\text{Signal}}{\text{Crossfeed}} \text{ (dB)} \quad (5)$$

Since the reproducing process is essentially a linear one, the derivation of the reproducing head signal in the presence of a typical medium can be simply done by using the reciprocity principle [2,3]. In other words, a reciprocal relationship occurs and the field distribution in the read gap region may be looked upon as a measure of the relative spatial sensitivity of the head to magnetization in the gap region. The properties of the medium which go into the calculation are listed below: transition excitation $M_t = 2.5 \text{ memu/cm}^2$, the head-medium spacing is $0.03 \mu\text{m}$.

The calculated SCR vs. inter-gap-separation characteristics are depicted in Fig. 3 [3]. SCR increases as the gap-center separation increases. For efficient use of the available storage space a short distance between the head gaps is required. An additional benefit from close write-to-read gap separation is fewer off-track errors due to the slope of the tape (and azimuth alignment of the head) as it

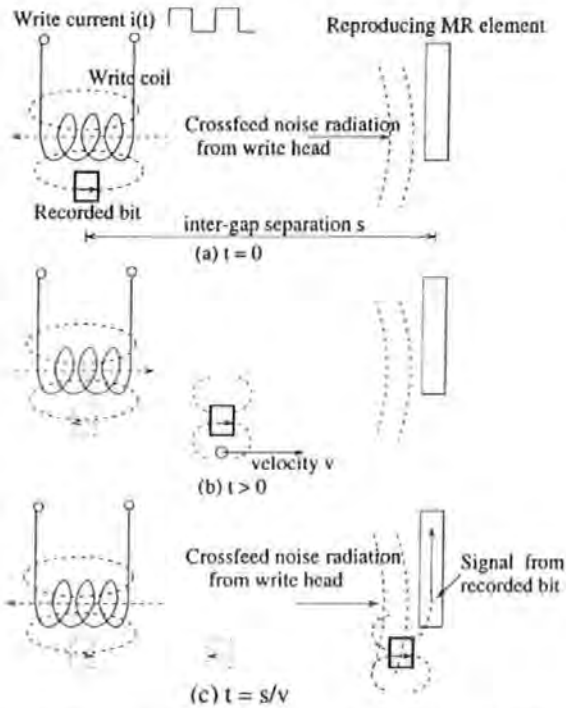


Fig. 1. Schematic illustration of crossfeed problem in RWW heads.

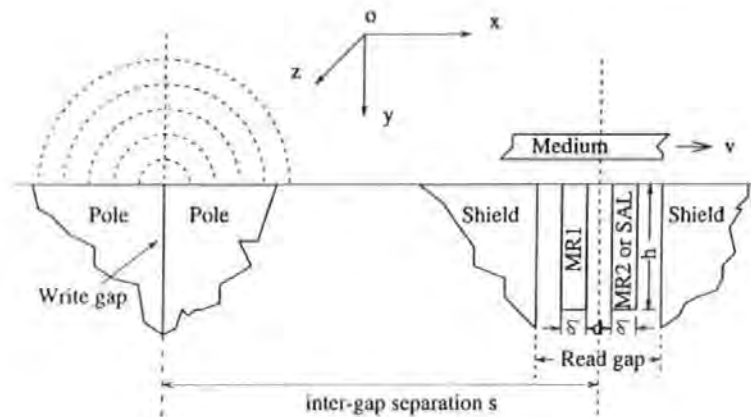


Fig. 2. Ideal model of an RWW head.

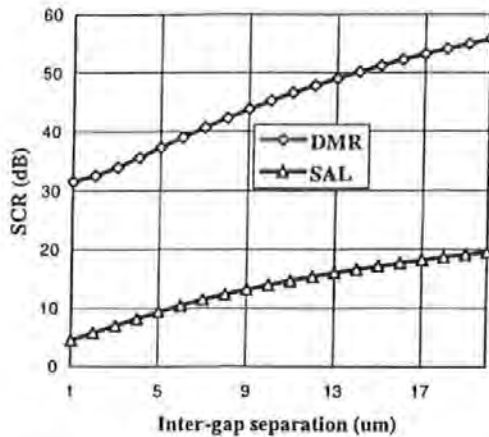


Fig. 3. SCR-inter-gap-separation characteristics of RWV heads.

passes over the head. In conclusion, the SCR in the DMR design is generally 4–5 times higher than that in the SAL reproducing design. Such a high SCR in the DMR design is because the leakage flux from the medium goes upward in the right stripe and returns downward in the left stripe, constituting a closed magnetic circuit. Both MR stripes have resistance change with same change polarity. Such anti-parallel field components will cause a remarkable signal output in the DMR head. In contrast, when considering crossfeed radiation from the write head, the field disturbance accepted by the two MR stripes is almost the same because these two stripes are located very close to each other with respect to the write gap. As a result, one MR stripe has resistance increase, and the other has resistance decrease. Obviously in the DMR case the output signals from these two stripes will cancel each other, thus causing an almost null final output.

3. Experimental measurements

Measurements with MR and DMR heads by re-connecting the terminals of dual-stripe magnetoresistive (DSMR) heads were done. The MR playback channel is $2.9 \mu\text{m}$ wide, the record channels is $3.6 \mu\text{m}$ wide. The write gap length is $0.35 \mu\text{m}$ and the read gap length is

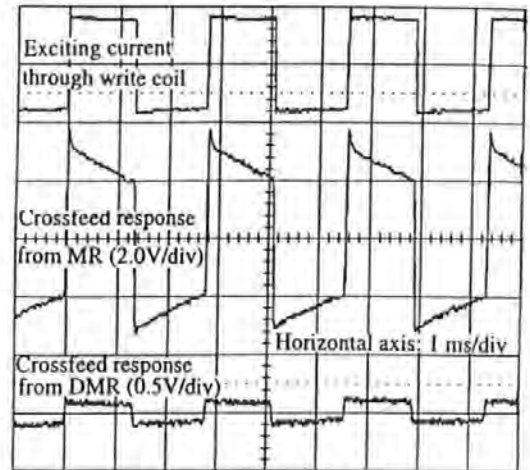


Fig. 4. The crossfeed responses against a square-wave excitation in the write coil. See text for detail.

$0.28 \mu\text{m}$. The gap-center separation is $2.32 \mu\text{m}$. The record channel is nine turns. In the measurement, the head assembly was put far away from the medium to measure noise interference occurring between the write and read elements. When a 50 mA square-wave recording current (optimum recording current) was flowing through the write coil of the write head, we observed the reproducing waveform (crossfeed noise response) from the MR sensor at a sense current of 12 mA on the oscilloscope, as shown in Fig. 4. The reproducing waveform from the DMR sensor is also pictured in Fig. 4. In the case of MR, the crossfeed response is 2.56 V (after an amplifier); in the case of DMR, the crossfeed response is just 62 mV (after the same amplifier). It is clear that the DMR head receives much little crossfeed noise from the recording coil than the MR sensor.

References

- [1] N. Smith, J. Freeman, P. Koeppe, T. Carr, *IEEE Trans. Magn.* 28 (5) (1992) 2292-2294.
- [2] C.D. Mee, *The Physics of Magnetic Recording*, North-Holland Personal Library, 1986.
- [3] C and C + + SoftBench User's Guide, HP LaserROM HP UX 9.0, June 1995.

Suppression of Crossfeed Field in a Read-While-Write Head

D.J. Mapps, Z.G. Wang, L.N. He and D.T. Wilton

Centre for Research in Information Storage Technology,
School of Electronic, Communication and Electrical Engineering, University of Plymouth, Devon PL4 8AA, United Kingdom

Abstract—The thrust of this work is to find a practical solution for the suppression of crossfeed field in a Read-While-Write (RWW) operation for tape and/or potentially disk magnetic recording applications. It is concluded that the shielding efficiency depends partly on the flux transport in the magnetic shields. It is advantageous to use magnetic materials with a low conductivity or to cut a notch in the metallic magnetic shields to prevent eddy currents.

I. INTRODUCTION

The magnetic recording process has to fulfill high requirements as to its reliability. Magnetic-tape units used in combination with digital electronic computers therefore contain multiple-head structures in which the information written on the tape by means of a magnetic recording head is read out immediately afterwards by a magnetic reproducing head adjusted to the same track and placed closely behind the recording head. For information being recorded and verified continuously, this means that the read head and write head are in operation simultaneously [1]. This will require work to suppress the so-called crossfeed field from the write head.

II. MODEL AND RESULTS

A read-while-write tape head is shown in Fig. 1. This is a typical thin-film head and the fabrication technique has been borrowed from the semiconductor industry for fabrication of integrated circuits. Different layers are deposited onto an insulating substrate (silicon). The copper has been shaped into a multi-turn conductor and magnetic top and bottom cores are jointed at the center of this conductor and there is no back gap. The front gap for an inductive head is controlled by a thin insulating layer. A Magneto-Resistive (MR) reproducing element is inserted between two shields. All the dimensions are taken according to a new generation head TR5 produced by Read-Rite company. The cores are $3.0 \mu\text{m}$ thick, and the throat height is $5 \mu\text{m}$. The write head gap is $1.20 \mu\text{m}$. The angle of the inclination of the top core near the zero-throat point

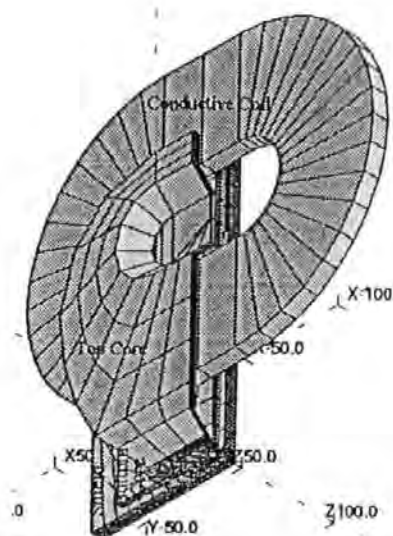


Fig. 1. A Read-While-Write head and the display of 3D finite element mesh. Due to the symmetry, only half of the structure is shown here.

is 45° . The tip widths of the top core, the bottom core and the two shields are $61 \mu\text{m}$, $100 \mu\text{m}$ and $140 \mu\text{m}$, respectively. The top core and the bottom core are $10 \mu\text{m}$ apart in the yoke region. Overall they are about $140 \mu\text{m}$ high and $140 \mu\text{m}$ wide. The head coils are assumed to be a single turn, and the applied magnetomotive force is 0.60 A-turns . This is approximately equivalent to a write current of 40 mA for a 15-turn coil. The MR stripe track width is $22.9 \mu\text{m}$, the thickness 500 \AA and the depth $2.5 \mu\text{m}$.

The ELEKTRA-3d Vector Fields Electromagnetics Analysis Package is used to compute electromagnetic fields including the effects of eddy currents, in three dimensions. The program incorporates state of the art algorithms for the calculation of electromagnetic fields and advanced finite element numerical analysis procedures. The art algorithms is based on a combination of vector magnetic potentials, in conducting media, and scalar magnetic potentials, in the rest of space, to model time-varying electromagnetic fields. Finite element discretization forms the basis of the methods used in these analysis programs. The display of the 3D finite element-mesh is also shown in Fig. 1.

Corresponding author: Z.G. Wang, SECEE, University of Plymouth, Drake Circus, Plymouth, Devon PL4 8AA, United Kingdom. FAX: +44-1752-232583, E-mail: zwang@plymouth.ac.uk

This work was performed under EPSRC GR/L39803.

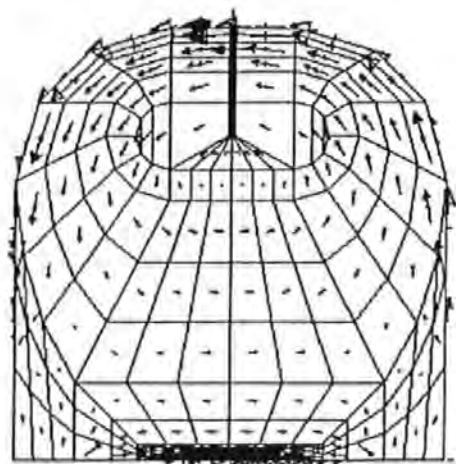


Fig. 2. Eddy current distribution in the conventional shield (the top one near the bottom core) under a write field of 50 MHz. The material of the shields is FeN. The finite-element mesh is also shown.

In the RWW operation, the shields serve mainly to transport part of the flux from the write head back to the writing coil. At the high frequencies encountered in digital recording, the conductivity of metallic magnetic materials represents an increased reluctance (above air) by eddy-currents phenomenon to the crossfeed fields. This causes the crossfeed fields to forcibly interfere with the MR element behind the shield. In this regard, the transporting efficiency is considerably improved when magnetic materials with a low conductivity are used. The shields with a low conductivity act more as alternative low-reluctance paths which divert the crossfeed fields away from the MR element. Recently, Fe-Al-O films with a nano-granular structure were successfully fabricated by RF magnetron sputtering[2]. These films exhibit good magnetic softness together with low electrical conductivity of 2.86×10^4 S/m. Nevertheless, in order to allow the head to write to the high coercivity (1650 Oe) metal particle medium, the core material is still expected to be chosen as an excellent soft magnetic film FeN with a saturation magnetization of 2.1 Tesla, an initial permeability of 3500 and a conductivity of 1×10^7 S/m. Due to the high conductivity, the flux penetrating through the shield induces an in-plane eddy current (in Fig.2) that in turn produces a counteracting field to block the penetrating flux through the shield. A possible way, we propose here, to prevent this eddy currents is to cut a notch in these metallic magnetic shields. As shown in Fig.3, a notch with a depth of $35 \mu\text{m}$ and a width of $2 \mu\text{m}$, ending at the nominal center of the coil, has been cut. Obviously, the eddy currents have been retarded and the strength of the eddy currents has been reduced to around half of that in the conventional case of Fig.2.

The work to suppress the crossfeed field involves both a novel reproductive mode[1], playing the key role in suppressing the crossfeed, and a shielding scheme, giving further suppression. The ELEKTRA analysis confirms that the shielding

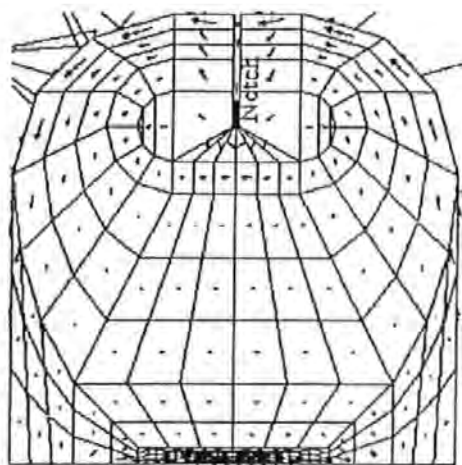


Fig. 3. Eddy current distribution in the improved top shield (FeN) with a notch, ending at the nominal center of the coil, under a write field of 50 MHz.

efficiency depends partly on the flux transport in the magnetic shields. It is advantageous to use magnetic materials with a low conductivity or to cut a notch in the metallic magnetic shields to prevent eddy currents.

REFERENCES

- [1] Z.G. Wang, D.J. Mapps, D.T. Wilton and L.N. He, *IEEE Trans. Magn.*, Vol. 33, No. 4, pp. 2531-2537, 1997.
- [2] W.D.Li, O.Kitakami, Y.Shimada, K.Ishiyama and K.I.Arai, *Journal of the Magnetics Society of Japan*, Vol.20, No.2, pp. 461-464, 1996.

Appendices

Software

This appendix lists some of the relevant software written in support of the project. The codes are Borland C++ 5.0, MATLAB 4.2C.1 and Turbo C 2.01, respectively, and the listings here do not (intentionally) use any platform specific or special language features.

A.1 Crossfeed Calculation: Borland C++

```
/* > proj0008.cpp --to calculate cross feed */
/* Frank Z. Wang, 1996 */
#include < math.h >
#include < conio.h >
#include < stdio.h >
#include < fstream.h >
#include < iomanip.h >
double H0=1.0;
double GAP=1.0;
double PI=3.1415926;
double x;
double y=0.5;
double z ;
```

SOFTWARE

```
double PHAI;
```

```
double PHA1(void)
```

```
{  
return PI-atan(y/z);  
}
```

```
double PHA2(void)
```

```
{  
return -atan(y/z);  
}
```

```
double PHA(void)
```

```
{  
PHAI=PHA2();  
if (z >0.0)  
PHAI=PHA1();
```

```
return PHAI;
```

```
}
```

```
double ROU(void)
```

```
{  
return sqrt(pow(y,2)+pow(z,2));  
}
```

```
double X1(void)
```

```
{  
return (x+GAP/2.0)/ROU();  
}
```

SOFTWARE

```
double X2(void)
{
return (x-GAP/2.0)/ROU();
}
```

```
double U31(void)
{
return log(X1()+sqrt(pow(X1(),2.0)+1.0));
}
```

```
double U32(void)
{
return log(X2()+sqrt(pow(X2(),2.0)+1.0));
}
```

```
double XY3(void)
{
return (cosh(U31()/3)/cos(PHA()/3));
}
```

```
double XY4(void)
{
return (cosh(U32()/3)/cos(PHA()/3));
}
```

```
double FY31(void)
{
return -4*cosh(U31()/3)*cos(PHA()/3)+0.5*log((XY3()+1)/(XY3()-1));
}
```

```
double FY32(void)
```


SOFTWARE

```
{  
return -4*cosh(U32()/3)*cos(PHA()/3)+0.5*log((XY4()+1)/(XY4()-1));  
}
```

```
double HY3(void)  
{  
return (H0/GAP)*(FY31()-FY32());  
}
```

```
double XZ3(void)  
{  
return (cosh(U31()/3)/sin(PHA()/3));  
}
```

```
double XZ4(void)  
{  
return (cosh(U32()/3)/sin(PHA()/3));  
}
```

```
double FZ31(void)  
{  
return -4*cosh(U31()/3)*sin(PHA()/3)+0.5*log((XZ3()+1)/(XZ3()-1));  
}
```

```
double FZ32(void)  
{  
return -4*cosh(U32()/3)*sin(PHA()/3)+0.5*log((XZ4()+1)/(XZ4()-1));  
}
```

```
double HZ3(void)  
{
```

SOFTWARE

```
return (H0/GAP)*(FZ31()-FZ32());  
}
```

```
double FX31(void)  
{  
return atan(sinh(2.0*U31()/3.0)/sin(2.0*PHA()/3.0));  
}
```

```
double FX32(void)  
{  
return atan(sinh(2.0*U32()/3.0)/sin(2.0*PHA()/3.0));  
}
```

```
double HX3(void)  
{  
return (H0/GAP)*(FX31()-FX32());  
}
```

```
double U21(void)  
{  
return (x+GAP/2.0)/y;  
}
```

```
double U22(void)  
{  
return (x-GAP/2.0)/y;  
}
```

```
double FX21(void)  
{  
return atan(U21());  
}
```

SOFTWARE

```
}
```

```
double FX22(void)
```

```
{
```

```
return atan(U22());
```

```
}
```

```
double HX2(void)
```

```
{
```

```
return (H0/GAP)*(FX21()-FX22());
```

```
}
```

```
double FY21(void)
```

```
{
```

```
return -0.5*log(pow(U21(),2)+1);
```

```
}
```

```
double FY22(void)
```

```
{
```

```
return -0.5*log(pow(U22(),2)+1);
```

```
}
```

```
double HY2(void)
```

```
{
```

```
return (H0/GAP)*(FY21()-FY22());
```

```
}
```

```
double main(void)
```

```
{
```

```
ofstream book_fileX3 ("DATA3");
```

SOFTWARE

```
for (z=-8.01;z< 8.0; z+ = 0.1)
{
for (x=-5.0;x< 6.0; x+ = 0.1)
book_fileX3 << setw(13) << z << setw(20) << x << setw(25) << HX3() <<
endl;
}
```

```
ofstream book_fileY3 ("DATAY3");
for (z=-8.01;z< 8.0; z+ = 0.1)
{
for (x=-5.0;x< 6.0; x+ = 0.1)
book_fileY3 << setw(13) << z << setw(20) << x << setw(25) << HY3() <<
endl;
}
```

```
ofstream book_fileZ3 ("DATAZ3");
for (z=-8.01;z< 8.0; z+ = 0.1)
{
for (x=-5.0;x< 6.0; x+ = 0.1)
book_fileZ3 << setw(13) << z << setw(20) << x << setw(25) << HZ3() <<
endl;
}
```

```
ofstream book_fileX2 ("DATAX2");
for (z=-8.01;z< 8.0; z+ = 0.1)
{
for (x=-5.0;x< 6.0; x+ = 0.1)
book_fileX2 << setw(13) << z << setw(20) << x << setw(25) << HX2() <<
endl;
}
```

SOFTWARE

```
ofstream book_fileY2 ("DATAY2");
for (z=-8.01;z< 8.0; z+ = 0.1)
{
for (x=-5.0;x< 6.0; x+ = 0.1)
book_fileY2 << setw(13) << z << setw(20) << x << setw(25) << HY2() <<
endl;
}
}
```

A.2 Crossfeed Calculation and Plotting: MATLAB

```
/* > projMM41.m -- to calculate and plot crossfeed */
/*Frank Z. Wang, 1996*/
clear
clg
x=(-5.0:0.1:+5.0);
z=(-5.0:0.1:+5.0);

load c:/BC5/BIN/practice/DATAY3;
load c:/BC5/BIN/practice/DATAY2;
*****

for i=1:1:17871;
a(i)=DATAY3(i,3);
end;
*****
```

SOFTWARE

```
for i=1:1:161;
for j=1:1:111;
b(j,i)=a(111*(i-1)+j);
end;
end;
*****

for i=1:1:161;
for j=1:1:111;
bR(j,i)=a(111*(i*(-1)+161)+j);
end;
end;
*****

for i=1:1:10;
for j=1:1:111;
bM(j,i)=a(j);
end;
end;

for i=11:1:161;
for j=1:1:111;
bM(j,i)=a(111*(i-10)+j);
end;
end;
*****

for i=1:1:90;
for j=1:1:111;
bRM(j,i)=bR(j,(i+10));
end;
end;
```

SOFTWARE

```
for i=91:1:161;
for j=1:1:111;
bRM(j,i)=bR(j,161);
end;
end;
```

```
for i=1:1:161;
for j=1:1:111;
bMS(j,i)=bM(j,i)+bRM(j,i);
end;
end;
```

```
for i=1:1:17871;
a(i)=DATAY2(i,3);
end;
```

```
for i=1:1:161;
for j=1:1:111;
bK(j,i)=a(111*(i-1)+j);
end;
end;
```

```
for i=1:1:161;
for j=1:1:111;
bbY(j,i)=bMS(j,i)-bK(j,i);
end;
end;
```

SOFTWARE

```
*****
*****
load c:/BC5/BIN/practice/DATAZ3;
*****

for i=1:1:17871;
a(i)=DATAZ3(i,3);
end;
*****

for i=1:1:161;
for j=1:1:111;
b(j,i)=a(111*(i-1)+j);
end;
end;
*****

for i=1:1:161;
for j=1:1:111;
bR(j,i)=a(111*(i*(-1)+161)+j);
end;
end;
*****

for i=1:1:10;
for j=1:1:111;
bM(j,i)=a(j);
end;
end;

for i=11:1:161;
for j=1:1:111;
```


SOFTWARE

```
bM(j,i)=a(111*(i-10)+j);
```

```
end;
```

```
end;
```

```
*****
```

```
for i=1:1:90;
```

```
for j=1:1:111;
```

```
bRM(j,i)=bR(j,(i+10));
```

```
end;
```

```
end;
```

```
for i=91:1:161;
```

```
for j=1:1:111;
```

```
bRM(j,i)=bR(j,161);
```

```
end;
```

```
end;
```

```
*****
```

```
for i=1:1:161;
```

```
for j=1:1:111;
```

```
bMS(j,i)=bM(j,i)-bRM(j,i);
```

```
end;
```

```
end;
```

```
*****
```

```
*****
```

```
for i=1:1:161;
```

```
for j=1:1:111;
```

```
bbZ(j,i)=bMS(j,i);
```

```
end;
```

```
end;
```

```
*****
```

SOFTWARE

```
for i=1:1:161;
for j=1:1:111;
bb(j,i)=abs(bbY(j,i))+abs(bbZ(j,i));
end;
end;
*****

for i=1:1:161;
for j=1:1:101;
bbDMR(j,i)=abs(bb(j,i)-bb((j+10),i))/2.0;
end;
end;
*****
*****

for i=1:1:30;
for j=1:1:101;
bbDMRM1(j,i)=bbDMR(j);
end;
end;

for i=31:1:161;
for j=1:1:101;
bbDMRM1(j,i)=bbDMR(j,(i-30));
end;
end;
*****

for i=1:1:131;
for j=1:1:101;
bbDMRM2(j,i)=bbDMR(j,(i+30));
end;
end;
```

SOFTWARE

```
for i=132:1:161;
for j=1:1:101;
bbDMRM2(j,i)=bbDMR(j,161);
end;
end;
*****

for i=1:1:161;
for j=1:1:101;
bbDMRS(j,i)=bbDMRM1(j,i)+bbDMRM2(j,i)+bbDMR(j,i);
end;
end;

*****
*****

for i=1:1:101;
for j=1:1:101;
bbDMRSS(j,i)=(bbDMRS(j,(i+30)))/5.04;
end;
end;

*****

cc=reshape(bbDMRSS,101,101);

*****

mesh(z,x,cc);

view(135,30);

OutStr=['point',10,'dB']
```

A.3 Stage Control: Turbo C

```

/* > movxyr.c --tomovelinearX - Ytable */
/*Frank Z. Wang, 1997*/
*****

#include < conio.h >
#include < stdio.h >
#include < bios.h >
#include < dos.h >

#define QUIT 'q'
#define UP 'H'
#define DOWN 'P'
#define RIGHT 'M'
#define LEFT 'K'
#define STETUP '+'
#define STEPDOWN '-'

short velx,vely,lowx,lowy,highx,highy,go;
char inchar;
int stepsize,x,y;

*****

move()
{

```

SOFTWARE

```
lowx = x % 256;
lowy = y % 256;
highx = x / 255;
highy = x / 255;
printf("%d %d %d %d %d %d %d /n",x,y,stepsize,highx,lowx,highy,lowy);
bioscom(1,velx,1);
bioscom(1,lowx,1);
bioscom(1,highx,1);
bioscom(1,vely,1);
bioscom(1,lowy,1);
bioscom(1,highy,1);
bioscom(1,go,1);
}
```

```
main()
{

int count1,count2,count3,count4,count5;
int i=0,j=0,ii=0,jj=0;
for (count1=1;count1≤4;count1++)
{
bioscom(0,243,1);
go=255; stepsize=1; x=8000; y=1000;
velx=17;
vely=18;
move();

for (count2=1;count2≤300;count2++)
{
```

SOFTWARE

```
i=i+1;
for (count3=1;count3≤30000;count3++)
j=j+1;
}

x=0; y=1000;
move();
for (count4=1;count4≤300;count4++)
{
ii=ii+1;

for (count5=1;count5≤30000;count5++)
jj=jj+1;
}
/*while ((inchar=getche()) != QUIT)*/
}
}
*****
```

A.4 Piezoelectric Ceramic Actuator Control: Turbo C

```
/* > piezoele.c --todrivemultilayerpiezoelectricceramicactuators */
/*Frank Z. Wang, 1997*/
#include < conio.h >
#include < stdio.h >
#include < bios.h >
```

SOFTWARE

```
#include < dos.h >
```

```
#include < conio.h >
```

```
*****
```

```
int main(void)
{
int count1, count2,count3,count4,count5;
int i=0,j=0,ii=0,jj=0;
int portcc = 435;
int porta =432;
int value =128;
int valuea =0;
int valueb =255;
outport(portcc, value);
for (count1=1;count1≤6;count1++)
{
outport(porta,valuea);
for (count2=1;count2≤900;count2++)
{
i=i+1;
for (count3=1;count3≤900;count3++)
j=j+1;
}
printf("Value %d sent to port number %d/n", valuea,porta);
outport(porta,valueb);
for (count4 =1;count4≤900;count4++)
{
ii=ii+1;
for (count5=1;count5≤900;count5++)
jj=jj+1;
```

SOFTWARE

```
}  
printf("Value %d sent to port number %d/n", valueb, porta);  
}  
}
```


List of Figures

1.1	The write and read heads for longitudinal recording (a) and Type 1 and 2 perpendicular recording, (b) and (c), respectively. Type 1 perpendicular recording requires a special write head and a soft magnetic layer under the perpendicular recording medium. Type 2 requires only a perpendicular medium and a special equalizer to process asymmetric bi-polarity readback waveform across a transition in an otherwise conventional system.	2
1.2	A typical design for a practical thin-film Inductive/Magneto-Resistive (MR) head, based on a shared-pole sensor-in-gap structure. In the read process, the magnetic field emanating from transitions is picked up by the magnetoresistive (MR) read element, inserted between shields.	3
1.3	Concept of Read-While-Write (RWW) operation. In the RWW operation, the read head (here is a SAL [Soft Adjacent Layer] biased MR head) may receive not only a signal flux from the medium but also a flux component from the write head.	5
1.4	Schematic illustration of four different sources of crossfeed field. They are: (a) Capacitive coupling from the writing to the reading bump; (b) Inductive coupling from the writing to the reading winding; (c) Magnetic flux leaking around the screens; (d) Magnetic flux penetrating through the screens. Here the reproducing head is an example of an inductive head. If an MR reproducing head is used, it is equivalent to a one-turn coil with respect to the crossfeed field source (b).	6
1.5	Schematic illustration of the crossfeed problem in RWW heads for the purpose of high reliability.	8

1.6	Tape skew.	10
1.7	The azimuth alignment of the head in hard disk drive.	10
1.8	A traditional sector servo system. Here the servo signal is intermittent because data sectors and servo sectors are distributed alternately over the hard disk surface, thereby yielding a possible misregistration from the track when the head is passing through data sectors.	12
1.9	Track and head configuration for misregistration Z_R . When exposed to the same stray field from a medium transition, one MR stripe has a resistance increase, and the other has a resistance decrease. The difference of these two stripes' signals is taken as DSMR's effective output whereas the sum of these two stripes' signals is taken as a PES (Position Error Signal) for servo purposes.	13
1.10	Illustration of fields in the (y,z) MR element plane from a recorded longitudinal medium. The biased MR element is shown in two positions to illustrate off-track asymmetry.	13
1.11	Normalized voltages amplitude versus the transverse misregistration Z_R of the head from the recorded track. Due to the intrinsic asymmetry of the 45° bias, the individual stripe's response is asymmetric and the peak shifts right (for MR1) or left (for MR2), respectively. But the DSMR signal retrieved from MR1 and MR2 is symmetry. When $-0.3 \mu m \leq Z_R \leq +0.3 \mu m$, a good linearity with PES can be seen.	15
1.12	Schematic diagram of the buried servo. A buried servo method can obtain a positioning signal continuously, in which servo and data share a medium layer by using the thin upper layer for data only and deeper layer for servo only. Both the data and the servo signals are reproduced by an identical MR sensor.	16
1.13	Schematic Tape Bearing Surface (TBS) view of a servo write head.	17
1.14	Walther's experimental situation in 1964.	19
1.15	Different screening configurations by Walther.	20
1.16	Schematic arrangement of the cores in a head in Tanaka's work.	23
1.17	Circuit diagram of the crosstalk canceller in Tanaka's work.	23

1.18	Recording gap layout of a 384 track fixed recording head in Coutelier's work.	24
1.19	Structure of the 4 MB FDD head in Murata's work.	25
1.20	Cross-section of the read/write head in Ruigrok's work.	26
2.1	SAL (Soft Adjacent Layer) scheme.	31
2.2	Schematic of a Dual Magnetoresistive head. DMR is a typical 2-terminal element because the two MR stripes are shorted at both ends.	32
2.3	Normalized spectral response function, $F(k)$, for the UMR(Unshielded MR), SMR(Shielded MR) and DMR(Dual MR). The DMR has been shown to provide a large reproduce sensitivity at high linear recording densities exceeding 100 kFCI[25][26].	33
2.4	Idealized model of a RWW head. Two replay modes will be considered: the SAL mode (SAL and MR) and the DMR mode (MR1 and MR2).	34
2.5	SCR-inter-gap-separation characteristics of RWW heads.	37
2.6	The higher: Idealized 3D model of a multi-track Read-While-Write (RWW) head. The recording gap length g is used as a size unit. Two replay modes will be considered: the SAL mode (SAL and MR) and the DMR mode (MR1 and MR2); The lower: Superposition of wedges to obtain finite gap, finite width head[38].	39
2.7	The calculated crossfeed response in arbitrary units of a SAL-MR head while 3 write heads are in operation simultaneously vs the MR head location (x,y,z) . In this case, $y=0$ and x and z range from $-5g$ to $+5g$	42
2.8	The calculated crossfeed response, in the same units as Figure 2.7, of a Dual-MR head while 3 write heads are in operation simultaneously vs the MR head location (x,y,z) . In this case, $y=0$ and x and z range from $-5g$ to $+5g$	43

2.9	Crossfeed response 2D slices of Figure 2.7 and Figure 2.8. Three write heads are operative simultaneously.	44
2.10	Crossfeed response 2D slices of Figure 2.7 and Figure 2.8. Three write heads are operative simultaneously.	45
2.11	Regions of model space.	47
2.12	Moving between modes in the Pre-Processor.	48
2.13	Front view with mesh elements. This is an example of the so-called separator design. The geometry and fields exhibit two-fold symmetry and hence only half of the structure, except for the coil, has been modelled here.	55
2.14	Side view with mesh elements. This is an example of the so-called separator design.	56
2.15	Bottom view with mesh elements. This is an example of the so-called separator design.	56
2.16	3D perspective view with mesh elements. This is an example of the so-called separator design.	57
2.17	The reference shared-pole design.	58
2.18	The improved (nonmagnetic) separator design.	59
2.19	The improved laminated-separator design.	60
2.20	Traditional planar coil structure.	61
2.21	Proposed tubular coil structure.	61
2.22	Fictitious field distribution comparison between planar coil structure and tubular coil structure. For a closed coil, two different sources of interference field can easily be distinguished, namely: (1) Positive-direction current carrying conductor (In abbreviation, positive conductor); (2) Negative-direction current carrying conductor (negative conductor). The primary motivation for the tubular coil scheme is to reduce the crossfeed by the property that the interference fields from the positive and negative conductors will cancel each other because they are so close to each other in the tubular coil scheme.	62

2.23 Flux density distribution in the mid-width plane ($z=0$) of magnetic materials for a tubular coil design at a selected applied magnetomotive force 0.60 AT.	63
2.24 Magnified flux density distribution around the write gap for a tubular coil head design.	63
2.25 The write field distribution in the TBS ($y=0$) in the shared-pole design at a selected applied magnetomotive force 0.60 AT.	65
2.26 The fictitious write field distribution in the TBS ($y=0$) in the shared-pole design with same pole width at a selected applied magnetomotive force 0.60 AT.	65
2.27 Flux density distribution in the mid-width plane ($z=0$) for a shared-pole design (with the planar coil) at a selected applied magnetomotive force 0.60 AT.	66
2.28 Flux density distribution in the mid-width plane ($z=0$) for a $3\ \mu\text{m}$ non-magnetic separator design (with the planar coil) at a selected applied magnetomotive force 0.60 AT.	67
2.29 Flux density distribution in the mid-width plane ($z=0$) for a $3\ \mu\text{m}$ laminated-separator (packing factor = 0.5) design (with the planar coil) at a selected applied magnetomotive force 0.60 AT.	67
2.30 Flux density distribution in the mid-width plane ($z=0$) for a shared-pole design at a selected applied magnetomotive force 0.60 AT. The shield serves mainly to transport part of the flux from the write head back to the writing coil. The (planar) coil is also shown here.	69
2.31 Flux density distribution in the mid-width plane ($z=0$) for a $3\ \mu\text{m}$ separator design at a selected applied magnetomotive force 0.60 AT. The shield serves mainly to transport part of the flux from the write head back to the writing coil. The (planar) coil is also shown here.	70

2.32 Flux density distribution in the mid-width plane ($z=0$) of magnetic materials for a $3 \mu\text{m}$ laminated-separator (laminating factor = 0.5) design at a selected applied magnetomotive force 0.60 AT. The laminated-separator and shield serve mainly to transport part of the flux from the write head back to the writing coil. The (planar) coil is also shown here. 71

2.33 The shield serves mainly to transport part of the flux from the write head back to the writing coil. Here is example of separator design. During the RWW process, the coils of an inductive write element are energized with a current. A portion of the resulting magnetic leak flux is radiated to the read gap in front of the TBS and then transported through the high-permeability poles and shields in the head structure. The details of this flux — transportation process and its overall efficiency (i.e., how much of the flux reaches the read gap) are determined by the head geometry and materials. 72

2.34 One-dimensional mapping of the vertical component B_y along the TBS (Tape Bearing Surface) ($z=0, y=0$) in a shared-pole design. . . . 74

2.35 One-dimensional mapping of the vertical component B_y along the TBS ($z=0, y=0$) in a separator design. 74

2.36 One-dimensional mapping of the vertical component B_y along the TBS ($z=0, y=0$) in a laminated-separator (laminating factor = 0.5) design. 75

2.37 Write field distribution with an underpole. In this scheme, a whole-plane shielding pole with a hole ($5 \mu\text{m}$ high) to let the tape go through is used. 78

2.38 Field mappings of crossfeed situations around the read gap region in the under-pole design, with the 0.60 AT magnetomotive force through the writing coil. 78

2.39	Write field distribution with an underlayer. In this scheme, a thick soft magnetic underlayer with high-permeability placed at a certain distance ($5 \mu\text{m}$) behind the tape covers both the write head and the read head.	79
2.40	Field mappings of crossfeed situations around the read gap region in the under-layer design, with the 0.60 AT magnetomotive force through the writing coil.	79
2.41	DMR (Dual Magnetoresistance) head replay processes. The figure illustrates the flux distribution of the 2-bit perpendicular recorded medium in the mid-width cut plane ($z=0$), with the replay DMR head located above the transition of those two bits.	82
2.42	DMR (Dual Magnetoresistance) head replay processes. The figure illustrates the flux distribution of the 3-bit longitudinal recorded medium in the mid-width cut plane ($z=0$), with the replay DMR head located above the central bit.	83
2.43	Field mappings of crossfeed situations around the read gap region in the shared-pole design, at a selected applied magnetomotive force 0.60 AT through the writing coil.	84
2.44	Field mappings of crossfeed situations around the read gap region in the non-magnetic separator design, at a selected applied magnetomotive force 0.60 AT through the writing coil.	85
2.45	Field mappings of crossfeed situations around the read gap region in the laminated separator design, at a selected applied magnetomotive force 0.60 AT through the writing coil.	85
2.46	SCR vs. gap separation characteristics. Here the thickness of the laminated-separator is $3 \mu\text{m}$ and the packing factor for the laminated-separator design is 0.5.	87
2.47	Lamination packing factor effect.	88
3.1	A typical thin-film-magnetoresistive head. This is the so-called separator design.	91

- 3.2 Eddy currents in a conductive sheet with an exciting coil in its geometric center. An applied field induces an eddy current that in turn produces a counteracting field. The two fields cancel at the center, but not at the edges (skin depth). 97
- 3.3 Eddy currents in a conductive sheet with an exciting coil at its edge. Induced circulating currents are still seen though they are seriously distorted when the coil is shifted at the edge of the sheet. 97
- 3.4 Field vs. MMF (Magneto-Motive Force). 101
- 3.5 Frequency dependence of the normalized field intensity and phase angle. 102
- 3.6 Field response vs. write current. 103
- 3.7 Magnetic flux and eddy current distribution in a typical RWW head. Due to the high conductivity, the flux penetrating through the shield induces an in-plane eddy current that in turn produces a counteracting field to block the penetrating flux through the shield. 104
- 3.8 Eddy current distribution in the conventional shield (Shield 1 near the bottom pole) under a 5 MHz co-sinusoidal write current at time = 0. The material of the shields is FeN with a conductivity of 1×10^7 S/m. The finite-element mesh is also shown. 107
- 3.9 Magnified eddy current distribution in the conventional shield (Shield 1) at time = 0. The material of the shields is FeN with a conductivity of 1×10^7 S/m. 107
- 3.10 Eddy current distribution in the low-conductivity (2.86×10^4 S/m) shield (the top one near the bottom pole) under a 5 MHz co-sinusoidal write current at time = 0. The material of the shields is Fe-Al-O. The finite-element mesh is also shown. 108
- 3.11 Magnified eddy current distribution in the low-conductivity Fe-Al-O shield (2.86×10^4 S/m) at time = 0. 108
- 3.12 Magnetic flux and eddy current distribution for head with a slot. The in-plane eddy currents have been retarded by the slot. 110

- 3.13 Eddy current distribution in the improved shield (Shield 1, FeN) with a slot, ending at the nominal center of the coil, under a 5 MHz co-sinusoidal write current at time = 0. 111
- 3.14 Magnified eddy current distribution around the slot in the improved shield (Shield 1) at time = 0. 111
- 3.15 Eddy current distribution along the vertical symmetric line ($z=0$, $x=40.2$) in the conventional shield (shield 1) under a 5 MHz co-sinusoidal write current at time = 0. 112
- 3.16 Eddy current distribution along the vertical symmetric line ($z=0$, $x=40.2$) in the improved shield (shield 1) under a 5 MHz co-sinusoidal write current at time = 0. 112
- 3.17 Comparison of normalized crossfeed response vs. phase angle for heads with and without slot. 113
- 3.18 Schematic of suppression the so-called crossfeed field radiation from the write head by a conductive ring around the MR reproducing element. 115
- 3.19 Bottom view of a shield-wing-interconnecting RWW head (Write poles are not shown here). Finite-element mesh is displayed. 115
- 3.20 Magnified eddy current distribution in the TBS around the joint region of the two shields under a 5 MHz co-sinusoidal write current at time = 0. 116
- 3.21 Crossfeed response vs. write field frequency. The improved stands for the shield-wing-interconnecting design and the traditional for the parallel-shield design. 116
- 3.22 Media cross-section and flux path for a basic keepered-longitudinal(perpendicular)-medium reproduction with a Dual MR head. A soft-magnetic keeper film is deposited on top of the medium layer and below the lubricating overcoat. During a write operation, flux from the recording head saturates the keeper above the medium region. The keeper layer could be biased by the stray flux from dual MR sensors during a read operation. 118

- 3.23 The stray flux density distribution of the DMR in the presence of a top keeper layer (without recording layer) at a selected sense current $I = 10$ mA. Sense current of the same magnitude and direction is sent through both elements producing opposing semi-saturated state in each sensor. The resulting bias field in front of the stripe-stripe-gap saturates a small region of the keeper layer underneath the gap. . . . 120
- 3.24 Releasing state. Flux distribution of the recorded bits (not including the contribution from the MR sense currents) in the mid-width cut plane ($z=0$), with the replay DMR head with an optimum sense current $I = 10$ mA at the top of the medium, is shown. The small saturated region in the top keepered layer, which is created by the resulting bias field in front of the stripe-stripe-gap, cuts off the return path of the medium transition flux through the top keepered layer due to saturated region's low permeability. The medium transition flux is therefore forcibly released from the shunting in the top keeper layer, which allows flux transitions to be picked up by the reproductive DMR head. 122
- 3.25 Shunting state. Flux distribution of the recorded bits in the mid-width cut plane ($z=0$), with the replay DMR head without any sense current is shown. The flux distribution from the perpendicular recording layer is well restrained beneath the top keeper layer and above the bottom keeper layer (underlayer). 123
- 3.26 Magnified write field distribution under a 5 MHz co-sinusoidal write current at time = 0 around the write gap in the presence of keepered medium. 125
- 3.27 Field mapping of crossfeed situation around the read gap region in the presence of keepered medium, under a 5 MHz co-sinusoidal write current at time = 0. 125
- 3.28 Eddy current distribution in the keeper layer under a 5 MHz co-sinusoidal write current at time = 0. 126

3.29	Schematic of eddy current in a conductive keeper due to the penetrating stray flux through the keeper layer.	126
4.1	A computer-controlled experimental apparatus for the assessment of heads. IBM PC-386 computer (right), two-stage positioning system (centre), MR/inductive head with its holder (up centre), circuits for write amplifiers and read amplifiers (lower centre), voltage booster for piezoelectric actuators (left, black), linear motor controller (left, white, underneath booster), power supply (far left, white) and signal generator (far left, above supply).	132
4.2	Magnified photograph near the heads.	133
4.3	Schematic of experimental apparatus for measuring crossfeed on an MR/inductive head.	134
4.4	Part of the crossfeed measurement system.	134
4.5	Part of analog and digital playback circuitry—sense current (analog and digital channels) and DC bias current (digital MR channels). . .	135
4.6	A new generation thin-film MR tape head product TR5 provided by Read-Rite.	136
4.7	Arrangement of the poles and shields for the single channel head TR5.	137
4.8	The reproducing waveform of TR5 (the lower) without any sense current through MR against a squarely-varying excitation (the higher) in the write coil at frequency of 36.4 kHz. The vertical scale is 50 mV/div and the horizontal scale is 10 μ s/div.	138
4.9	The reproducing waveform of TR5 (the lower) with a 10 mA sense current through MR against a squarely-varying excitation (the higher) in the write coil at frequency of 36.4 kHz. The vertical scale is 400 mV/div and the horizontal scale is 10 μ s/div.	138
4.10	The reproducing waveform of TR5 (the lower) with a 10 mA sense current through MR against a squarely-varying excitation (the higher) in the write coil at frequency of 364 kHz. The vertical scale is 400 mV/div and the horizontal scale is 1 μ s/div.	139

- 4.11 The reproducing waveform of TR5 (the lower) with a 10 mA sense current through MR against a squarely-varying excitation (the higher) in the write coil at frequency of 3.64 MHz. The vertical scale is 400 mV/div and the horizontal scale is 0.1 μ s/div. 139
- 4.12 The reproducing waveform of TR5 (the lower) with a 10 mA sense current through MR against a squarely-varying excitation (the higher) in the write coil at frequency of 36.4 MHz. The vertical scale is 400 mV/div and the horizontal scale is 0.01 μ s/div. 140
- 4.13 Measurement of crossfeed response of TR5 as a function of frequency, against a squarely-varying recording current of 40 mA_{0-p} (optimum recording current). 140
- 4.14 The reproducing waveform of TR5 against a TDK magnetic tape coupon, pre-recorded by a 9.6 kHz sinusoidally-varying recording field. The vertical scale is 200 mV/div and the horizontal scale is 1 ms/div. 142
- 4.15 The reproducing waveform of TR5 against a TDK magnetic tape coupon, pre-recorded by a 9.6 kHz squarely-varying recording field. The vertical scale is 500 mV/div and the horizontal scale is 1 ms/div. 142
- 4.16 A Dual-Stripe Magnetoresistive (DSMR) head stack, provided by Read-Rite, were originally designed for hard disk drives. 143
- 4.17 The reproducing waveform (the lower) with a 12 mA sense current through the single MR against a squarely-varying excitation (the higher) in the write coil. The vertical scale is 2.00 V/div and the horizontal scale is 0.1 ms/div. 144
- 4.18 The reproducing waveform (the lower) with a 12 mA sense current through the DMR against a squarely-varying excitation (the higher) in the write coil. 144
- 4.19 Philips Digital Compact Cassette (DCC) magnetic tape head, which serve 9 parallel digital tracks on tape. 146
- 4.20 The Philips DCC head has a track pitch of 195 μ m (130 tpi). The read elements are much smaller than the track pitch at 70 μ m. . . . 147

- 4.21 Schematic configuration of record and playback channels in the DCC head. Starting from the tape track indicated in the figure, the magnetic flux is transported across the MR element via magnetic flux guide layers. With the aid of the barberpole, the output characteristic of the MR element is linear (otherwise parabolic). 147
- 4.22 The crossfeed responses of the DCC head in MR sensor No.2, 3 and 4, respectively, against a squarely-varying excitation in write head No.3. The vertical scale is 50 mV/div and the horizontal scale is 1 ms/div. . 148
- 5.1 The Hewlett Packard 9000-715 workstation. A TOSCA model is on screen. 152
- 5.2 A recorded bit is being picked up by a DMR head. The leakage flux from the medium goes upward in the left stripe and returns downward in the right stripe. It constitutes a closed magnetic circuit. Obviously it causes an adequate signal output due to electrically parallel connection in the DMR head. 157
- 5.3 Resultant crossfeed field suppression by using a Dual MagnetoResistive head. Here the contribution from the medium is not included in the magnified flux density distribution. 158
- 5.4 A multi-track Read-While-Write (RWW) head. When an MR head is biased, the magnetic vector is placed approximately at 45 degrees to the current flow direction. To reduce Barkhausen noise a transverse field component is sometimes used. The field from the tape also has transverse components in it, especially if the track is narrow. For these reasons it is important to consider the cross-track direction for crossfeed within a combination head. 159

List of Tables

2.1	Crossfeed responses with three different RWW head designs. The thickness of the (non-magnetic) separator or the laminated-separator is $3 \mu\text{m}$. In the laminated-separator design, the packing factor is 0.5. The unit of response is $\text{T}\cdot\mu\text{m}^3$	76
2.2	Crossfeed responses in laminated-separator RWW head design with three different packing factors. The unit of response is $\text{T}\cdot\mu\text{m}^3$	77
2.3	Crossfeed responses in shared-pole RWW head with two additional improved different designs. The response's unit is $\text{T}\cdot\mu\text{m}^3$	80
2.4	The SCR(Signal-Crossfeed-Ratio) of various head designs. In the separator design the material of the separator is non-magnetic. In the laminated-separator design, the packing factor is 0.5.	87
3.1	Properties of soft magnetic materials.	105

Index

- 0-p (zero-peak value), 136, 137, 140, 143, 146, 149
- ABS (Air Bearing Surface), 40, 41
- AC (Alternating Current), 7, 17, 21, 28
- DC (Direct Current), 7, 28
- DCC (Digital Compact Cassette), 130, 133, 145–149
- DMR (Dual Magneto-Resistive), 30, 106, 109, 114
- DSMR (Dual Stripe Magneto-Resistive), 12, 13, 15, 143, 148–150
- ELEKTRA, 92, 94
- FEM (Finite Element Method), 24, 29, 86
- JPEG (Joint Photographic Experts Group), 26
- kFCI (kilo Flux Change per Inch), 28, 33
- MFM (Magnetic Force Microscopy), 117
- MMF (Magneto-Motive Force), 100, 101, 151
- MR (Magneto-Resistive), 3–7, 11, 12, 14, 28
- p-p (peak-peak value), 137, 141, 145, 149
- PES (Position Error Signal), 11, 13, 150
- RWW (Read-While-Write), 7, 8, 11, 15, 28, 68, 72, 76, 77, 84, 86, 88, 89, 92, 99, 104, 114, 115, 117, 123, 127, 149–151, 154, 156
- SAL (Soft Adjacent Layer), 5
- SCR (Signal-Crossfeed-Ratio), 36, 38, 81, 155, 164
- SRR (Shunting-Releasing Ratio), 121
- TBS (Tape Bearing Surface), 17, 40, 41, 64, 65, 68, 72–75, 80, 116, 155
- TOSCA, 46, 48, 52, 151, 152
- TR5, 130, 133, 135–137, 140, 141, 148, 149
- VCM (Voice Coil Motor), 11